

UNIVERSITÉ DU QUÉBEC À CHICOUTIMI

**THESIS PRESENTED TO THE
UNIVERSITY OF QUEBEC AT CHICOUTIMI
IN PARTIAL FULFILLMENT OF
THE REQUIREMENT FOR THE DEGREE OF
DOCTOR OF PHILOSOPHY IN ENGINEERING**

BY

YASSER ZEDAN

**MACHINABILITY ASPECTS OF HEAT-TREATED
Al-(6-11)% Si CAST ALLOYS: ROLE OF INTERMETALLICS
AND FREE-CUTTING ELEMENTS**

MAY 2010

UNIVERSITÉ DU QUÉBEC À CHICOUTIMI

THÈSE

PRÉSENTÉE À

L'UNIVERSITÉ DU QUÉBEC À CHICOUTIMI

COMME EXIGENCE PARTIELLE

DU DOCTORAT EN INGÉNIERIE

PAR

YASSER ZEDAN

**ASPECTS DE L'USINAGE DES ALLIAGES DE FONDERIE
Al-(6-11)% Si TRAITÉS THERMIQUEMENT : RÔLE DES
INTERMÉTALLIQUES ET DES ÉLÉMENTS DE
DÉCOLLETAGE**

MAI 2010

*Dedicated to my parents, my wife Noha,
and to my children Ali and Hana.*

RÉSUMÉ

Le besoin de combler le vide entre les procédés de coulé et d'usinage donne de bonnes raisons d'examiner les nombreux aspects affectant l'usinabilité des alliages de fonderie Al-Si. Les alliages quasi-eutectiques sont, parmi les alliages Al-Si, les plus difficiles à usiner, puisque les particules de la phase Si sont environ 10 fois plus dures que la matrice d'aluminium, lesquelles expliquent pourquoi les outils de coupe s'usent prématurément. Toutes ces difficultés nécessitent une meilleure compréhension des effets de la microstructure sur l'usinabilité de ces alliages.

Ce travail a été mené dans le but d'étudier un nouvel alliage expérimental appartenant au groupe des alliages de fonderie Al-Si quasi-eutectique contenant environ 10,8%Si, à savoir l'alliage 396. Suite à ce qui a été soulevé, l'objectif principal de ce travail est de rapporter les changements des critères d'usinage résultant des effets des intermétalliques de fer, à savoir α -Fe, β -Fe et « sludge »; de deux niveaux de Cu, à savoir 2,25 et 3,5%; et de deux niveaux de Mg, à savoir 0,3 et 0,6%. De plus, les effets des alliages sans Mg et modifiés au Sr ont également été étudiés en plus des effets des éléments de décolletage tels que Sn, Bi et Pb. Le traitement thermique T6 a été sélectionné pour établir le niveau de dureté des alliages étudiés à l'intérieur d'une plage de 110 ± 10 BHN, conforme à la plupart des niveaux de dureté pour les applications commerciales des alliages d'aluminium. La mesure de la dureté a été faite directement sur les blocs d'usinage pour assurer que les échantillons possèdent le niveau de dureté requis. Tous ces alliages ont également été testés mécaniquement de façon à obtenir une compréhension des effets des additifs sur les propriétés mécaniques de tractions pour les mêmes conditions appliquées aux blocs de test d'usinage.

Les tests d'usinage ont été faits sur une machine d'usinage horizontale haute vitesse Makino A88E sous des conditions fixes lesquelles incluent la vitesse de coupe, la vitesse d'avance, la longueur de la coupe, la géométrie de l'outil, le matériau de l'outil ainsi que le liquide de refroidissement. Les critères d'usinage observés sont les forces et les moments total de coupe, la durée de vie de l'outil en termes de nombre de trous percés ou taraudés jusqu'au bris de l'outil, la morphologie des copeaux et l'arête rapporté (BUE).

Les résultats démontrent que la présence de « sludge » sous la forme de points durs a un effet sur la force de coupe et la durée de vie de l'outil qui est réduite de moitié par rapport à l'alliage de base. La formation de la phase α -Fe dans l'alliage M1 a un effet bénéfique sur la durée de vie de l'outil, ainsi cet alliage est celui qui donne le plus grand nombre de trous percés comparativement aux alliages contenant le « sludge » ou β -Fe; ces résultats pourraient être expliqués par le fait que la formation des intermétalliques α -Fe avec leur morphologie de scripts chinois arrondis et de leur présence à l'intérieur des dendrites α -Al améliore l'homogénéité de la matrice par un durcissement des dendrites. L'augmentation du fer de 0,5% à 1% dans l'alliage 396-T6 contenant 0,5% Mn produit une amélioration distincte de l'usinabilité en termes de force de coupe et de durée de vie de l'outil. Lors des tests de taraudage, il a été trouvé que les outils en acier rapide sont considérablement plus sensibles aux phases intermétalliques de fer que les outils en carbure

utilisés pour le perçage L'ajout de Fe ou de Mn semblent avoir aucun effet sur l'arête rapporté (BUE) et sur la morphologie des copeaux comparativement à l'alliage de base.

L'augmentation des niveaux de Cu ou de Mg dans l'alliage 396-T6 ont tous des effets nuisibles sur la durée de vie du foret. Cette réduction de la durée de vie du foret pourrait être attribuée à la formation d'une grande quantité de blocs de la phase Al_2Cu et à la formation de plaques épaisses de la phase Al-Si-Cu-Mg. L'alliage expérimental sans Mg affiche les plus faibles force et moment de coupe en plus de produire le plus grand nombre de trous de tous les alliages étudiés. Cette observation pourrait être expliquée par une précipitation combinée des phases durcissantes Al_2Cu , Mg_2Si , Al_2CuMg et $Al_5Si_6Cu_2Mg_8$ dans les alliages contenant du Mg lesquels confèrent une plus grande résistance à l'alliage que la précipitation seule de la phase Al_2Cu de l'alliage sans Mg. Une comparaison entre l'alliage modifié et non-modifié (contenant les mêmes niveaux de Mg et de Cu) en terme de nombre de trous percés, révèle que la morphologie des particules de Si a un effet sur la durée de vie de l'outil.

L'ajout de petites, mais efficaces, quantités d'éléments de décolletages aux alliages de fonderie Al-Si améliore considérablement l'usinabilité de ces derniers. L'alliage contenant du Sn a un effet sur la durée de vie des forets en carbure et des tarauds en acier rapide. D'un autre côté, les alliages contenant du Bi mènent à un grossissement des particules de Si eutectique résultant à une détérioration de la durée de vie de l'outil. L'ajout simultané d'une petite quantité de deux ou de plusieurs éléments insolubles dans l'aluminium a un plus grand effet sur l'usinabilité en termes de réduction de la force et du moment de coupe que les ajouts individuels de chaque élément. L'ajout de Pb, Bi et Sn semble n'avoir aucun effet sur la formation de l'arête rapporté (BUE) ou sur la morphologie des copeaux excepté que l'alliage contenant du Bi montre un légère tendance à réduire la formation de l'arête rapporté (BUE) et il produit également des copeaux en forme d'éventail plus petit que ceux observés pour les alliages sans Bi.

Un examen visuel des copeaux révèle que la forme d'éventail est de loin la forme prédominante pendant le perçage, de plus elle est considérée comme la forme idéale pour beaucoup d'application de perçage. La fragmentation des copeaux des alliages contenant la phase Al_2Cu était supérieure à celle des alliages contenant la phase Mg_2Si . Ainsi, l'addition combinée de Cu et de Mg devrait raffiner davantage la taille des copeaux produits.

L'examen des forets usés a montré que le maximum d'usure prend place au coin extérieur de l'arête du foret, alors qu'un minimum d'usure se produit à, ou près de, la pointe du foret. Lorsque les coins du foret sont arrondis, le foret colle à la pièce et se brise si le procédé de coupe n'est pas arrêté à temps. Pour les tests de taraudage, le principal mécanisme d'usure observé est l'adhésion, même si une certaine abrasion pourrait se produire lors du taraudage des alliages contenant le « sludge » et le Bi. La rupture se produit fréquemment dans la patrie chanfreinée du taraud puisqu'elle génère une majeure partie de la force résultante, en raison de la plus grande section de copeaux apparentée aux dents du chanfrein.

ABSTRACT

The need for bridging the divide between the casting process and the machining process provides a strong motivation for examining the various aspects affecting the machinability of Al-Si casting alloys. Near-eutectic alloys are said to be the most difficult to machine of the various Al-Si alloys, as may be evidenced by the fact that the silicon phase present is almost ten times harder than the aluminum base alloy, which is why the cutting tools tend to wear out so rapidly; these difficulties have thus created the need for a more in-depth understanding of the effects of microstructure on the machinability of these alloys.

This study was conducted with the intention of investigating a new experimental alloy belonging to the Al-Si near-eutectic cast alloy group, containing about 10.8%Si, namely the 396 alloy. In the light of the above, the main purpose of the work is to report on the changes in the machinability criteria resulting from the effects of Fe-intermetallics, namely α -Fe, β -Fe, and sludge; the effects of two levels of Cu, namely 2.25% and 3.5%; and the effects of two levels of Mg, namely 0.3 and 0.6%. In addition to the preceding, the effects of Mg-free alloys and Sr-modification on these same alloys were also investigated together with the effects of free-cutting elements, specifically Sn, Bi, and Pb. Thus, a specific T6 heat treatment was selected to establish the hardness level for the alloys investigated within the range of 110 ± 10 BHN, conforming to most of the required hardness levels in the commercial application of aluminum alloys. Hardness measurements were carried out on heat-treated machinability test blocks to ensure that they possessed the required hardness levels. All of these alloys were also mechanically tested in order to acquire an understanding of the effects of additives on the tensile properties in the same conditions applied to the machinability test blocks.

Machining tests were carried out using a Makino A88E high-speed horizontal center machine under fixed machining conditions which include cutting speed, feed rate, length of cut, tool geometry, tool material, and coolant as applied to the examination of the alloys under discussion. It should be mentioned here that the pertinent machinability criteria relate the total cutting forces and moments, tool life expressed as the number of holes drilled/tapped up to the point of tool breakage, chip configuration, and built-up edge (BUE) evolution.

The results demonstrate that the presence of sludge in the form of hard spots has a significant effect on cutting forces and tool life, in that it decreases drill life by 50% compared to the base alloy. The formation of the α -Fe phase in the M1 base alloy has a beneficial effect on tool life in that this alloy produces the highest number of holes drilled compared to alloys containing sludge or β -Fe; this result may be explained by the fact that the formation of the α -Fe intermetallic with its rounded Chinese script morphology and its presence within α -Al dendrites is expected to improve matrix homogeneity via hardening of the soft α -Al dendrites. Increasing the Fe-content from 0.5% to 1% in the 396-T6 alloy containing 0.5%Mn produces a distinct improvement in alloy machinability in terms of

cutting force and tool life. In tapping tests, it was found that high-speed steel (HSS) tools are considerably more sensitive to the Fe-intermetallic phases than the carbide tools used for drilling. The addition of Fe and/or Mn appears to have no discernible effect on the built-up edge area (BUE) and chip configuration compared to the base alloy.

The increase in the levels of Cu and/or Mg in the 396-T6 alloy has a detrimental effect on drill life. Such an effect may be attributed to the formation of large amounts of the coarse blocklike Al_2Cu phase, together with the formation of thick plates of the Al-Si-Cu-Mg phase. The Mg-free experimental alloy displays the lowest cutting force and moment in addition to producing the highest number of holes in the alloys studied. This observation may be explained by the cooperative precipitation of the Al_2Cu , Mg_2Si , Al_2CuMg , and $\text{Al}_5\text{Si}_6\text{Cu}_2\text{Mg}_8$ hardening phases in Mg-containing alloys which confer greater strength on the alloy than would be the case with the precipitation of only the Al_2Cu phase in the Mg-free alloy. A comparison of the non-modified alloy and the Sr-modified alloy (containing the same level of Mg and Cu additions) in terms of the number of holes drilled, reveals that the morphology of Si particles has a noticeable effect in governing the tool life of near-eutectic Al-Si alloys.

The addition of small but effective amounts of free-machining elements to Al-Si casting alloys significantly improves the machinability of these alloys. The Sn-containing alloy has a beneficial effect on tool life for both carbide drills and HSS taps. On the other hand, the Bi-containing alloys lead to a noticeable coarsening of the eutectic Si particles resulting in a deterioration of tool life. The simultaneous addition of smaller amounts of two or more elements insoluble in aluminum has a greater effect on machinability in terms of reducing the drilling force and moment than individual additions of each element. The addition of Pb, Bi, and Sn appears to have no significant effect on the formation of built-up edge (BUE) or on chip configuration except that the Bi-containing alloy shows a slightly lower tendency to BUE formation, and it also produces finer fan-shaped chips than those observed in the Bi-free alloy.

A visual examination of the chips reveals that the fan shape is by far the predominant form during the drilling of the alloys studied, and also that it is considered to be the ideal chip type for most drilling applications. The chip breakability of alloys containing the Al_2Cu phase was superior to that of alloys containing Mg_2Si . Thus, combined additions of Cu and Mg are expected to further refine the size of the chips produced.

An examination of worn drills showed that the maximum wear takes place at the outer corner edge of the drill, while minimum wear occurs at, or near, the point of the drill tip. When the corners of the drill are rounded off, the drill then sticks to the workpiece and breaks if the cutting process is not halted in time. In tapping tests, the main wear mechanism observed is adhesion, although some abrasion may also occur during the tapping of the sludge-containing and Bi-containing alloys. Breakage occurs frequently at the chamfered part of the tap since it generates a major part of the resulting force, because of the larger chip cross-section related to the teeth of the chamfer.

ACKNOWLEDGMENTS

I would like to express my sincere gratitude to my supervisor, Dr. Fawzy H. Samuel, Professor at Université du Québec à Chicoutimi (Canada) and visiting Professor at King Saud University (Saudi Arabia) for motivating me to complete my Ph.D. degree; without his continuous guidance and support it would have been impossible to do so. I am much indebted to him for helping me so generously over the last four years. I feel privileged to have been able to work with someone whose dedication and contribution to the field of science will be a constant inspiration to me throughout my life.

I would also like to express my sincere thanks to Dr. Agnes Marie Samuel, Research Professor at Université du Québec à Chicoutimi (Canada) for her invaluable guidance and help during different stages of my research work.

Financial support in the form of scholarships received from the Natural Sciences and Engineering Research Council of Canada (NSERC), the Fondation de l'Université du Québec à Chicoutimi (FUQAC), General Motors Powertrain Group (U.S.A), and Corporativo Nemark (Mexico) is gratefully acknowledged.

I would like to extend my appreciation to Mr. Alain Bérubé of the TAMLA group, at UQAC, for his assistance with the castings and sample preparation, as well as to Mr. Lang Shi of the Microanalysis Laboratory, Earth and Planetary Sciences, McGill University for carrying out EPMA analyses.

Thanks are also due to Madame Marion Sinclair for her help in editing my thesis. Credit goes to the members of my family, especially to my mother, my wife, and my children, as well as to all my brothers and sisters for their sound advice and unfailing encouragement during the time it took to write my thesis.

PUBLICATIONS

Journal Papers

1. Y. Zedan, F.H. Samuel, A.M. Samuel, H.W. Doty, "Effects of Fe Intermetallics on the Machinability of Heat-Treated Al-(7-11)% Si Alloys," *Journal of Materials Processing Technology*, 2010, Vol. 210, pp. 245-257.
2. Y. Zedan, F.H. Samuel, A.M. Samuel, H.W. Doty, "**Effects of Additions of Pb, Bi, and Sn on the Machinability of Al-10.8% Si Casting Alloys,**" Prepared for Submission to *Journal of materials Processing Technology*, 2010.
3. Y. Zedan, F.H. Samuel, A.M. Samuel, H.W. Doty, "**Effects of Sn and Bi Addition on the Machinability of Heat-Treated B319.2 Cast Alloy,**" Prepared for Submission to *Materials Science and Engineering A*, 2010.
4. Y. Zedan, F.H. Samuel, A.M. Samuel, H.W. Doty, "**Machinability Aspects of Heat-Treated Al-10.8%Si Cast Alloys: Role of Cu-Rich Intermetallics,**" Prepared for Submission to *International Journal of Machine Tools & Manufacture*, 2010.

Scientific Posters

5. Y. Zedan, F.H. Samuel, A.M. Samuel, H.W. Doty, "**Factors Controlling The Machinability of Al-Si Casting Alloys,**" Poster Presented at "Journée des Etudiants du REGAL" (REGAL Students' Day), October 26, 2007, UQAC, Chicoutimi; Published in *The Encyclopaedia of Research on Aluminum in Quebec-2007 Edition* (Strategic Aluminium Research Network), October 26, 2007, UQAC, Chicoutimi, Les Presses de l'Aluminium (PRAL), Chicoutimi, Qc, Canada, 2008, Axis II-New Aluminium Products and Materials, p. 50.
6. Y. Zedan, A.M. Samuel, F.H. Samuel, H.W. Doty, "**Effects of Individual Additions of Pb, Bi, and Sn on the Machinability of Al-11Si-2.25Cu-0.3Mg Casting Alloys,**" Poster Presented at "Journée des Etudiants du REGAL" (REGAL Students' Day), October 21, 2009, ETS, Montreal; Published in *The Encyclopaedia of Research on Aluminum in Quebec- 2009 Edition* (Strategic Aluminium Research Network), October 21, 2009, ETS, Montreal, Les Presses de l'Aluminium (PRAL), Chicoutimi, Qc, Canada, 2010, Axis II-New Aluminium Products and Materials, P. 56.

TABLE OF CONTENTS

	Page
RÉSUMÉ	i
ABSTRACT	iii
ACKNOWLEDGMENTS	v
PUBLICATIONS	vi
TABLE OF CONTENTS	vii
LIST OF FIGURES	x
LIST OF TABLES	xv
CHAPTER 1 DEFINING THE PROBLEM	1
1.1 INTRODUCTION	2
1.2 OBJECTIVES	6
CHAPTER 2 REVIEW OF THE LITERATURE	8
2.1 INTRODUCTION	9
2.2 IMPORTANT ISSUES IN METAL-CUTTING OPERATIONS	10
2.3 MACHINING OF ALUMINUM ALLOYS	11
2.4 EFFECTS OF METALLURGICAL FACTORS ON MACHINABILITY OF Al-Si ALLOYS	13
2.4.1 Alloying Elements	13
2.4.1.1 Role of Si and Melt Treatment in Al-Si Alloys	14
2.4.1.2 Role of Fe Intermetallics in Al-Si Alloys	17
2.4.1.3 Role of Cu and Mg in Al-Si Alloys	19
2.4.1.4 Role of Free-Cutting Elements in Al-Si Alloys	23
2.4.2 Microstructural Features	29
2.4.3 Heat Treatment	31
2.5 MACHINING OPERATIONS	33
2.5.1 Drilling Process	34

2.5.1.1 Drill Nomenclature and Geometry	35
2.5.1.2 Operating Conditions	37
2.5.1.3 Dry Drilling of Aluminum Alloys	41
2.5.2 Tapping Operations	44
2.6 MACHINABILITY CRITERIA	47
2.6.1 Cutting Forces Experienced During Drilling Operations	48
2.6.2 Tool Wear and BUE Formation	52
2.6.3 Tool Life Criteria	55
2.6.4 Chip Formation in Drilling	59
CHAPTER 3 EXPERIMENTAL PROCEDURES	64
3.1 INTRODUCTION	65
3.2 ALLOY PREPARATION AND CASTING PROCEDURES	66
3.3 HEAT TREATMENT	71
3.4 METALLOGRAPHY-MICROSTRUCTURAL EXAMINATION	72
3.5 HARDNESS TESTING	75
3.6 TENSILE TESTING	76
3.7 MACHINING PROCEDURES.....	78
3.7.1 Cutting Tools	78
3.7.2 Cutting Parameters	79
3.7.3 Tool Life Criteria	81
3.7.4 Measurement of Machining Forces	83
3.7.5 Chip Form and BUE Evaluations	84
3.8 METHODOLOGY FOR THE DATA-PROCESSING OF DRILLING AND TAPPING TESTS	86
CHAPTER 4 EFFECTS OF IRON-RICH AND COPPER-RICH INTERMETALLICS ON THE MACHINABILITY OF HEAT-TREATED Al-10.8%Si CAST ALLOYS.....	96
4.1 INTRODUCTION	97
4.2 CHARACTERIZATION OF THE MICROSTRUCTURE	98
4.2.1 Silicon Particle Characteristics	99

4.2.2 Iron-Rich Intermetallics	104
4.2.3 Copper-Rich Intermetallics	109
4.3 HARDNESS AND TENSILE PROPERTIES	112
4.4 MACHINING BEHAVIOR	114
4.4.1 Effects of Fe-Intermetallics on Machinability	115
4.4.1.1 Cutting Forces and Moments	115
4.4.1.2 Tool Life	123
4.4.2 Effects of Cu and Mg Additions on Machinability	127
4.4.2.1 Cutting Forces and Tool Life	129
4.4.3 Evolution of Built-Up Edge (BUE) and Tool Wear Characteristics	144
4.4.4 Chip Characterization	153
CHAPTER 5 EFFECTS OF FREE-CUTTING ELEMENTS ON THE MACHINABILITY OF Al-Si-Cu-Mg CAST ALLOYS...	156
5.1 INTRODUCTION	157
5.2 MICROSTRUCTURE	159
5.2.1 Silicon Particle Characteristics	159
5.2.1 Effects of Free-Cutting Elements on Microstructure	164
5.3 HARDNESS AND TENSILE PROPERTIES	169
5.4 MACHINING BEHAVIOR	171
5.4.1 Cutting Forces and Tool Life	172
5.4.1.1 396 Alloys (Al-11% Si)	172
5.4.1.2 B319.2 Alloys (Al-7% Si)	184
5.4.2 Evolution of Built-Up Edge (BUE) and Tool Wear Characteristics ...	189
5.4.3 Chip Characterization	192
CHAPTER 6 CONCLUSIONS AND RECOMMENDATIONS.....	195
6.1 CONCLUSIONS	196
6.2 RECOMMENDATIONS FOR FUTURE WORK	202
REFERENCES.....	203

LIST OF FIGURES

CHAPTER 2

Figure 2.1	Nomenclature of a twist drill.	36
Figure 2.2	Undeformed chip width in the drilling process.	39
Figure 2.3	(a) Showing rake angle along the cutting edge moving across workpiece, and (b) showing variation in cutting speed with the cutting edges.	40
Figure 2.4	Tap and thread nomenclature.	45
Figure 2.5	(a) Basic elements of tap and forces on an elementary tooth; (b) change in torque during the tapping cycle.	47
Figure 2.6	Tool wear evolution: 1. initial wear; 2. slight wear; 3. moderate wear; 4. severe wear; and 5. worn-out.	50
Figure 2.7	Wear mechanisms as a function of temperature.	54
Figure 2.8	Some features of single-point tool wear in turning operations.	56
Figure 2.9	Characteristics of worn twist drill.	58
Figure 2.10	Types of drill wear.	58
Figure 2.11	Conical helical chip produced by the twisted part of the cutting lip.	61
Figure 2.12	Chip forms generated: (A) conical; (B) fan-shaped; (C) chisel-edge; (D) amorphous; (E) needlelike; (F) impacted.	63

CHAPTER 3

Figure 3.1	Electrical resistance melting furnace.	69
Figure 3.2	(a) Waffle-plate metallic mold; (b) machinability test block casting; and (c) machinability test block.	69
Figure 3.3	Blue M electric furnace.	71
Figure 3.4	Optical microscope-image analysis system.	72
Figure 3.5	Scanning electron microscope system used for this study.	74
Figure 3.6	(a) Schematic diagram of Brinell hardness test; (b) hardness measurement for machinability test block; (c) schematic of hardness indentations for test block.	76
Figure 3.7	(a) Actual tensile test bar casting; (b) MTS servohydraulic mechanical testing machine.	77
Figure 3.8	(a) Makino A88E CNC machining center; and (b) a close-up view of the test block, dynamometer, and cutting tool.	79
Figure 3.9	(a) Machinability test block after drilling and tapping; (b) detailed drawing of the tapped hole.	81

Figure 3.10	Thread gauge used in the current work.	82
Figure 3.11	(a) Kistler dynamometer with four sensors used in this study; (b) illustration showing the measurement chains for the 6-component forces and moment measurements.	84
Figure 3.12	Schematic diagrams showing the experimental set-up for carrying out the drilling and tapping tests.	85
Figure 3.13	Data processing for the drilling feed force-Fz component of the first group of holes (90-holes): (a) raw data of Fz component; (b) filtration (9-times) for Fz component.	90
Figure 3.14	(a) First difference of the filtered Fz, point detection within each cycle; (b) first and second difference of the filtered Fz component.	91
Figure 3.15	(a) Two points within each cycle: the red point represents the mean Fz during drilling cycle, while the green point represents the error value upon removing the drill from the hole; (b) output results for the drilling feed force for the first group of holes (90 holes) showing plots with or without error consideration.....	92
Figure 3.16	(a) Data processing for the tapping feed force-Fz component of the first group of holes (90-holes); (b) three points within each cycle, the upper point representing the mean $mF_{z_{up1}}$, the lower point representing the mean $F_{z_{down1}}$, and the middle point representing the error value of the signal.	95
CHAPTER 4		
Figure 4.1	Optical micrographs showing the effects of Sr-addition on Si morphology in grain-refined and heat-treated Al-10.8% Si alloy: (a) 0 Sr-M0 alloy; (b) 200 ppm Sr-M1 alloy.	101
Figure 4.2	Optical micrographs showing the effects of Cu and Mg on Si morphology in the grain-refined and heat-treated (a) M5 alloy; and (b) M6 alloy.	103
Figure 4.3	(a) Backscattered image, and (b) optical micrograph of the α -Fe phase observed in Sr-modified and grain-refined M1 alloy.	106
Figure 4.4	(a) Backscattered image, and (b) optical micrograph of sludge particles observed in Sr-modified and grain-refined M3 alloy.	107
Figure 4.5	(a) Backscattered image, and (b) optical micrograph of β -Fe and α -Fe observed in Sr-modified and grain-refined M4 alloy. Arrows indicate the effects of heat-treatment and Sr on the fragmentation of β -Fe.	108
Figure 4.6	Optical micrograph of (a) heat-treated Mg-free M9 alloy, and (b) heat-treated M6 alloy containing 0.6% Mg showing precipitation of both the blocklike Al_2Cu phase (marked A) and the $Al_5Si_6Cu_2Mg_8$ phase (marked B).	111
Figure 4.7	Effects of Fe-intermetallics on the machinability of M1, M3, and M4	

	alloys in terms of (a) mean total drilling force; (b) mean total drilling moment; and (c) mean power cutting required for drilling 90 holes.	121
Figure 4.8	(a) Photograph of drill illustrating area investigated; and (b) photograph showing the effect of sludge on the cutting drill edge after drilling the M3 alloy.	121
Figure 4.9	Effects of Fe-intermetallics on the machinability of M1, M3, and M4 alloys in terms of (a) mean total tapping force; and (b) mean total tapping moment required for tapping 90 holes.	122
Figure 4.10	Effects of Fe-intermetallics on the drill/tap life of the M1, M3, and M4 alloys in terms of the number of holes drilled and tapped.	126
Figure 4.11	Optical microstructure of the M4 alloy showing precipitation of (1) pre-eutectic β -Fe, and (2) post-eutectic β -Fe.	126
Figure 4.12	Effects of Cu, Mg, and Sr additions on the machinability of M1, M5, M6, M0, and M9 alloys in terms of (a) mean total drilling force; (b) mean total drilling moment; and (c) mean power cutting required for drilling 90 holes.	134
Figure 4.13	Comparison of tool life of M0, M1, M5, M6, and M9 alloys containing additions of different alloying elements in terms of the number of holes drilled and tapped.	134
Figure 4.14	Effects of Cu, Mg, and Sr additions on the machinability of M1, M5, M6, M0, and M9 alloys in terms of (a) mean total tapping force; and (b) mean total tapping moment required for tapping 90 holes.	135
Figure 4.15	Microstructure of the M6 alloy showing the influence of both Sr and Mg: (1) segregation of the Al_2Cu phase; (2) formation of thick plates of $Al_5Si_6Cu_2Mg_8$ phase; and (3) acicular silicon particles.	138
Figure 4.16	(a) Cross-section of drilled hole illustrating area investigated; and (b) optical microstructure of M6 alloy corresponding to the drill breakage portion showing the presence of large silicon particles, marked 1, and the coarse undissolved Cu-phase, marked 2, in this area.	138
Figure 4.17	SEM micrograph and EDX analysis showing the precipitation of hardening phases (a) Mg-containing M1 alloy; and (b) Mg-free M9 alloy (T6-heat treated conditions).....	143
Figure 4.18	Microstructure beneath the fracture surface of the non-modified M0 alloy. White arrows indicate broken acicular Si particles.	144
Figure 4.19	Photographs showing the progress of built-up edge (BUE) on the tip of the cutting edge (a) after drilling 90 holes, and (b) after drilling 2070 holes.	147
Figure 4.20	Photographs showing the effects of Cu- and Mg-addition produced in the heat build-up formation and the wear on the cutting-drill lip in M1, M6, and M9 alloys after different stages of drilling.	149

Figure 4.21	Photographs showing wear mode on cutting edge after drilling the M1 alloy.	149
Figure 4.22	Photographs showing the wear mode on the tap edge (a) new tap; (b) BUE on the relief face of the tap chamfer part; (c) material adhering to the first thread of tap; (d) broken tap in the workpiece; (e) photograph of tap illustrating area investigated.	151
Figure 4.23	A photograph showing the broken taps (a) new tap; (b) broken tap after tapping the M6 alloy; and (c) broken tap after tapping the M1 alloy.	152
Figure 4.24	Optical micrographs showing different types of chip obtained for M1, M6, M9, and A356.2 alloys after drilling the specified number of holes.	155
Figure 4.25	Effects of Cu and Mg on chip breakability in terms of the chips-per-gram criterion for the alloys investigated.	155

CHAPTER 5

Figure 5.1	Optical micrograph showing the effects of Sn, Bi, and Pb additions on the microstructure of heat-treated 396 alloys in (a) the M1 base alloy; (b) the M2 (M1 + 0.15% Sn); (c) the M7 (M1 + 0.5% Bi); and (d) the M8(M1 + 0.8% Pb).	163
Figure 5.2	(a) High magnification backscattered image of the M2 alloy showing precipitation of β -Sn, (b) X-ray image of Sn distribution for the same particles illustrated in (a).	166
Figure 5.3	EDX spectrum corresponding to β -Sn particles observed in M2 alloy containing 0.15% Sn.	166
Figure 5.4	Low magnification backscattered image obtained from the M7 (M1 + 0.5% Bi) alloy showing precipitation of Bi-containing particles.	167
Figure 5.5	(a) Backscattered image of the M7 (M1 + 0.5% Bi) alloy showing morphology of Bi-containing particles, X-ray image of (b) Bi and (c) Mg distribution for the same particles illustrated in (a).	167
Figure 5.6	(a) Backscattered image of the M8 (M1 + 0.8% Pb) alloy showing the precipitation of Pb-containing particles, (b) EDX spectrum corresponding to Pb-containing particles.	168
Figure 5.7	(a) Low magnification backscattered image obtained from the M12 (B319.2 + 0.15% Sn + 0.5% Bi) alloy showing the presence of Bi and Sn particles (bright white particles).	169
Figure 5.8	Effects of adding Sn, Bi, and Pb on the machinability of 396 (M1, M2, M7, and M8) alloys in terms of (a) mean total drilling force; (b) mean total drilling moment; and (c) mean cutting power required for drilling 90 holes.	177
Figure 5.9	Effects of adding Sn, Bi, and Pb on the drill/tap life of the M1, M2, M7, and M8 alloys in terms of the number of holes drilled and tapped.	177

Figure 5.10	(a) High magnification backscattered image showing molten Sn particles in the M2 (M1 + 0.15% Sn) alloy after machining processes, (b) X-ray image of Sn distribution for the same particles illustrated in (a).	178
Figure 5.11	Backscattered images of the M7 alloy showing the precipitation of Bi-particles and the corresponding X-ray images of Bi, Mg, and Sr.	182
Figure 5.12	Photographs after Bi addition showing wear occurring on (a) outer corner and (b) cutting drill lip of the M7 alloy after stripping the BUE in a solution of NaOH..	182
Figure 5.13	Effects of Sn, Bi, and Pb additions on the machinability of 396 (M1, M2, M7, and M8) alloys in terms of (a) mean total tapping force; and (b) mean total tapping moment required for tapping 90 holes.	183
Figure 5.14	Effects of Sn and/or Bi additions on the machinability of B319.2 (M10, M11 and M12) alloys in terms of (a) mean total drilling force; and (b) mean total drilling moment required for drilling 100 holes.	187
Figure 5.15	Effects of Sn and/or Bi additions on the machinability of B319.2 (M10, M11 and M12) alloys in terms of (a) mean total tapping force; and (b) mean total tapping moment required for tapping 100 holes.	188
Figure 5.16	Photographs showing the effects of Sn, Bi and Pb addition occurring in the heat build-up formation and the wear on the cutting drill lip in 396 (M1, M2, M7, M8) alloys after different stages of drilling.	192
Figure 5.17	Optical micrographs showing different types of chip obtained for M1, M2, M7, and M8 alloys after drilling the specified number of holes out of 1080 holes.	193
Figure 5.18	Effects of Sn, Bi, and Pb on chip breakability in terms of the chips-per-gram criterion for the alloys investigated.	194

LIST TABLES

CHAPTER 3

Table 3.1	Chemical composition of the 396, B319.2, and A356.2 base alloys.	66
Table 3.2	Nominal composition and codes for the alloys prepared in this study. ...	67
Table 3.3	Average chemical composition of the alloys discussed in this study.	70
Table 3.4	Schematic representation of the carbide drill and HSS tap, together with the terms used in describing their geometry.	80
Table 3.5	Cutting parameters applied for machinability testing.	81

CHAPTER 4

Table 4.1	Summary of eutectic Si-particle measurements for the alloys studied. ...	100
Table 4.2	Volume fraction of Fe- and Cu-intermetallics for the alloys studied.	110
Table 4.3	Summary of mechanical properties for the alloys studied.	113
Table 4.4	Effects of Fe-intermetallics on width of built-up edge (BUE) during drilling process.	147

CHAPTER 5

Table 5.1	Summary of the eutectic Si-particle measurements for the alloys studied.	161
Table 5.2	Summary of mechanical properties for the alloys studied.	171
Table 5.3	Effects of Sn, Bi, and Pb additions on the width of built-up edge (BUE).	190

CHAPTER 1

DEFINING THE PROBLEM

CHAPTER 1

DEFINING THE PROBLEM

1.1 INTRODUCTION

The need for bridging the divide between the casting process and the machining process provides a strong motivation for examining the various aspects affecting the machinability of Al-Si casting alloys, given that these alloys constitute more than 80% of all aluminum alloy castings. The reason for this widespread acceptance of Al-Si alloys may be found in the attractive combination of a number of parameters which include (i) physical properties; (ii) generally excellent castability; (iii) mechanical properties; (iv) corrosion resistance; (v) machinability; (vi) hot-tear resistance; (vii) fluidity; and (viii) weldability. These are, thus, the factors which have led the automobile, aerospace, defense, and engineering industries to make full use of Al-Si alloys. Machinability plays an important role in the selection of material for commercial exploitation. In general, more than 90% of manufactured parts need to be machined before they are ready for use. Machining is a manufacturing process by which unwanted material is removed to obtain the desired shape of a cast part. Reducing the machining time and extending cutting tool life both have great economic significance. Machinability is an interaction phenomenon between work piece (material type and form), cutting tool (material type and geometry), and cutting medium such as air and liquid in a

number of different removal sequences which include turning, drilling, tapping, milling, sawing, and cutting conditions (speed, feed, and depth of cut). The condition and physical properties of the work material have a direct influence on the machinability of the workpiece. Operating conditions, tool material and geometry, and workpiece requirements all exert an indirect influence on machinability and can often be used to overcome difficult conditions presented by the work material. On the other hand, they can also create situations which compound difficulty of machining if they are ignored. Machinability testing aims at evaluating the comparative machining performance of workpiece materials, cutting tools, and cutting fluids. This type of testing also aims at establishing conditions which will ultimately produce satisfactory finished parts with the desired dimensional surface finish and functional integrity in an economical fashion. The machinability of a particular material can be evaluated by assessing any one of the following five parameters:

- Tool life: the amount of material which may be removed before the tool either fails or wears out to a prescribed degree.
- Surface finish of test piece: the surface finish obtained under constant cutting conditions.
- Cutting force requirements: either the forces acting on the cutting tool or the required power consumption to obtain a given material-removal rate.
- Chip shape: the ease with which the chips can be evacuated from the area around the tool.
- Limiting rate of metal removal: the rate at which a material can be removed while maintaining a prescribed tool life.

When problems occur in industry, questions always arise as to the relationship between the microstructure and the machinability of the given alloys and to the way in which engineers can design and control the casting process to obtain a cast structure which will provide improved mechanical properties and machinability. These production problems are often attributed, wrongly or rightly, to difficulties relating to microstructure and casting. Adequate studies of the influence of microstructure on machinability, however, are relatively scarce to date. A thorough understanding of all the metallurgical factors affecting the machinability of aluminum alloys will contribute to selecting metallurgical designs which attempt to promote the optimum machining combinations essential to sustained productivity.

The principal salient metallurgical factors which govern the condition of the work material and which can influence the outcome of machinability are the following: (i) alloying elements, (ii) features of the microstructure, (iii) porosity, (iv) casting methods, (v) heat treatment, (vi) grain refining and modification, and (vii) the physical properties of the work material. Silicon and other hard phases act as abrasives in the relatively soft alloy matrices and tend to reduce cutting tool life. Copper and magnesium have been observed to increase alloy hardness, to improve the finish of machined surfaces, and to decrease the tendency of an alloy towards build-up on the cutting tool edge. Certain elements are known to enhance the wet machinability of aluminum and steel; these elements are referred to as free-machining elements and include bismuth (Bi), tin (Sn), lead (Pb), and cadmium (Cd). Sand castings require a greater amount of machining stock and have a coarser microstructure than either permanent mold castings or die castings and are, therefore, more

costly to machine, with die castings having been recorded as the least costly to machine. Treatment applied with the intention of refining primary silicon or modifying the morphology of eutectic silicon will improve tool life substantially. Heat treatment, applied to increase hardness, reduces the incidence of built-up edge on the cutting tool and improves the surface finish of the machined part. Porosity may lead to problems particularly in those workpiece areas where holes are to be drilled or tapped. Excess porosity resulting from improper gating, venting, and/or injection may result in poor machining characteristics. These conditions, individually or in combination, can influence and control the machinability of the alloy directly. Machinability problems during the machining of Al alloys are related either to tool wear, or to the quality of the machined surface, to chip disposal or to the presence of burrs, all of which appear to be specific problems restricting productivity.

Among the various Al alloys, aluminum-silicon alloys are said to be the most difficult to machine, as is evidenced by the fact that the silicon phase present is almost ten times harder than the base alloy, thus causing the cutting tools to wear out rapidly. For this reason, attempts have been made to optimize the selection of cemented carbide tools, cutting conditions, and tool geometry; the further investigation of the following points was also promoted: (i) the effects of flank build-up on tool wear, (ii) the effects of cutting fluids on machinability, and (iii) the improvement of machinability through the addition of certain elements. In order to understand the metallurgical factors affecting alloy machinability, a prior study was carried out investigating the possible effects that the addition of certain alloying elements would have on the microstructural characteristics and mechanical

properties of 396 near-eutectic alloy, B319.2, and A356.2 alloys. These alloying elements included Fe (0.5% to 1%), Mn (0.5% to 1%), Cu (2.25% to 3.25%), and Mg (0.3% to 0.5%), while the free-cutting elements included Pb, Sn, Bi, Zn, and In. Based on this study, certain alloys were selected for a further examination of the corresponding machinability characteristics since they constitute the focus of the current work.

1.2 OBJECTIVES

This study is part of a larger research project which was conducted to provide a better understanding of the effects that Fe-intermetallics, free cutting elements, matrix-hardening elements, and Sr-modification would have on the machinability characteristics of cast Al-Si near-eutectic alloys. The study was confined to a new experimental alloy belonging to this family, and which contains about 10.8% Si, namely the 396 alloy. Thus, drilling and tapping operations were carried out using a Makino A88E machine under fixed machining conditions of speed, feed, length of cut (depth of the hole drilled or tapped), tool geometry, tool material, and coolant as applied to the examination of the alloys under discussion. It should be mentioned here that the pertinent machinability criteria relate to force and moment as well as to tool life, chip configuration, and built-up edge (BUE) evolution. In keeping with these aims, the objectives of this study will cover the following:

1. specific T6 heat treatments selected to establish the hardness level for the alloys studied within the range of 110 ± 10 BHN;
2. effects of iron intermetallics (α -Fe, β -Fe, and sludge), and hardening alloying elements such as Cu (2.25 and 3.5%) and Mg (0.3 and 0.6%) intermetallics on the machining of modified and grain refined 396-T6 alloys;

3. effects of Sr-modification and the presence of a Mg-free alloy on the machinability behavior of heat-treated and grain refined Al-10%Si experimental alloys;
4. effects of free-cutting elements, such as Sn, Bi, and Pb on tool life, chip shape, and cutting force and moment of the 396-T6 alloys;
5. effects of the free-cutting elements, Sn, Bi, and Sn + Bi in the machining of modified and grain-refined B319.2-T6 alloys;

A thorough understanding of the role of all these factors in the alloys studied would make it possible to select materials and workpiece designs for obtaining optimum machining combinations critical to maximum productivity.

CHAPTER 2

REVIEW OF THE LITERATURE

CHAPTER 2

REVIEW OF THE LITERATURE

2.1 INTRODUCTION

Aluminum-silicon alloys, especially near-eutectic alloys containing ~11% Si, are widely used in the automotive industry because of their excellent foundry characteristics and mechanical properties. These alloys have, therefore, replaced iron and steel in many components, including transmission cases and intake manifolds, as well as in more critical components such as engine blocks, cylinder heads, and wheels;¹ this extended application of Al-Si alloys for automotive components has created the need for a more in-depth understanding of the effects of microstructure on the machinability of these components. The microstructure of Al-Si alloys is typically composed of an aluminum matrix containing eutectic silicon; the silicon can be present in the form of acicular needles, blocklike plates, or a refined fibrous structure, depending upon the level of chemical modification and the cooling rate of the cast section. In general, eutectic silicon is not uniformly distributed, but tends to be concentrated at the interdendritic boundaries.² These microstructural constituents also include Fe-intermetallics which commonly precipitate in the form of α - $\text{Al}_{15}(\text{Fe},\text{Mn})_3\text{Si}$ and β - Al_5FeSi phases, secondary eutectic phases such as Mg_2Si and Al_2Cu , and other complex intermetallics constituted from the remaining liquid during the final stages of solidification.³

2.2 IMPORTANT ISSUES IN METAL-CUTTING OPERATIONS

During the cutting process, the cutting tool comes into contact with the workpiece material and removes part of it. The main study areas in material cutting may be summarized into the following three groups:⁴

- (i) Aspects of the cutting tool involving the geometry of tool design. The properties of the cutting tool materials, tool failure mechanisms, and predicted tool life.
- (ii) The properties of the workpiece material including mechanical behaviour; the physical, chemical, and microstructural features; and the thermal properties.
- (iii) Operating parameters such as cutting speed, feed rate, and depth of cut.

The interaction between these three aspects of machining determines the efficiency of a given metal-cutting process. For example, in cutting a specific workpiece, as soon as the cutting tool is chosen, the operating parameter predetermines the rate of material removal, the ultimate quality of the machined surface, and the duration of tool life. If a different tool should be chosen, *e.g.* to obtain a different rake angle, the rate of material removal may not necessarily change, whereas tool life and the quality of the machined surface may do so. The reason for this is because the material behavior changes as a result of the changes brought about in the cutting stress distribution and the plastic strain distribution ensuing from prior changes in the geometry of the cutting tool.

The three most important machining parameters which determine the rate of metal removal are the cutting speed, the feed rate, and the depth-of-cut. Optimizing these three parameters results in minimizing the possibilities of tool failure, and thereby prolonging tool life. Tool life is influenced mainly by cutting speed, then by the feed rate, and to a

lesser degree, by the depth-of-cut.⁵ Experiments have shown that when the length-of-cut is about ten times greater than the feed rate, a further increase in this parameter will have no significant effect on tool life.⁶ In practice, the first step is to select the depth based on the tool, workpiece, power, and the rigidity of the equipment. Since depth-of-cut has the least influence on tool life, it is advisable to use the deepest cutting depth possible. The second step is to select the feed rate, in that it depends on the specification of the final machined surface. Under normal circumstances, the smaller the feed rate, the better the quality of the finish. Cutting speed also has a strong potential influence on tool life.

The mechanical properties of either tool materials or workpiece materials may change significantly with variations in the cutting speed. Higher cutting speeds can contribute to increasing the removal rate of unwanted material, but the effects on tool life will vary noticeably with the cutting conditions. The reason for this has been recognized as the rise in temperature at the contact area between the cutting tool and the workpiece. Increasing the feed rate also causes the temperature to rise, thereby increasing the contact stress and the plastic deformation of the workpiece material in the chip formation area.⁷

2.3 MACHINING OF ALUMINUM ALLOYS

Aluminum alloys are among the most machinable of the common metals. Compared to that of steel, the machinability of aluminum alloys features considerably lower cutting forces and substantially higher cutting speeds for which comparable tool-life values may be obtained. The economically optimal cutting-speed range for machining aluminum alloys has its lowest limits set by the occurrence of built-up edge material and the resulting rapid deterioration of surface quality. Aluminum alloys are thus usually machined by applying

cutting speeds of not less than 90 m/min.⁸ A higher cutting-speed limit for machining aluminum, however, cannot be defined exactly since such a limit would depend on tool wear or tool life, or the occurrence of deceptive chip formation; it should be noted that this limit may also vary in accordance with the alloy composition and the cutting parameters involved. When machining aluminum alloys, even though the specific cutting force is only about one fourth that of steel, the machining capacity required for economical machining is three times as high, since high cutting speeds may need to be applied.⁹

It may be said for aluminum alloys, in general, that their high thermal conductivity facilitates rapid heat dissipation from the locus of chip formation and that it also lessens the thermal load on the cutting-edge of the tool. The relatively low strength of these alloys, accompanied by low shear modulus, makes it possible for the emergence of a low penetration resistance of the material to the tool and leads to a considerably lower energy requirement than is, as a rule, necessary for machining ferrous materials.¹⁰ When they are cut under proper conditions using sharp tools, aluminum alloys acquire a fine finish through turning, drilling, and milling, thereby minimizing the necessity for further protracted grinding and polishing operations.

Aluminum is commonly machined by means of high-speed steel, diamond, and carbide tooling; cutting tools based on silicon-nitride ceramics are generally not used with aluminum because of the recognized high solubility of silicon in aluminum.¹¹ The major machinability assets related to aluminum alloys include tool life, chip characteristics, chip disposal, and surface finish. Standard twist drills are generally reasonably satisfactory for the drilling of aluminum alloys, although high spiral drills with a helix angle of 40-48°,

instead of the usual 24-28°, are recommended for deep holes. The point angle may also be increased to good advantage from the normal value of 118° to 130-140°. This procedure produces a narrower chip which is then more easily expelled through the flutes of the drill. Evacuation of the chips and how to stop them from welding to the drill flutes are two of the main problems arising at this juncture; thus, in this regard, ensuring an adequate supply of coolant is of paramount importance.¹²

2.4 EFFECTS OF METALLURGICAL FACTORS ON MACHINABILITY OF Al-Si ALLOYS

Three metallurgical factors have a major influence on machinability: these are the alloying elements, the features of the microstructure, and the selected heat treatment.

2.4.1 Alloying Elements

When pure aluminum is used unalloyed, it tends to adhere to the tool causing built-up edge to form, thus producing long chips which are too ductile to break. The addition of certain alloying elements improves machinability by reducing adherence to the tool and causing the chips to become more brittle. Constituents which are present in solid solution, such as copper, silicon, magnesium, and zinc, tend to increase the hardness of the aluminum matrix, thereby reducing not only metal pick-up from tools, but also burr formation, and the tearing of metal surfaces; whereas out-of-solution constituents promote the break-up of chips when combined with aluminum. In the cases where constituents such as Al_2Cu , $FeAl_3$, and Mg_2Si are not noticeably hard, machinability is observed to improve; on the other hand, rapid tool-wear occurs if constituents such as silicon or phases formed by boron, chromium, manganese, and titanium are extremely hard.^{13,14}

2.4.1.1 Role of Si and Melt Treatment in Al-Si Alloys

Silicon, which is the major alloying element in Al-Si alloys, improves the fluidity of the metal during casting by increasing the volume of the aluminum-silicon eutectic; this heightened level of fluidity makes it possible for molten metal to flow readily and easily into the thinnest sections of the mold.¹⁵ Additionally, this ease of flow helps to minimize shrinkage during solidification. In the solidified alloy, silicon tends to increase the strength values; improvements in the wear resistance can also occur when the silicon levels are in the moderate-to-high range. Increasing the amount of silicon, however, tends to decrease the ductility in cast aluminum alloys. The Al-Si binary system forms a simple eutectic at approximately 577°C with 12.5wt% Si. In general, alloys such as the 356 and 319 alloys containing less than 11wt% Si are referred to as hypoeutectic alloys, whereas those containing 11-12wt% Si are known as eutectic alloys, and those containing more than 12% are called hypereutectic alloys.¹⁶ The phase diagram also shows that the maximum solubility of 1.65% Si in Al occurs at 577 °C, this solubility then drop to a negligible level upon reaching room temperature.

Silicon (Si), either in its eutectic or primary form, is much harder than any other phase of the alloy microstructure. The Knoop hardness number of silicon crystals generally ranges from 1000 to 1300KHN, while the micro-hardness for an alloy matrix of an aluminum casting rarely exceeds 180KHN. Silicon is similar to iron, manganese, and chromium, in that its intermetallic impurity phases are noticeably abrasive in an otherwise soft matrix, and is thus the element which has the greatest tendency to decrease cutting tool life.¹⁷ A fine, well-modified eutectic silicon structure is far less detrimental to tool life than

heavy-element intermetallic impurity phases. The rate of wear on cutting tools increases, however, as the particle size of the silicon increases. If the eutectic silicon structure is coarse, tool life suffers.

Primary silicon crystals, even if well-refined and distributed, can be more detrimental than eutectic silicon; thus large unrefined primary crystals are likely to be devastating to tool life. Whether in permanent mold casting or sand casting, primary silicon is controlled by a refinement treatment which recommends adding a small amount of strontium to the molten alloy. Unrefined primary silicon particles are 8 to 10 times the size of refined silicon crystals, and they are likely to affect machinability to a significant degree.¹⁸ In conventional die casting, no supplemental refinement treatment is considered necessary. Primary silicon size in these die castings is small, even in the absence of phosphorus refinement, and its size and distribution are controlled by process parameters such as melt temperature, die temperature, and die-fill rate. Regardless of the casting method employed, primary silicon acts as a chip-breaker; although primary silicon crystals are extremely hard, they are also relatively brittle. When the cutting tool passes through the alloy matrix, it fractures the primary silicon particles. This fracturing, together with the natural hardness of the alloy and the work-hardening of the chips, causes the close tightly-curved chips to break into short ringlets with an appearance similar to that of grey iron chips.¹⁹

Tests carried out at the Alcoa Research Laboratories²⁰ demonstrated the effects of silicon particle size on the rate of tool-wear. In these tests, the silicon content was maintained constant at about 6wt% and the size variation was produced by means of different melting, casting, and thermal treatments. It was found that this wear rate is apt to

increase by a power of 1.7 of the silicon particle diameter, and that tool life decreases in machining Al-Si casting alloys as the silicon level of the alloy increases. This effect is relatively small, except when the silicon content exceeds about 12wt%. The amount of silicon in the alloy has a minor effect on the surface finish, and the same can be said for the size of the silicon particles. The size of the chips, the degree of burring, and the possible machining rate are also affected, although only moderately, by the amount and the size of the silicon constituent.

The effects of grain refinement, modification, and heat-treatment on the machinability of eutectic and hypereutectic Al-Si cast alloys were studied by Dwivedi *et al.*¹³ They concluded that the melt treatment, as applied to the alloys under examination, reduced the cutting force and cutting temperature because of the refining of hard brittle silicon particles, although heat treatment is known to increase both cutting force and cutting temperature; the same effect may be attributed to an increase in the hardness and strength of both alloys after heat treatment. Similar research results were also reported by Basavakumar *et al.*²¹ who studied the influence of melt treatments and turning inserts on the cutting force and surface integrity of turning in Al-12Si and Al-12Si-3Cu cast alloys. These researchers found that the addition of a grain refiner to the alloys mentioned, combined with a modifier, produces a conspicuously low level of cutting forces and creates an improved surface finish, compared to untreated alloys.

2.4.1.2 Role of Fe Intermetallics in Al-Si Alloys

Iron (Fe) combines with other elements to form a variety of intermetallic compounds depending on the composition of the alloys; although iron intermetallics improve strength and hardness, they tend to reduce ductility. Iron also tends to make the material brittle, and consequently it improves machinability in terms of the cutting force.²² Jorstad^{14,23} found that intermetallic phases which are formed out of heavy elements such as iron are liable to lead to a substantial reduction in tool life, although they have a negligible effect on tool-edge build-up. A number of Fe-rich intermetallic phases, including α $\text{Al}_{15}(\text{Fe},\text{Mn})_3\text{Si}_2$, β (Al_5FeSi) , π $(\text{Al}_8\text{Mg}_3\text{FeSi}_6)$, and δ $(\text{Al}_4\text{FeSi}_2)$, have been identified in Al-Si casting alloys.^{24,25} Depending on the temperature as well as on the chemical composition of the mix, among other factors, Fe may precipitate as an intermetallic compound displaying different morphologies, the most common being polyhedral crystals, “Chinese script,” and thin platelets which appear needlelike in two-dimensional optical micrographs.²⁶

In near-eutectic alloys with iron concentrations of between 0.5 and 1.2 wt%, primary crystals of Al_5FeSi (β -Fe) may appear under normal melt and casting conditions.²⁷ These crystals are needle-shaped and, as occurs with eutectic silicon needles, they may cause the mechanical properties of the alloy to deteriorate, in particular its ductility and toughness. Furthermore, these long iron-rich needles form during solidification and are usually associated with the shrinkage voids present in the solidified material.²⁸ Voids can cause problems to occur, particularly in those workpiece areas where holes are to be drilled or tapped. The length of these intermetallic β -AlFeSi phase platelets may be reduced by

decreasing the iron content of the alloy and/or by increasing the cooling rate. Since the $\text{Al}_{15}(\text{Fe},\text{Mn},\text{Cr})_3\text{Si}_2$ (α -Fe) phase is dendritic, it is therefore not so detrimental from the viewpoint of the machinability characteristics of the alloy, given that its Chinese-script morphology diminishes the shrinkage effect resulting from the concentration of stresses.²⁹ Although α -Fe compound is not formed under normal casting conditions, it may be stabilized by means of the addition of certain elements, such as Mn, Cr, or Co, which substitute for iron in the crystalline structure of the intermetallic compound. The most adequate Fe-to-Mn ratio for stabilizing the α -AlFeSi phase is 2:1;³⁰ iron, manganese, and chromium tend to segregate towards the bottom of aluminum melting and holding furnaces, thereby forming solid particles of α -phase ($\text{Al}_{15}(\text{Fe},\text{Mn},\text{Cr})_3\text{Si}_2$). This phase is denser than molten aluminum and forms solid particles of *sludge*. The tendency of a molten alloy to form sludge can be predicted by the holding temperature and its *sludge factor* ($\text{SF} = 1\% \text{Fe} + 2\% \text{Mn} + 3\% \text{Cr}$).³¹ This factor is an empirical formula applied to Al-Si-Cu alloys and is used to determine how much Fe, Mn, and Cr can cause sludge to form; it also serves as a rough guide to help to avoid sludging.

The sludge factor is useful for predicting susceptibility to sludge formation, although metal temperature and the agitation of the molten metal also influence this susceptibility to some extent. At higher holding temperatures, or with an agitated bath as occurs in induction furnaces, a sludge factor of 1.8 will normally result in sludge formation if a casting temperature of 650°C or more is maintained; despite this, for lower holding temperatures, a sludge factor of 1.4 or less may have to be applied. For alloys 319 and 413, the critical sludge factor is estimated at 2.1.³² The high Fe-content and low holding

temperature of the die casting alloy can cause furnace sludging to become an outright inconvenience. On other hand, the holding temperatures for sand and permanent-mold castings are too high for any appreciable sludging to occur, in view of the fact that the iron-rich phase remains in solution.³³ Sludge presents high hardness values, a high melting point, and a high specific gravity when compared to the matrix; thus sludging produces such deleterious effects as hard spot inclusions in casting, ultimately resulting in damage to the cutting tools during machining. In addition, this phenomenon restricts metal flow during casting and is detrimental to the mechanical properties.³⁴

2.4.1.3 Role of Cu and Mg in Al-Si Alloys

Based on the Al-Si system, the main alloying elements are copper (Cu) and magnesium (Mg). The addition of Cu to near-eutectic Al-Si alloys leads to a slight increase in alloy fluidity and to a depression in the Si eutectic temperature of $\sim 1.8^\circ\text{C}$ for every 1wt% Cu added. It has been observed that, at $\sim 548^\circ\text{C}$, the amount of Cu in solid solution in Al is about 5.7 wt%. This value decreases with decreasing temperatures, reaching 0.1-0.2 wt% at 250°C .³⁵ Copper forms an intermetallic phase with Al which precipitates during solidification either as blocklike Al_2Cu or in its eutectic form of Al- Al_2Cu .³⁶ In general, copper increases the strength and hardness of the aluminum alloy and improves the elevated temperature properties, all of which is accomplished through heat-treating, where the development of the Al_2Cu precipitate occurs; the final properties are dependent upon the precipitate developed.³⁷ Any excess copper, beyond the solid solubility limit in aluminum, forms large blocklike particles of the Al_2Cu intermetallic phase.

When Mg is present, the Cu-Mg intermetallic phase $\text{Al}_5\text{Mg}_8\text{Cu}_2\text{Si}_6$ precipitates during

a complex eutectic reaction which takes place in the final stages of solidification, and which reduces the eutectic temperature related to Cu-containing phases.³⁸ The addition of Mg is seen to result in an increase in the volume fraction of Cu-containing phases, with a tendency to segregate towards areas away from the eutectic Si regions, leading to the formation of the blocklike phase rather than that of the fine eutectic-like Al_2Cu . This segregation makes it more difficult to dissolve the Al_2Cu phase during solution heat treatment.³⁹ Addition of Mg to Al-Si alloys increases strength and reduces ductility; also, Mg has a negative effect on Sr-modification, in other words, it alters the microstructure, causing it to change from being well-modified to only partially modified.³⁵

Strontium (Sr) is thus commonly added to Al-Si casting alloys only in very small amounts to modify the eutectic silicon morphology from a coarser, flakelike form to a fine fibrous one. The change in the morphology of the Si, in turn, enhances the mechanical properties, particularly ductility. It has been observed, however, that the presence of Sr also leads to the segregation of the copper phase towards areas away from the Al-Si eutectic regions during the solidification process, thereby resulting in a slowing down of its dissolution during solution heat treatment. Also, due to this segregation, the Al_2Cu phase tends to precipitate in the blocklike form rather than in the fine eutectic form. The addition of strontium thus leads to an increase in the amount of the blocklike type of the Al_2Cu observed in the structure.⁴⁰

It should be mentioned here that an extensive number of articles have been published which deal with the formation of the as-cast microstructure^{2,35,36,41,42} as well as with the effects of solution heat treatment^{1,37,38,39,40} and aging^{43,44,45,46} on the microstructure and

mechanical behaviour of Al-Si-Cu-Mg alloys. Only a few studies so far, however, have dealt with the influence of Cu and Mg addition on the machinability of near-eutectic Al-10.8% Si cast alloys. Yamada and Tanaka⁴⁷ reported that when aluminum casting alloys contain both 1% Cu and 0.5% Mg, the finished surface in the turning process is considerably improved, and there is only a slight effect apparent with regard to tool wear and the cutting force. This improvement in the finished surface may be attributed to a significant increase in the hardness of the matrix. Such an increase in matrix hardness of up to about 80 BHN is effective in improving the finished surface of the alloys studied, since the shear angle increases noticeably with the increase in matrix hardness.

Jorstad^{14, 23} found that, in aluminum alloys containing copper and silicon, a small magnesium addition of about 0.3 wt% caused a significant increase in the material work-hardening ability and drastically reduced the tendency towards built-up edge formation on the cutting tool; Mg hardens the alloy matrix and by doing so reduces the friction between tool and work piece, resulting in shorter and tighter chips, as well as providing a better surface finish. Magnesium hardens the alloy, but does not increase abrasiveness since, in small amounts, it does not contribute to the formation of hard intermetallic phases.

Tash *et al.*¹⁸ investigated the effects of metallurgical parameters on the drilling performance of heat-treated Al-alloys containing different proportions of Mg and Cu. They showed that a small amount of Mg added to 319 alloys, about 0.1 wt%, improves alloy machinability and reduces the cutting force and moment, thereby allowing for a high number of holes to be drilled and tapped. The addition of Mg to 319 type alloys transforms a large proportion of the β -Fe platelets into the compact α -Fe script phase which is less

harmful to machinability.

Tests performed at Alcoa Research Laboratories²⁰ have demonstrated that copper in Al-Si alloys affords a smoother surface finish, smaller and more tightly coiled chips, and a reduced burring tendency, attributable largely to the strengthening aspect provided by this element. Tool-wear is not greatly influenced by copper content in Al-Si alloys, although this parameter can increase by as much as 50% in the presence of substantial quantities of undissolved Al-Cu and/or Al-Cu-Mg phases.

Tanaka and Hanasaki⁴⁸ studied the effects of the addition of Cu (0.3%-2.0%) and Mg (0.01%-2.0%) on the machinability of hypereutectic Al-Si alloys in relation to tool wear, roughness of the machined surface, cutting forces, and chip formation. Their results reveal that surface finish is significantly improved by adding about 0.5% Cu or 0.3 to 0.6% Mg to hypereutectic Al-Si alloys. When a sharp cutting tool is used, the addition of Cu and/or Mg hardly affects the cutting forces at all, although, as the tool grows blunt after greater cutting distances, the cutting forces increase as either Cu or Mg are added; the type of chips formed when hypereutectic Al-Si alloys are machined are known as the broken type, whereas additions of Cu and Mg refine the size of the chips. Chip-breakability increases in alloys with Al₂Cu or Si, and this tendency appears more conspicuous in wet cutting than in dry cutting. The increase in chip-breakability is a result of the fracture of second-phase particles during machining, according to Kamiya and Yakou.⁴⁹ A similar investigation was carried out by Grum and Kisin¹⁹ but this time with regard to the relationship between the microstructure of the alloy and the roughness of the machined surface. Increasing the size of the soft, aluminum-based grains produced an increase in the cutting force and in the

roughness of the machined surface. For good surface quality, therefore, it is important that the particles of the hard phase be extremely fine and uniformly distributed within the soft, aluminum-based phase.

2.4.1.4 Role of Free-Cutting Elements in Al-Si Alloys

One of the approaches suitable for improving machinability is the use of free-cutting alloys; these were developed from standard heat-treatable alloys to which elements have been added to form additional phases in the aluminum matrix. These phases improve the machinability of any given material because they provide a smooth surface, cause less tool wear, and produce chips which are more easily breakable.^{50,51} Free-cutting constituents tend to form in the presence of alloying elements and display the following properties: (i) they are insoluble in both liquid and solid aluminum, (ii) they have a low melting point with regard to aluminum, (iii) they do not form intermetallic compounds with aluminum or other alloying elements, and (iv) they have lower hardness values compared to the aluminum matrix. These conditions may be fulfilled by using lead (Pb), bismuth (Bi), tin (Sn), cadmium (Cd), indium (In), antimony (Sb), and a number of other elements which are, however, unusable from a practical point of view.⁵² These lubricity-imparting additives are not entirely soluble in the solidified Al-rich matrix phase of the castings, although they may combine with such alloying constituents as magnesium, and so forth. These additives are thus dispersed as small globular bodies in the cast metallurgical microstructure. The globules do not adversely affect the strength or hardness of the casting but enable it to be machined without the need for a cooling and lubricating machining fluid.⁵³ The minimum required amount of free-cutting additives depends on the casting composition and its

microstructure, as well as on the selected additive itself and the stringency of the machining operations involved. Preferably, the total addition of one or more of these soft lubricity-imparting elements should not exceed about 2 wt% of the casting in such a way as not to alter the other properties of the same casting to any significant degree. According to the inventor Young, bismuth and/or tin are the additives preferred by most researchers.⁵⁴ It should be remembered that if the amount of the additive is not high enough, the low melting point constituents will be too dispersed to have any significant impact on machinability.⁵⁵

In the early years of research into aluminum alloys, Sn was one of the first elements which was added to aluminum alloys in proportions of up to 2 wt%. At that time, its wider use was not accepted into practice because of a supposed worsening of corrosion properties, lower alloy ductility, and the high price. The lower strength values of the alloys containing added Sn resulted from the distribution of fine soft particles of β -Sn, mainly at the grain boundaries, as well as from the formation of other intermetallic compounds such as Mg_2Sn .⁵² When referring to the Al-Sn phase diagram,¹⁶ it will be observed that Al and Sn display mutual solid insolubility, with the maximum solubility of Sn in Al being about 0.1 wt% at approximately 627°C. This solubility then decreases, reaching a probable value of 0.05 to 0.07% Sn at the eutectic temperature, or considerably less at a lower temperature. The eutectic point occurs between 228°C and 229°C at 99.5% Sn, which is close to the melting point of tin.

Over the last few years, a tendency has emerged favoring the replacement of lead with other elements because of its harmfulness to living organisms, as well as for related

environmental reasons. Tin, and indium to a certain extent, are used most frequently as substitutes. With regard to as-cast billets of AlCuMgSn alloys containing only Sn for improving machinability, Smolej *et al.*⁵⁶ demonstrated that tin, together with phases based on aluminum and copper, formed nets enveloping the crystal grains of the matrix, although tin was not found in the crystal grains themselves. The size and distribution of free-cutting constituents in the matrix are important factors in the machinability of alloys. Tin constituents were observed to be smaller and more densely distributed compared to the free-cutting constituents in AlCu₅PbBi.

Zaima⁵⁷ reported that cutting efficiency improved in the Al-13%Si alloys containing 0.2~0.4%Sn; thus, the cutting resistance decreased, the cutting temperature dropped, and the progress of tool wear slowed down. The improvement in machined surfaces was not clearly defined, although the treatment of chips became easier because their shape had changed to a sheared form. On the other hand, in Al-23%Si alloys containing the same level of tin, *i.e.* about 0.2–0.4%Sn, the improvement in machinability was negligible. Neither the decrease in cutting force nor the drop in cutting temperature was at all obvious. The effects of the addition of tin on tool wear and machined surfaces were also not distinct. The chip shape of the original alloy was likely to be a sheared form, and the alloy containing tin produced finer chips of a similar shape.

Bismuth (Bi) is a brittle type of heavy metal of a silvery white appearance. It was once usually added to improve the machinability of free-cutting steels and aluminum.^{58, 59} Additions of bismuth produce continuous self-lubricity, and they also provide low friction and resistance to high seizure loads.^{60,61} According to the Al-Bi phase diagram,⁶² Al and Bi

dissolve completely into each other at temperatures above 1037°C thus forming a homogeneous melt. Below this temperature, however, there exists a miscibility gap in the liquid state. An Al-rich melt coexists with a Bi-rich melt which has the higher density. At 657°C, the Al-rich melt decomposes into a solid Al and Bi-rich melt, *i.e* it produces a monotectic reaction at 3.4 wt% Bi, whereas at 237°C, the Bi-rich melt itself solidifies. It should also be noted that the solubility of bismuth is less than 0.24 wt% at the monotectic temperature, whereas the limit of its solubility in aluminum at the eutectic temperature is assumed to be almost nil.

Bismuth appears to have significant potential as a nontoxic alternative to Pb for enhancing the machinability of Al alloys because of the similarity of features between lead and bismuth, *e.g.* a low solubility in aluminum alloys and a low melting point. It was assumed that an increase in the number of bismuth particles, which in fact also implies a decrease in the mean spacing of these particles, could be considered more effective in producing fine chips than would be an increase in the bismuth content. The reduction in mean spacing of Bi particles is achieved through a refinement in the α -Al grains of the matrix attributed to the high wettability of bismuth at the grain boundaries.^{63,64} Based on an examination of a cutting chip and a cut surface of the material containing bismuth, Tetsuya and Tetsuro⁶⁵ reported that the existence of molten bismuth seemed to play an important part in fracturing cutting chips of this particular material. Consequently, it was deduced that this type of distribution has a noticeable effect on the machinability of Al alloys.

Bismuth, a highly reactive element, reacts not only with Sr, Na, and Ca which

themselves contribute to the modification of the Si-phase, but also with Ni and Mg which were originally added to increase the strength of the alloy, so that the effectiveness of these elements ultimately decreases, as do the mechanical properties of the alloy.⁶⁶ Cho and Loper⁶⁷ demonstrated that bismuth in Al-Si alloys interacts with major modifiers, such as sodium and strontium. He postulated that the formation of a ternary Bi-Mg-Sr compound ($\text{Bi}_2\text{Mg}_2\text{Sr}$) and/or binary Bi-Sr compounds (Bi_3Sr , BiSr , Bi_2Sr_3 , and BiSr_2) would occur as a result. The Bi-phase, however, does not form an intermetallic compound with Al because it is independently distributed. Thus, the Bi-phase is not uniformly distributed throughout the Al-Si alloy structure and it also has a tendency to segregate thereby forming a coarse phase.⁶⁸

Antimony is responsible for the modification of the Si-phase, although it does not react with the highly reactive Bi. The addition of Sb to the eutectic Al-Si alloys containing Bi leads to modification of the Si-phase as well as to reduced segregation and coarseness of the Bi-phase; the function of Bi may thus be fulfilled to the maximum extent. Consequently, since Bi has a relatively high specific gravity (9.8 g/cm^3) and a low melting point (271°C), it is uniformly distributed in the Al-based matrix which has a relatively low specific gravity (2.7 g/cm^3) and a high melting point (660°C). There is thus a reduction in seizure behavior through heterogeneous distribution and segregation of the Bi-phase occurring in the matrix leading to an improvement in the mechanical properties of the alloy.^{69,70} Improvements in machinability by means of the addition of bismuth may be obtained either through the softening of the bismuth particles as a result of an increase in cutting temperature or by void formation due to a deformation mismatch between bismuth

and the aluminum matrix during machining. It is also possible that a combination of both these processes is at play during machining which ultimately gives rise to improvements in machinability.^{71,72}

Lead (Pb) was used for the purposes of this study because it has already been recognized as a free-machining element. It is considered that the addition of Pb to aluminum alloys is the most appropriate method for improving machinability; and although the process of adding Pb to 2xxx and 6xxx series alloys was already fairly well advanced, recent work has, however, involved replacing Pb in free-machining wrought alloys with more environmentally-friendly additives such as Sn or Bi based on new ecologically-oriented criteria.^{73,74} In fact, Pb has been found to be either equivalent to, or even more effective than, tin as a soft phase alloying addition made to aluminum and its alloys. Some unfavorable factors, however, such as the wide miscibility gap, large range of solidification, and high disparity in the densities of aluminum and Pb cause practical problems in the preparation of Pb-containing alloys with a uniform distribution of lead.^{75,76}

It should be mentioned here that most of the work carried out to date on free-machining aluminum alloys has involved wrought alloys. Only a few studies have dealt with cast alloys, thus producing conflicting results. Jorstad^{14, 23} added Pb, Sn, or Bi to A380 alloy as lubricating elements, but observed that no beneficial effect accrued in the form of decreased friction or attenuated tool wear. Alabi^{77,78} successfully added Bi or Bi-Sn to an Al-Si alloy used for air-conditioning components, not for machinability reasons, but to reduce friction in the component. Consequently, in view of the above, the purpose of this study is to examine near-eutectic Al-Si cast alloys containing ~11% Si, namely the 396

alloys, as a basis for understanding the role of the three free-machining elements, Pb, Bi, and Sn, when included in more complex systems for use in industrial applications.

2.4.2 Microstructural Features

In the 1960s, researchers first showed the possibility of obtaining a high-quality machined surface and surface layer by examining all the aspects of this problem, including the microstructure and measurement of the microhardness and residual stresses. Studies of the surface quality resulting from a machining process applied to aluminum alloys confirmed that the type of microstructure, *i.e.* the size of the individual grains, was of decisive importance.^{79, 80}

The effects of systematic variation of the microstructure in the workpiece materials reveals that this aspect has a dominant influence on chip formation in high speed machining either for continuous or for interrupted cutting. Continuous or segmented chip-formation is determined by the microstructural properties of the workpiece material, whereas machining parameters such as cutting speed and feed-per-tooth only determine the degree of segmentation.⁸¹ Schulz *et al.*⁸² reported that a transition from continuous to segmented chip-formation was yet to be observed for any precipitating sequence up to cutting speeds of 8000m/min. It is assumed that the different mechanisms of interaction between dislocations and precipitates are at the origin of the differences observed in chip-formation. The initiation of localised shear bands during chip-formation in the underaged microstructure is thought to be a consequence of local work-softening caused by shearing of coherent precipitates through dislocations. In contrast, the incoherent precipitates of the overaged state make it possible for the redistribution of slip bands, leading to homogeneous

plastic deformation and thereby to the development of continuous chips. During the fine-turning of alloys displaying similar mechanical properties, differences will appear in the roughness of the machined surface and in the magnitude of the cutting forces measured, all of which can be attributed to the influence of the microstructure of the workpiece according to Grum and Kisin.³

Dwivedi⁸³ studied the influence of a grain refiner (Al-5Ti-1B), a modifier (Sr), and an artificial aging treatment on surface roughness in the machining of cast Al-4%Si, Al-11%Si, and Al-17%Si alloys with and without magnesium. According to him, the grain refinement of hypoeutectic alloys, the grain refinement and modification of eutectic alloys, and the refinement of silicon particles in hypereutectic Al-Si alloys improve surface finish significantly under similar machining conditions. Heat treatment, however, adversely affects the surface roughness after machining, especially that of hypoeutectic and eutectic alloys compared to hypereutectic alloys.

When machining cast aluminum silicon alloys, the secondary dendrite arm spacing (SDAS) is the most important metallurgical factor affecting tool life. The larger the magnitude of the SDAS is, the lower its ultimate tensile strength and percentage of elongation will be. The abrasive resistance of the aluminum silicon alloys increases with increased SDAS magnitudes, however, because the perimeter length of the silicon particles increases with such SDASs. The SDAS is governed by the cooling rate of the aluminum alloy during the casting stage, when slower cooling rates generate larger SDAS magnitude values.⁸⁴ Szablewski *et al.*⁸⁵ clearly outlined the effects of SDAS on tool wear for uncoated carbide and PCD tool materials when machining W319 aluminum alloys at high cutting

speeds. When the SDAS was between 22-23 μm , the average silicon particle perimeter was $\sim 20 \pm 5 \mu\text{m}$; for SDASs of between 55-66 μm , however, the average silicon particle perimeter length increased to $\sim 80 \pm 10 \mu\text{m}$. Silicon particle size comes into play during the chip-formation stage of the cutting process; with reduced perimeter length, the particles will flow together and unite with the aluminum matrix. Thus the likelihood of the silicon particles coming into contact with the rake or clearance faces of the tool is attenuated. When the silicon particle perimeter length is greater than the cutting edge radius, however, the probability of the cutting edge being exposed to silicon particles during the shearing process increases. When large silicon particles are sheared in contact with the cutting edge, some sharp particle fragments will flow past the rake face while others will flow towards the clearance face. The fracturing of hard silicon particles thus has a major effect on increasing tool wear rate. It is clear then that more resistant tool materials need to be employed in order to reduce the tool wear rate when machining alloys with a larger SDAS.

Porosity is one of the defects normally present in Al-Si cast alloys. The formation of porosity is always considered to be a function of alloy composition, melt hydrogen level, and such foundry processing parameters as cooling rate, modification, alloying elements, grain refinement, inclusions, and so forth. Porosity is detrimental to the mechanical properties of the casting, particularly to ductility, fracture toughness, fatigue life, and in some cases, to the surface finish of the casting itself.

2.4.3 Heat Treatment

The role of heat treatment in the machinability of some of the more common alloys has been reported to a satisfactory degree in the literature.^{86,87} Heat treatment, which

increases hardness, will reduce the built-up-edge on the cutting tool and improve the surface finish of the machined part. For a specific cutting speed, tool life may be adversely affected by any increase in workpiece hardness, since the cutting loads and temperatures increase with the increasing hardness of the material. In drilling and turning, any increase in the cutting temperature is detrimental to tool life since it produces excessive accelerated heat-causing wear-out of the edge. In milling, the increased hardness values of the material produces higher impact loads when the inserts enter the cut, often resulting in the premature breakdown of the cutting edge.⁸⁸ Typical automotive machining techniques, however, usually require a minimum of workpiece hardness in order to avoid potential complications associated with built-up edge (BUE) on the cutting tool. Most automotive machine shops agree that a minimum hardness of 80BHN is desirable.^{14, 23} In fact, it is for this reason that 319-alloy intake manifolds are often aged to the T5 temper, and that 356 alloy manifolds usually require full heat treatment to the T6 temper.^{89,90,91}

Aging treatments are used to precipitate out the alloying elements which were originally placed and kept in solid solution by the solutionizing and quenching processes. By controlling the aging time and temperature, a wide variety of mechanical properties may be obtained; tensile strengths can be increased, residual stresses can be reduced, and the microstructure can also be stabilized. The precipitation process may be instigated at room temperature or may be accelerated by artificial aging at temperatures ranging from 90 °C up to 260°C. The basic requirements of the age-hardening of an alloy system are: decreasing solubility with decreasing temperature, and the formation of clusters of solute atoms coherent with the matrix; in other words, there should be an orientation relationship

between the precipitates and the matrix.⁹² The greater part of the increase in tensile properties which accompanies most heat treatments is a result of the formation of non-equilibrium precipitates, such as the θ phase, during the application of the aging treatments. Since the structure and morphology of the precipitates are controlled by the times and temperatures used in the heat-treatment sequences, it is possible for a considerable amount of control to optimize the strength, ductility, and toughness of these alloys. In the precipitation-strengthened alloys, it is possible for more than one phase to be precipitated in the matrix of a predominant phase. To obtain the best results, the precipitate phase should be hard and discontinuous, its particles small and numerous, while the morphology should be rounded rather than sharp-edged. On the other hand, the matrix should be soft and ductile so that if the cracks were to nucleate, it would be much safer for this to take place in the particles than in the matrix.⁸⁰

2.5 MACHINING OPERATIONS

Among the most typically used and widely known machining processes are turning, milling, and drilling. In addition to these machining processes, there are a large number of other cutting operations including sawing, reaming, tapping, planing, broaching, boring, and threading. Drilling and tapping operations were carried out using Makino A88E equipment to investigate the alloys under discussion in the present research. In keeping with these aims, drilling and tapping operations will be briefly described in the following sections.

2.5.1 Drilling Process

Drilling is a material removal process which has been widely used in manufacturing since the industrial revolution. It has been reported by several researchers in the field that drilling accounts for nearly 40% of all metal removal operations in the aerospace industry.^{93,94} Recent years have witnessed a noteworthy increase in the complexity and capabilities of metal cutting technology. Simple machine tools have been replaced by flexible and computer-integrated manufacturing systems. Drills and drilling processes have undergone noticeable changes over time; this is especially true for the past fifty years, when many research activities have been devoted to the drilling process. Chip-formation,^{95,96,97} drill geometry design,^{98,99,100} drilling forces,^{101,102} and drilling temperature^{103,104} have all been among the most exclusive topics selected by researchers for investigation. Based on related research findings, a number of drilling processes have been significantly improved and numerous new processes have been developed. Regardless of these achievements, industrial practice continually presents new challenges to the development and improvement of the drilling process.

One of the main challenges is the increasing demand for intensified throughput methods, since, typically, the drilling process is the bottleneck problem for productivity in automotive and aerospace manufacturing. It has been reported by one major automobile manufacturer that fully one-third of the cycle time in its engine plants is spent in carrying out drilling processes.¹⁰⁵ High throughput drilling requires a high-speed spindle machine, a sophisticated tool holder, and a specialized drill. Currently, it is quite common to have a machine with a spindle speed of 10,000-20,000rpm. Machines with a spindle speed of over

40,000rpm may also be found. On the other hand, drill geometry, drill material, and the requirements of the tool holder remain as challenges to be met utilizing the advanced machines to the maximum of their capability.^{105, 106, 107}

A further challenge to drilling process development and improvement is related to the machining coolant; this helps to obtain better process quality in terms of tool life, dimensional accuracy of the parts, surface finish, and chip evacuation. However, it also causes numerous ecological and health problems, and is accompanied by distinct economic drawbacks. The significance of the problem may be assessed by casting a glance at machining coolant consumption statistics, which attain about 750,000 tons in Germany and millions of tons worldwide. Many concerted efforts have been devoted in recent years to eliminating machining coolants and attempting to perform dry machining as an alternative. Not many successful applications have been developed, however, for dry drilling processes, mainly because of the extremely adverse conditions involved in such a process. This problem becomes more challenging when the ratio of hole depth to diameter is greater than three.^{108, 109}

2.5.1.1 Drill Nomenclature and Geometry

The most widely-used type of drill is the twist drill. The nomenclature listed below and illustrated in Figure 2.1 applies specifically to this particular type of tool.¹¹⁰ A drill is an end-cutting tool for producing holes; it has one or more cutting edges, as well as flutes to allow fluids to enter and chips to be ejected. This tool is customarily composed of a shank, a body, and a point; the shank is the part of the drill which is held and driven, being either straight or tapered. Smaller-diameter drills normally have straight shanks, whereas

larger drills have shanks ground to a taper and a tang to ensure accurate alignment and a positive drive. The flutes are grooves which are cut or formed in the body of the drill to allow fluids to reach the point and chips to reach the workpiece surface; although straight flutes are used in some cases, they are normally helical. The land, on the other hand, is the remainder of the outside of the drill body after the flutes are cut; it is cut back somewhat from the outside drill diameter in order to provide clearance. The margin is a short portion of the land which has not been cut away for clearance, thereby preserving the full drill diameter.

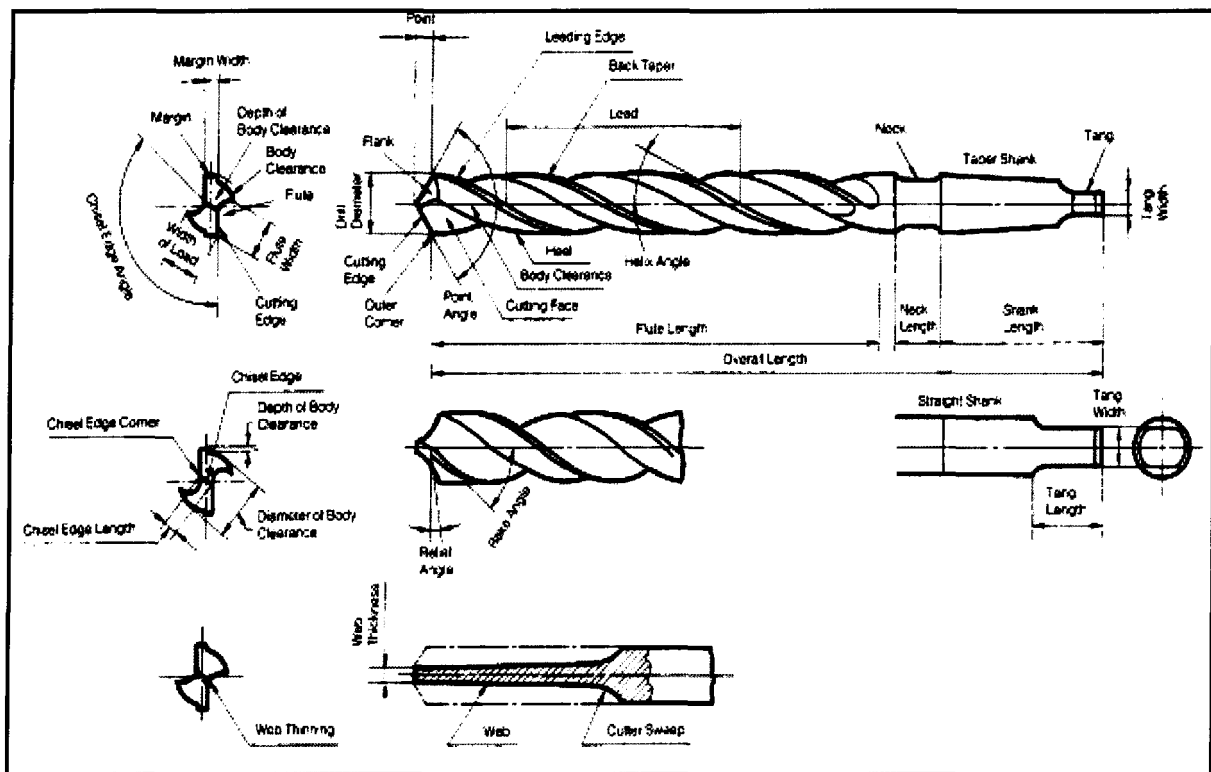


Figure 2.1 Nomenclature of a twist drill.¹¹¹

The web is the central portion of the drill body which subsequently connects the lands. The edge which has been ground on the tool point along the web is called the chisel

edge and connects the cutting lips as the primary cutting edges of the drill extending from the chisel point to the periphery of the drill. The web thickness is the smallest dimension across the web and is measured at the point unless otherwise noted; it will often increase upon going up the body away from the point, and it may have to be ground down during sharpening to reduce the size of the chisel edge in a process called 'web thinning'. The angle which the leading edge of the land makes with the drill axis is called the helix angle; drills having various helix angles are available for different operational requirements. The angle included between the drill lips is called the point angle and may be varied for different workpiece materials. The chisel edge angle is the angle between the lip and the chisel edge, when seen from the end of the drill.

2.5.1.2 Operating Conditions

The varying conditions under which drills are used make it difficult to lay down set rules for speeds and feeds. Drill manufacturers and a number of reference texts provide recommendations for proper speeds and feeds for drilling different types of materials. Drilling speed depends on respecting the following seven variables: (i) the type of material being drilled, for which the harder the material, the slower the cutting speed; (ii) the cutting tool material and diameter; (iii) the types and use of cutting fluids which might make it possible to increase in cutting speed; (iv) the rigidity of the drill press; (v) the rigidity of the drill, concerning which the shorter the drill, the better the outcome; (vi) the rigidity of the work setup; (vii) the quality of the hole to be drilled. Each variable should be considered independently prior to drilling a hole. Each variable, however, is significant in its own right, although the work material and its cutting speed should be considered the most

important factors. When the cutting speed has been selected for a particular workpiece material and condition, the appropriate feed rate must be established in accordance with this. Drilling feed rates are selected to maximize productivity while at the same time maintaining chip control. Feed in drilling operations is expressed in inches-per-revolution, or IPR, which is the distance the drill moves in inches for each revolution of the drill. The feed may also be expressed as the distance traveled by the drill in a single minute, or IPM, inches-per-minute, which is the product of the RPM and IPR of the drill. The undeformed chip width is equivalent to the length of the drill lip, which depends on the point angle as well as on the drill size. For a given set-up, the undeformed chip width is constant in drilling; the feed dimension specified for drilling is the feed-per-revolution of the spindle. A more fundamental quantity is the feed-per-lip, namely, half the feed-per-revolution for the common two-flute drill. The undeformed chip thickness differs from the feed-per-lip depending on the point angle, as shown in Figure 2.2. The width of cut b is given by

$$b = D / (2 \cdot \sin \rho), \text{ where } \rho \text{ is the half point angle of the drill.}$$

The drilling process, with all its complexity, may be attributed to the combined cutting and extrusion of metal at the chisel edge in the center of the drill. The high thrust force caused by the feeding motion first extrudes metal under the chisel edge; it then tends to shear metal under the action of a negative rake angle tool. The cutting action through the lips of the drill is not unlike that which occurs in other machining processes. Due to the variable rake angles and inclination angles, however, there are differences to be observed in the cutting action at different radius locations on the cutting edges.

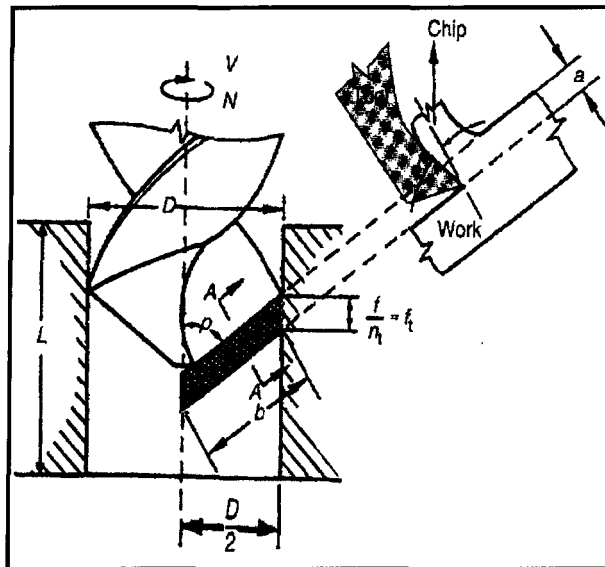


Figure 2.2 Undeformed chip width in the drilling process.¹¹²

Figure 2.3(a) shows the change of rake angle resulting from flute formation; the rake angle displays clear changes from negative to positive when the radius increases. Both lips for the twist drill operate at variable rake angles, inclination angles, and clearance angles along the cutting edge. The spindle speed is constant for any one operation; since the cutting speed varies all along the cutting edge, cutting speed is normally computed for the outside diameter. At the center of the chisel edge, the cutting speed is zero and at any point on the lip it is proportional to the radius for that point, as shown in Figure 2.3(b). Once the drill engages the workpiece, the contact is continuous until the drill breaks through the bottom of the part or is otherwise withdrawn from the hole.¹¹³

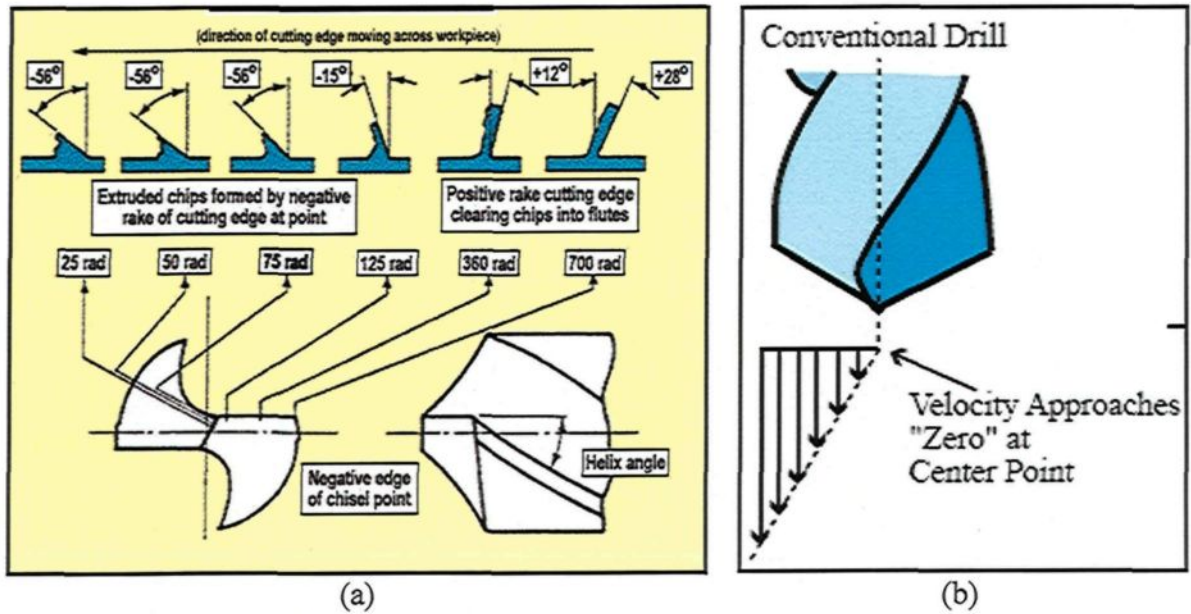


Figure 2.3 (a) Showing rake angle along the cutting edge moving across workpiece, and (b) showing variation in cutting speed with the cutting edges.

2.5.1.3 Dry Drilling of Aluminum Alloys

The machining of aerospace aluminum alloys with conventional tools cannot be carried out without a certain amount of difficulty. These materials tend to adhere to tool surface and burrs are formed inside the holes.¹¹⁴ Tool damage is caused mainly by the formation of an adhesion layer and a built-up-edge (BUE) entailing a reduction in tool life.¹¹⁵ Thus, cutting fluids play an important role in the machining process since they contribute to: (i) the reduction of friction in tool-workpiece contact; (ii) the removal of chips from the tool rake face; (iii) the drop in temperature in the contact zone; and (iv) the limitation of the diffusion of chemical species from the tool towards the chip and vice versa.¹¹⁶ The use of cutting fluids, however, seriously degrades the quality of the environment and increases the costs of machining, thus lubrication represents about 16-20% of the product cost. As a result, dry machining has been widely investigated over the last few years.¹¹⁷

Dry machining, and especially the drilling process itself, is considered to be among the most difficult of machining processes for accomplishing dry cutting in view of the special difficulties it presents such as cutting at close quarters or in a circumscribed space, as well as high cutting temperatures and the difficulty of chip-removal.¹¹⁸ The dry drilling of aluminum cast alloys in the absence of cutting fluids is known to involve a certain degree of difficulty particularly since these alloys display properties which are inimical to dry cutting, including high thermal expansion and low melting points.¹¹⁹ To control dry drilling of aluminum alloys, it is necessary to limit the generation of heat which activates the diffusion of chemical elements between tool and chip, and which facilitates the removal

of chips from the cutting area. The generation of heat depends mainly on tool geometry, the prevailing cutting conditions, and tool-chip friction.¹²⁰ The degree of difficulty in performing dry machining is a function of the cutting process, as well as of the work and tool materials put into use.¹²¹

In order to carry out the range of dry drilling, reaming, tapping, and end-milling operations successfully on aluminum alloys, it is essential to use tools with suitable coating systems and to apply a minimum quantity of lubricant. This is especially true when the L/D ratio, or the ratio of hole depth to diameter, is greater than three.¹²² Cselle¹²³ reported two coatings which were introduced to reduce friction in drilling, reaming, tapping, and milling. These coatings are somewhat similar to *Teflon* in that they adhere well to the tool surface while also providing a gliding or low-friction surface. In the case of both coatings, ultrafine-grain carbide with 10% cobalt was used because of its excellent heat-insulation characteristics. Good success has generally been reported when drilling steel and Al-9%Si using this coating.

Aronson,¹²⁴ Cselle,¹²³ Klocke and Eisenblatter,¹²⁵ Braga *et al.*,¹²⁶ and Heine¹²⁷ all reported on a method called *minimal quantity of lubricant* (MQL) in the development of a dry machining process. In this method, a small amount of the lubricant is delivered to the location of the process by means of either external or through-tool feeding. Since the consumption rate of the lubricant is only in the order of 0.01-0.5ml/min, the tool, the chip, and the workpiece remain dry and disposal costs can be minimized. This method has found a number of successful applications with regard to various materials and processes, as well as in the dry drilling of aluminum alloys. Aronson¹²⁴ reported a case in which 0.1ml of

lubricant per hole is combined with extremely high spindle speeds of 30,000 to 70,000 rpm, and a carbide tool. No detailed information was reported either on the type of coating used or on the type of aluminum alloy being drilled.

Klocke and Eisenblatter¹²⁵ reported on certain experiments conducted on a GD-AlSi₉Cu₃ workpiece with TiAlN+MoS₂ coated drills. The holes were 8.5mm in diameter and were drilled 30mm deep; the cutting speed was 300m/min at 11240rpm with a feed rate of 0.5mm/rev. In dry drilling operations conducted without MQL, the use of drill coating was non-significant because of the adhesion of material in the chip groove after only 16 holes. On the other hand, with MQL, it was found that there was no evidence of any wear or material adhesion to the tool after 128 holes.

Liu *et al.*¹²⁸ clarified the process of chip formation and the motion of chips within the flute in various cutting conditions, including the application of air blow drilling, MQL drilling techniques, and dry drilling. According to these researchers, there emerged a tendency for girdle chips to form in dry drilling as a result of the initial flow direction of the chips; this type of girdle chip then easily caused the chip/flute to clog because of an increase in the chip curl. The chip-removal was observed to be greatly improved in both air blow drilling and MQL drilling. Furthermore, the decrease in the curl size was more noticeable in MQL drilling than in air blow drilling as a result of the lubricant effect of the oil mist. With the progress of drilling, however, the interaction between the chips, the built-up edge formation, and the increase in chip ductility results in unstable chip formation. All the above applications involve either high spindle speed or special coatings, which is normally too expensive for most industrial applications. Discovering a cost-effective way to

carry out the dry drilling of aluminum alloys is thus greatly to be desired, yet it still remains a challenge.

2.5.2 Tapping Operations

Tapping is a machining process for producing internal threads. A tap is a cylindrical or conical thread-cutting tool having threads of a desired form on the periphery. Combining rotary motion with axial motion, the tap cuts or forms the internal thread.¹²⁹ The cutting tap generates the internal thread form as successive cutting edges on the chamfered section of the tap are rotated relative to the workpiece while being fed at a rate-per-revolution equal to the thread lead. Material is removed progressively from the wall of the hole until the final thread form is obtained with the first full thread on the main body of the tap.¹³⁰ The threaded parts are primarily used for force transmissions; the assurance of safety in force transmission depends notably on the quality of the threads, which in turn is dependent upon the nature of the cutting process.^{131,132} The cutting fluid is more important in tapping than it is in most other machining operations because the cutting edges are more susceptible to damage by heat and the chips have more chance of being trapped in the flute. The application of coatings to taps used for high-speed tapping becomes necessary in order to improve their performance in the face of difficulties with cooling, and dealing with a high volume of removal over short periods of time. The use of coatings by themselves, however, does not ensure long tool life when high-speed machining is applied. It is also necessary to obtain good edge geometry and a tough substrate, while the machine tool should be stable with a good fixing mechanism.¹³³

Screw threads have numerous dimensions; it is important in modern manufacturing

to have a working knowledge of screw thread terminology. Thus, a *right-hand thread* is a screw thread which requires right-hand or clockwise rotation to tighten it. A *left-hand thread* is a screw thread which requires left-hand or counter-clockwise rotation to tighten it. *Thread fit* is the range of tightness or looseness between external and internal mating threads. *Thread series* are groups of diameter and pitch combinations which are distinguished from each other by the number of threads-per-inch applied to a specific diameter. The two common thread series used in industry are the coarse and fine series, specifically known as UNC (Unified National Coarse Thread) and UNF (Unified National Fine Thread). Tap nomenclature is shown in Figure 2.4.¹³⁴

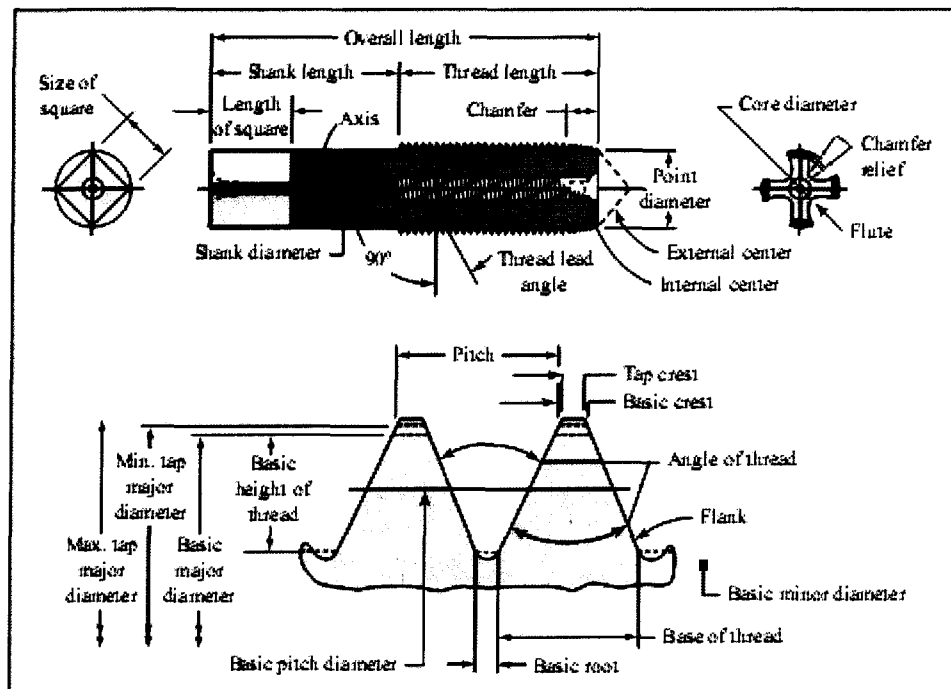


Figure 2.4 Tap and thread nomenclature.¹³⁴

One of the major problems arising in the tapping process is tap-breakage, resulting from excessive torque. Since tapping is often among the final operations performed on a

workpiece, the problem has the potential for being extremely costly. Tap-breakage may either ruin the almost completed workpiece, or else create a large down time reserved for removing the broken tap from the workpiece. Improved knowledge of torque in tapping and its relationship to tapping process faults such as axis misalignment, tap run-out, and poor hole quality is, therefore, critical to reducing the wear/vibration of the tap, and avoiding any breakage, while at the same time selecting productive tapping conditions. Knowledge of torque and thrust characteristics would also be useful in monitoring and control techniques for a computer-based tapping process.¹³⁵

In the context of tapping forces, it has been reported that the chamfer section of the tap generates a major portion of the resulting cutting force, because of a larger chip cross-section related to the teeth of the chamfer, as shown in Figure 2.5(a). Machining with a calibrating section does not contribute significantly to the resulting force since it is friction which affects this phase dominantly. For several practical reasons it is useful to decompose the resulting cutting forces acting on the tap to axial force and torque. The tapping process is also followed by the side force which arises from the unbalanced sum of tangential (F_t) and radial (F_r) forces acting on all the engaged teeth of the tap. During the tapping cycle, cutting forces undergo significant changes; thrust force and torque by full immersion of the chamfer section of the tap are used as representative values for such operations. Dynamic changes in the torque are shown in Figure 2.5(b) for two cases of tapping operations including tapping in a blind hole and in a through-hole. The maximum values which appear in phase B (and which are the same for the axial thrust force) are significant for phases in technology design related to the choice of fixture, tool, and tool holder. Besides applying

maximum values, it is useful to predict the changes in thrust and torque for the whole tapping cycle with regard to the implementation of the automatic monitoring of high volume production.¹³⁶

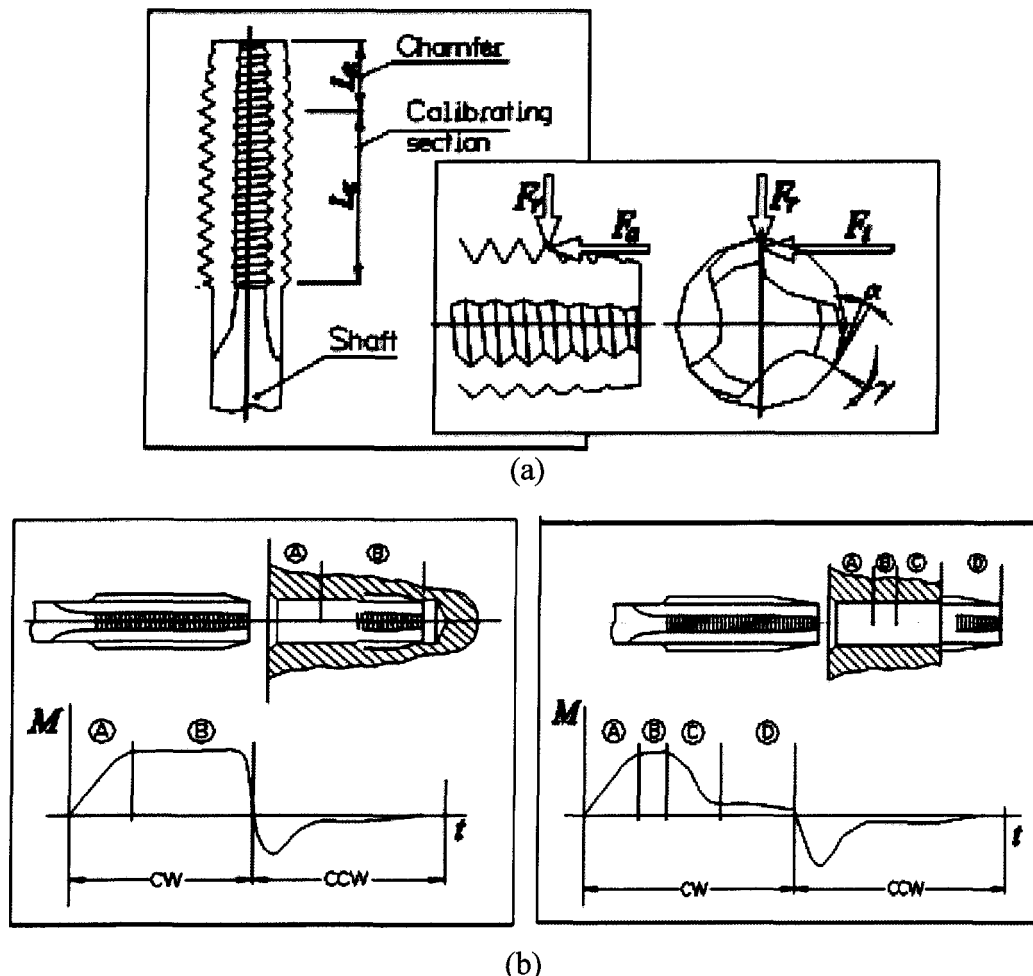


Figure 2.5 (a) Basic elements of tap and forces on an elementary tooth; (b) change in torque during the tapping cycle.¹³⁶

2.6 MACHINABILITY CRITERIA

Machinability may be deemed an interactive phenomenon between work piece (material type and form), cutting tool (material type and geometry), and the cutting medium such as air and liquid, in a number of different removal sequences which include turning,

drilling, tapping, milling, sawing, and cutting conditions (speed, feed, and depth of cut). In a collective sense, the significant terms, as related to the subject of machinability, are (i) specific power consumed, cutting forces, and temperature rise; (ii) tool life, wear level, and fracture probability; (iii) chip control including chip breakability, chip shape, and built-up edge; (iv) dimensional tolerances in terms of surface roughness, microstructure, and burr formation; (v) machining rate; and (vi) overall cost. Some of these parameters are, however, easy to evaluate and interpret and consequently commonly used; tool life and tool wear come under this category together with surface roughness. All effort-related parameters are relatively more difficult to evaluate, but can often provide an explanation for good or bad machinability results. The factors affecting machinability have already been discussed; the four methods used to judge machinability, however, will be dealt with in the following subsections.

2.6.1 Cutting Forces Experienced During Drilling Operations

Mean steady state values of the torque and feed force developed during drilling operations have been the subject of considerable investigation to date. There are three distinct cutting edges in a typical drill: (i) the main cutting edge; (ii) the chisel edge; and (iii) the margin cutting edge. The contribution of the main cutting edge to the thrust force and drilling torque experienced by a drill bit is approximately 40 and 80%, respectively. Experimentally, these values may be found to vary from 25 to 60% for the thrust force, with values greater than 80% for the torque. The chisel edge cutting action may be divided into two separate cutting mechanisms: (i) the outer section which produces a chip, having been modelled using orthogonal cutting theory; and (ii) the centre portion which produces

no chips and has been modelled as an indenter. The chisel edge contributes about 57 and 8% of the total thrust and torque, respectively. The margin cutting edge has not been studied extensively, but its contribution to a sharp drill is believed to be non-significant. The friction between the margin cutting edge and the newly formed hole walls has been reported to be about 12% of the torque while its contribution to the thrust is even less significant.¹³⁷

As manufacturing technology has moved towards the stage of full automation over the years, the monitoring of tool-wear condition has acquired a certain amount of significance in the prevention of tool failure strategies. It has thus now become possible to increase machine utilization and decrease production costs in an automated manufacturing environment. Although tool wear and tool breakage are still unsolved primary problems in the metal cutting process, a considerable amount of research has been reported in the literature.^{138,139} Wear is the loss of material at the cutting lip of the drill bit resulting from the physical interaction between the cutting tool and the workpiece material. Abrasion, adhesion, diffusion, and fatigue are the main mechanisms which cause wear in cutting tools. Tool wear in drilling is a progressive procedure but it continues to occur at an accelerated rate once a drill becomes dull. During this procedure, the cutting forces increase, the temperature of the tool rises, and then drill point deformation occurs followed by the immediate loss of the sharp edges. After a certain limit, tool wear may cause catastrophic and sudden failure of the tool without any warning which causes considerable damage to the workpiece and even, ultimately, to the machine tool. This scenario may be seen illustrated in Figure 2.6 showing a classification of the wear stages as (i) initial wear;

(ii) slight wear (regular stage of wear); (iii) moderate wear (micro-breakage stage of wear); (iv) severe wear (fast wear stage); and (v) worn-out (or tool breakage), all recorded as functions of tool life.¹⁴⁰

Measuring the thrust force (which is the force component in the cutting direction) and torque (which is the moment about the axis of rotation of the tool) is known to be one of the most commonly used techniques for monitoring conditions of tool wear. Thrust force and torque determine the energy required for chip generation; in addition, the effects of tool wear, drilling process parameters, plowing in the drill center chisel edge, chip generation on the major cutting edge, and the deformation of tool-and work-materials may be revealed simply by analyzing the change in thrust force and torque. Also, it is relatively easy to measure cutting forces using dynamometers mounted on a tool holder.¹⁴¹

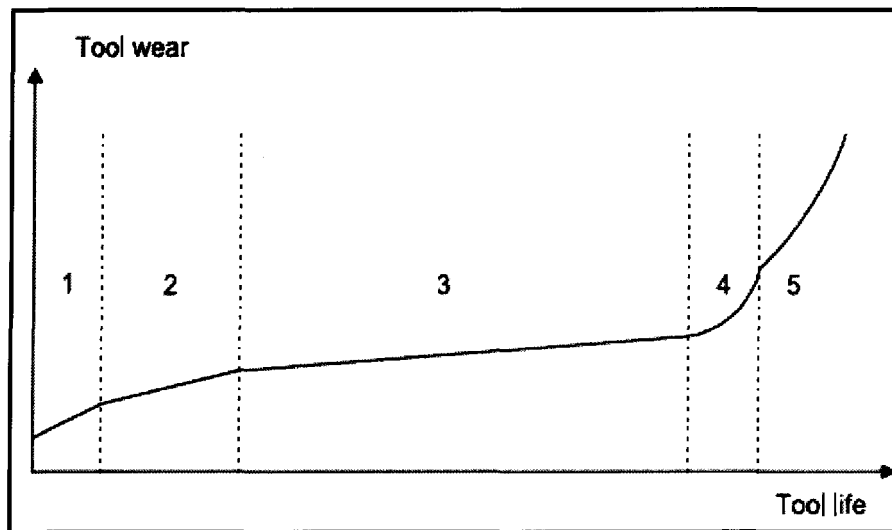


Figure 2.6 Tool wear evolution: 1. initial wear; 2. slight wear; 3. moderate wear; 4. severe wear; and 5. worn-out.¹³⁹

Cutting forces increase as the drill tool wears down and they will further increase suddenly when the tool breaks. For monitoring systems, thrust and torque can be selected

separately as measurement signals.¹⁴² Thrust force is also known to be one of the most useful dynamic parameters in the drilling process. Thangaraj and Wright¹⁴³ used the rate of change in thrust forces to predict drill failure, while Brinksmeier¹⁴⁴ selected torque to predict tool fracture. The major drawback with cutting forces is their dependence on cutting conditions including cutting velocity, feed, and depth of cut. Owing to the complexity of the cutting tool, most research on tool-wear monitoring for drills must be based on an analysis of experimental data. Subramanian and Cook¹⁴⁵ established thrust and torque as a function of workpiece material hardness, average flank wear, drill diameter, feed rate, and radius at the cutting edge. These researchers also found that tool life is strongly affected by workpiece material hardness; they demonstrated that monitoring drill conditions which made use of the thrust force and/or torque was effective only when a close tolerance range was maintained on the workpiece hardness at about 5%.

Bandyopahyay *et al.*,¹⁴⁶ who used dynamic system technology to monitor tool wear, claimed that the increase in force magnitude because of tool wear is non-significant, thus not to be used for tool-wear monitoring; it should be noted, however, that only drills showing relatively little drill wear were used in their tests. Jalali¹⁴⁷ established a tool life model by means of which it has been possible to observe that the thrust force and torque when machining the last hole is 50% greater than when machining the first hole. It was also observed that the cutting forces increase as tool wear increases; this finding was based on the existence of an increase in friction between tool and workpiece which occurs during the cutting process.

2.6.2 Tool Wear and BUE Formation

Tool machining is the radical process of friction and wear; tool wear during cutting not only decreases the service life of cutting tools, but also leads to the increased roughness of the cutting surfaces of a workpiece. Aluminum alloys, especially die-cast aluminum alloys, are widely used for machining work, in which drilling is one of the most important machining methods available for application to these alloys. As more and more automotive or computer-controlled machines are used, manufacturers need to increase the service life of cutting tools in order to increase machining effectiveness and to lower manufacturing costs.¹⁴⁸ Nevertheless, the effects of aluminum workpiece microstructure on tool wear do not appear to have received sufficient attention. In spite of the large amount of data and knowledge which has been accumulated on the subject, tool wear is still not fully understood. Cutting tools wear out mainly because (i) normal loads on the wear surfaces are heavy and also because (ii) the cutting chips and workpiece which apply these loads move rapidly over the wear surface. The cutting action and the friction of the contact surfaces increase the temperature of the tool material, which further expedites the physical and chemical processes associated with tool wear. These forces and motions are necessary for material removal and thus cutting tool wear is an inevitable production problem for manufacturing industries.¹⁴⁹

Two major types of gradual tool wear in metal cutting have been reported, namely, temperature activated diffusive wear or mechanically activated wear in terms of adhesive, abrasive, and/or fatigue mechanisms. The particular type of wear which prevails in a specific machining operation depends on the cutting-tool material, on the workpiece

material being machined, and on the cutting conditions themselves.¹⁵⁰ Several investigations have shown that tool wear is mainly the result of abrasion at low speed conditions. When the cutting speed is increased, the temperature at the tool rake face may increase as a result. This behaviour stems from the intensive deformation associated with large shear strains in the primary shear zone as well as the friction effects occurring along the tool-chip interface.¹⁵¹ Consequently, diffusion is considered to be the dominant wear mechanism for tools at higher cutting speeds. The atoms which are diffused from tool to chip are carried away by the flow of work material along the contact surface. The material transfer towards the chip leads either to the formation of an adhesion layer and a built-up edge or to the formation of a crater on the tool rake face in extreme cutting conditions, ultimately leading to a noticeable reduction in tool life. Thus, the magnitude of the tool-chip interface temperature causes a shift from abrasion to adhesion, or from adhesion to the diffusion-wear process.¹²²

In machining processes, tool life is usually determined by using criteria based on tool-wear. Figure 2.7 shows the intensity of tool wear, δ , as a function of the cutting temperature, T , in relation to different wear mechanisms. As shown in this figure, it will be observed that the adhesion mechanism is the wear mechanism which operates for the widest range of cutting temperatures. Generally, adhesion wear involves the direct transfer of tool particles to the metallic chips; however, tool wear may also occur through the transfer of macroscopic fragments from the workpiece material onto the tool surface. These fragments are mechanically unstable, and can thus be removed from the tool surface by the action of the high strength cutting forces which are thereby produced. In this process, tool

particles are abruptly removed giving rise to tool wear.¹⁵²

The workpiece material adheres to the rake face of the tool in two different and almost simultaneous forms. The first one is the most frequently occurring and involves the formation of built-up-edges (BUE) through the adhesion of workpiece materials to the cutting edge of the tool. In the second case, the material transferred is poured into wider areas on the flute of the drill.¹¹¹

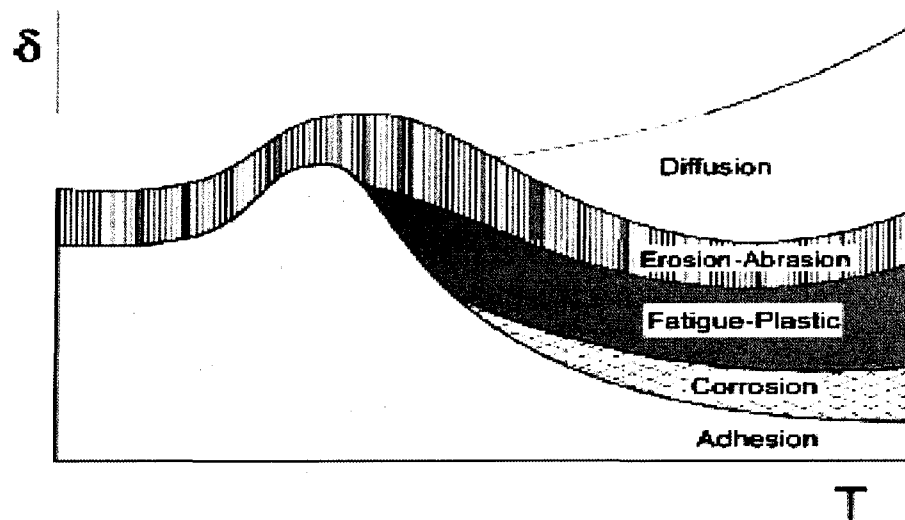


Figure 2.7 Wear mechanisms as a function of temperature.¹⁵²

The matrix hardness of the workpiece has a noticeable effect on the tool-wear failure mechanisms. A softer matrix causes adhesive wear whereas a harder one causes fatigue or abrasive wear. Workpiece materials with significantly different hardness values in their cutting zone tend to cause adhesive wear on the corresponding inserts. In general, tool wear is closely related to the hardness of the workpiece, as well as to the deformability of the matrix around the Si grains, and to the size of pro-eutectic Si phase in the work material itself. When the matrix of the workpiece is hard and resists deformation, the work material is also difficult to deform in the shear zone in front of the cutting edge and on the

tool surface in such a way that the Si grains are secured firmly in position. As a result, the grains have a strongly abrasive action on the tool cutting edge and flank. An increase in the hardness of the matrix results in a greater width of the flank wear.¹⁵³

2.6.3 Tool Life Criteria

A tool life criterion may be defined as a predetermined threshold value of tool wear measurement or the observable occurrence of that same phenomenon. In practical machining operations, the wear of the face and flank of the cutting tool is not uniform along the cutting edges; it is, therefore, necessary to specify the location and the extent of the wear when deciding on the amount of wear allowable before regrinding or disposal of the tool.⁴ Figure 2.8 shows a typical worn down single point tool; as shown in the central portion of the active cutting edge, or zone B, the wear land is usually fairly uniform. In order to allow for variations which may occur, however, the average wear land width in this region is designated VB , and the maximum wear land width is designated VB_{\max} ; among the criteria proposed by the *ISO* for defining the effective tool life for sintered-carbide tools, one or the other of the following criteria is recommended:

$$VB = 0.3 \text{ mm, or } VB_{\max} = 0.6 \text{ mm if the flank is irregularly worn,}$$

$$\text{or } KT = 0.06 + 0.3f, \text{ where } f \text{ is the feed.}$$

Drilling is known as a common machining process. As already mentioned earlier, it has been reported that fully one third of material removal processes performed in the industry relate to drilling operations;¹⁵⁴ these are usually conducted after such pre-processes as turning and milling. The downtime due to drill breakage, therefore, is critical with respect to the economics of machining operations. If a broken drill piece becomes lodged in

the workpiece, the workpiece will have to be reprocessed or otherwise discarded and replaced.

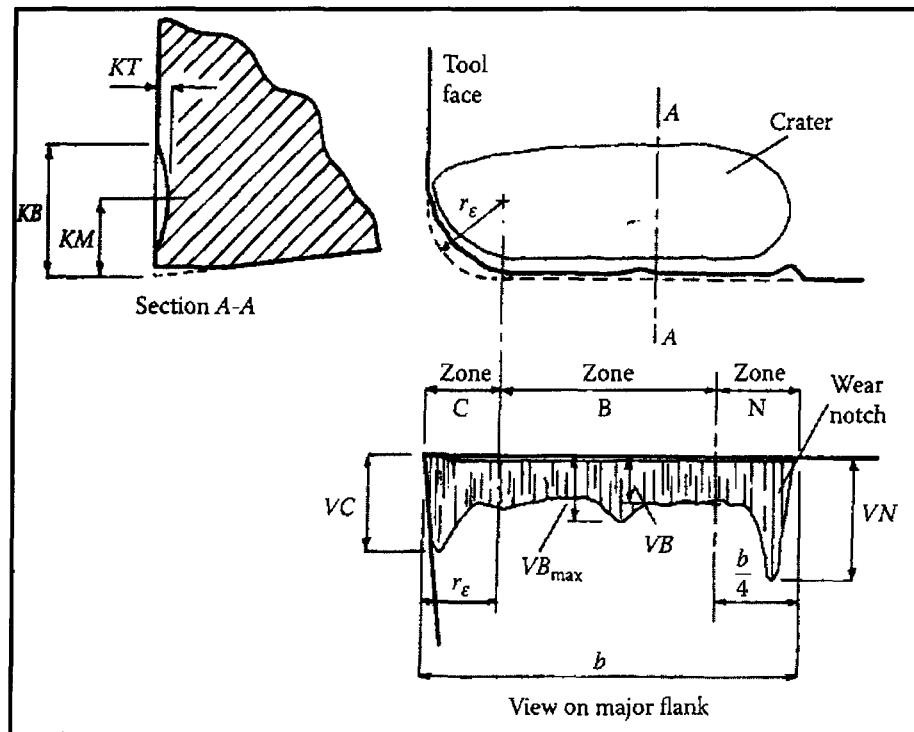


Figure 2.8 Some features of single-point tool wear in turning operations.⁴

Unfortunately, there is no reliable method of predicting drill life, since drill breakage is usually a random process; even drills from the same batch may fail at random. The primary reason for such random drill failure is the presence of inhomogeneities in the workpiece or the drill materials, accompanied by the unavoidable asymmetry induced by the grinding of the cutting edges.¹⁵⁵ Drill performance is traditionally determined by the failure of the drill. In a given drilling operation, the performance criterion should be governed by the drill life, and expressed as the number of holes to failure or the equivalent drilling time. In general, the failure of a twist drill occurs through one of two modes: either fracture or chipping, or excessive wear.¹⁵⁶ Experiments performed by Thangaraj and

Wright¹⁴³ indicate that, under normal cutting conditions, failure as a result of fracture was more commonly observed with small-sized drills *i.e.* $\leq 3\text{mm}$ diameter, while excessive wear was the dominant failure mode with large-sized drills *i.e.* $\geq 3\text{mm}$ diameter. A worn drill generates vibration signals indicative of the drill condition. The vibration can cause the drill to “wander” from its true center, or else these vibrations may result in a tapered or oversized hole. These defects are of particular importance for high speed precision drilling. This process is common in the aircraft industry, such as for the machining of aluminum alloy parts, and in the automobile industry, such as for the machining of cast iron parts.

Drills were easily worn out by friction, heat, and so forth, and they occasionally broke when subjected to severe cutting forces at the lips, which are the main cutting regions and the weakest parts of the drill bit. Cutting tool wear occurs along the cutting edge and the adjacent surfaces. The location and the size of these wear surfaces play an important role in determining the useful life of the cutting tool. There are two main regions of tool wear in a cutting tool, namely, flank wear on the tool flank face and crater wear on the tool rake face. Figure 2.9 shows the characteristic appearance of a worn twist drill. Kanai and Kanda¹⁵⁷ classified the wear on large drills of diameter $\geq 6\text{mm}$ into several types. These types of wear are known as: outer corner wear, flank wear, margin wear, crater wear, and chisel edge wear, as shown in Figure 2.10 together with chipping at the lip. The dominant types of wear which result in drill failure and breakage are called: chisel wear, outer corner wear, flank wear, and margin wear. In practical situations, however, corner wear instead of flank wear or crater wear is used to predict the tool wear in drilling operations.

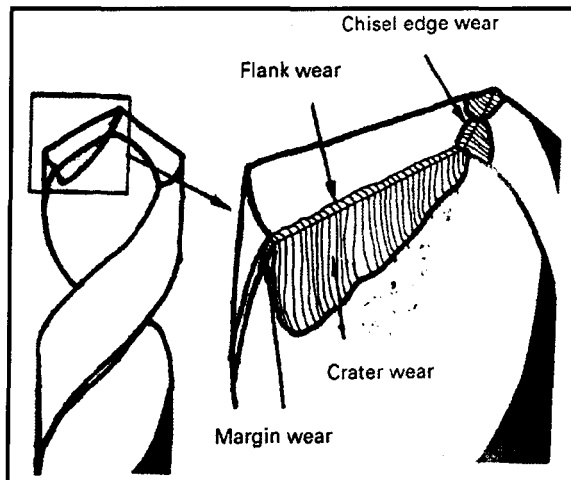


Figure 2.9 Characteristics of worn twist drill.¹⁴⁹

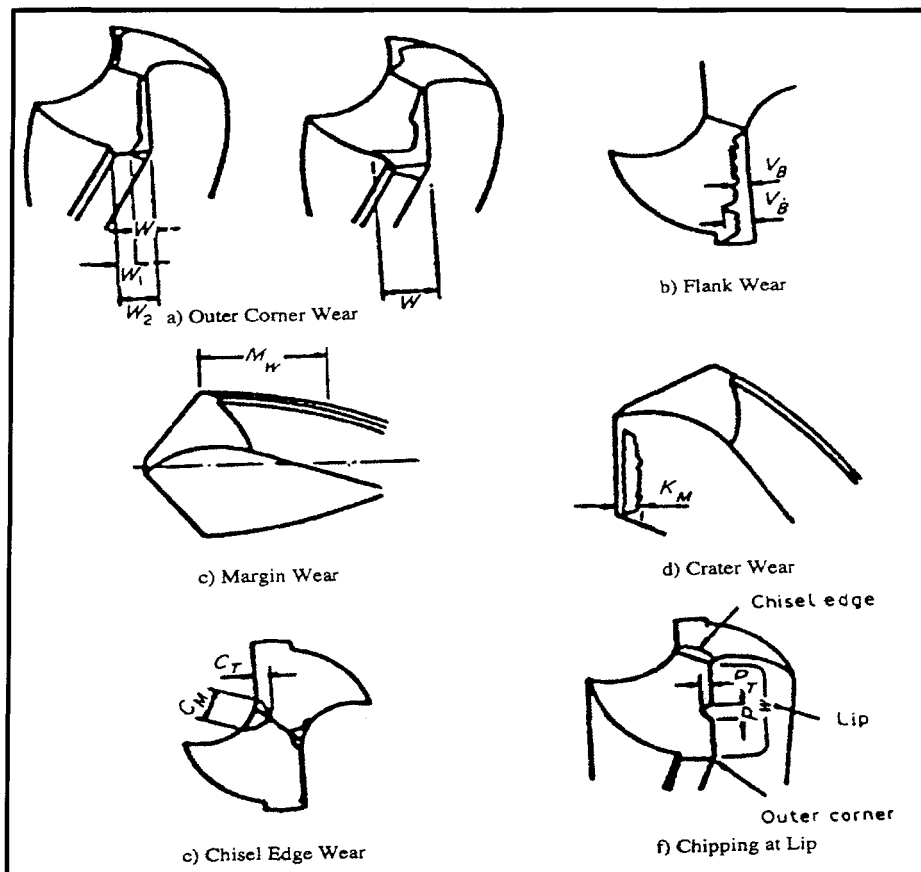


Figure 2.10 Types of drill wear.¹⁵⁷

2.6.4 Chip Formation in Drilling

Small well-broken chips are desirable in drilling operations; the reason for this is that as the chips get larger, they move less easily through the flutes, thereby increasing torque requirements, perhaps causing drill breakage. During formation, the chips rotate with the drill and collide with the hole wall or interior of the flute; this impact produces a bending moment in the chip. The chip will fracture, once the bending moment causes it to exceed a critical strain. There is, thus, a clear need for the parameters of chip size and shape to be studied in detail by the industry as a formal research topic in order to identify the conditions which will ultimately promote better chip evacuation.¹⁵⁸ A punctual examination of the chips being produced upon machining a particular workpiece will provide a considerable amount of information as to how well the job is proceeding, how tool wear is progressing, and why premature tool failure has occurred, or in other words, why a shortened tool life intervenes.¹⁵⁹

Chip-formation and the chip-breaking mechanism has been the subject of studies for a number of years; starting with the *Merchant* chip formation model in 1945, numerous other studies have contributed to the understanding of this area of research.^{3,5,6,8,11} Although the level of understanding has been adequate, the results from previous studies were based on simple cutting tools having the same tool geometry and cutting parameters along the cutting edge. There has been very little research carried out on such complicated cutting tools as drills whose geometry and cutting parameters differ along the cutting edge.¹⁶⁰ To simplify the drill cutting process, the drill cutting edge is conventionally treated as a summation of several small segments with each segment having homogenous geometry and

cutting parameters. There are differences between chip formation in drilling and conventional cutting processes. These differences include the following: (i) chip formation is not completed when chips leave the cutting edge; chips will be further deformed as a result of the interaction of the chips with the drill flute and hole-wall; (ii) chip flow direction is restricted by the cutting speed difference along the cutting edge since the cutting speed is much slower at the point close to the drill center, or inner cutting edge, than it is close to the drill peripheral point, or outer cutting edge, where the initial chips are cone shaped and tend to flow towards the drill center; and (iii) the chip-flute interaction is a combined effect of the drill point geometry in terms of point angle and the drill flute geometry represented by the helix angle. Furthermore, this interaction will alter the chip deformation after it leaves the cutting edge; it may also result in different chip lengths and shapes.¹⁶¹

In one of the few studies carried out on drilling chip formation, Nakayama and Ogawa¹⁶² reported that chip size in the drilling process is governed by its formation geometry at the cutting edge, as well as its thickness, curl, and characteristic length, as determined by the point at which the chip breaks in the generation cycle. Figure 2.11 shows the details of the three components of chip curl by indicating the following points. First is the side-curl, which is the result of velocity differences across the cutting lip since the cutting speed varies proportionally with the distance from the drill center, as shown by ω_z . The second rotation, ω_c , is about the drill axis; it accounts for the twisted, non-planar rake face, and for the increasingly positive rake angle having a radial distance from the drill axis. This term, ω_c , will also reflect the changes in the rake angle caused by built-up-edge

(BUE). The final rotation ω_x is about the cutting edge of the drill; this component is caused by the natural up-curl of the chip because of its strain-hardening properties and the obstruction presented by the web of the drill. Given the three components of angular velocity, ω_c , ω_z , and ω_x , based on Nakayama's analysis, the chip experiences a helical motion with the angular velocity, ω_h , which is the resultant of these three angular velocity components.

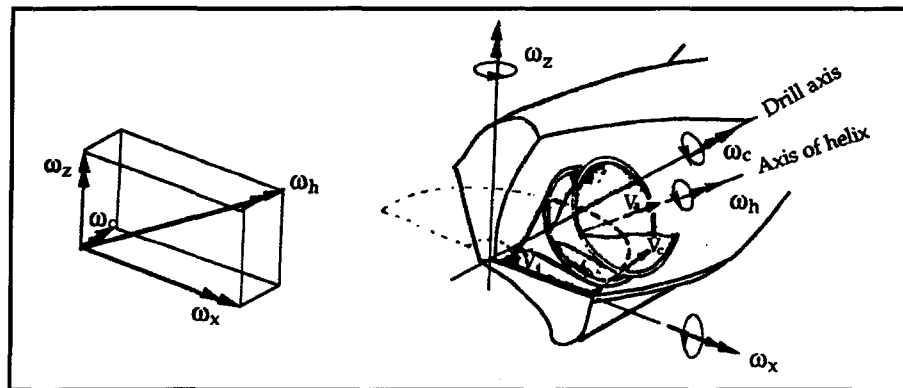


Figure 2.11 Conical helical chip produced by the twisted part of the cutting lip.¹⁶²

Most ductile materials do not break during drilling but form continuous chips instead. Based on the various chip formation mechanisms, continuous chips can be categorized as spiral chips or as string chips. When chips are initially generated, the inner chip is inherently shorter than the outer one because the inner cutting edge moves significantly more slowly than the outer cutting edge. This difference in length within the chip proper forces it to flow towards the drill center instead of perpendicular to the cutting edge. Furthermore, the center part of the drill flute forces the chip to curl and form a spiral shape. When spiral chips move into the drill flute, however, they are constrained to rotate constantly on their own axis in order to maintain a spiral shape, as shown in Figure 2.11.

This rotating motion causes the spiral chips to encounter difficulty maintaining their shape as the hole gets deeper. If the chips cannot keep up with the rotation, they will either break or be forced to move along the flute without spinning and thus to form string chips.⁹⁶

During the transition from spiral chips to string chips, there are a few types of intermittent shapes which emerge, depending on the material, the chip thickness, and the size of the drill. Although initial drill chips are all spiral cones, they will ultimately change into various other shapes upon drilling deeper as a result of the interaction between the drill flute and the hole wall. Batzer *et al.*⁹⁵ studied the effects of cutting conditions on the drilling process in order to acquire a better understanding of chip-formation mechanics; they were able to record the entire range of chip forms as created by drilling experiments, with the exception of dust-like chips, as shown in Figure 2.12. Figure 2.12A shows conical chips; the diameter of the conical chip must be small enough to allow it to move through the flute/hole wall cavity without breaking. Figure 2.12B shows fan-shaped chips; these are formed when conical chips cannot curl sufficiently to follow the flute and fracture prior to a complete revolution. Chisel-edge chips, as shown in Figure 2.12C, form because of the extrusion of metal from the chisel edge. These chips are long and narrow, streaming out of the drill along the interior of the flute at the web. When this chip forms, there is a second chip type also forming at the same time along the cutting edge; these two chips may or may not interact. To eliminate the chisel-edge chip, it may be necessary to decrease the feed and thereby the amount of metal to be extruded. Amorphous chips, which have a somewhat wrinkled, uncurled appearance, are shown in Figure 2.12D. These chips do not have enough consistent curl to assume a fan shape and are guided, unbroken, up the flutes. As is

apparent from their size, they are the heaviest chip form and the least desirable. Needle chips, as may be seen in Figure 2.12E, are caused by a severe up-curling of the chip; there appears to be no clear demarcation between the needlelike, or acicular, and the fan-shaped chips. While these latter are the smallest chip form next to dust-like chips, they are likely to be undesirable. Figure 2.12F does not show any of the primary chip forms, but rather aggregations of smaller chips which have amalgamated while moving up the flute; these are thus heavier than primary chips and tend to take on the shape of the flute. They are undesirable precisely because they clog the flutes, thus to eliminate this type of chip form, it may be necessary to reduce either the feed, or the speed, or both, or to use a drill with a larger flute cavity.

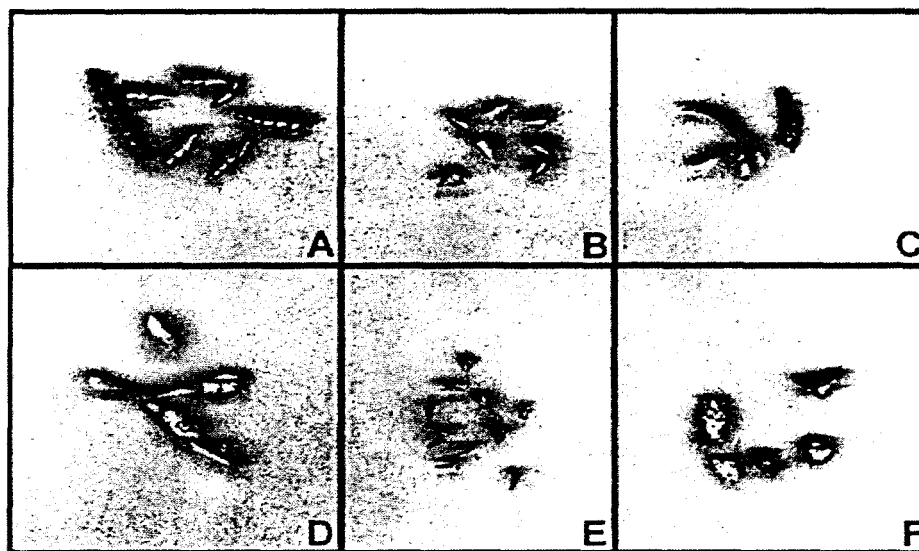


Figure 2:12 Chip forms generated: (A) conical; (B) fan-shaped; (C) chisel-edge; (D) amorphous; (E) needlelike; (F) impacted.⁹⁵

CHAPTER 3
EXPERIMENTAL PROCEDURES

CHAPTER 3

EXPERIMENTAL PROCEDURES

3.1 INTRODUCTION

With regard to experimental procedures, this chapter provides details of (i) the alloys and melt additives investigated, (ii) the general melting and casting procedures applied, and (iii) the various techniques used for microstructural investigation, hardness testing, tensile testing, and machinability testing. The study was conducted to investigate a new experimental alloy belonging to the Al-Si near-eutectic cast alloy group, and which contains about 10.8%Si, namely the 396 alloy. Machining tests were carried out using a Makino A88E high-speed horizontal center machine under fixed machining conditions which include cutting speed, feed rate, length of cut, tool geometry, tool material, and coolant as applied to the examination of the alloys under discussion. The operations were set in motion with a view to studying the machining performance of grain-refined, heat-treated 396, B319.2, and A356.2 alloys. It should be mentioned here that machining performance implies cutting force and moment as well as tool life, chip configuration, and built-up edge (BUE) evolution.

3.2 ALLOY PREPARATION AND CASTING PROCEDURES

The 396, B319.2, and A356.2 base alloys used in this study were supplied in the form of 12.5-kg ingots. The chemical composition of the ingots is shown in Table 3.1. Eight alloys were prepared using the 396 alloy, they were then classified into three groups according to the additives used, namely Fe-intermetallic elements, matrix-hardening elements, and free cutting elements; three alloys of the B319.2 commercial Al-Si alloy were used to investigate the role of free-cutting elements, namely Sn, Bi, and Sn + Bi in connection with the machinability performance of these alloys.

Table 3.1 Chemical composition of the 396, B319.2, and A356.2 base alloys

Alloy	Element (wt %)								
	Si	Cu	Mg	Fe	Mn	Sr	Ti	Al	Mn/Fe
396	10.89	2.243	0.309	0.464	0.492	0.014	0.057	bal.	1.06
B319.2	7.16	3.32	0.29	0.29	0.27	0.019	0.27	bal.	0.95
A356.2	6.93	0.173	0.4168	0.112	0.289	0.017	0.16	bal.	2.58

In addition, two further experimental alloys were prepared using the Al-10.8%Si-Cu-Mg and the Al-10.8%Si-Cu alloy groups. These two alloys were selected to study the effects of Sr-modification and the presence of a Mg-free alloy on the machinability of Al-Si near-eutectic alloys. For the purposes of comparison, the B319.2 and A356.2 commercial alloys were used here to compare the machinability of these alloys with that of 396 alloys. It should be kept in mind that the bulk of the experimental work was carried out using 396 alloys. The nominal composition and respective codes of the alloys prepared for the present study are provided in Table 3.2. The as-received 396, B319.2, and A356.2 ingots were cut into smaller pieces, dried, and melted in charges of 100kg each for the preparation of the

various alloy compositions. Melting was carried out in a SiC crucible of 120-kg capacity, using an electrical resistance furnace in which the melting temperature was maintained at $750 \pm 5^\circ\text{C}$, as shown in Figure 3.1.

Table 3.2 Nominal composition and codes for the alloys prepared in this study

Alloy Type		Alloy Code	Nominal Composition
396 alloy	Effects of Fe-intermetallics	M1	396 + 200 ppm Sr + 0.2% Ti
		M3	M1 + 0.25% Fe + 0.25% Mn
		M4	M1 + 0.5% Fe
	Effects of hardening/alloying elements	M5	M1 + 1% Cu
		M6	M1 + 1% Cu + 0.25% Mg
	Effects of free-cutting elements	M2	M1 + 0.15% Sn
		M7	M1 + 0.5% Bi
		M8	M1 + 0.8% Pb
Experimental alloys		M0	Non-modified Al-10.8% Si-Cu-Mg alloy
		M9	Al-10.8% Si-3.5% Cu (Mg-free alloy)
B319.2 alloy		M10	B319.2 + 0.15% Sn
		M11	B319.2 + 0.5% Bi
		M12	B319.2 + 0.15% Sn + 0.5% Bi
A356.2 alloy		M13	A356.2 + 0.15% Sn

All the alloys were grain-refined by adding 0.20 wt% Ti as Al-5%Ti-1%B in rod form and modified by adding 200 ppm Sr in the form of an Al-10%Sr master alloy by means of a perforated graphite bell. Taking the grain-refined and modified alloy, coded M1, as a reference, additions of Fe, Mn, Cu, Mg, Sn, Bi, and Pb were then added to the M1 alloy to study the effects of these elements on the machinability characteristics of the grain-refined and modified alloy. Iron and Mn were added in the form of Al-25%Fe and Al-25%Mn master alloy, respectively, where Cu, Mg, and free-cutting elements including Sn, Bi, and Pb were added in the form of pure metal.

It should be mentioned here that measured quantities of pure aluminum, silicon, copper, and magnesium were used to prepare two further experimental alloys, namely the non-modified M0 alloy and the M9 alloy, which belong to the Al-Si-Cu alloy group, in order to study the effects of Sr-modification and that of Mg-free alloys, respectively, on the machinability of Al-10.8%Si near-eutectic alloys. The melt was degassed by means of a graphite impeller rotating at ~150 rpm for ~15-20 min, using pure dry argon at a gas flow rate of 0.4 m³/hr, to ensure homogenous mixing of the additives. It should be noted that, for all the castings involved, the humidity level was between 18 and 20%. The surface oxides and inclusions were skimmed off carefully prior to pouring. Samplings for chemical analysis were also taken concurrently for each melt condition; the chemical analysis was carried out at the GM facilities in Milford, NH, using a Spectrolab Jr CCD Spark Analyzer. The averages obtained for three different chemical analysis samples and the respective codes for the various alloys prepared from the base alloys 396, B319.2, and A356.2 are all listed in Table 3.3.

The melt was poured into a graphite-coated waffle-plate metallic mold which had been preheated to 450°C to prepare the castings for machinability studies, as shown in Figure 3.2(a); eighteen machinability test blocks were cast. The test blocks were subsequently cut from each casting and then machined to the final testing form having the overall dimensions of 300mm length, 175mm width, and 30mm thickness, with five ribs each approximately 25mm wide, separated by gaps of 16mm, as shown in Figures 3.2(b) and (c).

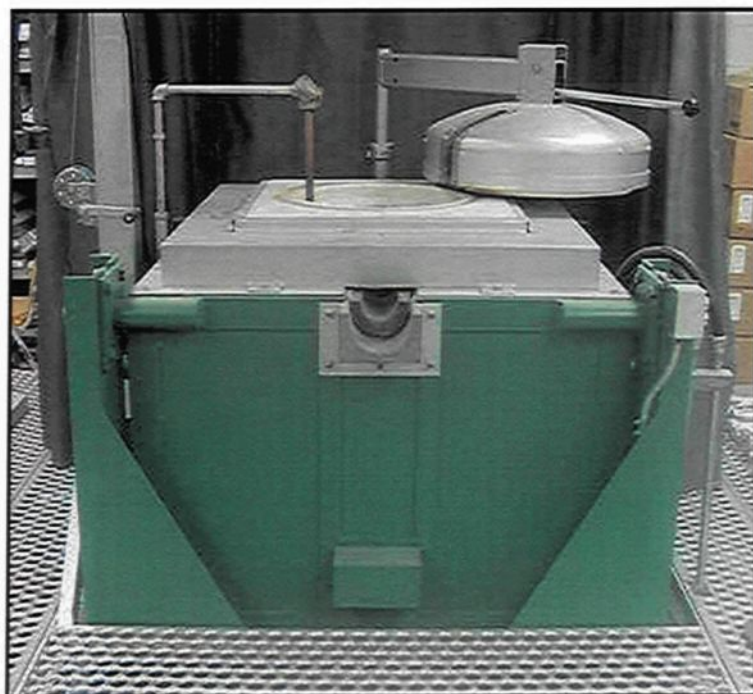


Figure 3.1 Electrical resistance melting furnace.

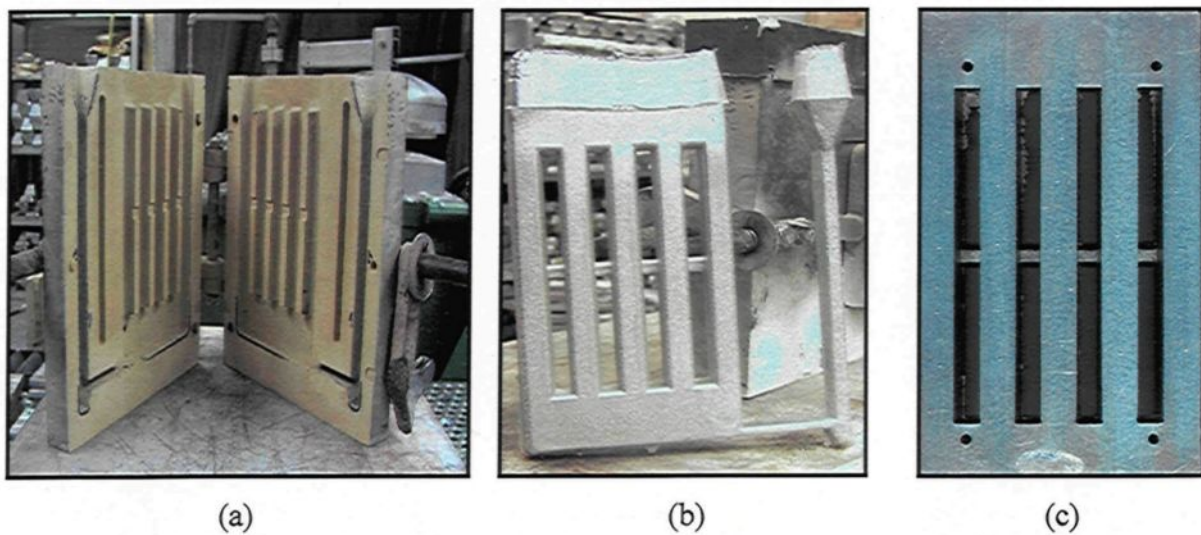


Figure 3.2(a) Waffle-plate metallic mold; (b) machinability test block casting; and (c) machinability test block.

Table 3.3 Average chemical composition of the alloys discussed in this study

Alloy code	Chemical composition (%wt)													
	Si	Cu	Mg	Fe	Mn	Sr	Ti	Sn	Pb	Bi	Zn	Al	Mn/Fe	S.F ^d
396 alloys														
M1 ^a	11.38	2.22	0.335	0.466	0.547	0.0183	0.16	0.00	0.00	0.00	0.00	bal.	1.17	1.561
M2	11.32	2.26	0.348	0.462	0.523	0.0238	0.17	0.18	0.00	0.00	0.00	bal.	1.13	1.508
M3	11.40	2.25	0.341	0.739	0.782	0.0238	0.16	0.00	0.00	0.00	0.00	bal.	1.06	2.304
M4	11.48	2.25	0.341	0.974	0.584	0.0226	0.16	0.00	0.00	0.00	0.00	bal.	0.60	2.142
M5	11.38	3.31	0.347	0.502	0.591	0.0250	0.17	0.00	0.00	0.00	0.00	bal.	1.18	1.685
M6	11.52	3.42	0.584	0.466	0.582	0.0229	0.16	0.00	0.00	0.00	0.00	bal.	1.25	1.631
M7	10.97	2.28	0.381	0.461	0.591	0.0191	0.13	0.00	0.00	0.50	0.00	bal.	1.28	1.64
M8	10.70	2.33	0.293	0.376	0.561	0.0244	0.29	0.00	0.79	0.00	0.00	bal.	1.48	1.498
Experimental alloys														
M0 ^b	10.84	2.81	0.30	0.57	0.56	0.000	0.11	0.00	0.00	0.00	0.00	bal.	0.98	1.71
M9 ^c	10.77	3.67	0.002	0.57	0.55	0.002	0.11	0.00	0.00	0.00	0.00	bal.	0.97	1.67
B319.2 alloys														
M10	7.76	3.39	0.306	0.306	0.295	0.018	0.16	0.16	0.00	0.0	0.14	bal.	0.96	0.896
M11	7.45	3.34	0.386	0.295	0.286	0.011	0.15	0.03	0.00	0.52	0.13	bal.	0.97	0.869
M12	7.33	3.29	0.377	0.291	0.286	0.009	0.15	0.15	0.00	0.56	0.13	bal.	0.98	0.864
A356.2 alloy														
M13	6.93	0.173	0.416	0.112	0.289	0.016	0.16	0.15	0.00	0.00	0.00	bal.	2.58	0.69

Alloying elements added to the base alloy are shown in bold type;

a: Grain-refined and modified 396 alloy, used as a reference alloy;

b: Experimental non-modified alloy;

c: Experimental Mg-free alloy;

d: Sludge Factor.

3.3 HEAT TREATMENT

The heat treatments were selected in such a way as to establish the hardness level as a common factor for all the alloys studied, within the range of 110 ± 10 BHN. This range is the one most frequently used in the majority of commercial applications for aluminum alloys. It was thus possible to carry out solution heat treatments at $490^{\circ}\text{C}/8$ h for the 396 and B319.2 alloys, and at $540^{\circ}\text{C}/8$ h for the A356.2 alloy. The solution heat-treated samples were quenched in warm water at 65°C , followed by artificial aging at 200°C for 5 hours for the 396 and B319.2 alloys, and 5 hours at 180°C for the A356.2 alloy, *i.e.* T6 tempered. Both solution and aging heat treatments were carried out in a forced-air Blue M electric furnace equipped with a programmable temperature controller accurate to within $\pm 2^{\circ}\text{C}$, as shown in Figure 3.3.



Figure 3.3 Blue M electric furnace.

3.4 METALLOGRAPHY-MICROSTRUCTURAL EXAMINATION

Samples measuring 25mm x 25mm for metallographic examination were sectioned from the machinability test blocks and mounted in bakelite using a Struers Labopress-3 Mounting Press. These samples were then ground and polished to the desired fine finish on 9, 6, 3, and 1 μ m diamond lap wheels. After that, the microstructure was examined using an Olympus PMG3 optical microscope, as shown in Figure 3.4. The eutectic silicon-particle characteristics, including particle area, length, roundness (%), aspect ratio, and density (particles/mm²) were measured and quantified using a Clemex image analyzer system in conjunction with the optical microscope. For each sample, 50 fields were examined at a magnification 500x, in such a way as to cover the entire sample surface in a regular and systematic manner.

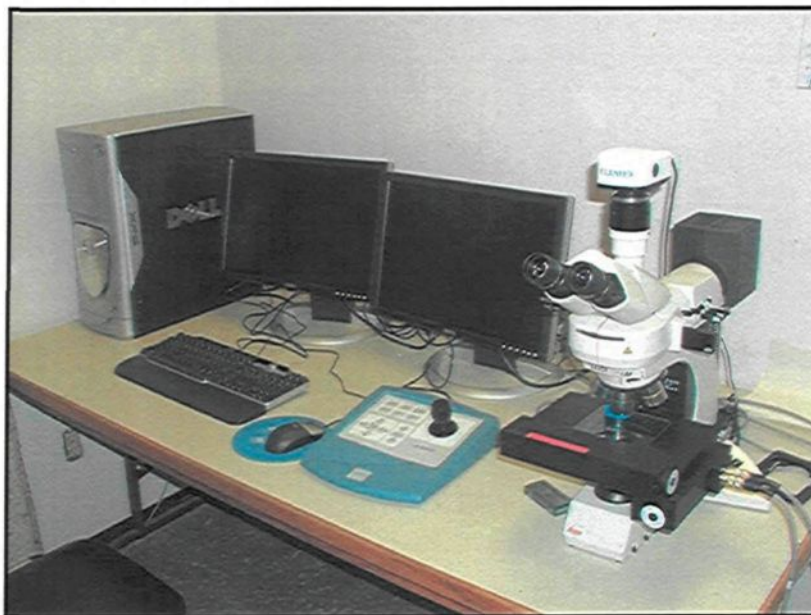


Figure 3.4 Optical microscope-image analysis system.

The various phases observed were identified using an electron-probe microanalyzer (EPMA) in conjunction with energy dispersive X-ray analysis (EDX) and wavelength dispersive spectroscopic analysis (WDS), using a JEOL JXA-8900L WD/ED combined microanalyzer operating at 20kV and 30nA, with an electron beam size of $\sim 2 \mu\text{m}$. Mapping of certain specific areas of the polished sample surface was also done to show the distribution of free-cutting elements in the alloy matrix.

The surface or volume fractions of the intermetallic phases were quantified using a JEOL JXA-8900L model electron probe microanalyzer with a special built-in software based on phase brightness. The brightness of each phase is a function of its average atomic number. The atomic number of the measured phase should be greater than that of the aluminum base matrix, *i.e.* greater than 13. The quantification process is based on the elimination technique which calculates the surface fraction of each phase by subtracting the surface fraction of the brighter phases from the total surface fraction of the other phases present within the matrix. Fifteen fields were measured in each case at a magnification of 100x.

A scanning electron microscope (SEM) was used to examine the characteristics of the hardening precipitates for both the 396-M6 alloy and the Mg-free M9 experimental alloy. The intended purpose of applying the SEM technique is mainly to investigate the distribution, size, and density of the hardening precipitates in the casting structure. The SEM used in the current study is a JEOL 840A Scanning Electron Microscope (SEM) attached to an EDAX Phoenix system designed for image acquisition and Energy Dispersive X-ray (EDX) analysis. The SEM was operated at a voltage of 15 kV, with a

maximum filament current of 3 amperes. Figure 3.5 shows a photograph of the SEM in question.



Figure 3.5 Scanning electron microscope system used for this study.

The samples for precipitate characterization were prepared from the machinability test blocks; they were then subjected to grinding and polishing procedures to produce a mirror-like surface by applying the same procedures as those used for preparing the samples for the characterization of eutectic silicon particles. The polished samples were further subjected to a chemical micro-etching process. The Keller etching reagent used for this study was 0.5 mL hydrofluoric acid, HF, (48%), *i.e.* a 48% concentration solution of 0.5 mL HF with the remaining 99.5 mL being water. This etchant was applied to the samples at room temperature for a length of time ranging from a few seconds to a few minutes based on the chemical composition of the alloys and the heat treatment procedures applied to them.

3.5 HARDNESS TESTING

The Brinell hardness test involves embedding a steel ball of a specific diameter, using a kilogram load, into a test block. The Brinell Hardness Number (BHN) may be obtained upon dividing the kilogram load by the surface area of the indentation, in square millimetres, as follows:

$$BHN = \frac{2F}{\pi D \left(D - \sqrt{D^2 - d^2} \right)}$$

where BHN is the Brinell hardness number, F is the imposed load in Kgf, D is the diameter of the spherical indenter in mm, and d is the diameter of the resulting indenter-impression in mm, as shown in Figure 3.6(a). The load is applied for a standard length of time, usually 25-30 seconds, and the diameter of the indentation is measured using a low-power microscope. Hardness measurements were thus carried out on the heat-treated machinability test blocks using a Brinell hardness tester, as shown in Figure 3.6(b), using a steel ball of 10mm diameter and a load of 500kg applied for 30s. The tester or testing machine was checked for calibration by taking at least five hardness readings on a standard test block before proceeding to the measurement of the test blocks proper. Four blocks were randomly selected from among the eighteen test blocks used for each alloy condition. The Brinell hardness values for each test block represent the average of at least forty indentation readings obtained from both faces of the five ribs, namely, four indentations per rib face for such a block, as shown in Figure 3.6(c). The average hardness of the four

blocks selected per alloys was then obtained and designated as representing the hardness value for that alloy condition.

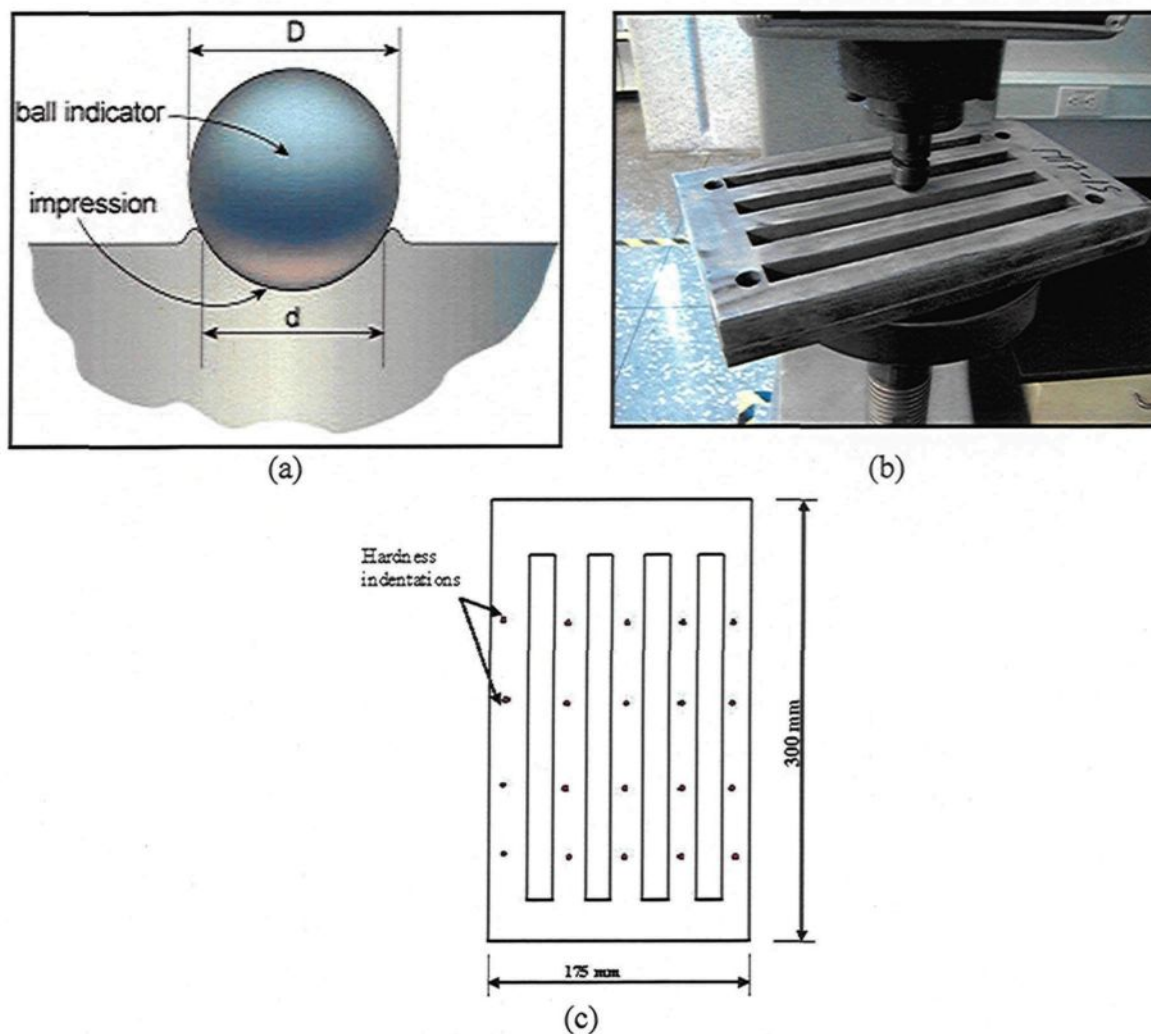


Figure 3.6 (a) Schematic diagram of Brinell hardness test; (b) hardness measurement for machinability test block; (c) schematic of hardness indentations for test block.

3.6 TENSILE TESTING

Tensile test bars were produced by pouring the degassed molten metal at 450°C into a preheated permanent steel mold, type ASTM B-108; each mold casting provided two tensile bars, each with a gauge length of 50mm and a cross-sectional diameter of 12.7mm,

as shown in Figure 3.7(a). Five bars were prepared for each alloy composition. The test bars were solution heat-treated at 490°C for 8 h, then quenched in warm water at 65°C, followed by artificial aging at 200°C for 5 h (*i.e.* T6 tempered). The heat-treated test bars were pulled to fracture at room temperature at a strain rate of 4×10^{-4} /s using a Servo-hydraulic MTS Mechanical Testing machine, as shown in Figure 3.7(b).

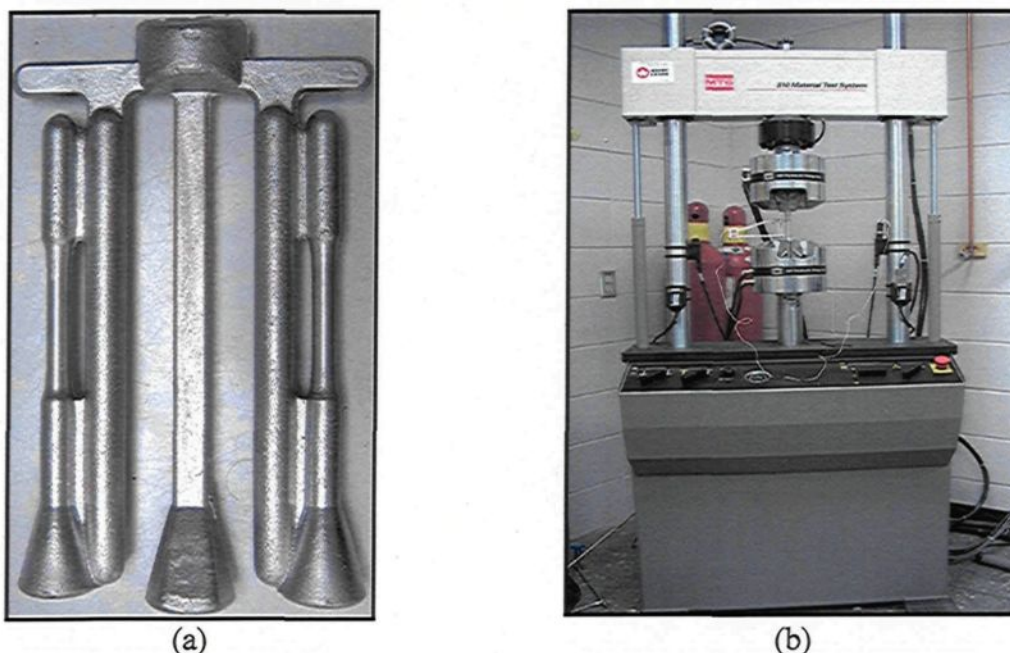


Figure 3.7 (a) Actual tensile test bar casting; (b) MTS servohydraulic mechanical testing machine.

A strain gauge extensometer was attached to the test bar to measure percentage elongation throughout the period of load application. The tensile data were analyzed using the TestWorks 4 software adapted for tensile testing. From the data acquisition system of the MTS machine, the yield stress (YS) was calculated at a 0.2% offset strain, the fracture elongation was estimated in terms of the percent elongation (%El) over a 50mm gauge length, and the ultimate tensile strength (UTS) value was also obtained. The average YS,

%El, and UTS values obtained from the five samples tested were considered to be the values representing a specified alloy/condition studied. It should be kept in mind that all of these alloys were mechanically tested in order to acquire an understanding of the effects of the additives on the mechanical properties at the same specific T6 heat treatments which were applied to the machinability test blocks.

3.7 MACHINING PROCEDURES

Drilling and tapping tests were carried out using a Makino A88E high-speed 5-axis, high-power horizontal machining center with a maximum power reading of 40HP (30kW) and a maximum rotation speed of 18,000 rpm, shown in Figure 3.8. The experimental set-up consisted of the A88E machine, a dynamometer with four sensors, charge amplifiers, and an A/D converter; this set-up was used for the online measurement of drilling/tapping forces and moments; also, a toolmaker's microscope was used for observing BUE formation and tool-wear characteristics.

3.7.1 Cutting Tools

Type K-quality cemented carbides are used, as a rule, for the short-chipping of Al-Si alloys. The K-types tend to display a lesser degree of adhesion to the work material, which is of particular importance when cutting high-Si aluminum alloy. High speed steel designated as HSS is not suited for cutting Al-Si alloys at higher cutting speeds. A cemented carbide drill is 50% harder and has almost four times more thermal conductivity than an HSS drill. The harder cemented carbide drill has a higher elastic modulus and produces less wear and deformation compared to the HSS drill.

The drills utilized for the purposes of this study were made of uncoated ISO K20 carbide or RT 150 GG according to Gühring specifications. A straight flute and coolant-fed carbide “G” drill with an average diameter of 6.5mm, 2-flute, 120° point angle and 90mm total length was used to drill two rows of blind holes in each rib, *i.e.* 36 holes per rib of the waffle-plate, producing 180 holes per casting block. Titanium-nitride coated HSS cutting taps, M8*1.25-6H, with three spiral flutes were used subsequently for the tapping process. Tapping was carried out for the drilled holes of the full plate immediately after drilling. Schematic representations of the carbide drill and HSS tap, together with the terms used in describing their geometry, are provided in Table 3.4.

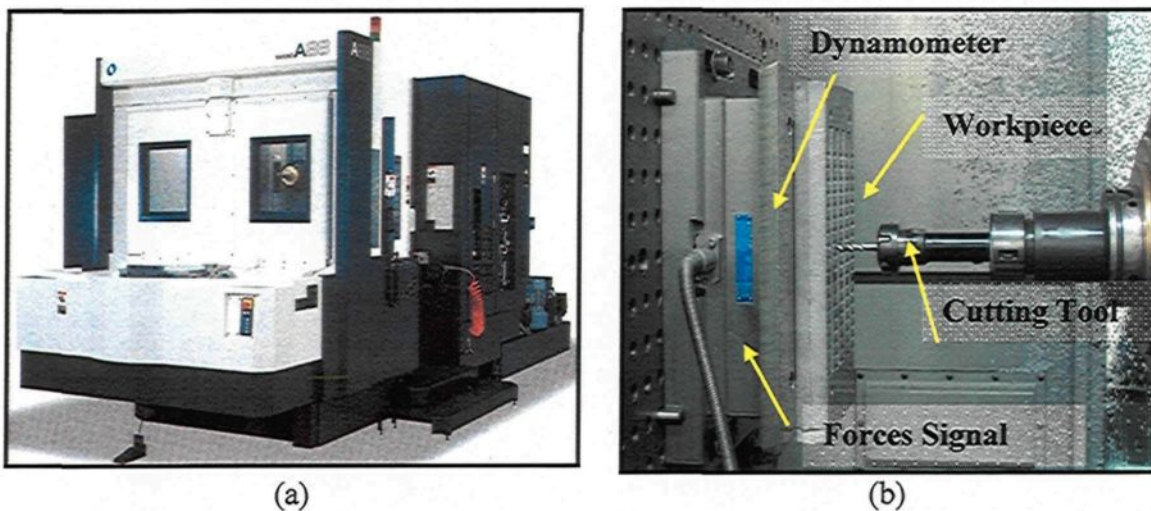


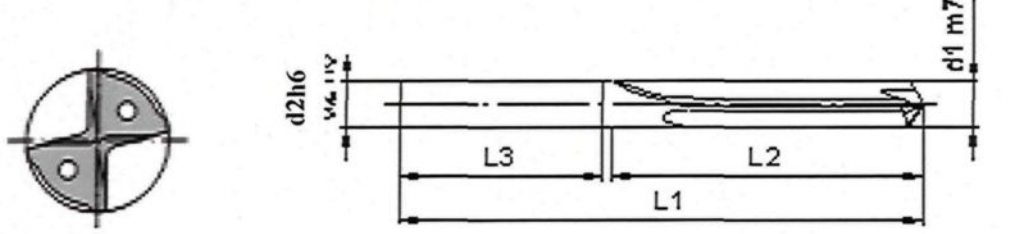
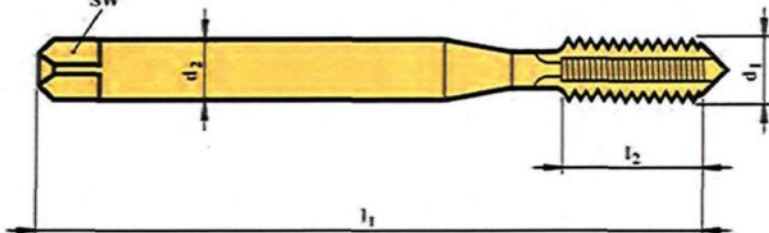
Figure 3.8 (a) Makino A88E CNC machining center; and (b) a close-up view of the test block, dynamometer, and cutting tool.

3.7.2 Cutting Parameters

All alloy conditions were tested under the same cutting parameters for drilling and tapping tests. The drilling tests were carried out at rotational speeds of 11000rpm using a feed rate of 1.117m/min with each hole being 28.38mm deep. The tapping tests were conducted at low cutting speeds, *i.e.* 400rpm, using a feed rate of 0.56m/min with each

tapped hole being 20.76mm deep. The cutting parameters for drilling and tapping tests are listed in Table 3.5.

Table 3.4 Schematic representation of the carbide drill and HSS tap, together with the terms used in describing their geometry

<p>Drill geometry</p>	 <p>Straight flute and coolant-fed carbide "G" type drill ($d_1 = 6.5\text{mm}$, $d_2 = 8\text{mm}$, $L_1 = 90\text{mm}$, $L_2 = 53\text{mm}$, $L_3 = 36\text{mm}$, point angle = 120°, helix angle = 0°)</p>
<p>Tap geometry</p>	 <p>TiN-coated HSS cutting taps, Class to fit 2B, Helix 40° RH ($d_1 = 7.939\text{mm}$, $d_2 = 8\text{ mm}$, $Sw = 6.197\text{ mm}$, $L_1 = 90\text{ mm}$, $L_2 = 20\text{ mm}$)</p>

The machinability test block after drilling and tapping is shown in Figure 3.9(a) and the detailed dimensions for the tapped hole are listed in Figure 3.9(b). Since increasing temperatures and the potential accumulation of hot chips at the bottom of the hole tend to present serious problems, a pressurized coolant was pumped through the drill to ensure adequate cooling and chip evacuation. A synthetic metalworking fluid concentrate, known

as CIMTECH[®] 310, composed of 5% cutting fluid + 95% liquid, was applied to avoid the possible adverse effects of any heat generated during machining.

Table 3.5 Cutting parameters applied for machinability testing

Parameters	Drilling	Tapping
Speed	234.5m/min or 11000rpm.	9.57m/min or 400rpm.
Diameter	Solid carbide “K20” drills: 6.5mm	TiN-coated HSS cutting taps, M8*1.25 UNC. 2B
Tolerance	m7	H4/H5
Depth of hole	Length of cut $\leq 4.5 \times D$ (28.38mm)	Length of cut $\leq 3 \times D$ (20.76mm)
Feed rate	1.117m/min	0.56m/min
Coolant	Synthetic metalworking fluid concentrate CIMTECH [®] 310 (5% cutting fluid + 95% liquid)	

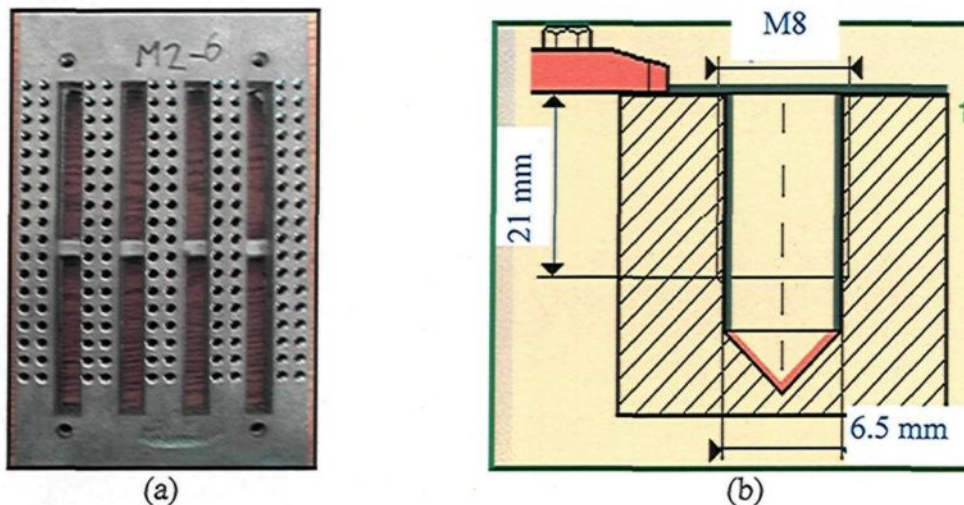


Figure 3.9 (a) Machinability test block after drilling and tapping; (b) detailed drawing of the tapped hole.

3.7.3 Tool Life Criteria

Unfortunately, there is no reliable method for predicting drill life, considering that drill breakage is a stochastic process. Even drills from the same batch tend to fail at random tool life durations. The primary reasons for such random drill failure include the presence

of inhomogeneities in the workpiece and drill materials, as well as the unavoidable asymmetry induced during the grinding of cutting edges. In this study, each alloy condition was tested with a new drill until it broke or until all of the block samples were drilled out. It should be mentioned here that each drilling and tapping test was carried out at least two or three times to validate the results of drill/tap life. If the drill broke down during the drilling process, one of two options was followed: (i) drilling was halted, then the test was changed to another series; or (ii) in the case when the drill broke as a result of the presence of a defect or large inclusion, the test was resumed for the remaining blocks of the same alloy condition using a new drill. Failure is said to occur, in the case of the tapping process, either when the drill fails or the tap gage no longer goes into the hole. The total number of holes drilled with a single drill/tap was counted as well as the number of holes drilled/tapped to the point that the hole was no longer up to specifications, as determined when a Go/No-Go gauge could no longer be inserted into the hole.

A Go/No-Go gauge test was carried out after the drilling and the tapping of each test block to check the dimensional accuracy for both drilled and tapped holes, as shown in Figure 3.10. Reference diameters of 6.5024 to 6.5278 mm and 7.02056 to 7.15518 mm from the Go-NoGo gauge test were applied to the drilling and tapping processes, respectively.

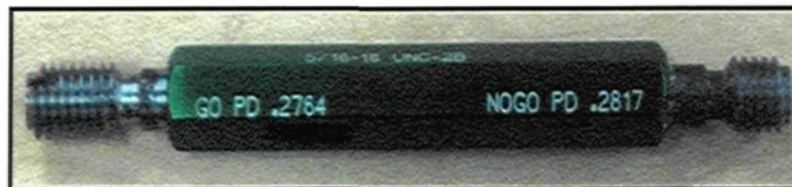


Figure 3.10 Thread gauge used in the current work.

3.7.4 Measurement of Machining Forces

It is customary to monitor forces in a cutting process in order to follow the development of cutting tool wear. The desired cutting conditions were established by numerical program prior to the machining tests. While the linear transverse motions of the machine table were controlled in the X and Y directions, a feed force was applied in the Z direction for drilling and tapping operations. A Kistler, model 9255B, 6-component piezoelectric quartz crystal dynamometer was used during drilling and tapping tests for the online measurement of the cutting forces and moments. The measuring system using piezoelectric force differs from other methods of measurement. The cutting forces acting on the quartz crystal elements are converted to a proportional electric charge in Pico-Coulombs (PC). Figure 3.11(a) illustrates the Kistler dynamometer with four sensors as used in this study, while the schematic depicted in (b) shows the measuring chains for the 6-component forces and moment measurements. Each of the sensors has three pairs of quartz plates, one sensitive to pressure in the z direction and the other two pairs responsive to shear in the x and y directions, respectively. The four sensors of the dynamometer, therefore, provide eight electric charges corresponding to the values of the eight components of the cutting forces in the x, y, and z directions, namely $F_{x_{1+2}}$, $F_{x_{3+4}}$, $F_{y_{1+4}}$, $F_{y_{2+3}}$, F_{z_1} , F_{z_2} , F_{z_3} , and F_{z_4} , as shown in Figure 3.11(b).

The output charges from the dynamometer were guided by an amplifier through the eight-core connecting cables, type 1677A5/16779A5. The charge amplifier converts these charges into proportional voltage signals which are subsequently converted into force signals by an analog-to-digital (A/D) converter using a data acquisition system. These force

signals are independently monitored and recorded for each test block in the LabVIEW program where Cut Pro 8.0 software was used for cutting force measurements. Figure 3.12 shows the experimental set-up which was organized, including a Kistler dynamometer, charge amplifiers, an A/D converter, and a LabVIEW program, for the measurement of the drilling and tapping forces. A toolmaker's microscope was used to examine BUE evolution and tool wear characteristics, also a Go/No-Go gauge test was applied to assess the dimensional accuracy control for both drilled and tapped holes.

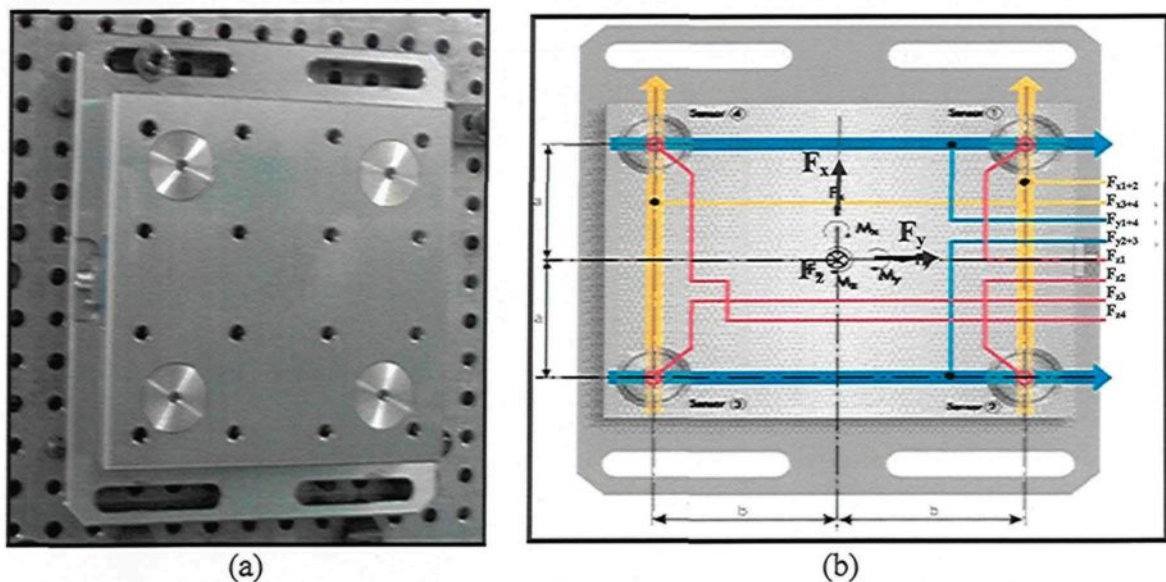


Figure 3.11 (a) Kistler dynamometer with four sensors used in this study; (b) illustration showing the measurement chains for the 6-component forces and moment measurements.

3.7.5 Chip Form and BUE Evaluations

The chips produced during the drilling tests were collected for the purposes of examining their size and shape after drilling each block. Chip size was studied using the number of chips-per-gm criterion. The built-up-edge (BUE) width of the drill was observed at the end of each casting block tested while the failure of the first and second teeth of the

tap was also checked using a toolmaker's microscope (TM-505 type) at a magnification of 30x. It should be kept in mind that all of these examinations were conducted periodically throughout the drilling and tapping tests for each alloy composition to monitor the condition of the cutting tools used and to evaluate the machining performance of the alloys studied.

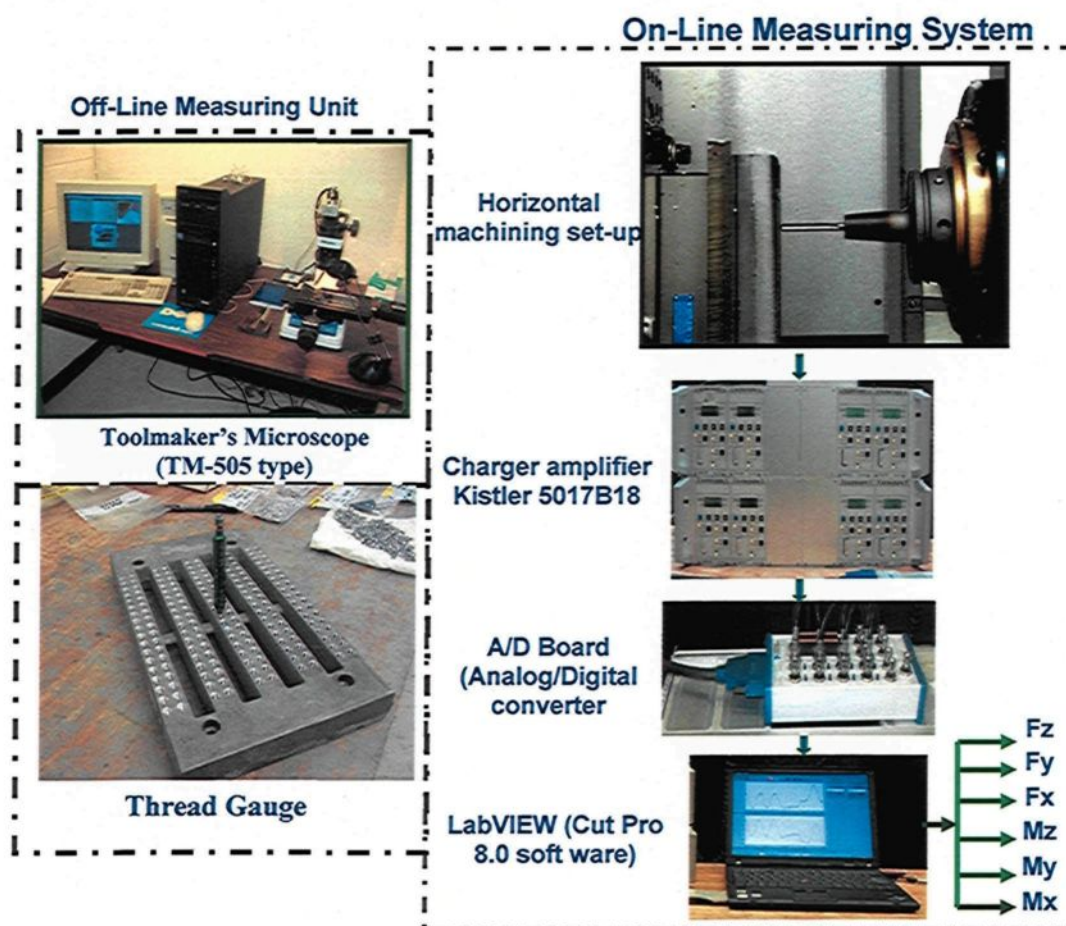


Figure 3.12 Schematic diagrams showing the experimental set-up for carrying out the drilling and tapping tests.

3.8 METHODOLOGY FOR THE DATA-PROCESSING OF DRILLING AND TAPPING TESTS

As mentioned earlier in section 3.7.4 of this chapter, to investigate the machinability characteristics of a material, it is customary to monitor the forces in a cutting process in order to follow the development of cutting tool wear. In our study, a Kistler 6-component piezoelectric quartz crystal dynamometer with four sensors was used during the drilling and tapping tests for online measurement of the cutting forces and moments. The four sensors of the dynamometer provide eight electric charges corresponding to the 8 components of the cutting forces in the x, y, and z directions, namely, F_{x1+2} , F_{x3+4} , F_{y1+4} , F_{y2+3} , F_{z1} , F_{z2} , F_{z3} , and F_{z4} . A charge amplifier converts these charges into proportional voltage signals by means of an A/D converter connected to the data acquisition system. These force signals are independently monitored and recorded for each test block, using the LabView program of the Cut Pro 8.0 software.

This section presents the force and moment calculations which were used for processing the drilling and tapping test data. The drilling moment M_z and feed force F_z are of particular interest in analyzing the drilling process. The deflective forces F_x , F_y perpendicular to the rotary axis provide additional information on the machining process. Matlab programs were developed for the processing of drilling and tapping data related to all the conditions studied in the present work. These programs are similar to those produced in an earlier study on the machining behaviour of 356 and 319 alloys carried out by Tash⁸⁰ from this research group. Complete details of these programs may be found in Appendix B of that study.⁸⁰ Essentially, the methodology followed for processing the drilling and tapping data consists of four steps as follows:

Step 1: Separation of the 6-components of force and moment, in order to process the data for obtaining the F_z component

The three forces F_x , F_y , F_z and the three moments M_x , M_y , M_z were first calculated from the eight-channel force components by applying the following sets of equations:¹⁶³

$$F_x = F_{x1+2} + F_{x3+4};$$

$$F_y = F_{y1+4} + F_{y2+3};$$

$$F_z = F_{z1} + F_{z2} + F_{z3} + F_{z4};$$

$$M_x = b. (F_{z1} + F_{z2} - F_{z3} - F_{z4});$$

$$M_y = a. (-F_{z1} + F_{z2} + F_{z3} - F_{z4}); \text{ and}$$

$$M_z = b. (-F_{x1+2} + F_{x3+4}) + a. (F_{y1+4} - F_{y2+3})$$

where a ($= 80$ mm) is the distance of the sensor axes from the X-axis; and b ($= 80$ mm) is the distance of the sensor axes from the Y-axis, as shown in Figure 3.11. It should be mentioned that the 6-component measuring system provides the following resultants: (i) the 3-components of the resultants of all the applied forces, including their direction but not their location in space; and (ii) the 3-components of the resultant moment vector related to the coordinate origin. The sampling rate of these charges or force components is 1000Hz which implies that each force component is measured at every 0.001s of the drilling tests; thus 1600 sample points per cycle or hole were acquired for calculating the mean value of cutting feed force (F_z) and 1200 sample points per cycle for the other five components of force and moment, F_x , F_y , M_x , M_y , and M_z in each signal of 90 cycles or holes per signal. Standard deviations were calculated based on the procedures outlined by Tash.⁸⁰

As an example of data processing, the drilling data for the 396-M1 alloy is presented here to show the methodology for the first group of holes (viz., 90 holes representing half a block). Matlab graphs representing the steps of data processing for the drilling force are shown in Figures 3.13 to 3.15.

Step 2: Filtration of raw data to obtain a smooth signal and remove fluctuations

The drilling feed force, Fz component, as shown in Figure 3.13(a), was separated and the relevant data was analysed and processed. The Fz component signal was filtered nine times by using a low pass filter whereby a smooth signal was produced, as shown in Figure 3.13(b). The function 'K1= Filter (b, 1, K1)' filters the data in vector K1, namely Fz, with the filter described by the numerator coefficient vector b and the denominator coefficient vector a(1).

Step 3: First Difference of the filtered signal to remove changes that represent error which helps in detection of all cycles within the signal

The first and second differences were taken for filtered signals in order to detect the beginning and the end of each cycle/hole. In connection with the first difference, the pointed peaks having a constant value were obtained in the majority of the cycles after applying the first difference, as presented in Figure 3.14(a).

Step 4: Second Difference of the filtered signal to obtain one peak data point within each cycle

The second difference was applied to the pointed peak (or plateau) signal obtained in the first difference in order to detect one peak data point at constant intervals within each cycle, as indicated by the faint blue horizontal dashed signal in Figure 3.14(b). Two points

were determined for each cycle relative to the peak data point detected in the second difference, as shown in Figure 3.15(a). The upper point represents the mean cutting feed force, $F_{z_{up}}$, without error consideration during the cutting cycle, while the lower point represents the error value ($F_{z_{down}}$) when the drill is removed from the hole. The output results for drilling feed force (mFz) of the first group of holes (90-holes), with or without error consideration, are shown in Figure 3.15(b).

The margin for error was taken into consideration and incorporated into the Matlab drilling programs for the six-component force and moment by using the following equations:

- (i) $mF_x = F_{x_{up}} - F_{x_{down}} ;$
- (ii) $mF_y = F_{y_{up}} - F_{y_{down}} ;$
- (iii) $mF_z = F_{z_{up}} - F_{z_{down}} ;$
- (iv) $mM_x = M_{x_{up}} - M_{x_{down}} ;$
- (v) $mM_y = M_{y_{up}} - M_{y_{down}} ;$ and
- (vi) $mM_z = M_{z_{up}} - M_{z_{down}} .$

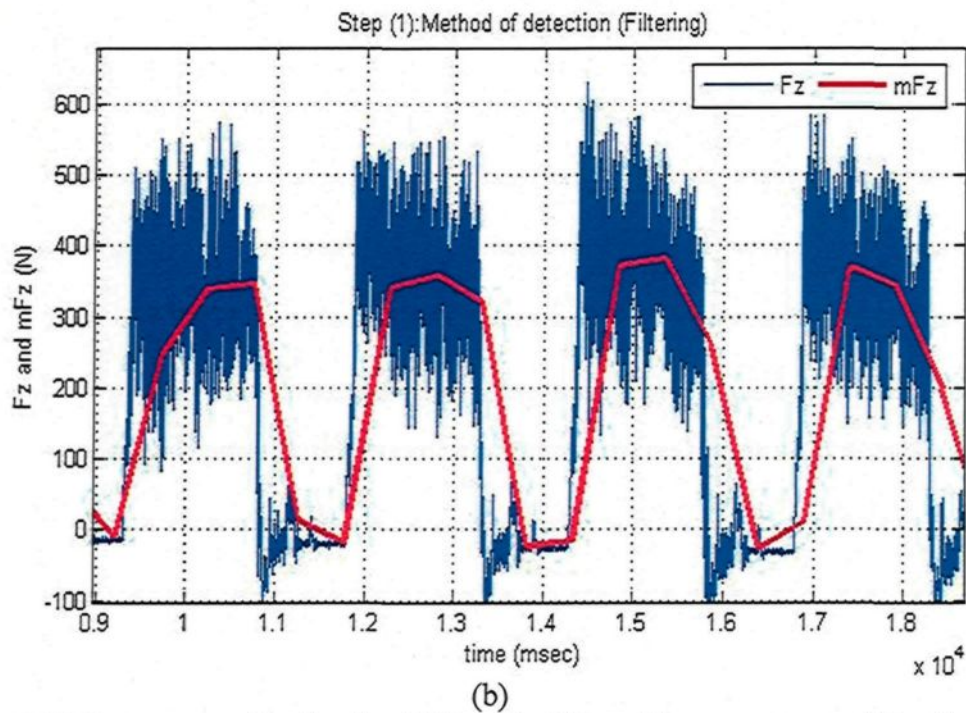
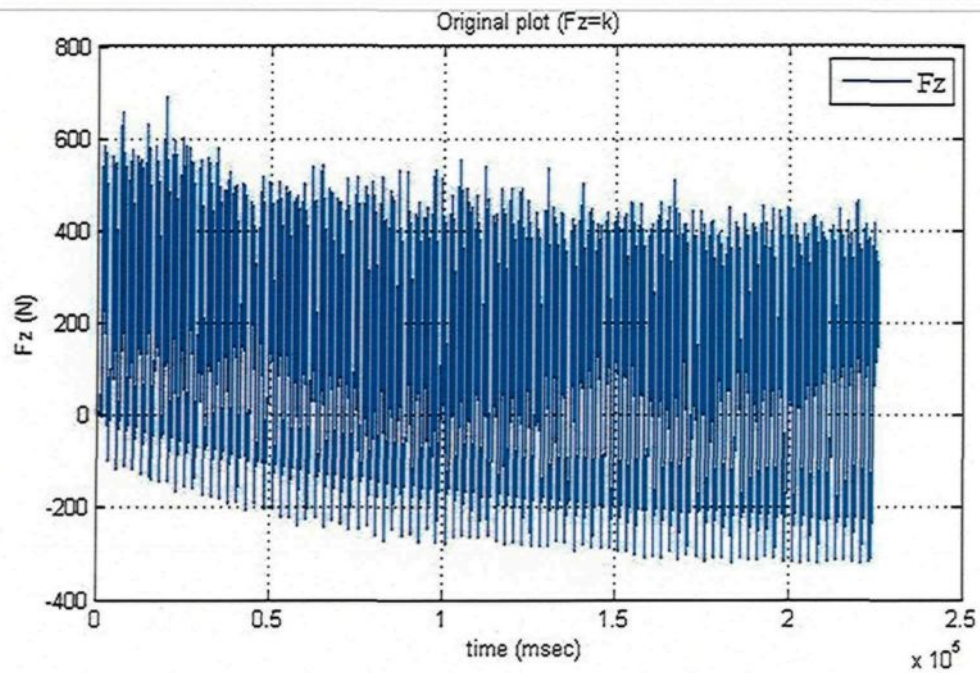
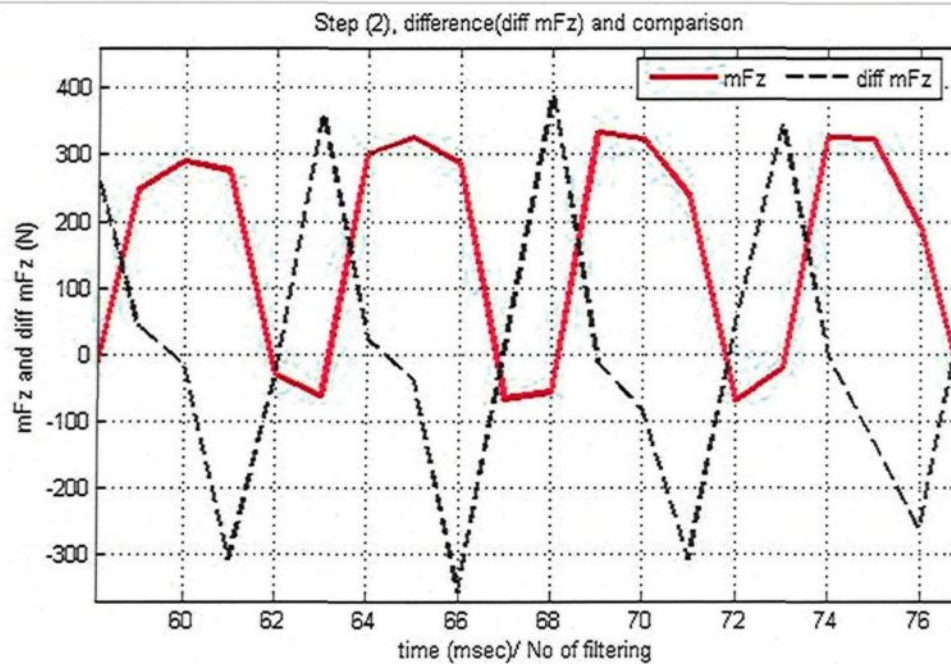
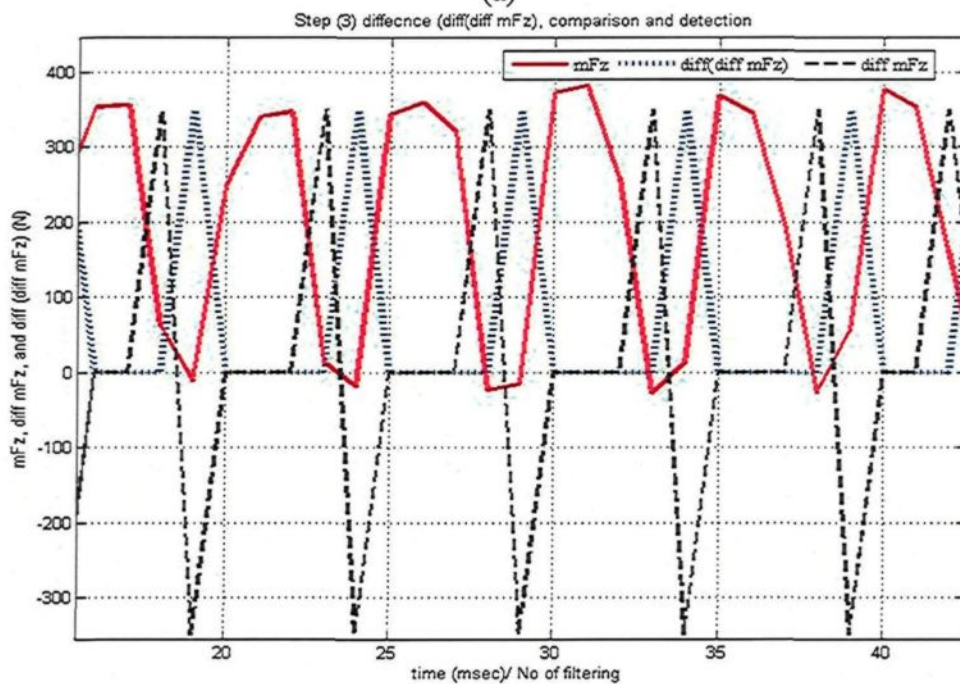


Figure 3.13 Data processing for the drilling feed force- F_z component of the first group of holes (90-holes): (a) raw data of F_z component; (b) filtration (9-times) for F_z component.



(a)



(b)

Figure 3.14 (a) First difference of the filtered Fz, point detection within each cycle; (b) first and second difference of the filtered Fz component.

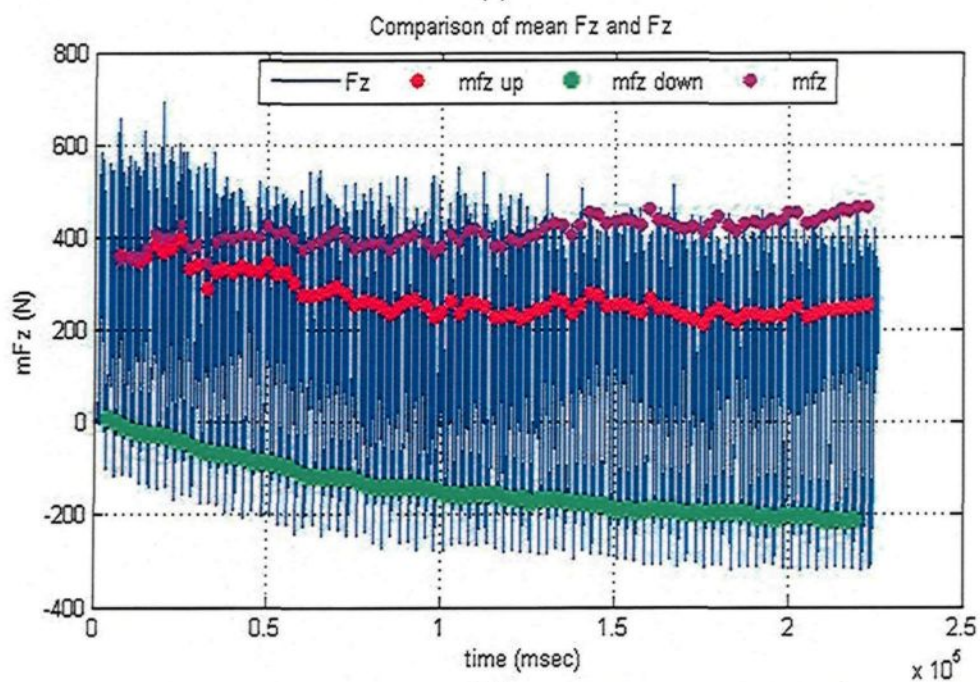
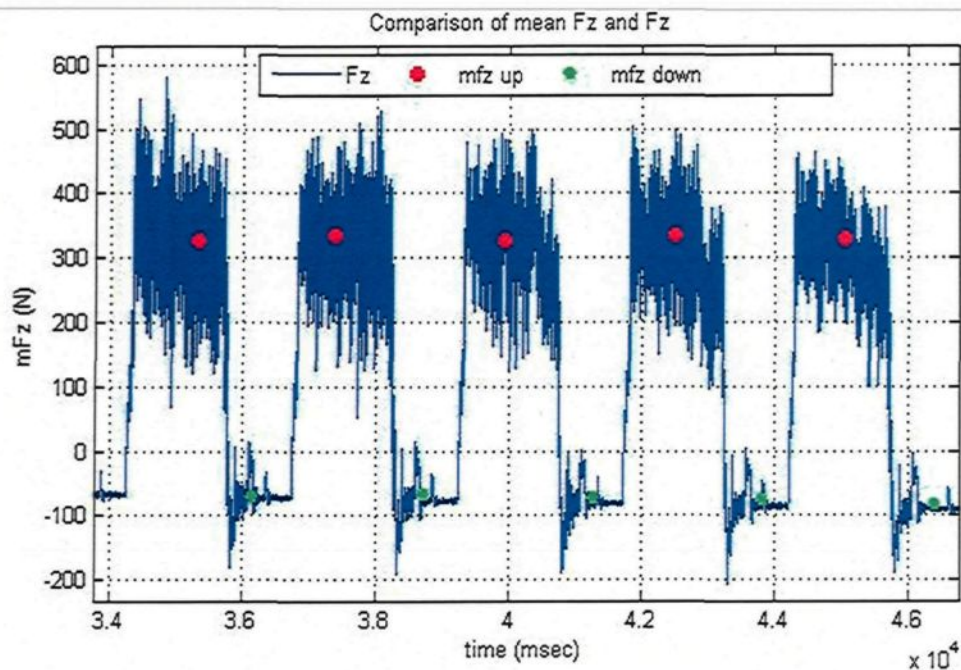


Figure 3.15 (a) Two points within each cycle: the red point represents the mean F_z during drilling cycle, while the green point represents the error value upon removing the drill from the hole; (b) output results for the drilling feed force for the first group of holes (90 holes) showing plots with or without error consideration.

The same methodology as that used for data processing of the drilling test results was applied to calculate the mean value of tapping force and moment. The tapping feed force was first separated and the data was processed according to the same procedures applied for the drilling tests. A smooth signal was obtained by using the same filter as that used for the drilling data calculations. Slow changes within the signal were removed by taking the first difference of filtered signals, as shown in Figure 3.16(a).

The second difference was applied to the peak or plateau obtained in the first difference to detect one point at constant intervals within the signal. Three points were determined within each cycle relative to the point detected in the second difference, as shown in Figure 3.16(b), where the upper or red point represents the mean tapping feed force ($mF_{z_{up1}}$) during the cutting cycle of the tap, while the green point represents the mean tapping feed force ($F_{z_{down1}}$) resulting from the friction between the internal thread and the tap teeth after removal of the tap from the tapped hole; the third or black point represents the error value of the signal ($F_{z_{down2}}$). It should be mentioned that the sampling rate of the tapping force components is 2000Hz which means that each force component is measured at every 0.0005s of the tapping test; thus 2000 sample points per cycle were used in calculating the mean value of the tapping force and moment. The error, which occurs when the tap enters or is removed from the drilled holes, was taken into consideration and incorporated into the Matlab tapping program in the form of the following set of equations:

(i) $mF_{z_{up}} = F_{z_{up1}} - F_{z_{down2}}$; (ii) $mF_{z_{down}} = F_{z_{down1}} - F_{z_{down2}}$; and (iii) $mF_z = F_{z_{up}} - F_{z_{down}}$.

Likewise, using similar calculations, the two forces F_x , F_y , and the three moments M_x , M_y , and M_z were obtained for all the alloys/blocks investigated.

All components of the mean drilling/tapping cutting force and moment were determined for all conditions used in this study, namely for the M1 through M14 alloys. The Matlab output results for all components of force and moment, together with their standard deviations in both drilling and tapping tests, were transferred onto an Excel data sheet and followed by calculations to obtain the total mean cutting force and moment. It should also be mentioned that the x and y force components were too small relative to the z force component; that is to say, the z force component was the dominant force in each case, and the small value of the deflective forces F_x , F_y indicate that the machine performance was high. The total forces, *i.e.* the resultants of the x, y, z components, were thus used in this study for a more accurate representation of the data.

Consequently, the total cutting force and total cutting moment in both drilling and tapping tests, as well as the cutting power of the drilling test, were calculated and used to evaluate the drilling and tapping process in this study by employing the following expressions:

$$F_t = [(F_x)^2 + (F_y)^2 + (F_z)^2]^{1/2}$$

$$M_t = [(M_x)^2 + (M_y)^2 + (M_z)^2]^{1/2}$$

$$P_c = (\pi * M_z * n) / 30, \text{ where } n \text{ represents drill speed}$$

The standard deviation calculation for the total cutting force and total cutting moment were carried out by applying the following equations:⁸⁰

$$\sigma_f = (F_x^2 * \sigma_x^2 + F_y^2 * \sigma_y^2 + F_z^2 * \sigma_z^2)^{1/2} / (F_x^2 + F_y^2 + F_z^2)^{1/2}$$

$$\sigma_m = (M_x^2 * \sigma_x^2 + M_y^2 * \sigma_y^2 + M_z^2 * \sigma_z^2)^{1/2} / (M_x^2 + M_y^2 + M_z^2)^{1/2}$$

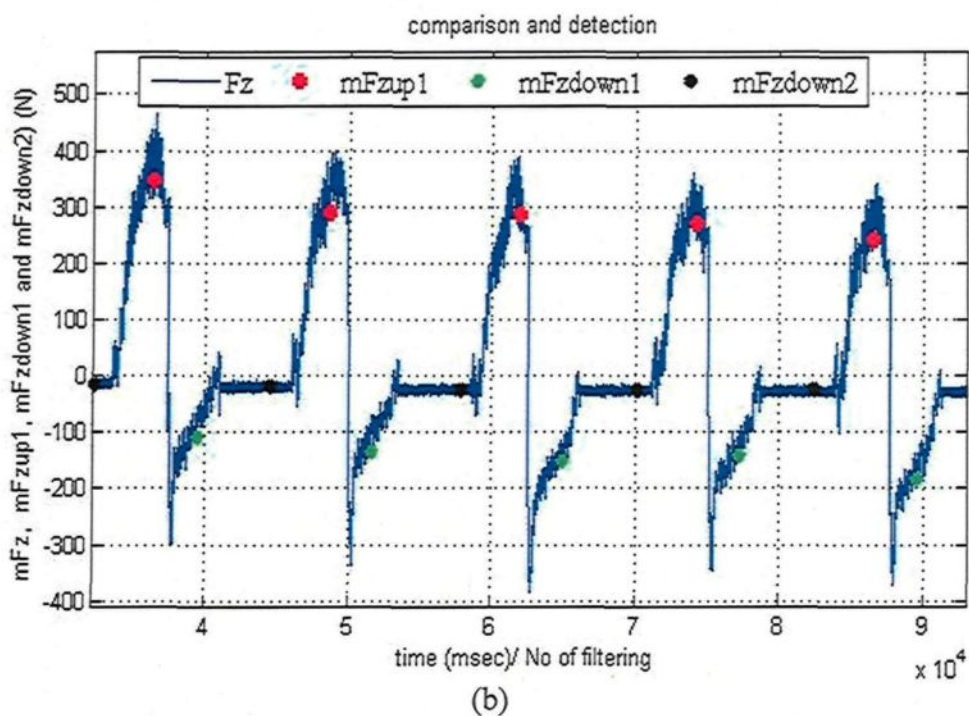
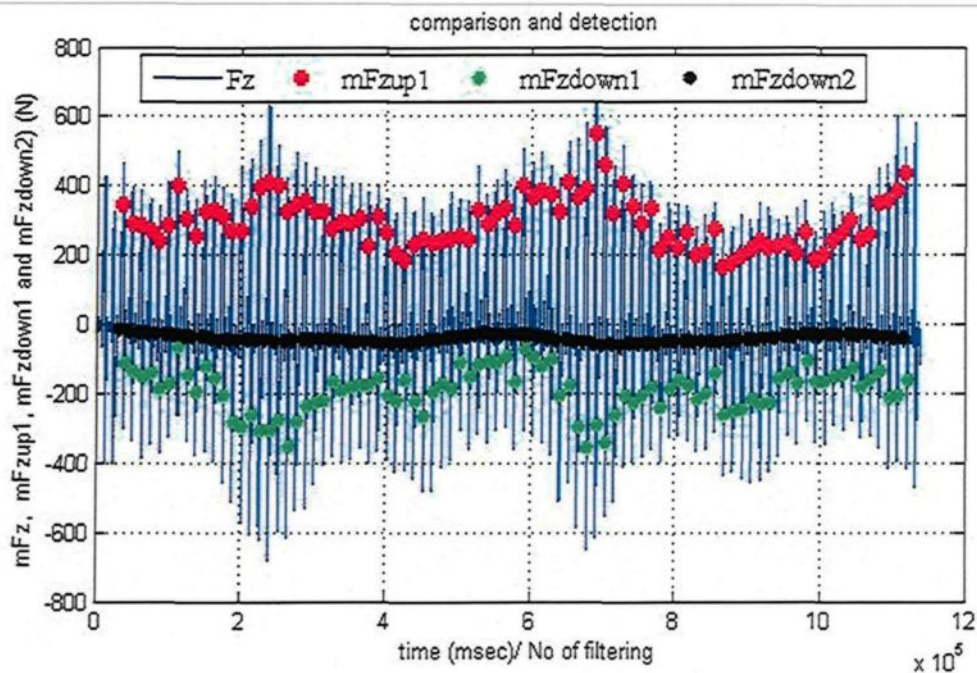


Figure 3.16 (a) Data processing for the tapping feed force- F_z component of the first group of holes (90-holes); (b) three points within each cycle, the upper point representing the mean mF_{zup1} , the lower point representing the mean F_{zdown1} , and the middle point representing the error value of the signal.

CHAPTER 4

EFFECTS OF IRON-RICH AND COPPER-RICH INTERMETALLICS ON THE MACHINABILITY OF HEAT- TREATED Al-10.8%Si CAST ALLOYS

CHAPTER 4

EFFECTS OF IRON-RICH AND COPPER-RICH INTERMETALLICS ON THE MACHINABILITY OF HEAT-TREATED Al-10.8%Si CAST ALLOYS

4.1 INTRODUCTION

Aluminum-silicon alloys having the same chemical composition can have different microstructures and mechanical properties either because of variations in the casting process, or as a result of using a modifier, and/or through the selection of a given heat treatment process for the alloy. This sequence of possibilities implies that different processing techniques can result in a whole range of mechanical properties, which then reflects on the characteristics of the machining process itself. The combination of alloying elements and liquid alloy treatments is a satisfactory option for obtaining improved control of the microstructure during solidification, and hence of improving the machinability performance. A number of elements are traditionally thought to provide any given alloy with a certain degree of natural lubricity. Other elements are known to increase matrix hardness, while still others result in the formation of hard intermetallic phases. All of these should be expected to have some effect on alloy machinability. Alloys containing copper, magnesium, or zinc, predominantly, as elements entering readily into solid solution with aluminum, generally possess the best machining characteristics.

It should be mentioned here that numerous studies have been carried out integrating the formation of the as-cast microstructure as well as the effects of solution heat treatment and aging on the microstructure and mechanical behaviour of Al-Si-Cu-Mg alloys. Only a few studies so far, however, have dealt with the influence of alloying elements and melt treatment on the machining performance of near-eutectic Al-10.8%Si cast alloys. In the light of the above, the main purpose of this chapter is to report on the changes in the machinability criteria resulting from the effects of Fe-intermetallics, namely α -Fe, β -Fe, and sludge; two levels of Cu, namely 2.25 and 3.5%; and two levels of Mg, namely 0.3 and 0.6%. In addition to the preceding, the effects of Mg-free alloys and Sr-modification were also investigated.

4.2 CHARACTERIZATION OF THE MICROSTRUCTURE

The constituents or phases existing in the workpiece play a prominent role in its machinability and may be described as soluble and non-soluble types. The soluble phases contain elements which dissolve in the aluminum matrix during heat treatment and are distinguished by relatively soft particles. The insoluble phases are those which do not dissolve during heat treatment, yet they typically contain a large amount of iron (Fe) and consist of hard brittle particles when compared to the soluble phases. From a machinability point of view, the insoluble particles represent abrasive areas in the metal which are likely to cause excessive tool wear; the presence of these particles is, therefore, intentionally maintained at a low level.

A metallographic study was conducted using samples which had been sectioned from the heat-treated machinability test block with the aim of examining the specific

changes resulting from Sr-modification and the addition of alloying elements, from the viewpoint of both the microstructure and the chemical composition. With this in mind, the characteristics of the eutectic silicon particles and the volume fraction of the insoluble intermetallic phases were measured and quantified. The results obtained were then discussed, in-depth, to explain the influence of the relevant additives on the machinability behavior.

4.2.1 Silicon Particle Characteristics

The morphology of eutectic Si plays a vital role in determining the machinability characteristics of cast Al-Si near-eutectic alloys. A fine, well-modified eutectic silicon structure is far less detrimental to tool life than heavy element intermetallic phases; tool life, will however, decrease in the presence of a coarse eutectic silicon structure. Table 4.1 summarizes the silicon particle characteristics obtained from quantified measurements of the alloys investigated. As can be seen from this table and from Figure 4.1(a), the Si particles are present in the form of coarse acicular plates with an aspect ratio of 3.51 in the T6 heat-treated condition for the non-modified experimental M0 alloy. The addition of 200 ppm of Sr transforms the morphology of Si particles from an acicular form to a fibrous one, as may be observed in the M1 alloy which has an aspect ratio of 1.77; this addition also increases the roundness ratio from 32.8% to 70%, as shown in Figure 4.1(b). The average Si particle length decreases from 20.80 μm in the M0 alloy to 2.96 μm in the M1 alloy, while the average area decreases from 65.70 μm^2 to 4.30 μm^2 , *i.e.* by about 86% and 93%, respectively. As a result of the decrease in the size of the particles, the density of the Si particle increases from 2604 to 28,000 particles/ mm^2 , implying that the eutectic Si particles

were fibrous and finely divided in the presence of Sr, as indicated in the micrograph shown in Figure 4.1(b). The Si phase in the unmodified alloy was to be observed in the form of large plates having sharp sides and ends, known as acicular silicon; the α -Fe Chinese-script was also observed interspersed with the Si particles. It is worth noting that, of all the alloys investigated, the M0 alloy reveals the highest values for average Si particle area and length, whereas the M1 alloy shows the lowest. Such values indicate that any further addition of alloying elements will decrease or weaken the effects of Sr as a modifier, as a result of the interaction of these elements with Sr to form complex intermetallic compounds.

Table 4.1 Summary of eutectic Si-particle measurements for the alloys studied

Alloy Code	Particle Area (μm^2)		Particle Length (μm)		Roundness Ratio (%)		Aspect Ratio		Density (particles/ mm^2)
	Av	SD	Av	SD	Av	SD	Av	SD	
M0	65.70	84.10	20.80	17.10	32.80	18.20	3.51	2.32	2604
M1	4.30	6.51	2.96	2.49	70.00	17.30	1.77	0.78	28000
M3	4.98	4.67	3.34	2.07	68.30	16.10	1.71	0.66	27883
M4	4.89	4.62	3.49	2.02	67.10	15.80	1.70	0.89	27022
M5	10.00	7.60	4.80	2.49	60.00	16.50	1.71	0.61	12542
M6	7.89	8.18	4.60	3.40	55.60	18.50	1.95	0.92	19252
M9	61.30	86.10	18.10	17.80	35.80	23.60	3.56	2.43	3064

It is interesting to note from Table 4.1 that the increase in the level of Fe and/or Mn in the M3 and M4 alloys, respectively, has only a slight influence on the values of the average Si particle area, length, roundness, aspect ratio, and density as compared to the M1 alloy. On the other hand, it is also clear that increasing the level of Cu and Mg leads to an increase in the average length and area of the Si particles in general.

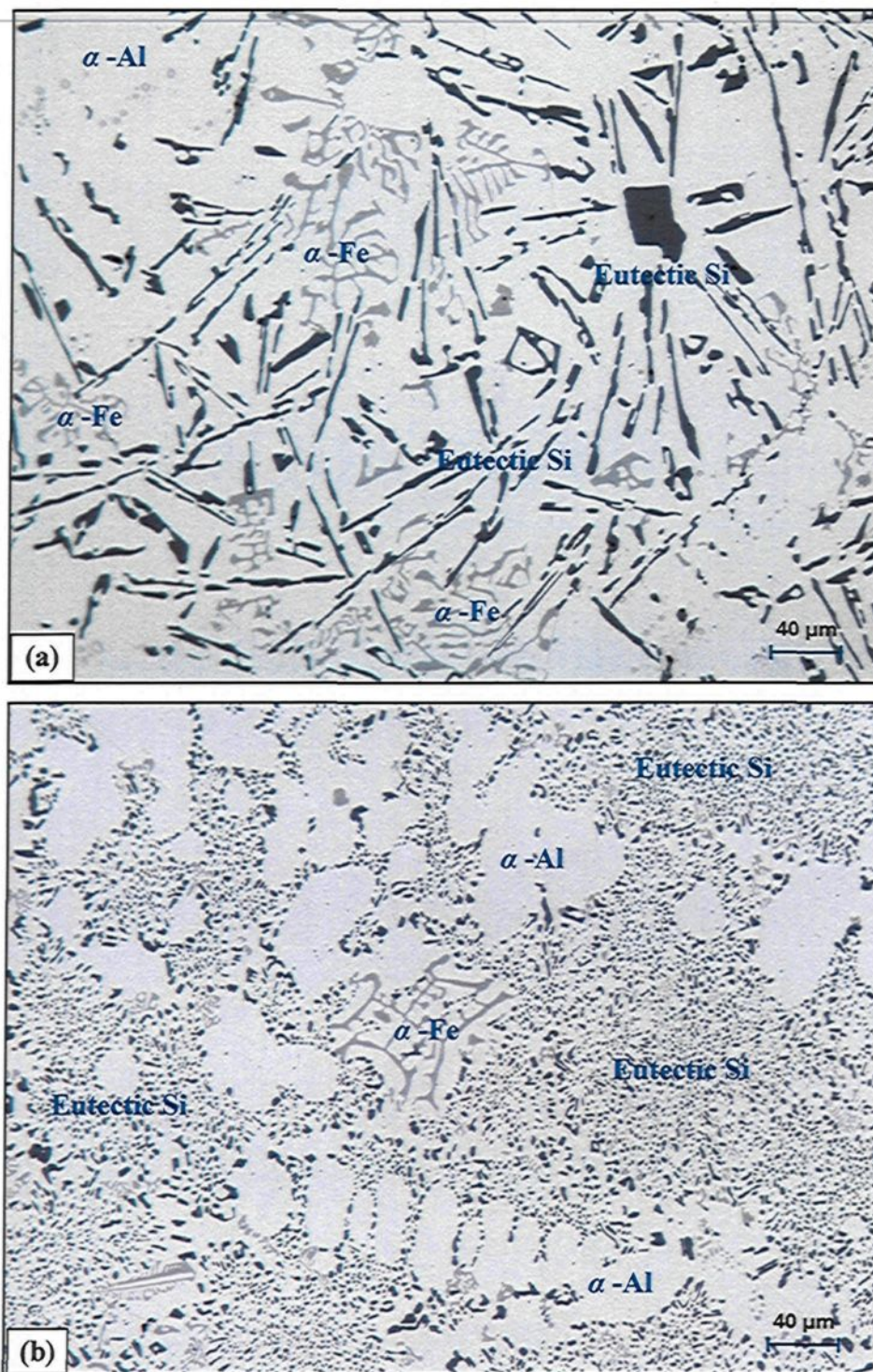


Figure 4.1 Optical micrographs showing the effects of Sr-addition on Si morphology in grain-refined and heat-treated Al-10.8% Si alloy: (a) 0 Sr-M0 alloy; (b) 200 ppm Sr-M1 alloy.

As shown in Table 4.1, the Si-particle length increases from 2.96 μm in the M1 alloy to 4.80 μm in the M5 alloy which contains 3.31%Cu and 0.35%Mg, and to 4.60 μm in the M6 alloy containing 3.42%Cu and 0.58%Mg, while the average particle area increases from 4.30 μm^2 to 10.00 μm^2 and 7.89 μm^2 , respectively. Moreover, the aspect ratio of the Si particle increases from 1.77 in the M1 alloy to 1.95 in the M6 alloy, *i.e.* it increases by about 10%. The presence of Mg and Cu also affects the roundness ratio of the eutectic Si particles; increased Mg content results in a clear reduction in the roundness ratio which is most pronounced at a higher Cu content, as in the M6 alloy, while the roundness ratio decreases from 70% in the M1 alloy to 55.6% in the M6 alloy. Thus, from the point of view of these observations, the addition of Mg and Cu may be deemed to diminish the effects of Sr as a Si-particle modifier, and to decrease the particle density as a result. Figure 4.2 show how the increase in the level of Cu and Mg hinders the modification effect of Sr when these elements are added to the Sr-modified M1 alloy. The microstructures reveal that certain Si areas are fully modified, whereas others are only partially modified. This observation is in satisfactory agreement with those of Joenoes and Gruzleski,¹⁶⁴ who reported that about 1% Mg is capable of refining the Si phase slightly and that it also has a negative effect on Sr modification, that is to say, it changes the microstructure from being a well-modified one to being a partially modified one, due to the fact that both Mg and Cu react with the Si and Sr in the alloy to form $\text{Mg}_2\text{Sr}(\text{Si},\text{Al})$ and Al-Cu-Sr compounds, respectively. As a result, there is less Sr available to obtain the same level of modification in the eutectic Si particles than would be expected with the amount added, which was ~ 200 ppm.

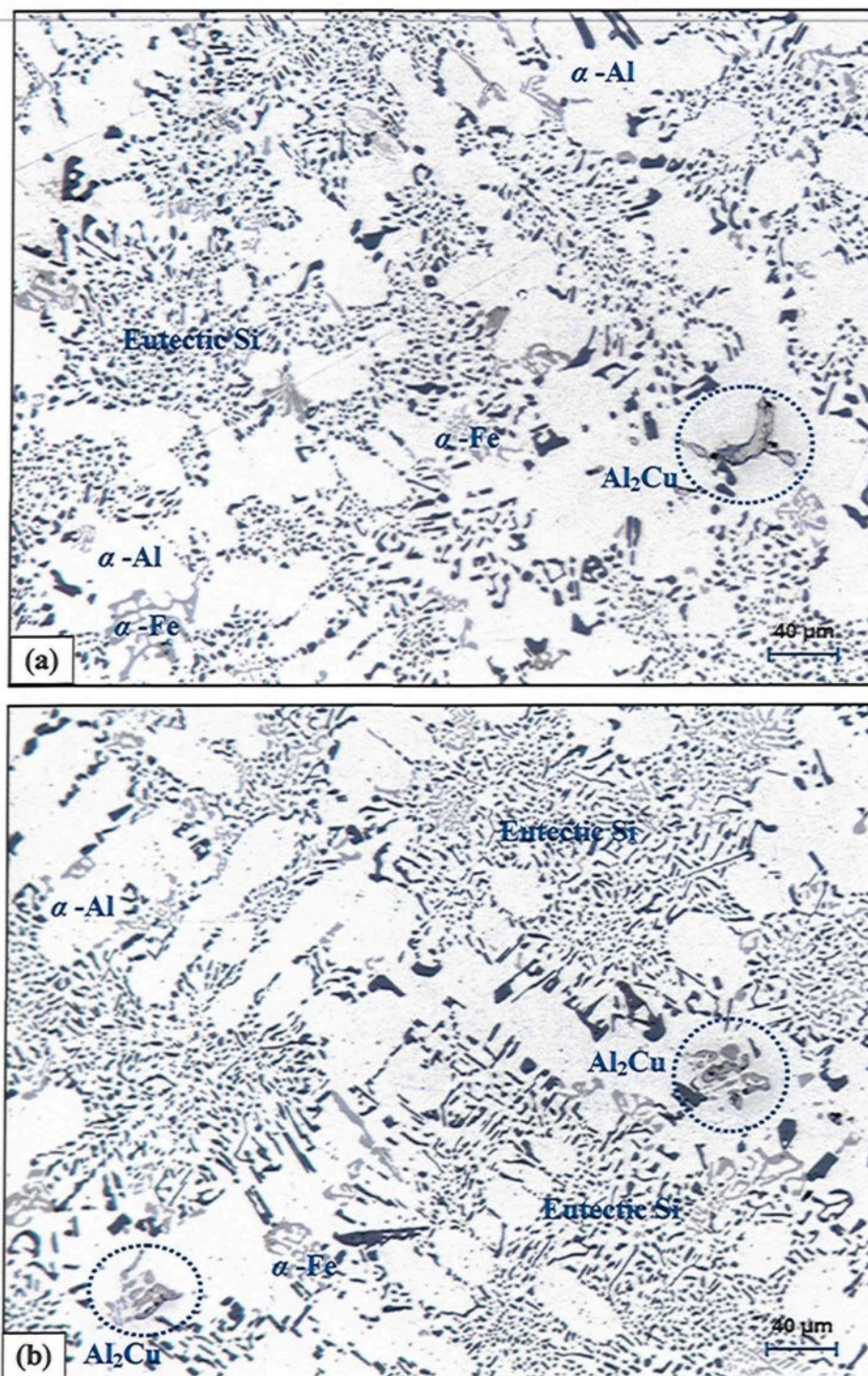


Figure 4.2 Optical micrographs showing the effects of Cu and Mg on Si morphology in grain-refined and heat-treated (a) M5 alloy; and (b) M6 alloy.

4.2.2 Iron-Rich Intermetallics

The solid-state solubility of Fe in Al is very low, the greater part of the Fe being present in the form of intermetallic compounds, the nature of which depends mainly on the alloying elements present.¹⁶⁵ Of the many existing AlFeSi intermetallics, the most important are generally thought to be the α -Fe, β -Fe, and sludge intermetallic phases. The conditions which control the formation of the α -Fe phase, as opposed to the β -Fe phase, are still not completely understood. In this study, it was observed that the addition of Sr and the presence of transition elements such as Mn in the M1 alloy are capable of promoting the development of the intermetallic α -Fe phase with its commonly observed *Chinese-script* morphology. The formation of the α -Fe phase reduces the possibility of the formation of the β -Fe phase. As may be seen in Figure 4.3, the coarse α -script particles are always seen to occur within α -Al dendrites in the M1 alloy indicating that they correspond to a predendritic reaction and tend to nucleate in the liquid alloy prior to solidification. The large size of these particles indicates the existence of a high diffusion rate of Fe occurring at high melt temperatures. The α -Fe phase has the composition $\text{Al}_{12}(\text{Fe}, \text{Mn}, \text{Cu})_3\text{Si}_2$, in other words 16.31% Fe, 9.93% Si, 13.5% Mn, 3.43% Cu.¹⁶⁶ This phase is reported as having a hexagonal structure with the parameters $a = 12.3\text{\AA}$, $c = 26.3\text{\AA}$, and a density of 3.58 g/cm^3 . The platelet-like β -Fe phase was not in evidence because of the higher Mn/Fe ratio in the M1 alloy of ~ 1.17 ; this ratio promotes the formation of the α -Fe phase at the expense of the β -Fe phase.¹⁶⁷

The α -Fe phase may precipitate either in the form of the Chinese-script phase or else as compact polygonal or star-like particles termed *sludge* with a composition close to that

of the α -Fe phase. This sludge precipitation depends upon the levels of Fe, Mn, and Cr present in the alloy, and the processing parameters which include melt holding temperature, pouring temperature, melt additives, and cooling conditions.¹⁶⁸ In this study, when the iron and manganese levels are increased from ~ 0.5 wt% in the M1 alloy to ~ 0.78 wt% in the M3 alloy, the predominant shape of the Al(Fe,Mn)Si phase, with a composition of $\text{Al}_{12}(\text{FeMnCu})_3\text{Si}_2$ is polyhedral or star-like and is located within the α -Al dendrites, as shown in the optical micrograph (b) in Figures 4.4.

When the iron content increases from ~ 0.5 wt% in the M1 base alloy to ~ 1 wt% in the M4 alloy, Chinese-script α -Fe and platelet-like β -Fe compounds form with the same level of Mn, *i.e.* ~ 0.54 wt %, as may be seen in Figures 4.5(a) and (b). The β -Fe occurs in the form of thin platelets which appear to resemble needles in a two-dimensional optical micrograph. On the other hand, fragmentation of the β -Fe was observed to result from the modifying effect of Sr and solution heat treatment, leading ultimately to the breakdown of the β needles into small thin fragments via two mechanisms:¹⁶⁹ (i) splitting of the needle/platelets into two halves through the formation of longitudinal cracks, which is enhanced greatly by the brittle nature of the β -Fe phase, and (ii) fragmentation through Si rejection. These observations confirm the findings of Villeneuve and Samuel¹⁷⁰ on the fragmentation and dissolution of the β -Fe phase during the solution heat-treatment of Al-13%Si containing different levels of iron at 540°C. The composition of the β -Fe phase is $\text{Al}_5(\text{Fe,Mn})\text{Si}$ having 20.49% Fe, 17.87% Si, and 6.21% Mn. It was found that the volume fraction of iron phases increased with the addition of increasing levels of Fe and/or Mn, as presented in Table 4.2.

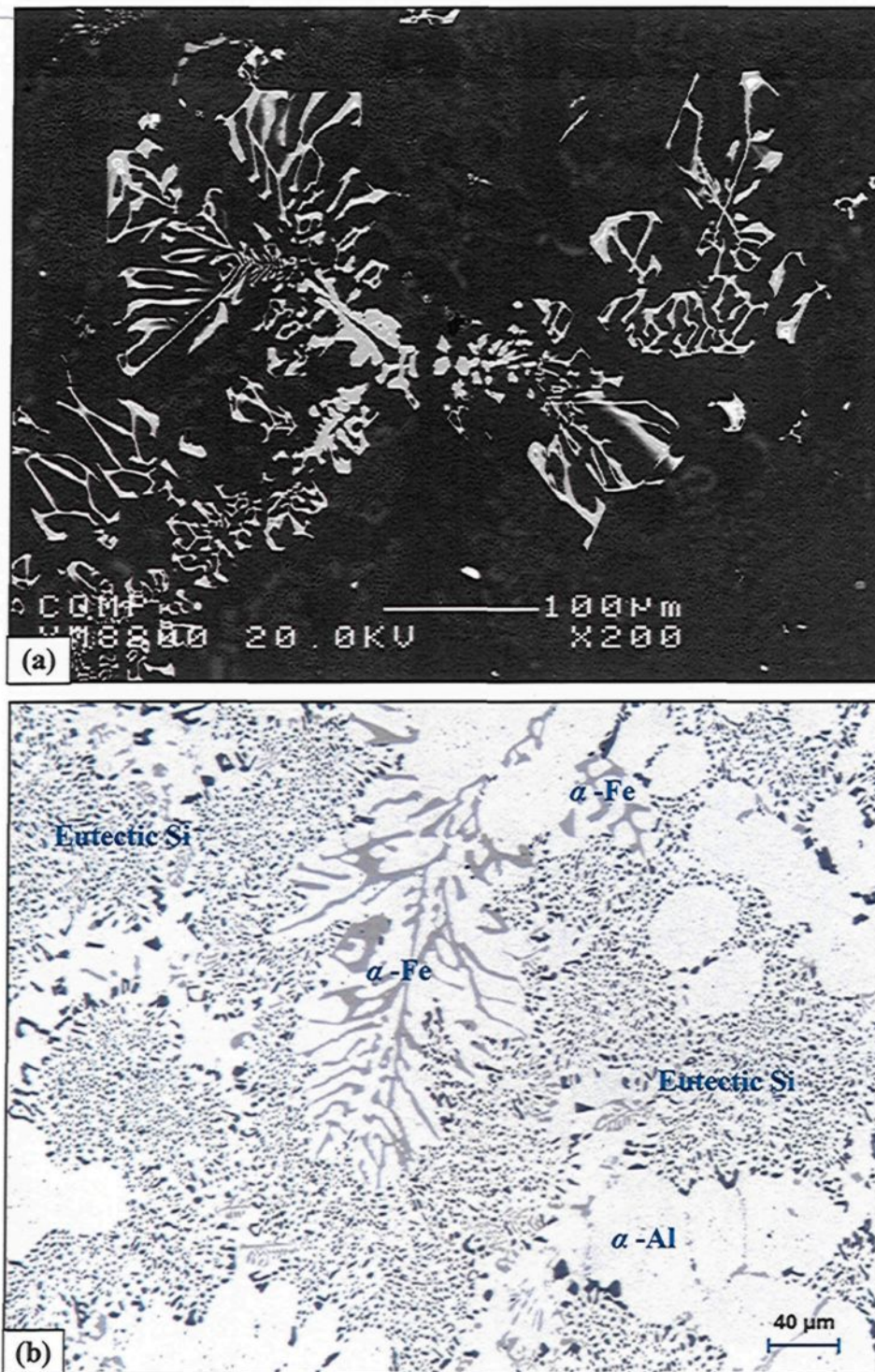


Figure 4.3 (a) Backscattered image, and (b) optical micrograph of the α -Fe phase observed in Sr-modified and grain-refined M1 alloy.

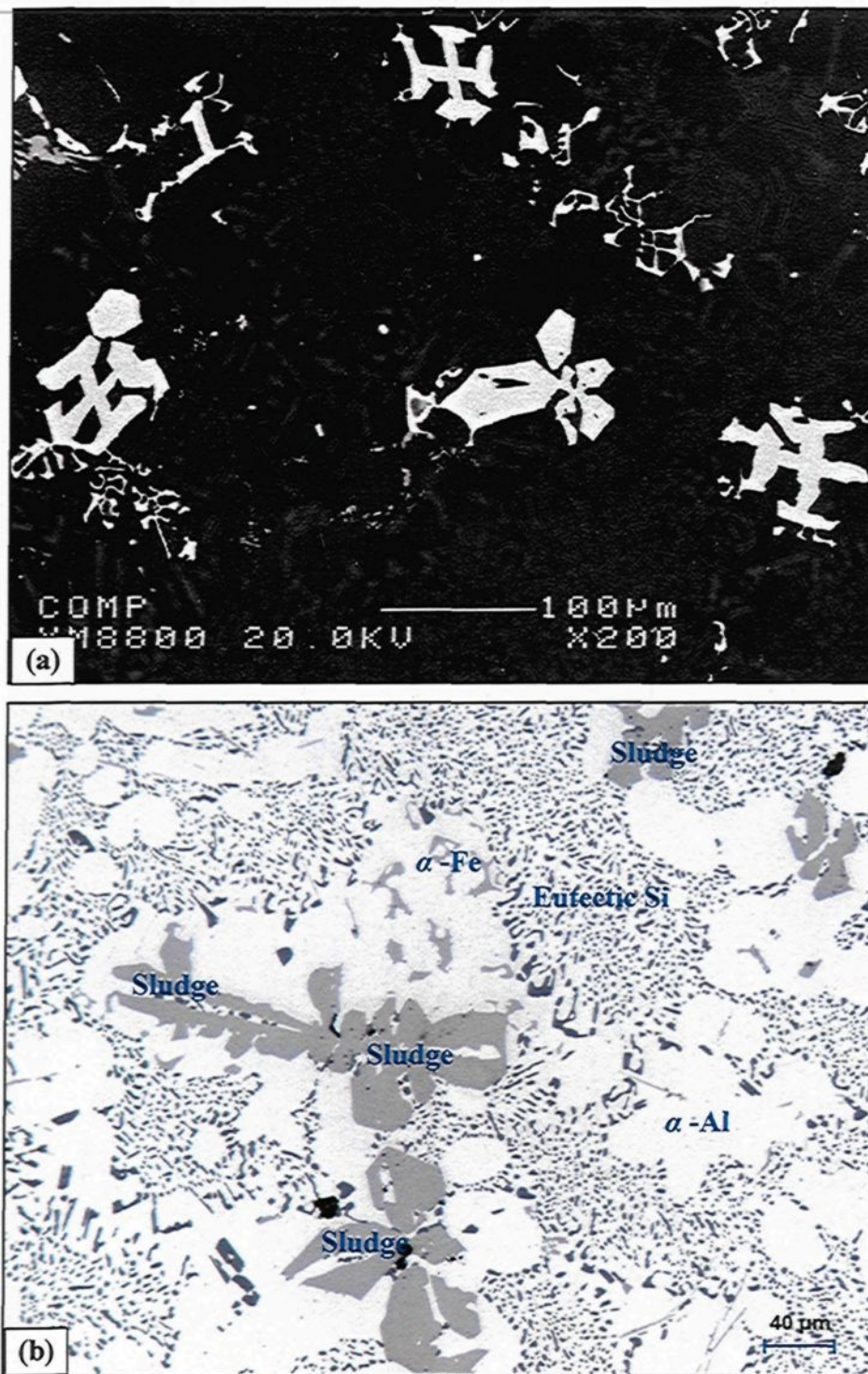


Figure 4.4 (a) Backscattered image, and (b) optical micrograph of sludge particles observed in Sr-modified and grain-refined M3 alloy.

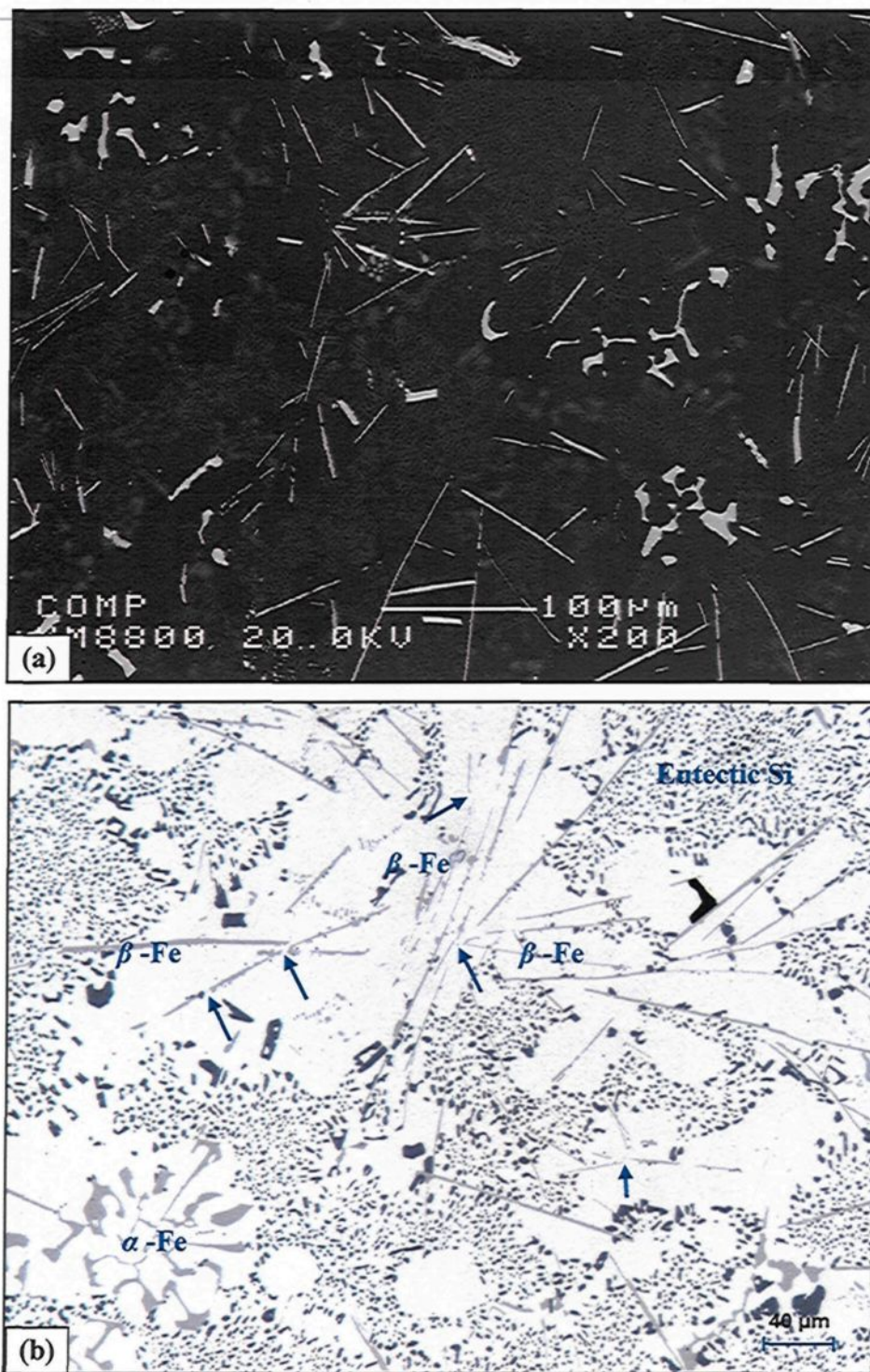


Figure 4.5 (a) Backscattered image, and (b) optical micrograph of β -Fe and α -Fe observed in Sr-modified and grain-refined M4 alloy. Arrows indicate the effects of heat-treatment and Sr on the fragmentation of β -Fe.

4.2.3 Copper-Rich Intermetallics

Alloying elements such as copper and magnesium determine which constituents will precipitate. Copper is a significant alloying addition made to aluminum because of its observable solubility and marked strengthening effect. Consequently, many commercial alloys contain Cu as either the major addition or as one of the principal alloying elements. Copper is frequently used in combination with magnesium, thereby improving the aging characteristics of the alloys.¹⁷¹ Figure 4.6(a) shows the microstructure of an experimental Mg-free M9 alloy which contains 3.67% Cu, consisting of unmodified acicular Si particles, as well as the α -Fe Chinese-script phase interspersed throughout the Si particles. The fact that the Fe-intermetallic particles are small in size, and that they occur interspersed in the Si phase, indicates that they precipitated in co-eutectic or post-eutectic reactions. The copper phase, marked A in this figure, may be seen mainly as pockets of the blocklike Al_2Cu phase nucleating either within the aluminum matrix or at the interface of such pre-existing constituents as Si or intermetallic particles.

The presence of Mg improves strain hardenability and strengthens the material according to the amount present in means of a solid solution.¹⁷² It was found that precipitation in the Al-Cu-Mg-Si alloys depends not only on the Mg content, but also on the Cu:Mg ratio in solid solution. For a Cu:Mg ratio of 2.0 (at.%), preferential precipitation of Mg_2Si occurs, while a ratio close to 8.0 promotes the formation of the Al_2Cu compound. The increase of Mg content in solid solution contributes to the precipitation phenomenon since clusters of Mg are the precursors in the formation of Mg_2Si in Al-Mg-Si alloys.¹⁷³ It was also observed that heightened Mg levels promote the precipitation process. In Mg-

containing alloys, the $\text{Al}_5\text{Si}_6\text{Cu}_2\text{Mg}_8$ intermetallic phase is reported to take place at the end of the Al- Al_2Cu eutectic reaction. The amount of this phase is found to increase progressively with an increase in Mg content. Thus, increasing the Mg content to ~0.6 wt%, thereby creating the M6 alloy, results in the formation of thick plates of $\text{Al}_5\text{Si}_6\text{Cu}_2\text{Mg}_8$, observed as grey particles in Figure 4.6(b) and marked B therein, which appear to be growing out of the Al_2Cu phase particles, marked A. The atomic weight of Cu being higher than that of Mg, the Al_2Cu phase appears brighter than the $\text{Al}_5\text{Si}_6\text{Cu}_2\text{Mg}_8$ phase shown in this figure. It is interesting to observe that the presence of Sr results in severe segregation of both $\text{Al}_5\text{Si}_6\text{Cu}_2\text{Mg}_8$ and Al_2Cu phase particles to areas away from the eutectic silicon colonies. As a result of this type of segregation, Al_2Cu may be observed mostly in the form of the blocklike phase containing high copper concentrations which are relatively difficult to dissolve during solution treatment. As confirmed through the volume fraction measurements, it was found that the volume fraction of the blocklike Al_2Cu phase increases from 0.15% in the M1 alloy containing 2.22wt% Cu to 1.71% in the M6 alloy containing 3.42wt% Cu, as shown in Table 4.2.

Table 4.2 Volume fraction of Fe- and Cu-intermetallics for the alloys studied

Alloy Code	Volume Fraction (%)	
	Fe-intermetallics	Undissolved Cu-intermetallics
M1	3.17 ± 0.51	0.15 ± 0.07
M3	4.98 ± 0.71	0.22 ± 0.12
M4	5.51 ± 0.81	0.3 ± 0.29
M5	3.12 ± 0.14	1.70 ± 0.4
M6	3.07 ± 0.86	1.71 ± 0.39
M9	3.22 ± 0.77	1.73 ± 0.39

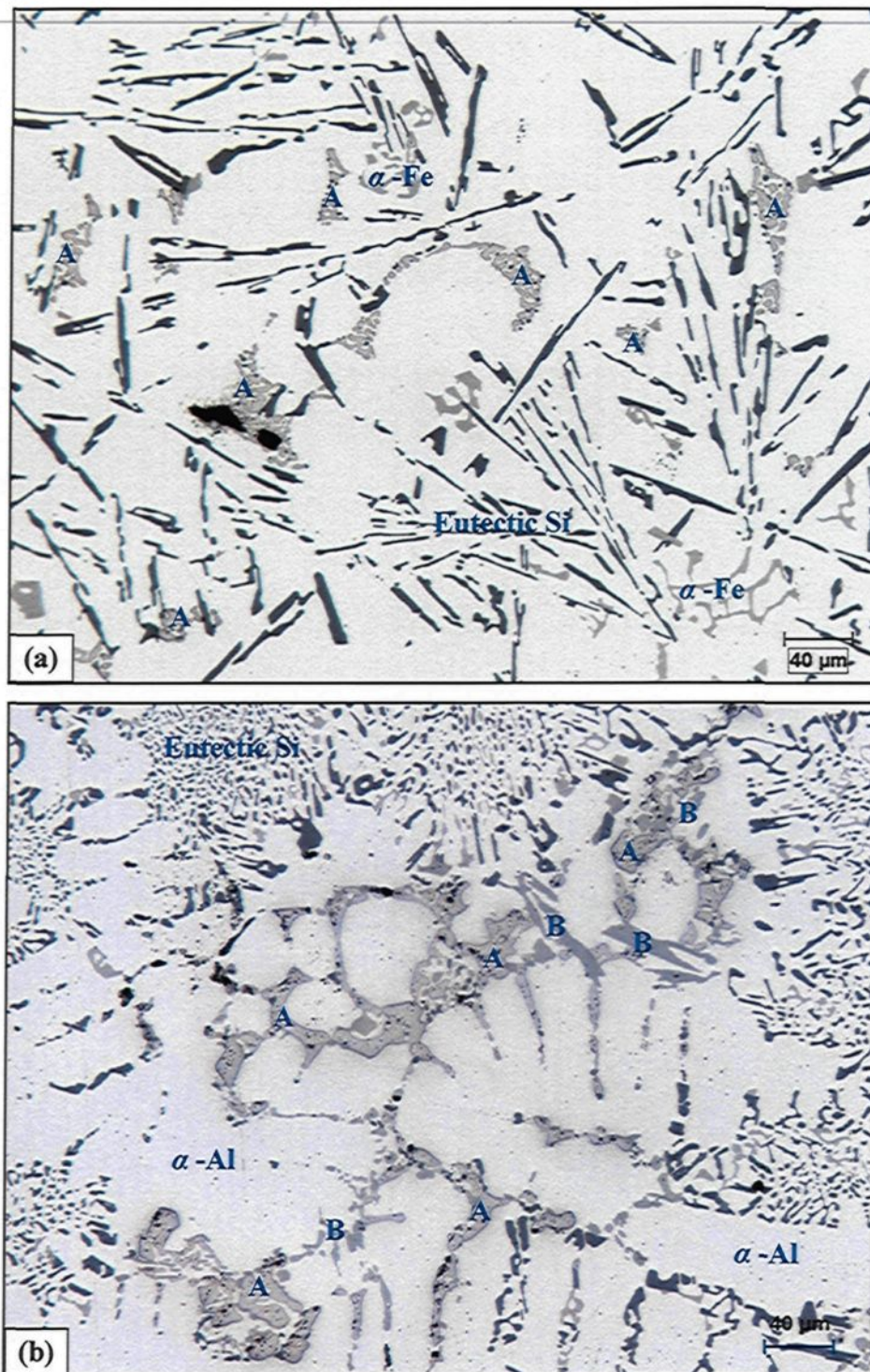


Figure 4.6 Optical micrographs of (a) heat-treated Mg-free M9 alloy, and (b) heat-treated M6 alloy containing 0.6% Mg showing precipitation of both the blocklike Al_2Cu phase (marked A) and the $\text{Al}_5\text{Si}_6\text{Cu}_2\text{Mg}_8$ phase (marked B).

4.3 HARDNESS AND TENSILE PROPERTIES

With regard to machinability, it was reported that heat treatment which increases hardness would reduce the built-up edge (BUE) on the cutting tool and would improve the surface finish of the machined part. A minimum hardness value situated in the range of 90-100 BHN for an alloy casting is to be recommended since this would tend to avoid difficulties associated with built-up edge on the cutting tool. Thus, a specific T6 heat treatment was selected to establish the hardness level for the alloys investigated within the range of 110 ± 10 BHN. Such a hardness range is considered suitable because it conforms to most of the required hardness levels observed in the commercial application of aluminum alloys. Hardness measurements were carried out on the heat-treated machinability test blocks to ensure that they possessed the required hardness levels. The average hardness value and standard deviations for each alloy composition studied are provided in Table 4.3. The corresponding hardness data indicate that the decrease in the hardness value of the Sr-modified M1 alloy compared to the non-modified M0 alloy is mainly the result of changes in the morphology of the eutectic Si particles, from brittle coarse acicular plates in the M0 alloy to a rounded fibrous form, as shown in Figures 4.1(a) and (b). Also, Sr leads to a depression in the eutectic temperature causing a shift of the eutectic point to a higher Si content, resulting in an increase in the amount of soft α -Al formed.⁴⁰

From Table 4.3, it will be observed that an increase in Fe and/or Mn content results in a slight increase in hardness values. It was also found that the addition of combined Cu and Mg to the M1 alloy, creating the M6 alloy, produces a considerable increase in the hardness values.

Table 4.3 Summary of mechanical properties for the alloys studied

Alloy Code	BHN (MPa)	YS (MPa)	UTS (MPa)	EI (%)
M0	119 ± 3.45	346.11 ± 5.92	382.78 ± 2.36	0.92 ± 0.09
M1	108 ± 3.56	358.1 ± 1.55	394.04 ± 6.27	0.98 ± 0.12
M3	111 ± 4.39	326.84 ± 2.13	354.72 ± 4.86	0.84 ± 0.04
M4	113 ± 3.95	320.4 ± 12.7	339.5 ± 9.85	0.51 ± 0.02
M5	117 ± 3.19	358.94 ± 7.45	369.99 ± 8.54	0.76 ± 0.14
M6	120 ± 4.45	392.7 ± 6.8	396.14 ± 6.8	0.66 ± 0.02
M9	104 ± 4.55	200.65 ± 4.70	300.82 ± 19.16	1.70 ± 0.47

There is a distinct possibility that the hardness increment in M5 and M6 alloys may be attributed to the formation of hard and brittle intermetallic phases of Al_2Cu and Al_2CuMg , as well as to an increased bonding of the silicon particles with the matrix, in which the thermal energy is sufficient to precipitate such intermetallics phases as are coherent with the matrix.¹⁷⁴ It should be mentioned that the hardness values of the machinability test blocks, however, still fall within the required range.

Tensile testing was also carried out to assess the changes occurring in the aluminum matrix and eutectic silicon as a result of the addition of Sr and other alloying elements. Table 4.3 provides the tensile properties including the YS at a 0.2% offset strain, the UTS, and the %EI for the alloys investigated. The modified M1 alloy displays somewhat higher YS, UTS, and %EI values than the unmodified M0 alloy, because of the improved eutectic silicon phase morphology caused by Sr modification. It will also be noted that as the percentage of Fe and/or Mn increases beyond 0.75%, the YS, UTS, and ductility decrease to a significant degree, a fact which may be attributed to the presence of the β -Fe phase in the structure of the M4 alloy. The high stress concentrations at the sharp edges of the β -

phase, as well as the weak bonding between the β -phase and the Al matrix, enhance crack initiation and thus decrease the ductility of this alloy.¹⁷⁵ With regard to the addition of Cu and Mg to the M1 alloy, it may be observed that at high Mg levels of ~ 0.6 , the ductility is considerably lower, as observed in the case of the M6 alloy. Such a result may be attributed to the influence of both Sr and Mg on the severity displayed by the Al_2Cu phase segregation, resulting in the formation of large amounts of the coarse blocklike form of the phase, as shown in Figure 4.6(b). Table 4.2 also provides the measurement of the volume fraction for the undissolved Al_2Cu phase. Further effects may be attributed to the formation of hard brittle $\text{Al}_5\text{Si}_6\text{Cu}_2\text{Mg}_8$ particles which remain largely unaffected by solution heat-treatment, as confirmed by the research carried out by Mohamed *et al.*¹⁶⁶ It was also found that the Mg-free M9 alloy displays a significant reduction in the YS and UTS values compared to the M1 reference-alloy. This observation is in satisfactory agreement with results obtained from previous work⁴⁴ which reported that the addition of Mg proves to be an excellent way of achieving a high level of tensile strength, however at the expense of ductility.

4.4 MACHINING BEHAVIOR

The upcoming sections will discuss the machinability behavior of the alloy conditions investigated in this work with respect to the total cutting force and moment, tool life expressed as the number of holes drilled/tapped up to the point of tool breakage, chip configuration, and built-up edge (BUE) evolution. The drilling and tapping tests were carried out under fixed machining conditions of speed, feed, depth of hole drilled/tapped, tool geometry, tool material, and coolant.

4.4.1 Effects of Fe-Intermetallics on Machinability

The number of insoluble phases present in the microstructure is dependent upon the Fe level in the alloy. Lowering the Fe content is extremely effective in suppressing the formation of the needle-like β -Fe intermetallic phase and in preventing sludge formation, thereby ultimately improving tool life. The modification of Fe intermetallics, through the addition of such suitable neutralizers as Mn and Cr, converts the β -Fe platelets into the more compact and less harmful α -Fe scriptlike phase. This phase shows an irregular, curved crystal growth which conforms to the complicated shape of the interdendritic spaces during solidification. The α -Fe has a non-faceted interface with the aluminum matrix, and exhibits no growth twinning which allows for a better bonding with the aluminum matrix. The β -Fe, on the other hand, grows in a lateral or faceted mode which is poorly bonded to the aluminum matrix.¹⁷⁶

4.4.1.1 Cutting Forces and Moments

The mean total drilling force, the mean total drilling moment, and the mean drilling power together with the corresponding standard deviation bars based on the mean value of 90 holes were all used as a way of evaluating the effects of the iron intermetallics, namely, α -Fe, β -Fe, and sludge, on the drilling process. Consequently, certain alloys responding to specific criteria were selected; these include heat-treated, Sr-modified, and grain-refined Al-10.8%Si near-eutectic alloys, represented respectively by (i) 396 + 200 ppm Sr + 0.2% Ti reference alloy coded M1 containing α -Fe; (ii) M1 + 0.25%Fe + 0.25%Mn alloy coded M3 containing sludge; and (iii) M1 + 0.5%Fe alloy coded M4 containing β -Fe and α -Fe, yielding hardness values of 108, 111, and 113 BHN, respectively.

The results obtained from the drilling tests reveal that the mean total drilling force, the mean total drilling moment, and the mean drilling power all increase as the number of holes drilled increases; this is clear from Figures 4.7(a), (b), and (c), respectively. With regard to this observation, the mean total drilling force of the M1 alloy increases from 317.97N after drilling 90 holes to 645.38N after drilling 2160 holes, a corresponding increase of 106%; this analysis agrees with the mean total drilling moment of the M1 alloy which was found to have increased by virtually the same amount, *i.e.* 105%. It will also be seen that the mean drilling power of the M1 alloy increases from 1.89 kW after drilling 90 holes to 4.42 kW after drilling 2160 holes, thus corresponding to an increase of 134%. A similar trend was also observed during the drilling of the M3 and M4 alloys. This rapid increase in the drilling force, moment, and power in conjunction with the progress of the cutting process during the machining of the 396 alloy containing 10.8%Si may be attributed to the presence of the silicon phase which is almost ten times harder than aluminum matrix.

The addition of 0.25%Fe and 0.25%Mn to the M1 base alloy, producing the M3 alloy which contains sludge as a predominant phase, leads to an extremely rapid increase in the total drilling force from 334.48N after drilling 90 holes to 586N after drilling only 540 holes, a corresponding increase of 75% over the evaluation period of 540 holes; similar behavior was also observed with regard to the total drilling moment and power, as shown in Figure 4.7. This significant increase in cutting force may be explained by the formation of the hard complex intermetallic sludge phase as the predominant phase in the M3 alloy. The sludge may be seen clearly in the backscattered image and optical micrograph shown earlier in Figure 4.4. It has also been reported that the microhardness of sludge usually lies

between 500 and 900 BHN, as compared to a matrix hardness of 108 BHN for the 396 alloys.^{14, 23} The sludge phase may act as an abrasive in an otherwise relatively soft matrix and it is capable of causing excessive tool wear, thereby increasing the cutting force and moment. Figure 4.8 shows aggressive wear on the drill edge after drilling 540 holes during the machining of the sludge-containing M3 alloy. It should also be noticed that the fluctuations of the total drilling force and moment values during the drilling of the M3 alloy results from the distribution and the size of the sludge particles within the alloy structure itself.

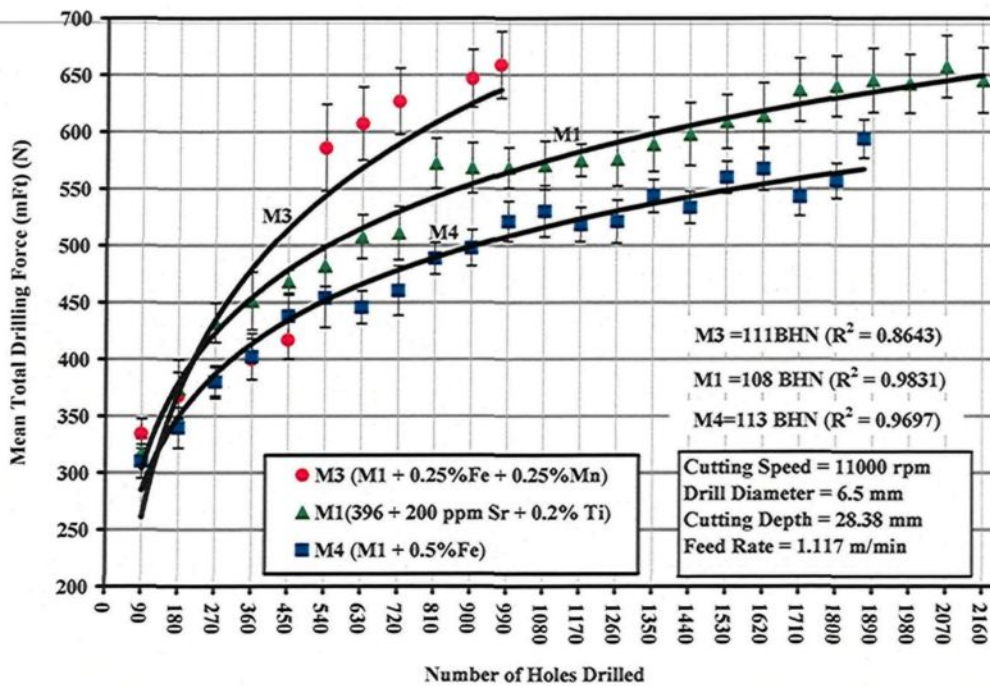
The addition of 0.5%Fe to the M1 base alloy, thereby producing the M4 alloy which contains a relatively thin form of β -Fe as the predominant phase, results in a considerable improvement in alloy machinability through (i) a lowering of the drilling force by 10%, ranging from 6% to 14%, (ii) a lowering of the drilling moment by 14%, ranging from 9% to 20%, and (iii) a decreasing of the drilling power by 24%, ranging from 15% to 30%, over the evaluation period of 1867 holes compared to the M1 alloy, as shown in Figures 4.7(a), (b), and (c). The preceding observations may be understood in the light of the effects which the presence of the β -Fe phase is known to have on ductility. As was listed earlier in Table 4.3, the ductility of the M4 alloy decreases noticeably, by about 50%, compared to the M1 alloy. The lower ductility value displayed by the β -Fe-containing M4 alloy lessens the drill-chip friction which in turn decreases the drilling forces, moment, and power. It has been reported by a number of observers that, as the ductility increases, plastic deformation takes place in the cutting zone and consequently cutting resistance becomes greater, causing the cutting force to be higher.^{177,178}

Tapping is known as a complex cutting process because of the multi-flute/multi-land engagement between the tap and the hole. In contrast to other machining processes such as turning and milling, tapping does not attain significantly high cutting speeds. Although modern machines are capable of high-speed rotations, the volume of material to be removed at once in tapping is relatively high. Also, a fast reversion in the change from the cutting cycle to the return cycle would be required, while the synchronism between rotation and axial displacement could create additional difficulties for certain machines.¹³³ As a result of a number of problems, some of which were pointed out above, the normal cutting speeds used in tapping operations are relatively low, *i.e.* around 10 m/min (400 rpm), compared to the high speeds involved in the drilling processes, *i.e.* around 234 m/min (11000 rpm).

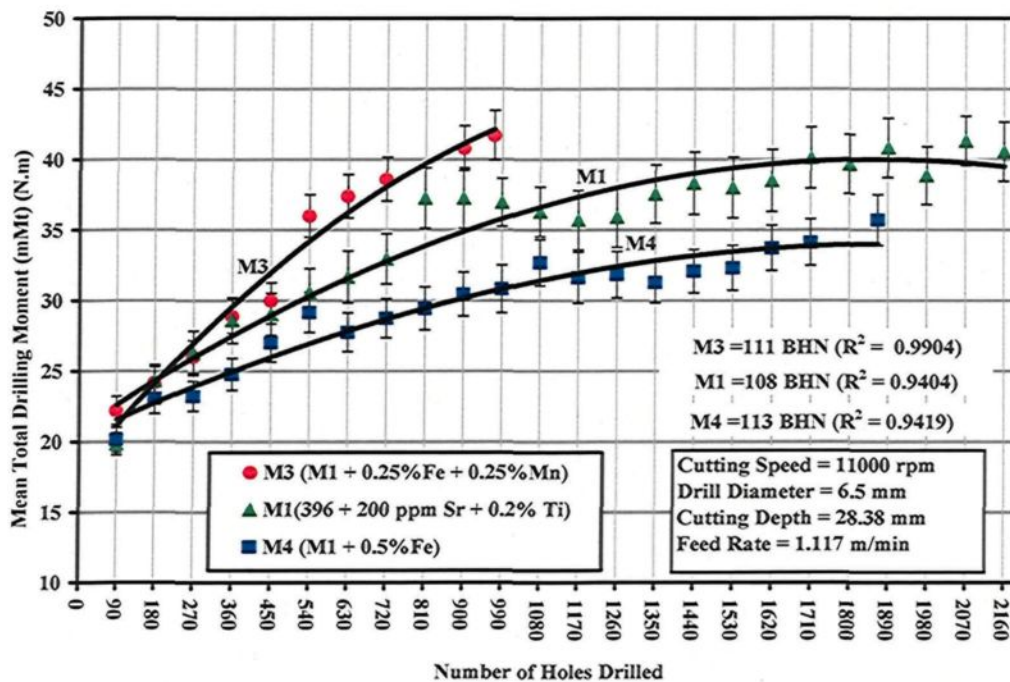
In the tapping test, the mean total tapping force and mean total tapping moment were used as criteria for characterizing the alloys studied. The effects of Fe-intermetallics on the tapping force and moment for the M1, M3, and M4 alloys are shown in Figures 4.9(a) and (b). It will be clearly observed that the presence of sludge as the predominant phase in the M3 alloy results in a noticeable increase in the tapping force and moment compared to the M1 alloy containing the α -Fe phase. In this regard, the M3 alloy required an average 30% higher tapping force ranging from 12% to 48% and displaying an average 15% higher tapping moment ranging from 10% to 20% compared to the M1 alloy. It should be mentioned that HSS taps were used for the tapping test instead of a carbide drill which was used for the drilling tests; the sludging produced in this way led to such

deleterious effects as hard-spot particles in the alloy structure, ultimately resulting in a significant increase in the tapping force and moment.

It will also be observed that the thin β -containing M4 alloy has the same effect on the tapping force and moment as the one observed in the drilling test, since the tapping force was reduced by 11% ranging from 2% to 20% compared with the M1 alloy. The tapping moment was decreased by almost the same ratio. This reduction occurring in the tapping force/moment values of the M4 alloy may be explained in the same manner as were the effects resulting from the presence of the β -Fe phase during drilling the tests.



(a)



(b)

Figure 4.7 Contd.

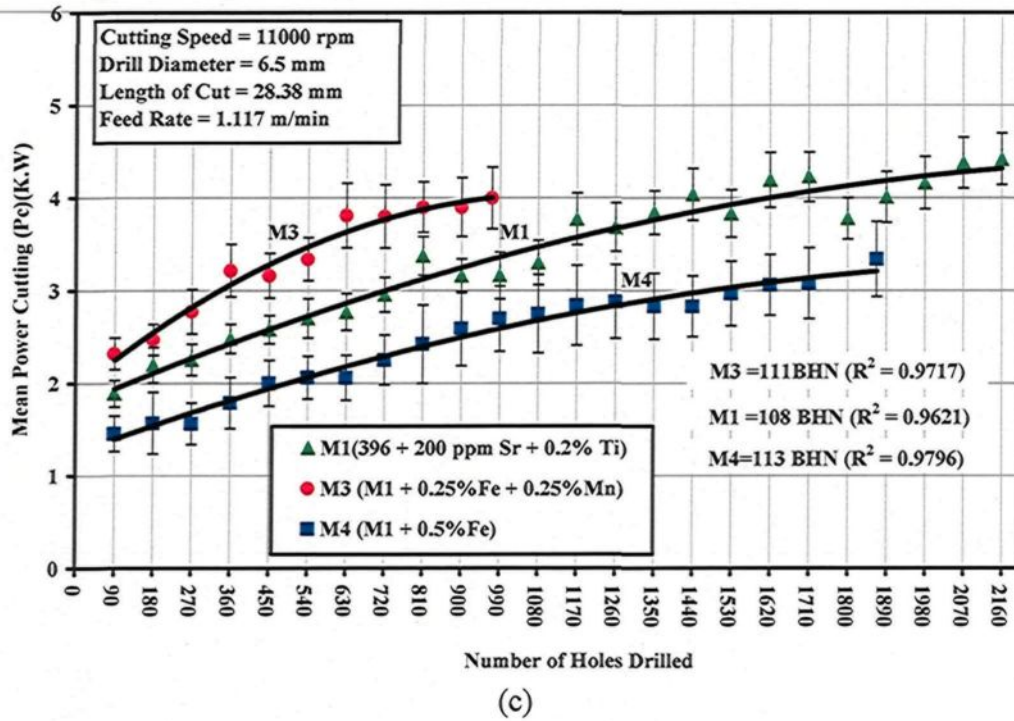


Figure 4.7 Effects of Fe-intermetallics on the machinability of M1, M3, and M4 alloys in terms of (a) mean total drilling force; (b) mean total drilling moment; and (c) mean power cutting required for drilling 90 holes.

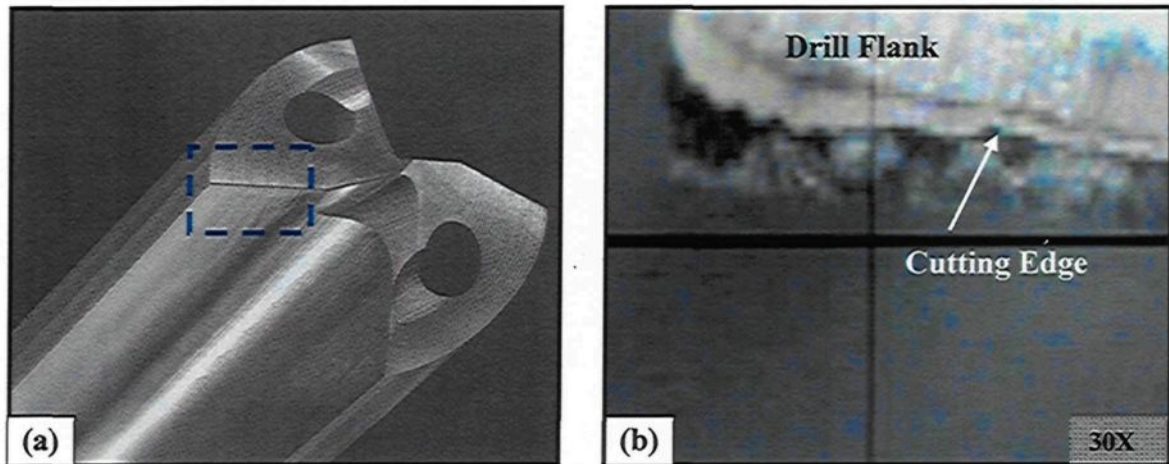
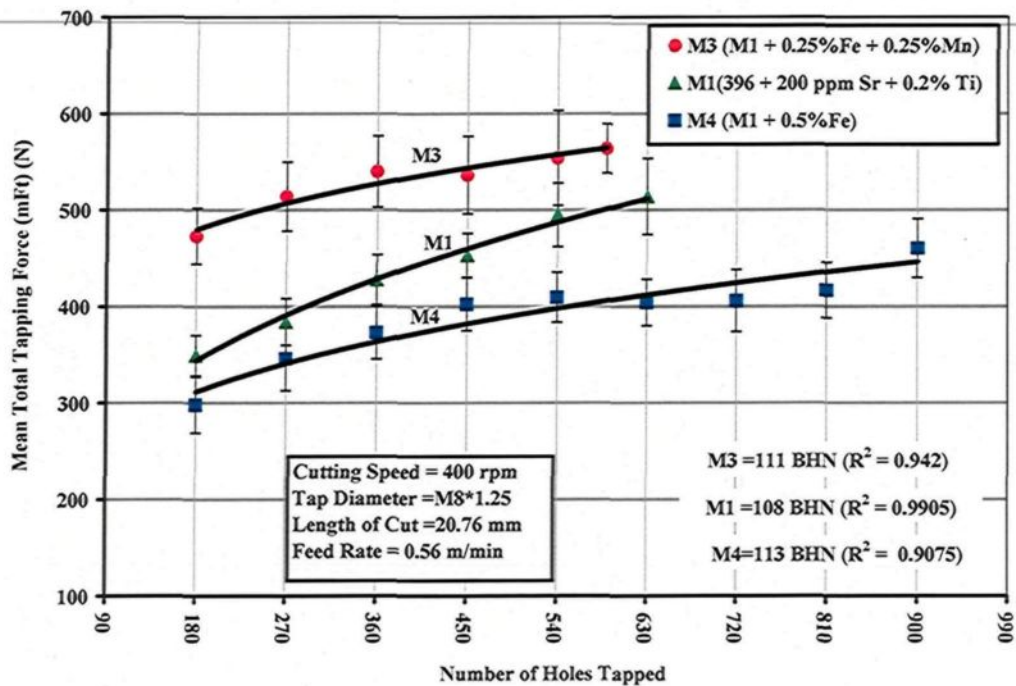
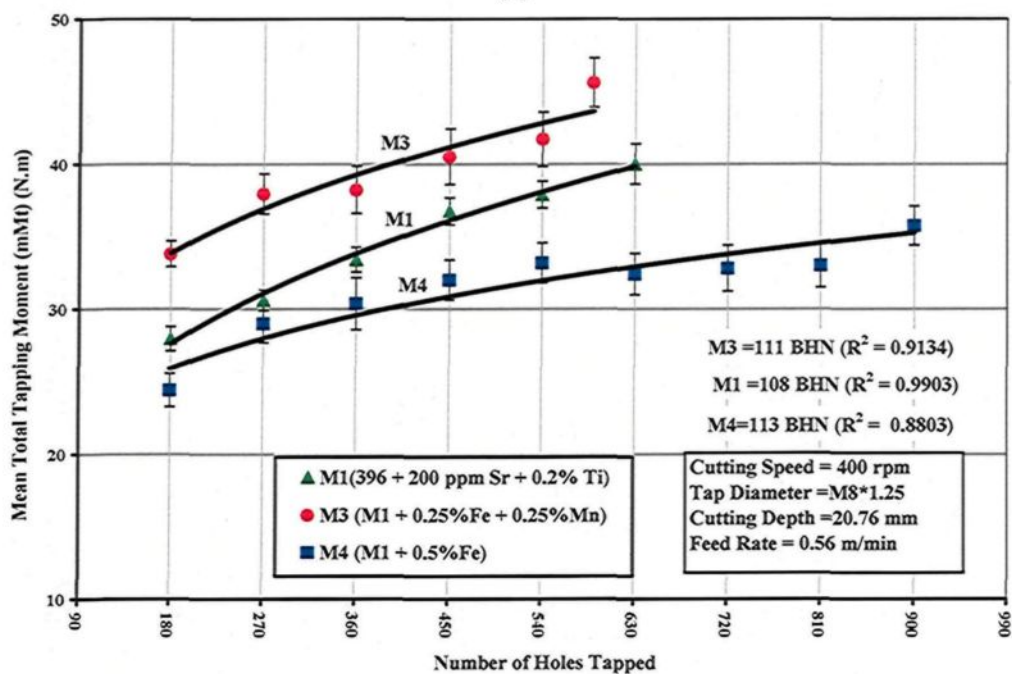


Figure 4.8 (a) Photograph of drill illustrating area investigated; and (b) photograph showing the effect of sludge on the cutting drill edge after drilling the M3 alloy.



(a)



(b)

Figure 4.9 Effects of Fe-intermetallics on the machinability of M1, M3, and M4 alloys in terms of (a) mean total tapping force; and (b) mean total tapping moment required for tapping 90 holes.

4.4.1.2 Tool Life

The dominant variables governing tool life are: the silicon content, the temperatures occurring at the contact surfaces of workpiece and tool, the hard-spot or sludge inclusions, and the non-metallic inclusions.¹⁷⁹ For each alloy composition, the tool life criterion was expressed in terms of the number of holes drilled/tapped up to the point of tool breakage. It should be kept in mind that each of the drilling and tapping tests was carried out at least twice to validate the reported values of tool life, as shown in Figure 4.10.

The base alloy M1 shows the highest number of holes, 2160, followed by the M4 alloy containing 0.5%Fe with ~1867 holes, and finally the M3 alloy with 0.25%Fe + 0.25%Mn showing only 971 holes. It is thus clear that the base alloy M1, containing mainly α -Fe, produces the highest number of holes drilled; this result may be explained by the fact that the formation of the α -Fe intermetallic phase and its within the α -Al dendrites rounded Chinese-script morphology is expected to improve matrix homogeneity by means of hardening of the soft α -Al dendrites, as shown previously in Figure 4.3. The formation of the coarse α -Fe phase may be related to the presence of Sr which seems to cause a significant segregation of Fe towards certain zones of the molten metal, leading to the precipitation of the α -Fe phase, which is then followed by the formation of the α -Al dendrites surrounding it. In addition, the interface between the α -Fe and the aluminum matrix is atomically rough, contributing to a greater stability of the α -Fe phase within the matrix during machining, and thereby also improving overall alloy machinability.

A comparison of the M1 and M3 drilling results, notably in terms of number of holes drilled, reveals that the M3 alloy, which contains mainly sludge of the hard-spot type

as the predominant phase, is more sensitive to tool wear than is the M1 alloy. Hence the presence of sludge has a significant effect on tool life, in that it decreases drill life from 2160 holes in the M1 alloy to 971 holes in the M3 alloy, a corresponding decrease of 50%. From the preceding, it is clear that the sludge phase has high hardness values, a high melting point, and a high specific gravity compared to the matrix, and it is consequently capable of causing damage to cutting tools; this phase is liable to cause rapid tool wear and to bring on all of the attendant problems accompanying a dull tool, confirmed by drill wear examination using a toolmaker's microscope, as shown in Figure 4.8(b).

On the other hand, the M4 alloy containing mainly β -Fe as the predominant phase, displays an increase in the length of drill life by 48% compared to the M3 alloy; showing a slightly lower number of holes drilled compared to the M1 alloy having 1867 holes with 2160 holes drilled in M1 alloy. It is interesting to note that increasing the iron level from ~0.5 to 1% while maintaining the same Mn level of ~0.5% proves to be most effective in terms of cutting force and tool life in the drilling and tapping processes. This observation may be explained by the fact that the detrimental effects of Fe may be partially neutralized by adding Mn in proportions greater than half the Fe concentration. As shown in the discussion on microstructure and illustrated in Figure 4.5, the fragmentation of β -Fe and the production of a relatively finer β phase will tend to have a direct influence on increasing the homogeneity of the matrix and hence prolonging tool life as a result of solution heat treatment and the addition of Sr. This outcome is also consistent with results recorded by Komiyama *et al.*¹⁸⁰ who showed that Mn has a powerful effect on alloy properties although only at iron contents of greater than 1%.

It is important to report that the M4 alloy yielded the lowest drilling force, moment, and power of the Fe-intermetallic alloy group attributable to the presence of β -Fe which diminishes ductility and tensile strength, thereby decreasing the cutting resistance with respect to drilling force and moment. By contrast, the β -Fe causes a slight shortening of drill life compared to the α -Fe containing M1 alloy. If the β -Fe phase particles are considered inclusions in the alloy structure, then, as has been reported, the reduction in the cutting tool life will depend mainly on non-homogeneities and hard-spots, as well as inclusions.⁹ As a result, it may be concluded that drill life is strongly dependent on the critical size and distribution of the β -Fe phase. The optical micrograph of the M4 alloy shown in Figure 4.11, reveals two distinct types of β -Fe platelets including the smaller co-eutectic or post-eutectic β particles (marked 2) which is the predominant phase, and the large pre-eutectic β particles (marked 1), each corresponding to the precipitation sequence related to the Al-Si eutectic reaction. The effects of Sr on the fragmentation and dissolution of β platelets was observed for the smaller co-eutectic β particles, whereas the large pre-eutectic β particles remained unaffected, as shown in the same figure. The pre-eutectic β -Fe phase platelets are the most pernicious in that they contribute to the deterioration of tool life because of their size and shape.

In tapping tests, it was found that high-speed steel tools react considerably more sensitively to the Fe-intermetallic phase than do the carbide tools used for drilling. The high speed steel tap (HSS-E) broke down after tapping only 630, 589, and 900 holes in the M1, M3, and M4 alloys, respectively, as shown in Figure 4.10.

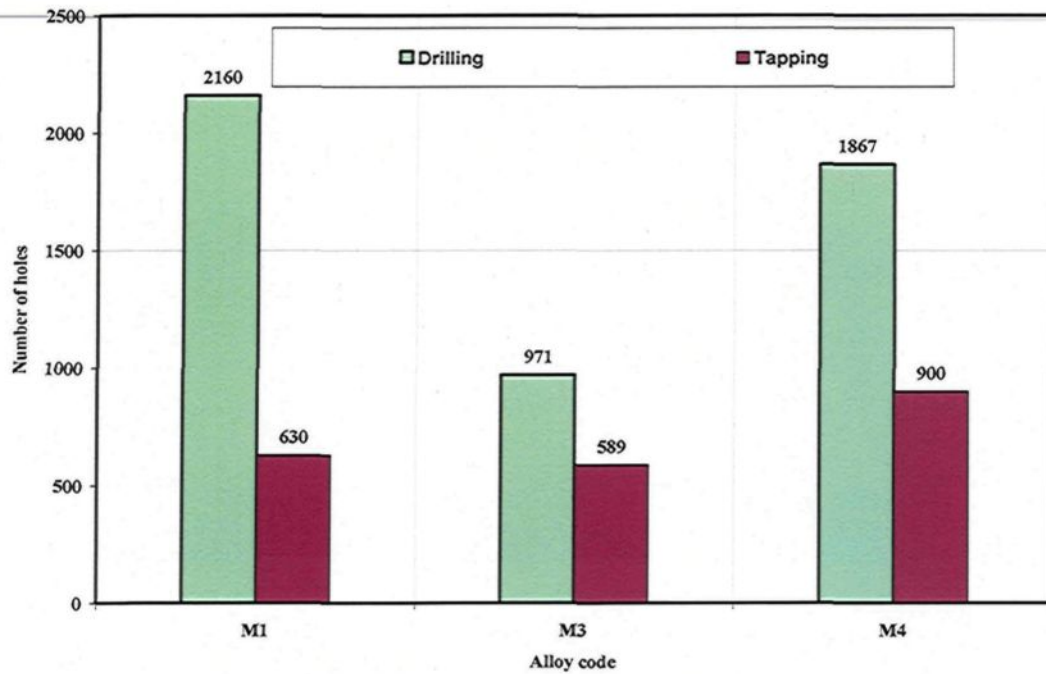


Figure 4.10 Effects of Fe-intermetallics on the drill/tap life of the M1, M3, and M4 alloys in terms of the number of holes drilled and tapped.

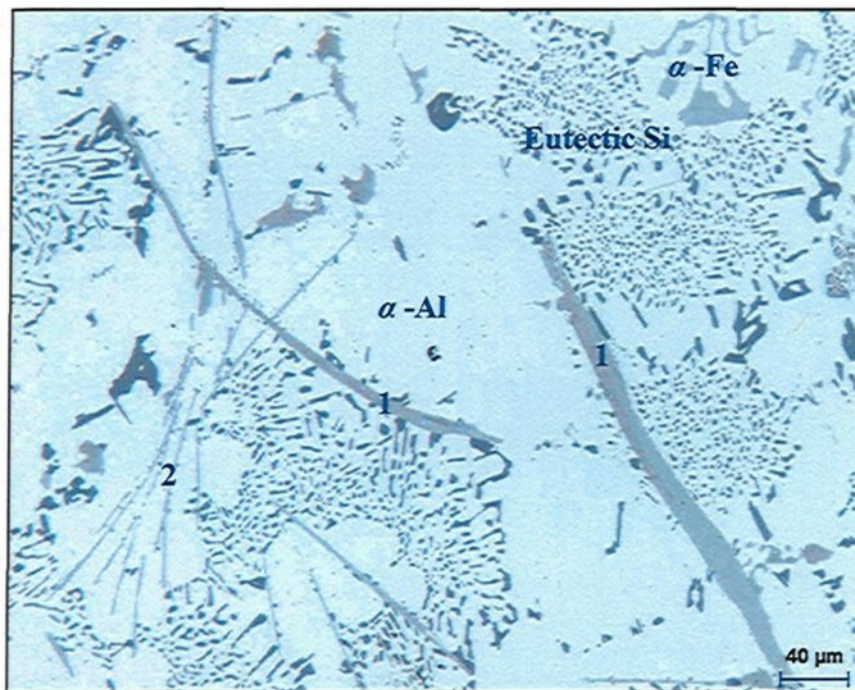


Figure 4.11 Optical microstructure of the M4 alloy showing precipitation of (1) pre-eutectic β -Fe, and (2) post-eutectic β -Fe.

4.4.2 Effects of Cu and Mg Additions on Machinability

Cast aluminum-silicon alloys contain mainly Cu and Mg as the major alloying elements. Magnesium is normally used to improve the mechanical properties of the alloy through the precipitation of the Mg_2Si and Al_2CuMg intermetallics.¹⁸¹ The Cu and Mg content of the alloys determines the precipitation strengthening and the volume fraction of Cu-rich and Mg-rich intermetallics obtained.¹⁸² Regulating the morphology, volume fraction, and distribution of these intermetallics will improve the alloy matrix homogeneity and hence improve its machinability.¹⁸³ With regard to machinability as one of the characteristics of a given alloy, there are studies in the literature reporting the effects of metallurgical characteristics as being important factors in this context; these characteristics comprise the chemical composition, the microstructure, and the morphology of second phase particles of the alloy.¹⁸⁴ A particular characteristic of the two-phase and multiphase microstructures of Al-Si alloys is the fact that the matrix phase is soft and highly ductile whereas the second phase is considerably harder. In order to obtain a good surface finish, it is important that the particles of the hard phase be fine and uniformly distributed within the soft, aluminum matrix.²¹

Conversely, most aluminum alloys are fairly soft in relation to cast iron and steel, and are commonly machined by high speed steel (HSS) tools, although an exception to this may be observed with aluminum-silicon alloys.¹⁸⁵ Near-eutectic Al-Si alloys are said to be the most difficult to machine out of the various types of Al-Si alloys, as is evidenced by the fact that the silicon phase present is almost ten times harder than the aluminum base alloy, thus causing the cutting tools to wear out rapidly.¹⁸⁶ For this reason, consistent attempts

have been made to optimize the selection of cemented carbide tools,¹⁸⁷ cutting conditions, and tool geometry; investigation of the following points was also recommended: (i) the effects of flank build-up on tool wear,¹⁸⁸ (ii) the effects of cutting fluids on machinability,¹²⁶ and (iii) the improvement of machinability through the addition of certain elements.¹⁸⁹ Although Cu and Mg are the main additives used to strengthen the alloys in the Al-Si systems, their effects on the machinability of near-eutectic Al-Si casting alloys has rarely been taken into account.

The presence of Cu leads to the formation of Al₂Cu particles, which when refined and dispersed, improve machinability by causing a decrease in plasticity, and ultimately result in chip embrittlement.¹⁹⁰ In the research¹⁹¹ carried out on the relationship between chip breakability and aging treatment in Al-Cu and Al-Cu-Si alloys, chip breakability successfully improved with the increased size of second-phase particles accompanied by advanced aging. In this case, however, it was pointed out that chip breakability was also related to the cracking of the second-phase particles and the ductility of the matrix around them. Nevertheless, these facts suggest that the chip breakability of Al alloys is expected to improve with the dispersion of some kind of second-phase particle, since this could be the cause of the chip breaking through cracking during machining; it should be remembered that there are various second-phase particles, including precipitates and crystallized particles, in commercial Al alloys.⁴⁹ The production of small brittle chips favors intermittent cutting, making chip extraction away from the cutting easier, while at the same time inhibiting the formation of a built-up edge on the cutting edge of the tool.

4.4.2.1 Cutting Forces and Tool Life

Drilling and tapping tests were carried out under constant cutting conditions to investigate the influence of Cu and Mg additions as well as of Sr-modification on the machining behaviour of a number of grain-refined and T6 heat-treated Al-10.8%Si near-eutectic alloys. The alloys in question were represented by the following:

396 + 200 ppm Sr + 0.2%Ti, coded M1 alloy;

M1 + 1%Cu, coded M5 alloy;

M1 + 1%Cu + 0.25%Mg, coded M6 alloy;

non-modified Al-10.8%Si-Cu-Mg experimental alloy, coded M0 alloy; and

Mg-free Al-10.8%Si-3.5%Cu experimental alloy, coded M9 alloy,

yielding 110 ± 10 BHN hardness level.

The results from drilling tests reveal that the mean total drilling force, moment, and power increase as the number of holes drilled increases, as shown in Figures 4.12(a), (b), and (c). From this figure, it will be observed that the drilling force, moment and power display a virtually linear trend during the drilling of the Mg-free M9 alloy, while in comparison the M1 base alloy shows a rapid increase in the cutting force. More specifically, the mean total drilling force of the M1 alloy increases by 103% over the evaluation period of 2160 holes. In contrast, the mean total drilling force of the Mg-free M9 alloy increases from 204N after drilling 90 holes to 316.8N after drilling 3240 holes, *i.e.* approximately a 55% increase. This analysis is in agreement with the mean total drilling moment and power of the M1 alloy which was found to have increased by 105% and 134%, respectively, as shown in Figures 4.12(b) and (c). On the other hand, the mean total drilling

moment and the mean drilling power of Mg-free M9 alloy increased by 53% and 60%, respectively.

The machining characteristics of the Al-10.8%Si near eutectic alloy depend mainly on the shape, size, and distribution of α -Al dendrites, eutectic Si morphology, and Al₂Cu particles in the interdendritic region. Figures 4.12(a), (b), and (c) show that the addition of 1% Cu to the M1 alloy, thereby producing the M5 alloy, has only a slightly diminishing effect on the drilling force and moment as well as on drilling power, compared to the case of the M1 alloy. On the other hand, the increase in the level of Cu and Mg from 2.2% and 0.3% in the M1 alloy to 3.4% and 0.6%, creating the M6 alloy, has a noticeable effect in increasing the mean total drilling force, mean total drilling moment, and mean power cutting by 25%, 20%, and 15%, respectively, compared to the M1 alloy.

Tool life is measured in terms of the number of holes drilled/tapped under constant machining conditions in M0, M1, M5, M6, and M9 alloys, as shown in Figure 4.13. In this figure, it will be observed that the M5 alloy containing high levels of Cu or the M6 alloy containing high levels of Cu and Mg, in the form of additions, all have a detrimental effect on drill life, whereas the drill life of the M1 alloy decreases from 2160 holes/drill to 810 holes/drill and 990 holes/drill in the M5 and M6 alloys, thus corresponding to a reduction in drill life by 63% and 58%, respectively.

It will also be clearly observed that the Mg-free M9 alloy displays a significant decrease in the total drilling force, in the total drilling moment, and in the total drilling power compared to the M1 reference alloy; specifically the M9 alloy required an average of 50% lower mean total drilling force ranging from 35% to 65%, and exhibited an average

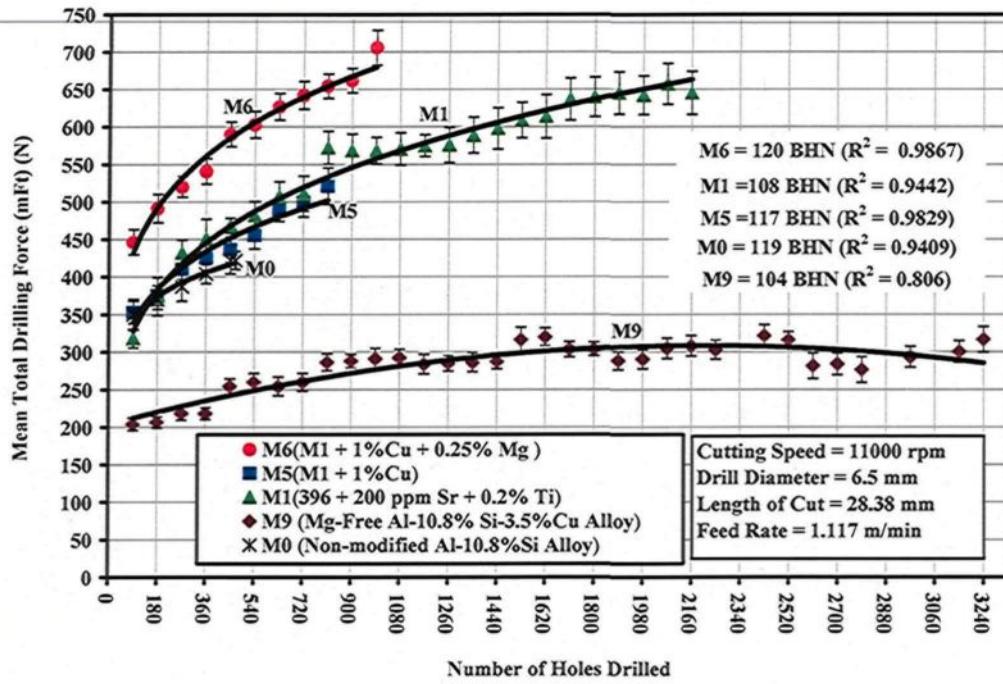
of 52% lower total drilling moment ranging from 35% to 69%, as well as approximately 64% less drilling power ranging from 58% to 70% compared to the M1 alloy over the evaluation period of 2160 holes, as shown in Figure 4.12.

It is interesting to observe that the Mg-free M9 alloy produces the highest number of holes with 3240 holes/drill; this is followed by the M1 alloy containing 0.3% Mg having 2160 holes/drill, and lastly by the high Mg-content M6 alloy containing 0.6% Mg with 990 holes/drill, as shown in Figure 4.13. It is thus clear that a high Mg-content of about 0.6% will cause a certain amount of deterioration in tool life, producing higher cutting force and moment, and lowering the number of holes drilled. These conclusions are in satisfactory agreement with results obtained by Jorstad^{14, 23} who reported that a small Mg addition of about 0.3%, in Al-Si-Cu alloys hardens the alloy but does not increase abrasiveness since it does not contribute in any way to the formation of the coarse hard Al-Si-Cu-Mg intermetallic phase.

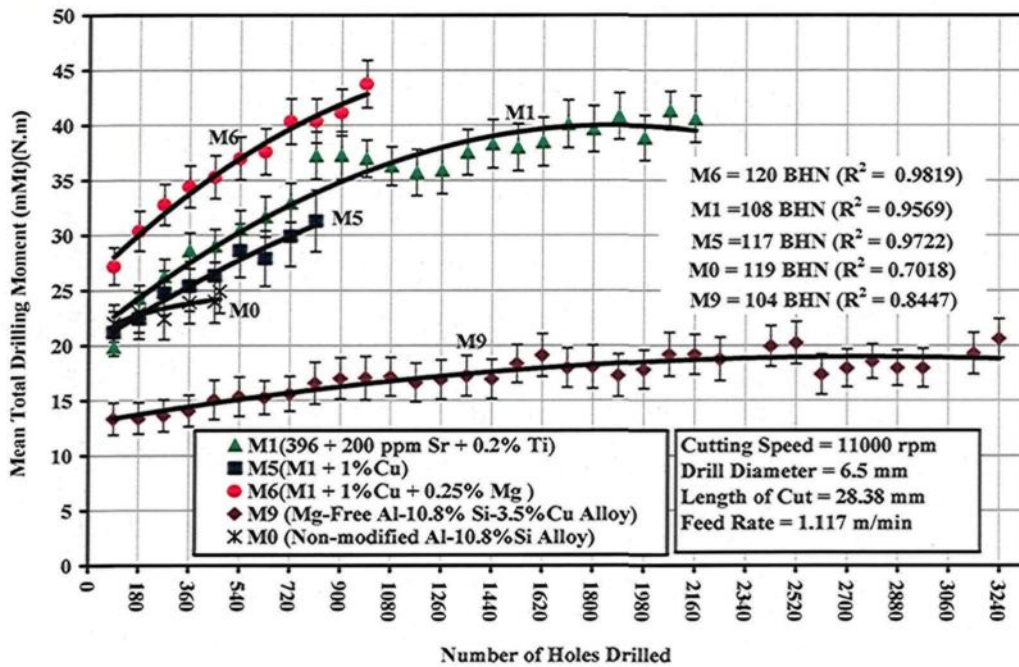
The microstructure of the non-modified Al-10.8%Si alloy consists mainly of the eutectic mixture (α -Al + Si) with some elongated α -Al dendrites and a few primary silicon particles. The silicon crystals, which have three-dimensional complex shapes and are extremely brittle, segregate to the grain boundaries of the α -Al matrix. Strontium, a surface active element, is a well-known additive in cast Al-Si alloys; it is commonly added to transform the shape of the eutectic silicon from acicular into fibrous particles. For the purposes of comparison, the non-modified Al-10.8% Si experimental alloy, coded M0, was used in this study to compare the machining behaviour of the non-modified alloy with that of the modified M1 alloy. It will be observed that the non-modified M0 alloy has some

slight effect in decreasing the mean total force, moment, and the mean power cutting by 9%, 13%, and 11%, respectively, when compared to the Sr-modified M1 alloy, as shown in Figures 4.12(a), (b), and (c). On the other hand, the non-modified M0 alloy has a detrimental effect on drill life, since the M0 alloy produces only 468 holes/drill compared to 2160 holes drilled in case of the the Sr-modified M1 alloy.

Figures 4.14(a) and (b) show the effects of Cu, Mg, and Sr additions on the mean total tapping force and the mean total tapping moment of the alloys investigated. As will be observed from the figures, the tapping results reveal that the alloys studied follow the same trend as those observed during the drilling tests. The addition of 0.25% Mg and 1% Cu to the M1 alloy generates high tapping force and moment in the M6 alloy which is created by these additions. On the other hand, the addition of only 1% Cu to the M1 alloy has little influence in lowering the tapping force and moment as opposed to the M1 base alloy. The non-modified M0 alloy, however, displays a significant decrease in the tapping forces, while the Mg-free M9 alloy generates the lowest tapping force and moment of all the alloys studied. Referring back to Figure 4.13 which shows the effects of the relevant additions to tap life in terms of the number of holes tapped, it was found that the M9 alloy showed the highest number of holes tapped with 3150 holes/tap, followed by the M6 alloy having 1314 holes/tap, then by the M5 alloy yielding 720 holes/tap, the M1 alloy producing 630 holes/tap, and lastly the non-modified M0 alloy with 540 holes/tap.



(a)



(b)

Figure 4.12 Contd.

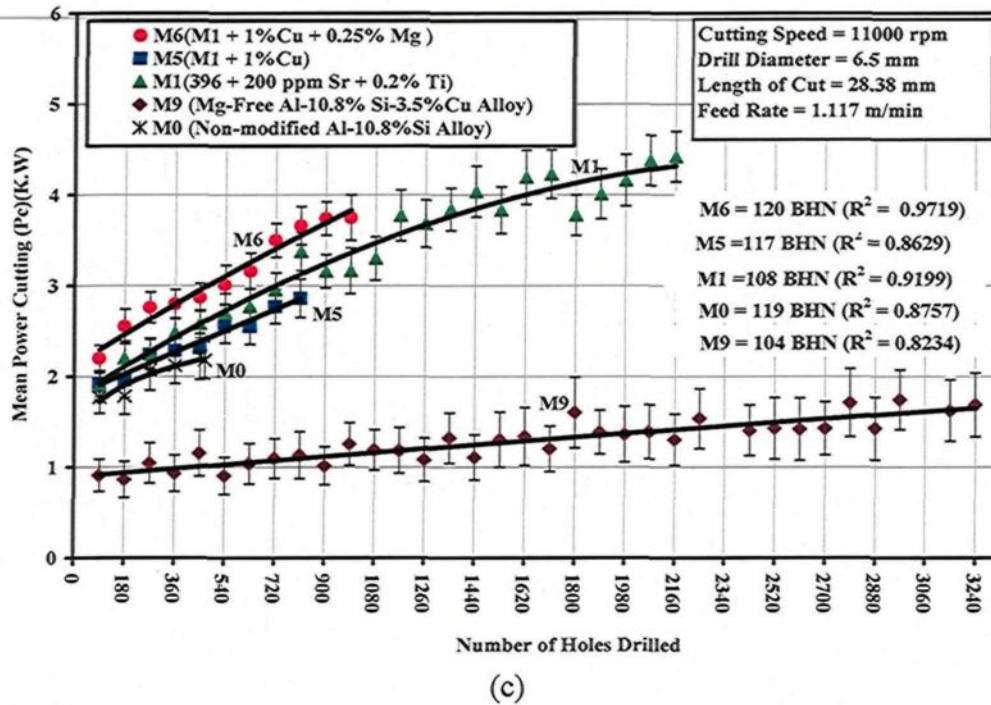


Figure 4.12 Effects of Cu, Mg, and Sr additions on the machinability of M1, M5, M6, M0, and M9 alloys in terms of (a) mean total drilling force; (b) mean total drilling moment; and (c) mean power cutting required for drilling 90 holes.

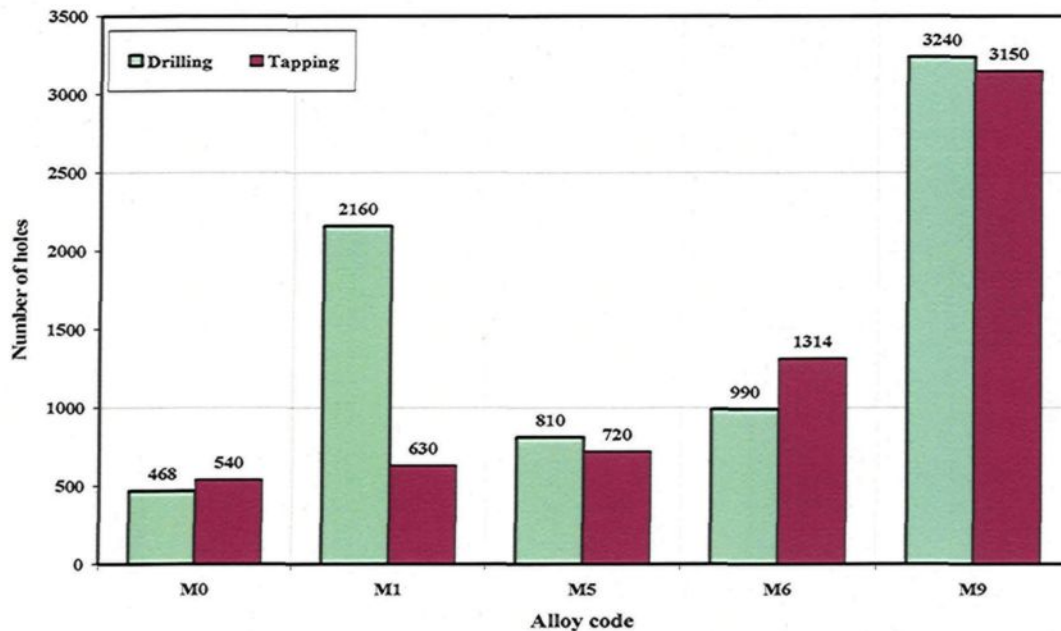
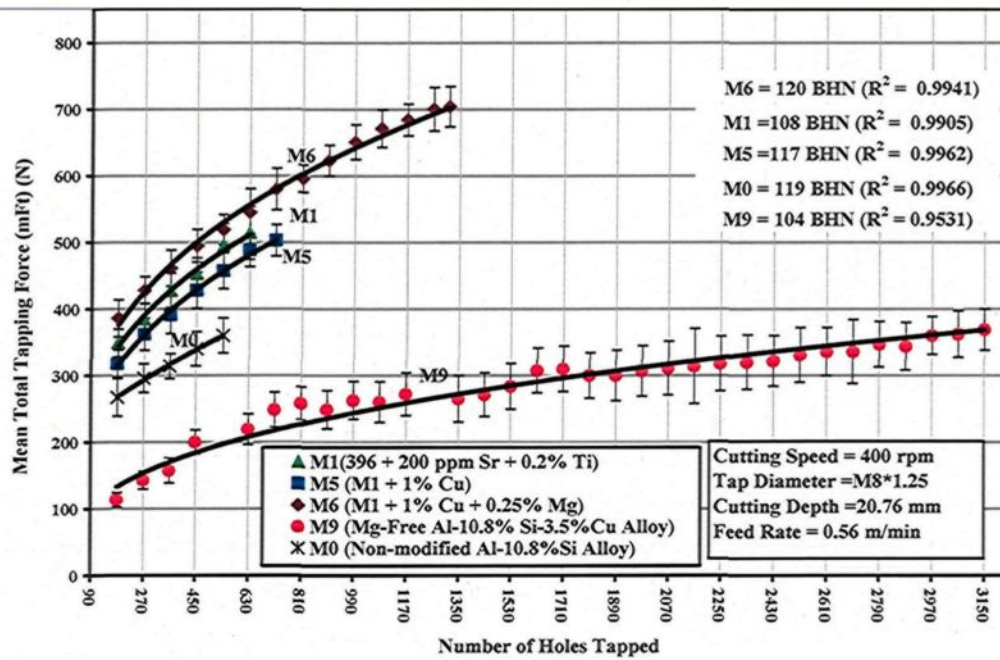
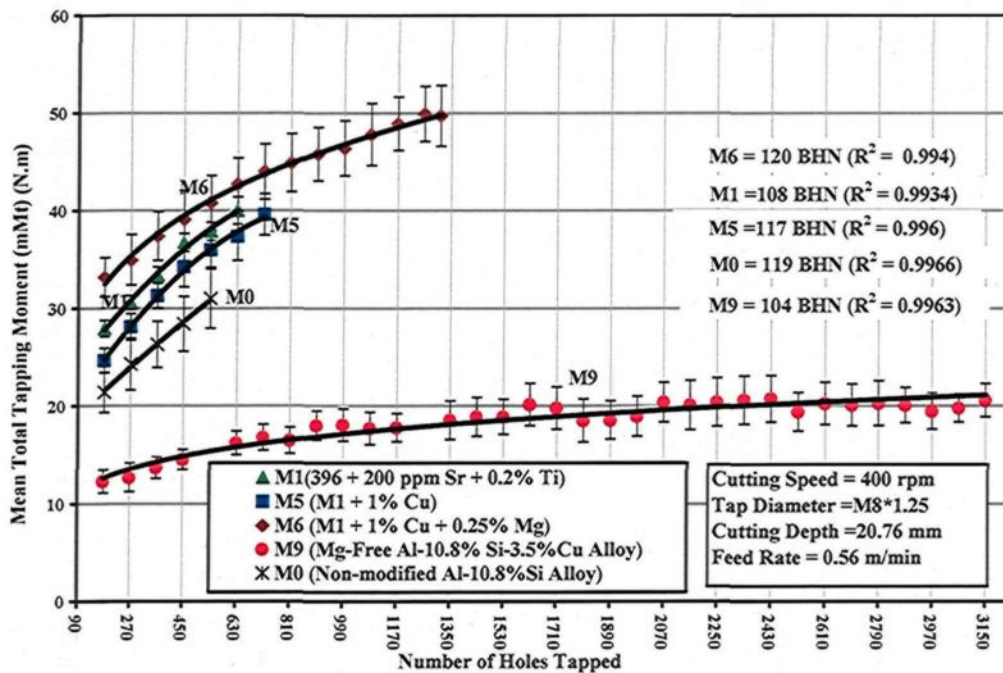


Figure 4.13 Comparison of tool life of M0, M1, M5, M6, and M9 alloys containing additions of different alloying elements in terms of the number of holes drilled and tapped.



(a)



(b)

Figure 4.14 Effects of Cu, Mg, and Sr additions on the machinability of M1, M5, M6, M0, and M9 alloys in terms of (a) mean total tapping force; and (b) mean total tapping moment required for tapping 90 holes.

The higher drilling force, moment, and power generated during the machining of the M6 alloy and the significant reduction in the drill life of the M5 and M6 alloys when compared to the M1 alloy may all be explained in terms of the following effects. Firstly, silicon particle measurements show that an increase in the level of Cu and Mg supplied to the Sr-modified M1 alloy results in an increase in Si-particle size, area, length, and aspect ratio; it also reduces the roundness ratio and particle density. These additions result in altering the microstructure of the M5 and M6 alloys from well-modified to partially-modified, as was confirmed earlier from Table 4.1 and Figure 4.2, since the silicon particles increase in size from $4.3\mu\text{m}^2$ in the M1 alloy to $10.00\mu\text{m}^2$ and $7.89\mu\text{m}^2$ in the M5 and M6 alloys, respectively. The fracturing of hard coarse silicon particles thus has a major effect on drill breakage. Studies carried out at Alcoa Research Laboratories²⁰ also reported the influence of silicon particle size on the rate of tool wear; it was found that the wear rate is apt to increase by a power of 1.7 of the silicon particle diameter, and that tool life decreases in machining Al-Si casting alloys as the number of silicon particles in the alloy increases.

Secondly, the volume fraction of the undissolved blocklike Al_2Cu phase increases with an increase in Cu-content. In addition, the influence of both Sr and Mg on the segregation of the Al_2Cu phase is expected to increase the severity of the segregation, resulting in the formation of large amounts of the coarse blocklike form of the phase. The increase in the level of Mg-content to $\sim 0.6\text{wt}\%$, creating the M6 alloy, also results in the formation of thick plates of the $\text{Al}_5\text{Si}_6\text{Cu}_2\text{Mg}_8$ phase which is, in itself, an insoluble, brittle hard intermetallic phase. Evidence for the severity of copper segregation, together with the formation of thick plates of the Al-Si-Cu-Mg phase as well as of acicular silicon particles

was shown clearly in the microstructure of the M6 alloy, Figure 4.15. It is important to mention here that the volume fraction of the undissolved Cu-rich intermetallic phase increases from 0.15% in the M1 alloy to 1.70% and 1.71% in the M5 and M6 alloys, respectively, as listed previously in Table 4.2. From the machinability point of view, such undissolved phase particles represent the abrasive area of the matrix with the potential for causing drill breakage. It has been reported that tool wear can be increased by as much as 50% through the presence of substantial quantities of undissolved Al-Cu and Al-Cu-Mg-Si phases.²⁰ Figure 4.16(b) shows the microstructure of the M6 alloy portion in which the drill was broken during machining; it will be observed that the segregation of the hard second-phase constituents which include Al_2Cu , $\text{Al}_5\text{Si}_6\text{Cu}_2\text{Mg}_8$, and coarse Si particles are detrimental to tool life, thus if their presence is necessary, it is best that they should be as fine and as dispersed as possible. With this limiting condition in mind, König and Erinski¹⁹² reported that the dominant variables influencing tool life and tool wear in the Al-Si alloys are: the morphology of eutectic silicon, the inhomogeneities of the alloy structure, and an interrupted regime of cutting resulting from the coarse undissolved particles.

It should be remembered here that in high copper-content alloys the complete dissolution of the Al_2Cu phase is not usually possible. The slow dissolution rate of blocklike Al_2Cu phase particles during solution heat treatment is attributed to their lower interfacial area corresponding to the large blocklike morphology and slower interface mobility because of curvature effects, or faceted morphology, which consequently lower the driving force for the dissolution of Al_2Cu phases in the Al matrix.¹⁹³

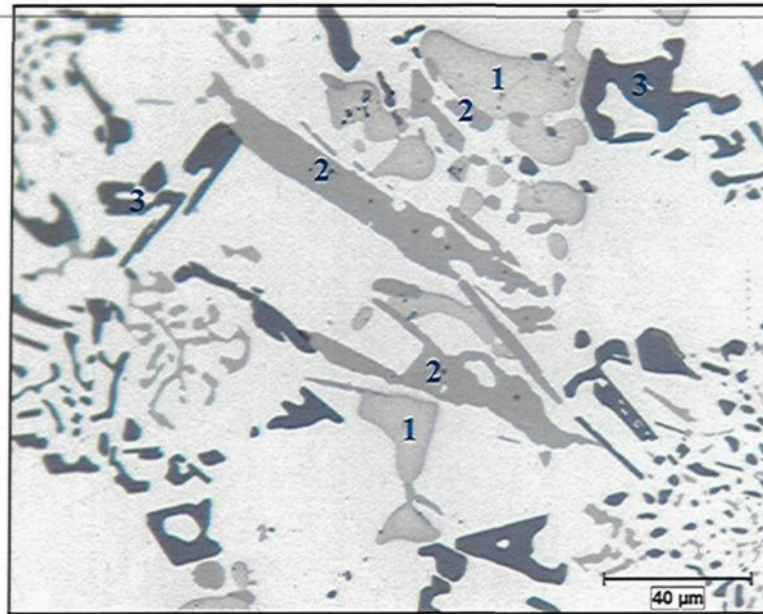


Figure 4.15 Microstructure of the M6 alloy showing the influence of both Sr and Mg: (1) segregation of the Al_2Cu phase; (2) formation of thick plates of $\text{Al}_5\text{Si}_6\text{Cu}_2\text{Mg}_8$ phase; and (3) acicular silicon particles.

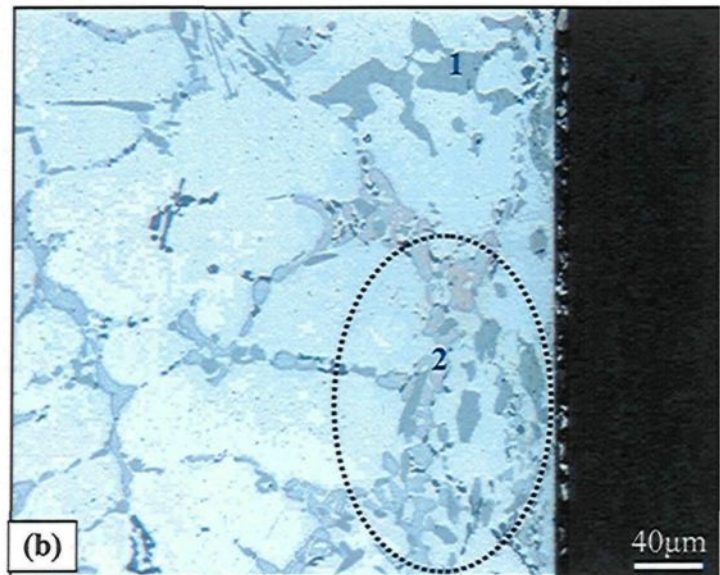
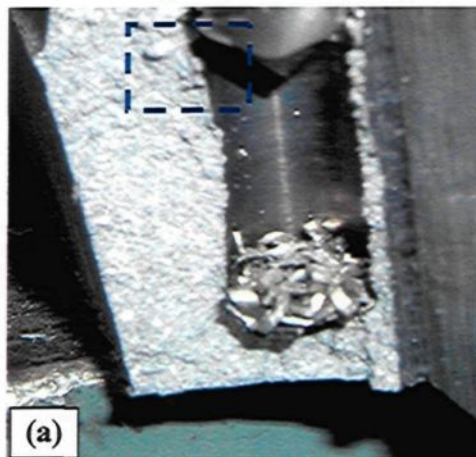


Figure 4.16 (a) Cross-section of drilled hole illustrating area investigated; and (b) optical microstructure of M6 alloy corresponding to the drill breakage portion showing the presence of large silicon particles, marked 1, and the coarse undissolved Cu-phase, marked 2, in this area.

The solution time must then be chosen carefully to allow for the maximum dissolution of this intermetallic phase. Solution-treating the alloy for long periods of time, however, is an expensive practice and may not be necessary to obtain the required alloy strength. Moreover, the coarsening of microstructural constituents and the possible formation of secondary porosity which tends to form after prolonged annealing temperatures can have a deleterious effect on machinability properties.¹⁹⁴

Thirdly, the hardness values of the M5 and M6 alloys increase with increasing Cu and Mg levels, as confirmed previously by the hardness measurements reported in Table 4.3. It is presumed that tool life is adversely affected by an increase in workpiece hardness, since the cutting loads and temperatures increase with increasing hardness values of the material, thereby reducing tool life even further.

The noticeable difference to be observed in the drilling force, moment, and tool life between the Mg-free M9 alloy belonging to the Al-10.8%Si-3.5%Cu alloy group and the M1 alloy containing 0.3%Mg may be attributed to the presence of Mg which has proved to be an excellent way of achieving a high level of tensile strength and hardness, however, at the expense of elongation. When approximately 0.3%Mg is added to the M1 alloy, a more marked response to artificial aging is evidenced in the yield strength and ultimate tensile strength values obtained for the T6 treatment compared to the M9 alloy which is a Mg-free alloy; the M1 alloy, however, shows higher values for YS and UTS, by 44% and 24%, respectively, than the M9 alloy, as listed previously in Table 4.3. These observations are in satisfactory agreement with those of previous researchers^{195, 196} and can be explained by the cooperative precipitation of the Al_2Cu , Mg_2Si , Al_2CuMg , and $Al_5Si_6Cu_2Mg_8$ hardening

phases in Mg-containing alloys which confer greater strength on the alloy than on the precipitation of only the Al_2Cu phase in the Mg-free M9 alloy. Scanning electron microscopy (SEM) in conjunction with an EDX analysis system was used to examine the distribution, size, and density of the hardening precipitate phases for Mg-containing M1 alloy and the Mg-free M9 alloy. In this regard, Figure 4.17(a) shows the SEM micrograph of the M1 alloy belonging to the Al-Si-Cu-Mg alloy from which more complex intermetallic phases may emerge, depending on the ratio of the different elements present in the alloy. Such hardening phases may include Al_2Cu , Al_2CuMg , and $\text{Al}_5\text{Si}_6\text{Cu}_2\text{Mg}_8$ among others, since the EDX analysis of these phases shows four peaks of Cu, Mg, Al, and Si. The identification of these phases, however, presents a certain amount of difficulty since most of them display the morphology of needles or very fine plates. On the other hand, in Figure 4.17(b) which shows the SEM micrograph of the M9 sample which belongs the Al-Si-Cu alloy, it will be observed that there is a dense precipitation of Al_2Cu phase; this behavior is to be expected since Al_2Cu precipitates are the ones responsible for strengthening for this alloy which has already undergone aging to the maximum strength or T6-condition.

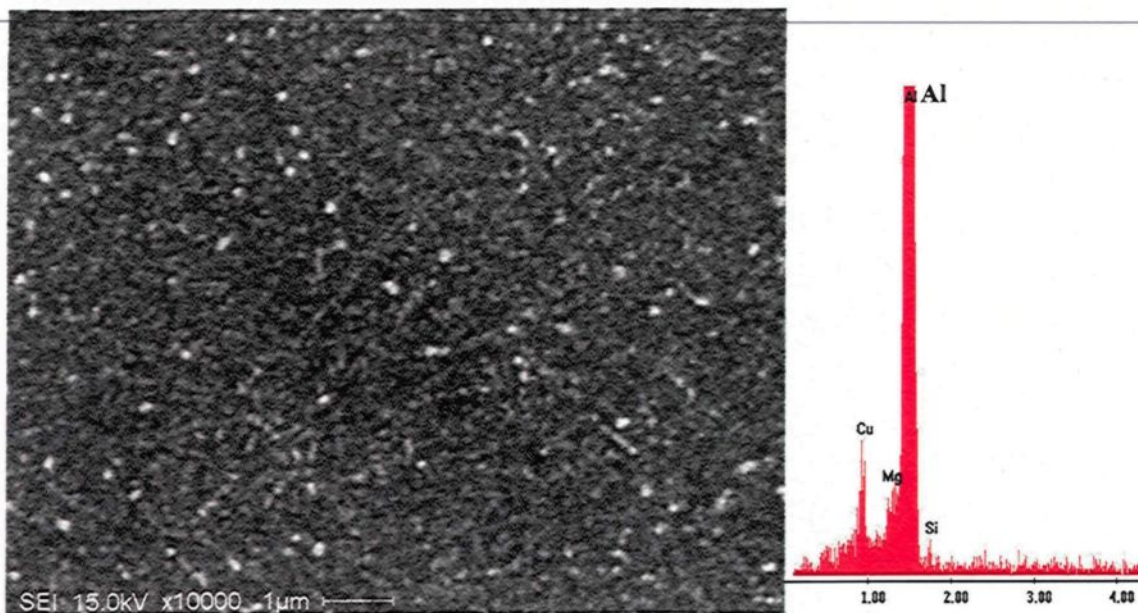
From the machinability point of view, a material having high yield strength, *i.e.* the sufficient force required per unit of area to create permanent deformation, necessitates a high level of force to initiate chip formation during machining operations. Thus, the smaller the strength of the alloy, the lower the cutting force required during machining since specific cutting pressures decrease with a decrease in tensile strength, as depicted during the machining of the M9 alloy. It is interesting to note that the M1 alloy displays a higher drilling force and moment than the Mg-free M9 alloy in spite of a higher Cu content of

3.67% in the M9 alloy compared to 2.22% in the M1 alloy. Thus, the effects of Cu addition in improving the mechanical properties of the alloy are, however, less pronounced than those of Mg, particularly at high levels of Mg-content. In other words, the addition of small amounts of about 0.3% Mg is observed to be more effective than a Cu addition of 3.5%.

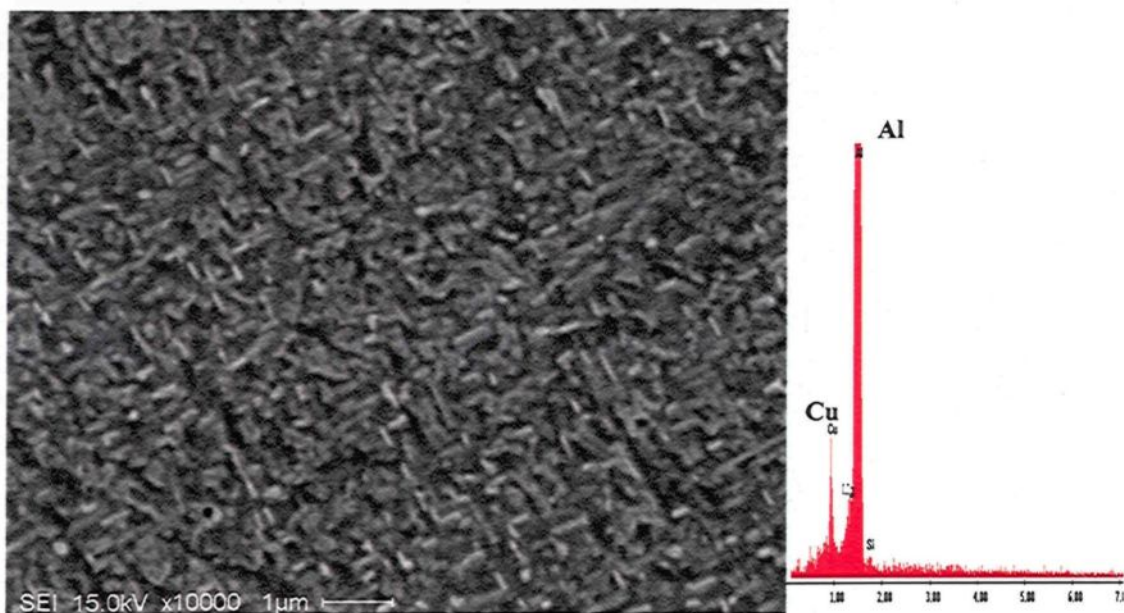
In spite of the M9 alloy being a non-modified alloy, it produces a longer drill/tap life compared to the Sr-modified M1 alloy containing the same level of Si. This observation may be explained based on the fact that tool life is closely related to the hardness of the workpiece, as well as to the deformability of the matrix around the Si particles. Thus, when the workpiece made of the M1 alloy is hard, thereby resisting deformation, the work material is also difficult to deform in the shear zone ahead of the cutting edge and on the tool surface in such a way that the Si particles are secured firmly in position. Consequently, the particles have a strongly abrasive action on the tool cutting edge resulting in a high cutting force as well as in a short tool life.¹⁵³

The lower drilling force and moment generated during the machining of the non-modified M0 alloy over the evaluation period of 468 holes, compared to the M1 alloy, may be explained by the fact that the acicular Si particles were part of the main fractured mechanisms in the near-eutectic Al-Si alloy,¹⁹⁷ as confirmed by the microstructure beneath the fracture surface of the non-modified alloy shown in Figure 4.18. It was reported that the strength of Si particles was 500-900 MPa for the fine eutectic Si particles whereas it was as low as 200 MPa for the coarse non-modified Si particles.¹⁹⁸ Consequently, the non-modified acicular silicon structure provides an easy path for fracture, resulting in decreases in the cutting force during the machining of the M0 alloy.

A comparison of the non-modified M0 alloy and the Sr-modified M1 alloy (containing the same level of Mg and Cu additions) in terms of the number of holes drilled, reveals that the morphology of Si particles has a noticeable effect in determining the tool life of near-eutectic Al-Si alloys. As was indicated previously in a discussion on Si-particle characterization, the addition of 200 ppm Sr to the M1 alloy leads to a decrease in Si particle area, length, and aspect ratio from $65.7\mu\text{m}^2$, $20.8\mu\text{m}$, and 3.51 in the M0 alloy to $4.3\mu\text{m}^2$, $2.96\mu\text{m}$, and 1.77 in the M1 alloy, respectively. As a result, the Si appears in the form of finely-distributed fibrous particles instead of displaying an acicular shape and large plates with sharp sides and edges. In fact, Miller¹⁷ stated that the rate of drill wear increases as silicon-particle size increases, thus if the eutectic silicon structure is coarse, tool life suffers and results in drill breakage. Hence, the drill life of the non-modified M0 alloy decreases by 78% compared to the Sr modified M1 alloy having 2160 holes with 468 holes drilled in the M0 alloy, even though the mean total drilling and moment force for the non-modified M0 alloy were lower than those for the Sr-modified M1 alloy. It should be kept in mind that when the perimeter of the silicon particles is greater than the cutting edge radius, the probability of the cutting edge being exposed to silicon particles during the shearing process increases. When large silicon particles are sheared in contact with the cutting edge, some sharp particle fragments will flow past the rake face while others will flow towards the clearance face. The shearing of large hard silicon particles thus has a significant effect on drill breakage.



(a)



(b)

Figure 4.17 SEM micrograph and EDX analysis showing the precipitation of hardening phases (a) Mg-containing M1 alloy; and (b) Mg-free M9 alloy (T6-heat treated conditions).

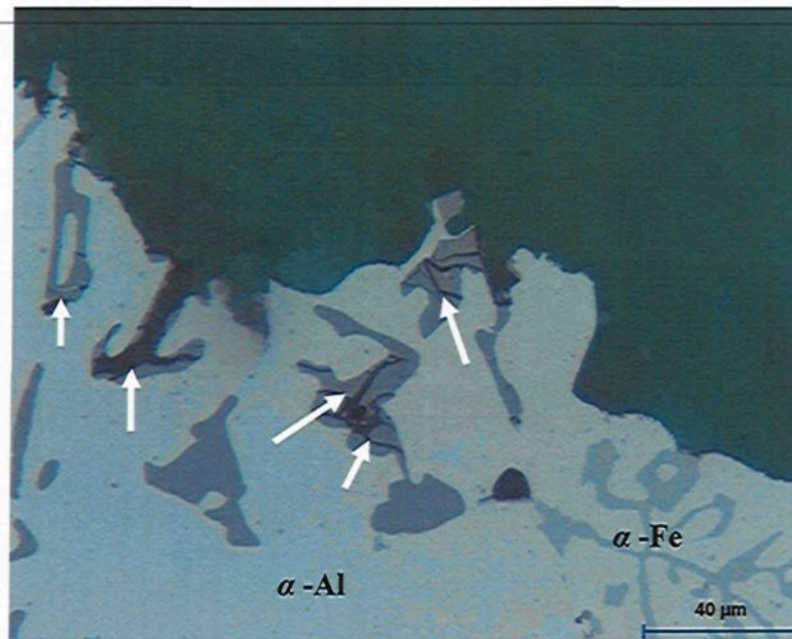


Figure 4.18 Microstructure beneath the fracture surface of the non-modified M0 alloy. White arrows indicate broken acicular Si particles.

4.4.3 Evolution of Built-Up Edge (BUE) and Tool Wear Characteristics

As a result of high temperatures, small particles of metal tend to adhere to the edge of the cutting tool thereby leading to build-up. The presence of built-up edge is capable of inducing a number of effects including an alteration in tool geometry, thereby reducing the contact area of the chip with the rake face.¹⁹⁹ Consequently, the shear plane angle increases while the cutting and feed forces diminish. The fragments of BUE, which are constantly breaking away, leave a very rough surface finish, which is why high cutting speeds must be applied if surface quality is important. In practice, the size and shape of the BUE vary greatly with the work material and the prevailing cutting conditions.²⁰⁰ For any material with its cutting conditions, the built-up edge seems to reach an equilibrium size and shape fairly early on. Built-up edge should be capable of supporting the high compressive force and shear stress imposed by the cutting process thereby rendering it unable to grow

indefinitely. As the BUE grows in height and changes in shape, the stress system also changes and parts of the built-up edge are broken away.²⁰¹ Williams and Rollason²⁰² suggest that the introduction of a second phase into a metal structure lowers its ductility, allowing fracture somewhere along the rake face after severe deformation. The occurrence of BUE is also affected by feed rate in uncut chip thickness, rake angle, tool material, and lubrication. For example, the BUE disappears completely at high speeds in accordance with the commercial purity of the aluminum alloy.

The tendency of each alloy to adhere and build up on the cutting edge of the tool was detected through a high magnification top-view of the projected area looking at the actual build-up on the drill; this was carried out using a toolmaker's microscope (TM-505 type) at a magnification of 30x. Figures 4.19 (a) and (b) show photographs of the progress of edge build-up on the cutting-drill lip from the beginning to the end of drilling a 396 alloy block casting. Table 4.4 also lists the effects of Fe-intermetallics on the evolution of BUE width for the M1, M3, and M4 alloys as drilling progresses. An analysis of the edge build-up and an examination of the corresponding photographs indicate that there is little change to be seen in the width of the BUE after drilling different numbers of holes. This fact may be attributed to the amount of the deposit, or BUE, which gradually increases; when this exceeds a critical size, however, it separates from the cutting face and adheres to the lower surface of the chip. It is assumed that when the deposit reaches this critical size, it will slide completely, or partly, off the cutting face under the action of a sufficiently strong lateral force, and then subsequently be eliminated with the chip itself. Immediately after the elimination of the existing deposit, a new deposit will begin to form; it will proceed to grow

gradually and will ultimately change or modify the tool geometry. It should be noted here that the drilling tests were carried out at high cutting speeds of around 11000 rpm and a high feed rate of about 1.117 m/min. Based upon research, it was reported that with the higher rates of metal removal, *i.e.* at a higher speed or feed rate, a BUE will no longer be discernible, since the transition from the built-up edge to the flow zone is strongly influenced by both speed and feed; also the flow zone occurs in the range of cutting conditions commonly encountered in industrial machining operations.²⁰⁰ It is not possible to draw a firm conclusion here, however, because of the intermittent peeling off of the BUE during drilling cycles.

A study of the build-up measurements for the M1, M3, and M4 alloys also strongly indicates that the width of the built-up edge has no clear-cut trend except for the fact that the alloy containing sludge as a predominant phase in the M3 alloy shows a slightly lesser build-up width compared to the M1 alloy; it should be noted that all the alloy composition variations left a readily discernible deposit on the tool edge, even after only 90 holes were drilled. Surprisingly, the addition of 0.25%Fe + 0.25%Mn (M3) or 0.5%Fe (M4) to the base alloy, which would initially have been expected to reduce the build-up tendency through the abrasive action of hard intermetallic phases, did not measurably reduce the built-up width compared to the one observed for the M1 base alloy. These results are consistent with the work of Jorstad^{14, 23} who reported that heavy elements such as iron, manganese, and nickel have a negligible effect on microhardness and on the tool-edge build-up in 380 alloy die castings.

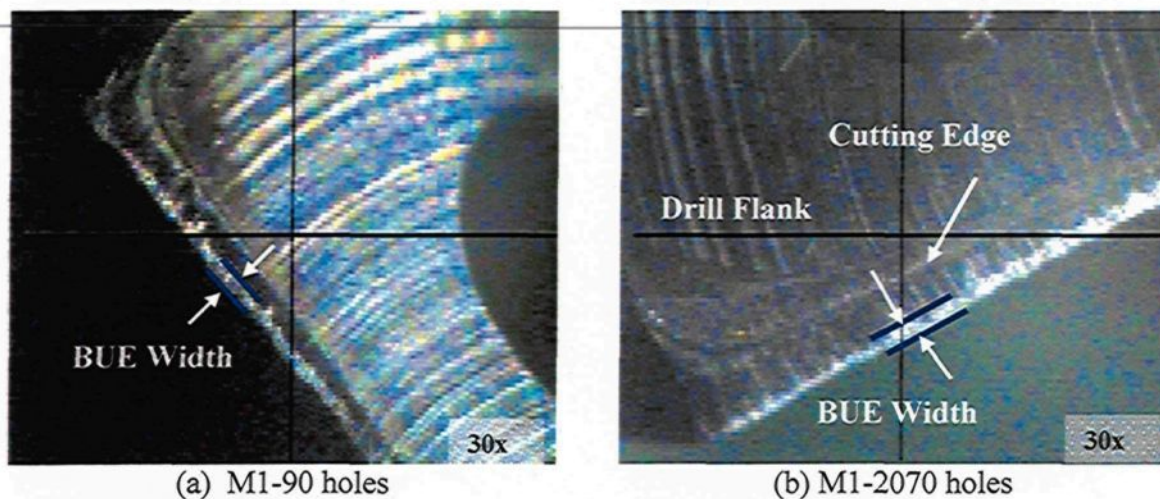


Figure 4.19 Photographs showing the progress of built-up edge (BUE) on the tip of the cutting edge (a) after drilling 90 holes, and (b) after drilling 2070 holes.

Table 4.4 Effects of Fe-intermetallics on width of built-up edge (BUE) during drilling process.

Alloy	BUE width (mm) after drilling the specified numbers of holes								
	No. of holes drilled →	180	360	540	720	900	1080	1620	Average
M1 (containing α -Fe Phase)		0.163	0.162	0.160	0.169	0.179	0.179	0.169	(0.168)
M3 (containing sludge phase)		0.160	0.158	0.155	0.159	0.150	-	-	(0.156)
M4 (containing β -Fe and α -Fe phases)		0.177	0.166	0.170	0.175	0.174	-	0.173	(0.170)

Figures 4.20(a), (b), and (c) show the effects of Cu- and Mg-addition produced in the heat build-up formation on the cutting-drill lip in M1, M6, and M9 alloys after the completion of different stages of drilling. An examination of these photographs indicates that Mg-containing alloys including the M1 alloy with 0.3%Mg, and the M6 alloy with 0.6% Mg all show an appreciably lower tendency to BUE formation compared to the Mg-free M9 alloy. It should also be kept in mind that the Mg-containing alloys have the

greatest degree of hardness compared to the M9 alloy, as listed in Table 4.3. Owing to its high hardness and low ductility values, the M6 alloy shows little tendency towards BUE formation on the cutting tool lip; on the other hand, the higher ductility of the M9 alloy increases its BUE width slightly compared to the M1 alloy, as shown clearly in Figure 4.20. These results are in satisfactory agreement with Jorstad^{14, 23} who reported that an addition of 0.3%Mg to the Al-Si-Cu alloy causes a noticeable increase in the material work-hardening and significantly reduces the tendency towards BUE formation.

Drill wear has a strong effect on hole quality and on dimensional accuracy, potentially reaching a threshold level, thereby causing the catastrophic failure of the drill. In this study, no systematic measurements of flank wear on the cutting edge were considered, although it should be kept in mind that the determining factor in drill life is governed by the quality of the hole produced when using the Go-NoGo gauge test. Figure 4.20(d) shows the state of drill wear on the cutting-drill lip after stripping the adherent workpiece material using a solution of sodium hydroxide (NaOH). It will be seen from this figure, that maximum wear takes place at the outer corner edge, whereas minimum wear occurs at or near the point of the tip, in view of the fact that the maximum rotational force and the maximum drill-to-workpiece contact occur further away from this point. The outer corner thus tends to become abraded more rapidly, whereas at the point of the tip, little rotational force is experienced and this force is more like “pushing” into the workpiece, rather than cutting into it. When the corners of the drill are rounded off, as shown in Figure 4.21, the drill then sticks to the workpiece and breaks if the cutting process is not halted in time.

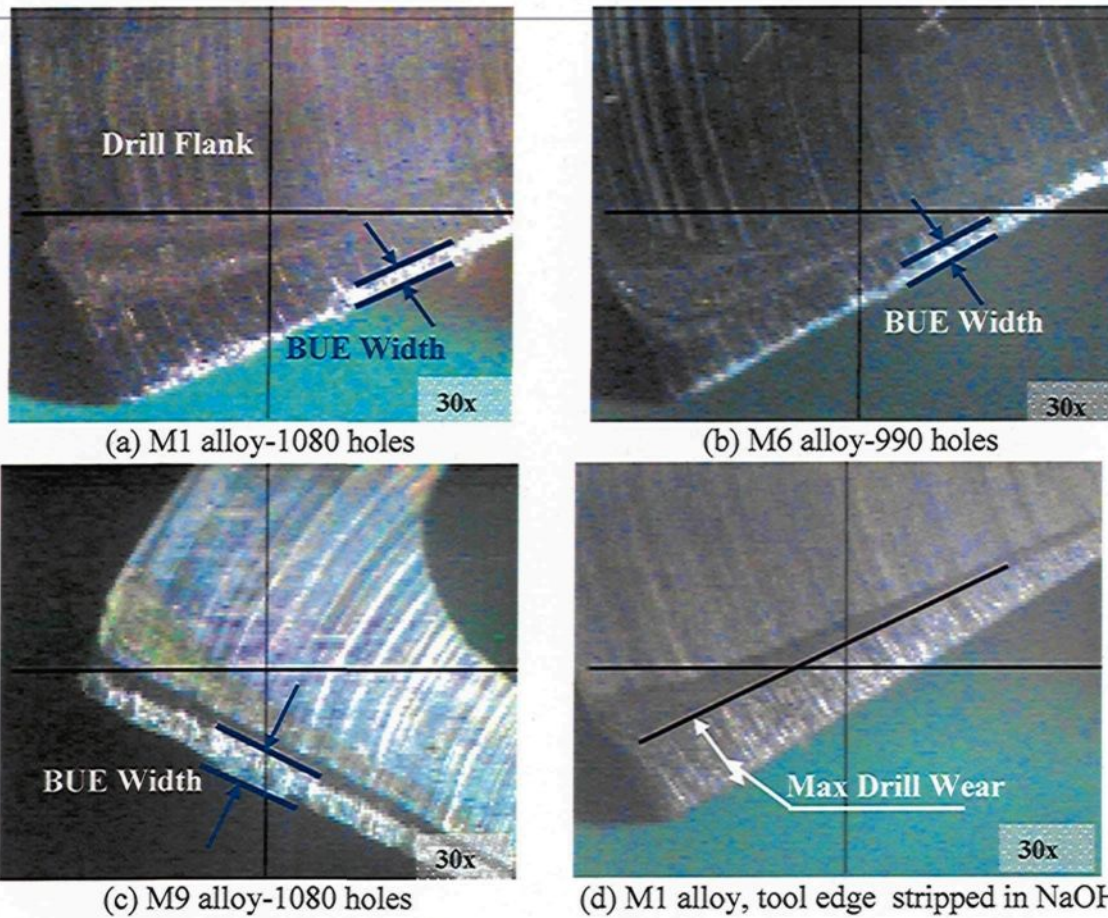


Figure 4.20 Photographs showing the effects of Cu- and Mg-addition produced in the heat build-up formation and the wear on the cutting-drill lip in M1, M6, and M9 alloys after different stages of drilling.

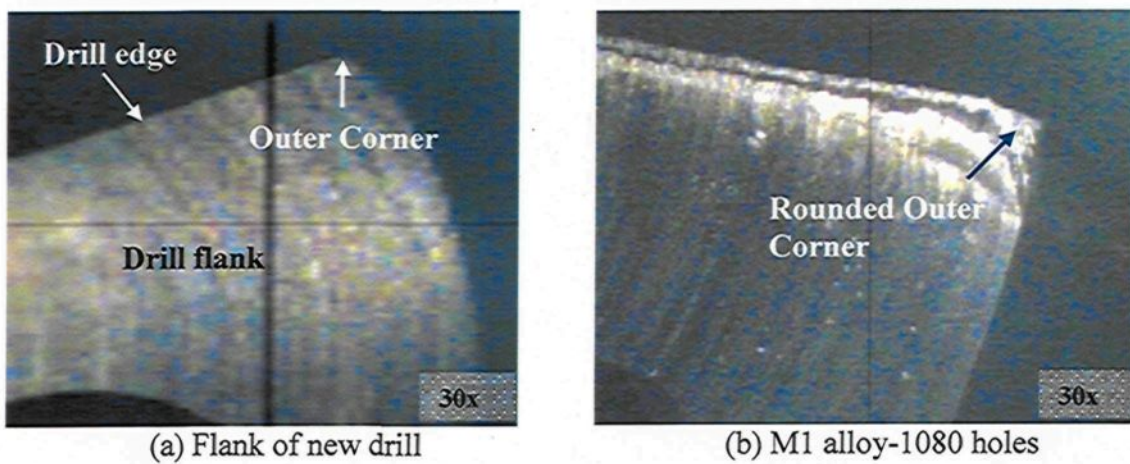


Figure 4.21 Photographs showing wear mode on cutting edge after drilling the M1 alloy.

Tool wear is a critical topic affecting the economics of machining, especially in connection with the tapping process, since it is one of the last operations to be performed within most operation sequences.²⁰³ It has been reported that the total tapping load consists of the base load and a chip-packing load. The base load results from chip formation and tool/workpiece friction, whereas the chip-packing load is the result of chip clogging in the flutes, and is random in nature. It should be noted that the chip-packing load may be many times that of the base load, depending on tap geometries and the machining conditions.²⁰⁴

In the present study, the tapping tests (M8 x 1.25) were performed in the blind holes at low cutting speeds of about 9.57 m/min; measuring the tool wear on tap tools, however, represents an extremely challenging task. There are several edges whose flanks are not entirely flat; similarly, the rake faces are also not flat; thus a Go-NoGo gauge criterion was required to assess tap life. The main wear mechanism observed was adhesion, although some abrasion may also have occurred during the tapping of the sludge-containing M3 alloy, while the main type of wear was flank wear. The adhesion of material to the relief face of the taps was the main cause of the ending of tool life. The material adhered mainly to the last edges of the chamfered part and to the first edges of the cylindrical part, as shown in Figure 4.22 (b) and (c); this observation may be attributed to the fact that these edges are responsible for cutting the last and extremely small depth-of-cut, at a relatively low speed, high pressure, and high temperature. The adhesion was not exactly the same as a built-up edge (BUE), but it seemed to follow the same mechanism as that for the building and the breaking of the tap. Figures 4.23 show photographs of broken taps; as is evident, the breakage occurred at the chamfered part of the tap in view of the fact that it generates a

major part of the resulting force, because of the larger chip cross-section related to the teeth of the chamfer.

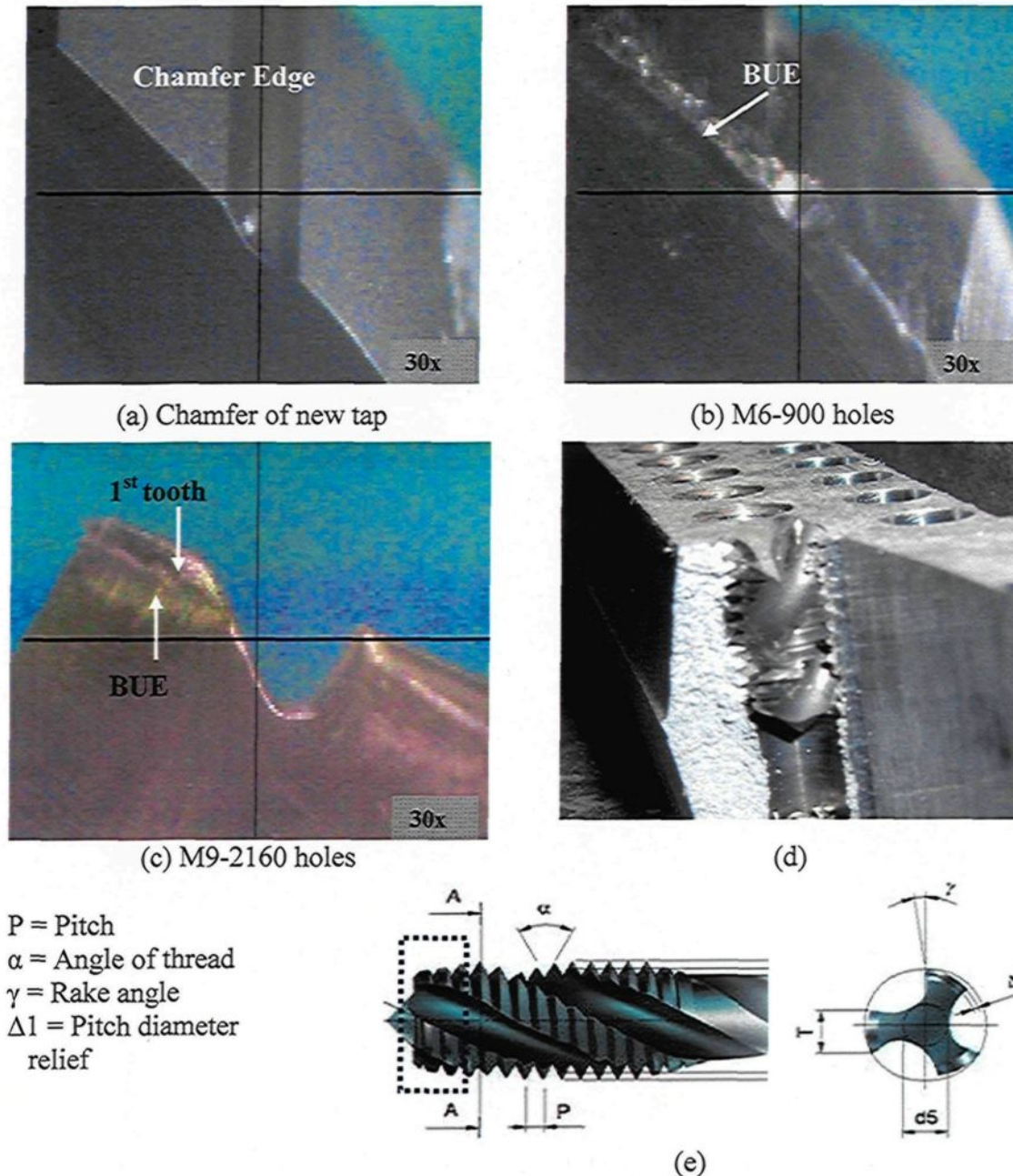
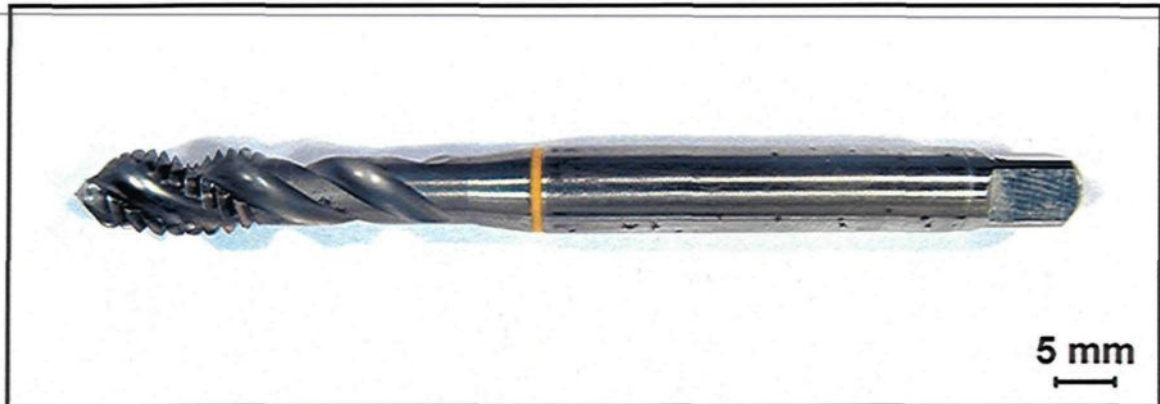
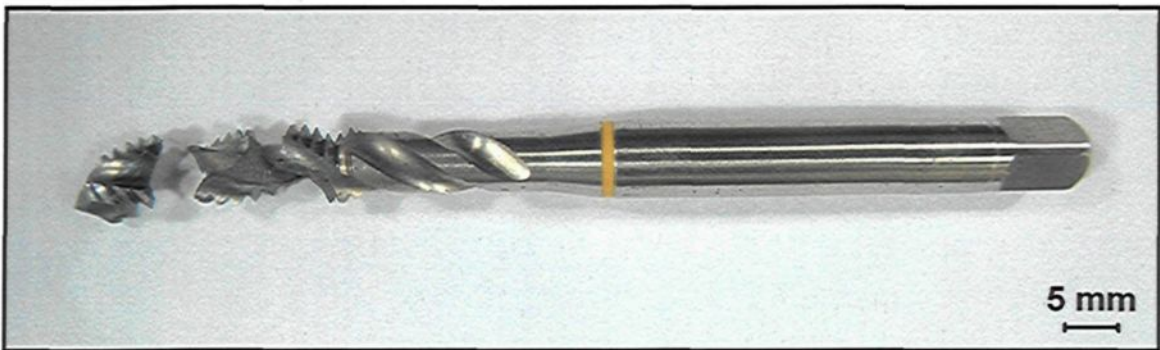


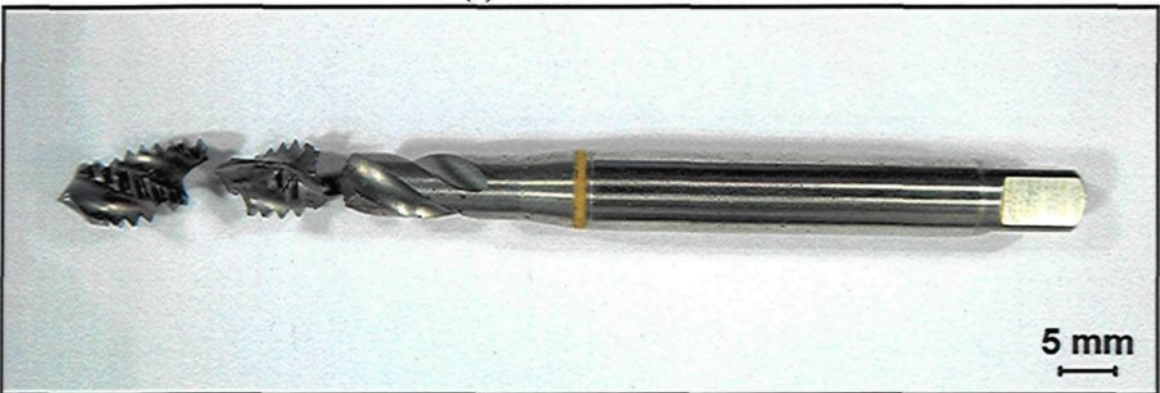
Figure 4.22 Photographs showing the wear mode on the tap edge (a) new tap; (b) BUE on the relief face of the tap chamfer part; (c) material adhering to the first thread of tap; (d) broken tap in the workpiece; (e) photograph of tap illustrating area investigated.



(a) M9-2160 holes



(c) M6-1314 holes



(e) M1-630 holes

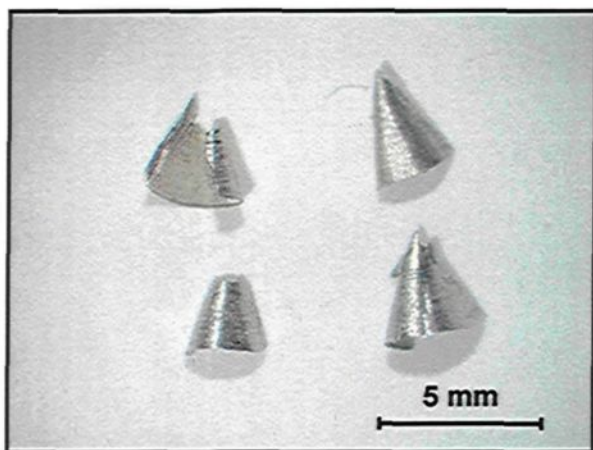
Figure 4.23 A Photograph showing the broken taps (a) new tap; (b) broken tap after tapping the M6 alloy; and (c) broken tap after tapping the M1 alloy.

4.4.4 Chip Characterization

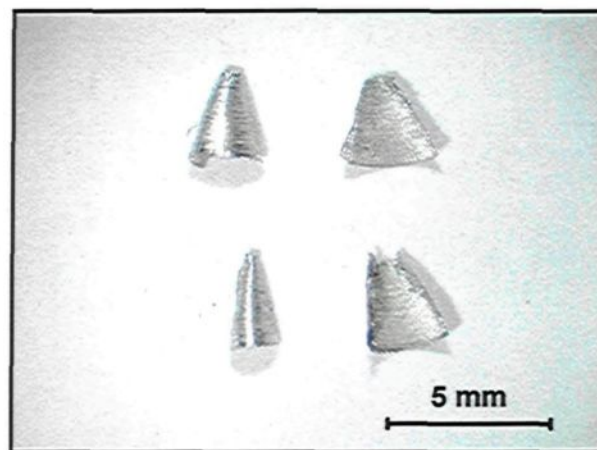
During the drilling process, the chip is formed within a closed space; hence it is extremely difficult to observe the process of its formation or its motion within the flute directly. The main problems arising in the drilling of aluminum cast alloys are the adhesion, or welding, of the chip to the drill, and chip/flute clogging.⁹⁵ Small well-broken chips are to be desired, because, as they get larger, they become unable to move easily through the flutes.⁹⁶ Fan-shaped chips were formed during the machining of the alloys studied, namely the M1, M3, M4, M5, M6, M9, and M0 alloys, as shown in Figure 4.24. These chips are formed when conical chips are unable to curl sufficiently to follow the flute; they tend to fracture prior to the completion of one revolution. The fan shape was by far the predominant form and is considered to be the ideal chip form for most drilling applications. The results show that the addition of iron and manganese, creating the M3 and M4 alloys, produces no discernible effect on the chip configuration compared to the 396 base alloy, as shown in Figure 4.24 (a). It was also found that there is no clear demarcation between needle- and fan-shaped chips. It has been observed that it is the marked change in the radius of the chip about the lip axis which results in the needle shape; this type of radius change occurs when the built-up edge alters the geometry of the drill cutting surface.

Figures 4.24(b), (c), and (d) show the effects of Cu and Mg on the typical chip formation produced during the drilling of Sr-modified, grain-refined, heat-treated 396 alloys. The difference in the chip morphology may be also observed from the histogram provided in Figure 4.25 which evaluates chip breakability in terms of the number of chips-per-gram for alloys investigated. With regard to these figures, it may be concluded that the

chip breakability of the alloy containing Al_2Cu , namely the M9 with 3.6% Cu, was superior to that of the alloy containing Mg_2Si which is the A356.2-M13 alloy with 0.4% Mg; further combined additions of Cu and Mg will refine the size of the chips in the M1 and M6 alloys. For comparison purposes, the A356.2 alloy which belongs to the Al-Si-Mg group was used in this study to investigate the effects of the Mg_2Si phase; from the point of view of chip breakability, however, this alloy produces larger chips of a fanlike shape than were observed in the Al-Si-Cu alloys under study, as shown in Figure 4.24(d). These results are in agreement with Kamiya and Yakou⁴⁹ who studied the role of second-phase particles namely Al_2Cu , Al_6Mn , Mg_2Si , and Al-Fe-Si with regard to chip breakability in aluminum alloys; they found that the chip breakability of alloys containing Al_2Cu or Si was excellent compared to those containing Mg_2Si or Al-Fe-Si phases. It was reported that the fractured second-phase particles acted as the cause of chip-breaking during machining.



(a) M1 alloy (1080 holes)



(b) M6 alloy (990 holes)

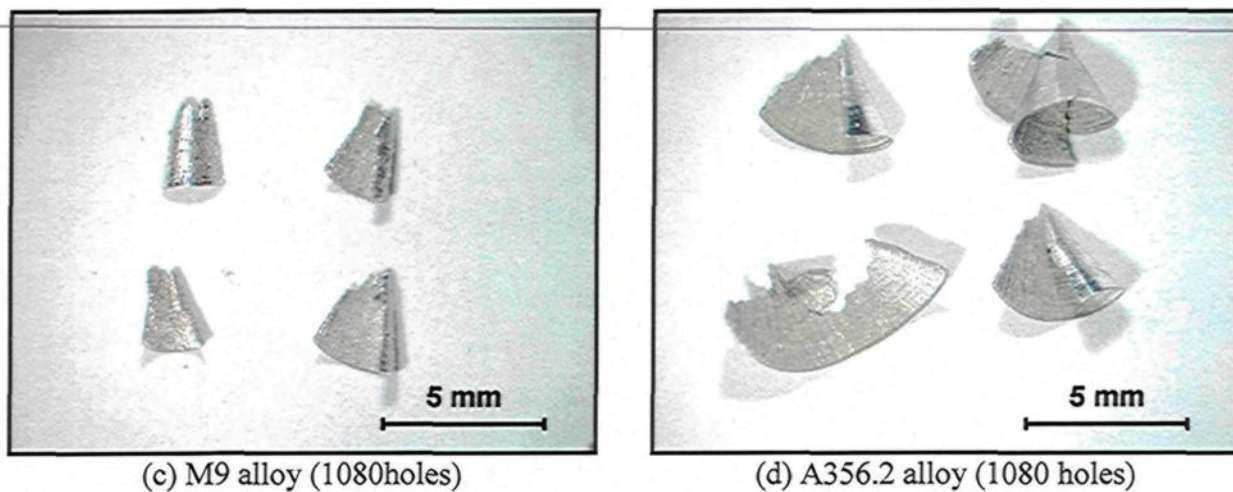


Figure 4.24 Optical micrographs showing different types of chip obtained for M1, M6, M9, and A356.2 alloys after drilling the specified number of holes.

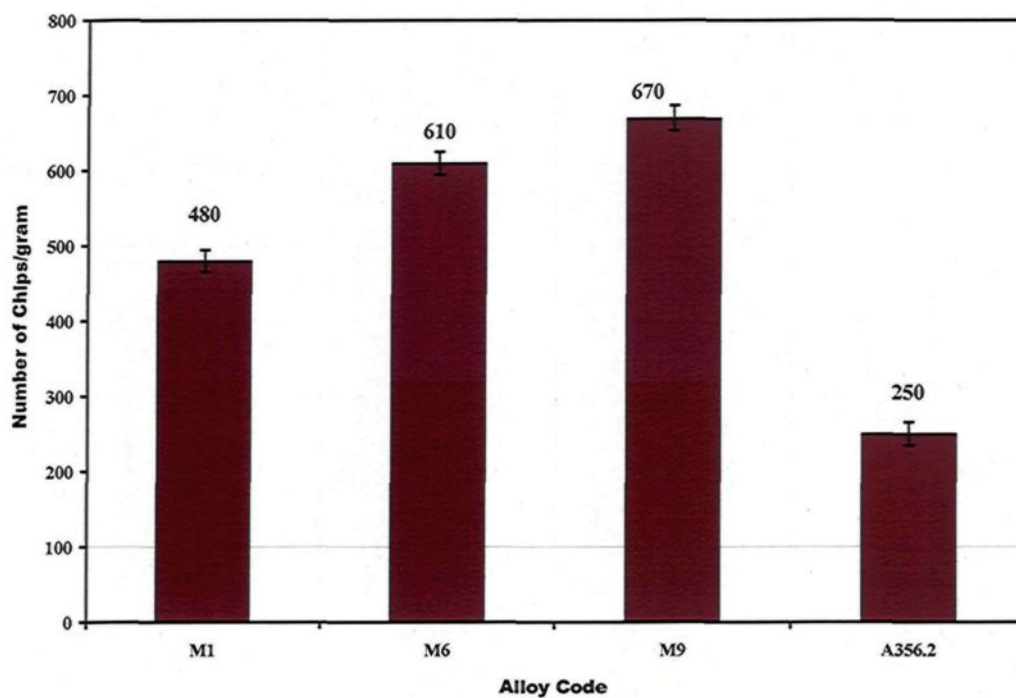


Figure 4.25 Effects of Cu and Mg on chip breakability in terms of the chips-per-gram criterion for the alloys investigated.

CHAPTER 5
EFFECTS OF FREE-CUTTING ELEMENTS ON THE
MACHINABILITY OF Al-Si-Cu-Mg CAST ALLOYS

CHAPTER 5

EFFECTS OF FREE-CUTTING ELEMENTS ON THE MACHINABILITY OF Al-Si-Cu-Mg CAST ALLOYS

5.1 INTRODUCTION

The three main aspects of good machinability are prolonged tool life, low cutting force or power requirements, and chip form. Lower cutting forces result in lower tool-wear rates, better dimensional accuracy, and extended tool life.⁵ Chip shape is the most important factor in obtaining smoothness of the drilling process which will proceed easily if the chips are well-broken. Most ductile materials, however, do not break during drilling and form continuous chips instead.⁹⁵ The main problems arising in the drilling of aluminum cast alloys are considered to be the adhesion, or welding, of the chip to the drill with the concomitant chip-flute clogging. All of these problems are closely related to the process of chip formation and chip removal within the flute itself. Therefore, chip form is often used to assess the machinability of soft, ductile alloys, especially aluminum alloys.⁹⁶

Certain elements known to enhance the wet machinability of aluminum and steel are referred to as free-machining elements. These low melting point elements are added to aluminum alloys to improve their machinability through the formation of insoluble globules which are effective chip breakers resulting in small, easily evacuated chips. The most common free-machining elements include bismuth (Bi), tin (Sn), lead (Pb), and indium (In); because of the harmful effect of Pb on the environment and the high price of In, both

Bi and Sn are the most preferable of choices as free-machining elements.²⁰⁵ There are a number of studies on the machinability of alloys containing low melting-point elements which address Al-Si alloy castings; these have revealed that the dry drilling performance of a cast Al alloy B319 was improved when these new elements, namely Bi, Sn, and Pb, were added.⁵³ Tin was found to be more effective than Bi for improving dry machinability,⁷³ although Bi continues to be preferred over Sn when considering the mechanical properties in the alloy and the hot cracking in the casting.

Previous studies have indicated that the performance of Bi and Sn in Al alloys differ in several ways: (i) the solidification of the embedded Bi in an Al alloy is found to take place over a wide temperature range at a contact angle between 72 ° and 80 °,²⁰⁶ although Sn displayed wetting at the Al grain boundaries;²⁰⁷ (ii) Bi does not display a unique orientation relationship with the Al, whereas Sn possesses a well-defined orientation relationship with it;⁷⁰ (iii) Bi is distributed as inclusions located at the Al grain boundaries and within the grains, but most of the Sn resides in the Al boundaries, primarily at triple junctions; (iv) Sn reduces the hardness and tensile strength, displaying a high tendency toward the formation of Mg₂Sn, because of the high diffusivity of Sn in the Al matrix.²⁰⁸

It should be mentioned here that most of the work carried out to date on free-machining aluminum alloys has involved wrought alloys; only a few studies have dealt with cast alloys. Consequently, in view of the above, the purpose of this chapter is to examine the near-eutectic Al-Si cast alloys containing ~11% Si, namely the 396 alloys, as a basis for understanding the role of the three free-machining elements, Pb, Bi, and Sn, when included in more complex systems for use in industrial applications. In this chapter,

an investigation will be also carried out to study the effects of free-cutting elements namely Sn, Bi, and Sn + Bi on the machinability of hypoeutectic B319.2 cast alloys containing 7% Si with the aim of examining the effects of silicon content on the machining behavior of these alloys.

5.2 MICROSTRUCTURE

The microstructure of Al-Si alloys depends on the chemical composition, casting process, and the heat treatment applied. Optical microscopy and electron probe microanalysis were used to characterize the effects of free-machining elements on the microstructure of the alloys investigated. The metallographic samples were sectioned from the heat-treated machinability test block, as described earlier in Chapter 3.

5.2.1 Silicon Particle Characteristics

The machining characteristics of near-eutectic Al-Si cast alloys depend not only on the chemical composition but, more importantly, on microstructural features such as the morphology of dendritic α -Al, and other intermetallics which are present in the microstructure. The morphology and size of eutectic Si, as well as the precipitation-hardening phases during heat treatment, also exert an important influence on the machining properties. Figures 5.1(a), (b), (c), and (d) show the effects of Sn, Bi, and Pb additions on the microstructure of 396 alloys. Table 5.1 summarizes the eutectic Si-particle characteristics obtained for the alloys investigated. It will be observed that the addition of 0.15% Sn to the M1 alloy, producing M2 alloy, leads to a slight coarsening of the eutectic Si particles, as seen in Figure 5.1 (b) which illustrates that the average roundness and density, in particles/mm², decrease by 7.14% and 17.8%, respectively. The corresponding

data show also that the addition of 0.15% Sn has little effect on the values of the average particle area, particle length, and aspect ratio compared to the M1 alloy, as provided in Table 5.1.

Bismuth has a slightly modifying effect on Al-11% Si alloys. It has been reported that bismuth in aluminum alloys interacts with such major modifiers as sodium and strontium.⁵¹ Small amounts of bismuth, from 0.005% up to 0.05%, are reported to counteract the effects of strontium and nullify modification. Also, it has been proposed that the higher the residual bismuth content, the greater the amount of strontium required for optimum modification.⁵⁸ It should be noted, too, that bismuth forms no known compounds with aluminum or with silicon.⁶⁰ The addition of 0.5% Bi to the 396 alloy counteracts the modifying effect of Sr, as is clearly shown in Figure 5.1(c), leading to a noticeable coarsening of the Si crystals. The eutectic Si-particle analysis of the average particle area showed a jump in this parameter from $4.30\mu\text{m}^2$ in the M1 alloy to $40.60\mu\text{m}^2$ in the M7 alloy. Also, particle length increased from $2.96\mu\text{m}$ in the M1 alloy to $13.30\mu\text{m}$ after the addition of Bi. On the other hand, the average roundness and density decrease significantly, by 56% and 84%, respectively. The impairment of Sr modification in the presence of Bi may be interpreted in terms of a Bi-Mg-Si interaction and/or a Bi-Sr interaction. It is possible that a ternary compound, $\text{Bi}_2\text{Mg}_2\text{Sr}$, and/or the binary compounds, Bi_3Sr , BiSr , Bi_2Sr_3 , and BiSr_2 , may form, resulting in a reduction in the amount of Sr available for modification.⁶⁷

The addition of 0.8% Pb to the M1 alloy is illustrated in Figure 5.1(d); a coarser and partially modified eutectic structure is thus to be observed with this addition, while the

modification level corresponds to that of a class 3 type, namely, partial modification. The corresponding data, see Table 5.1, on the average particle area, particle length, and aspect ratio, respectively, show an increase from $4.30\mu\text{m}^2$, $2.96\mu\text{m}$, and 1.77 in the M1 alloy to $11.6\mu\text{m}^2$, $6.18\mu\text{m}$, and 2.40 in the M8 alloy. On the other hand, the average roundness and density decrease from 70% and 28000 particles/ mm^2 in the M1 alloy to 45.6% and 15000 particles/ mm^2 , respectively, in the M8 alloy.

Table 5.1 also summarizes the eutectic Si-particle characteristics obtained from the image analysis measurements for the B319.2 alloy with respect to the Sn, Bi, and Sn +Bi additions. It will be observed that the addition of these elements yields behavior which is similar to that displayed by the 396 alloy in which the addition of 0.15%Sn has little influence on the eutectic Si particles; on the other hand, a marked effect will be observed with the addition of either 0.5% Bi or the combined addition of 0.15% Sn + 0.5% Bi to the B319.2 alloy, as listed in Table 5.1.

Table 5.1 Summary of the eutectic Si-particle measurements for the alloys studied

Alloy Code	Particle Area (μm^2)		Particle Length (μm)		Roundness Ratio (%)		Aspect Ratio		Density (particles/ mm^2)
	Av	SD	Av	SD	Av	SD	Av	SD	
(a) 396 alloy (Al-10.8%Si)									
M1	4.30	6.51	2.96	2.49	70.00	17.30	1.77	0.784	28000
M2	4.72	6.10	3.00	2.22	65.00	16.20	1.69	0.681	23000
M7	40.60	60.80	13.30	13.70	30.70	18.20	3.39	2.07	4500
M8	11.6	12.9	6.18	5.18	45.60	20.50	2.40	1.44	15000
(b) B319.2 (Al-7%Si)									
M10	7.44	10.60	4.33	3.73	60.00	18.90	2.07	1.05	12000
M11	21.20	16.90	7.30	9.90	45.00	19.60	3.49	2.43	8000
M12	19.90	12.51	6.80	5.30	49.50	20.90	3.51	2.48	9100

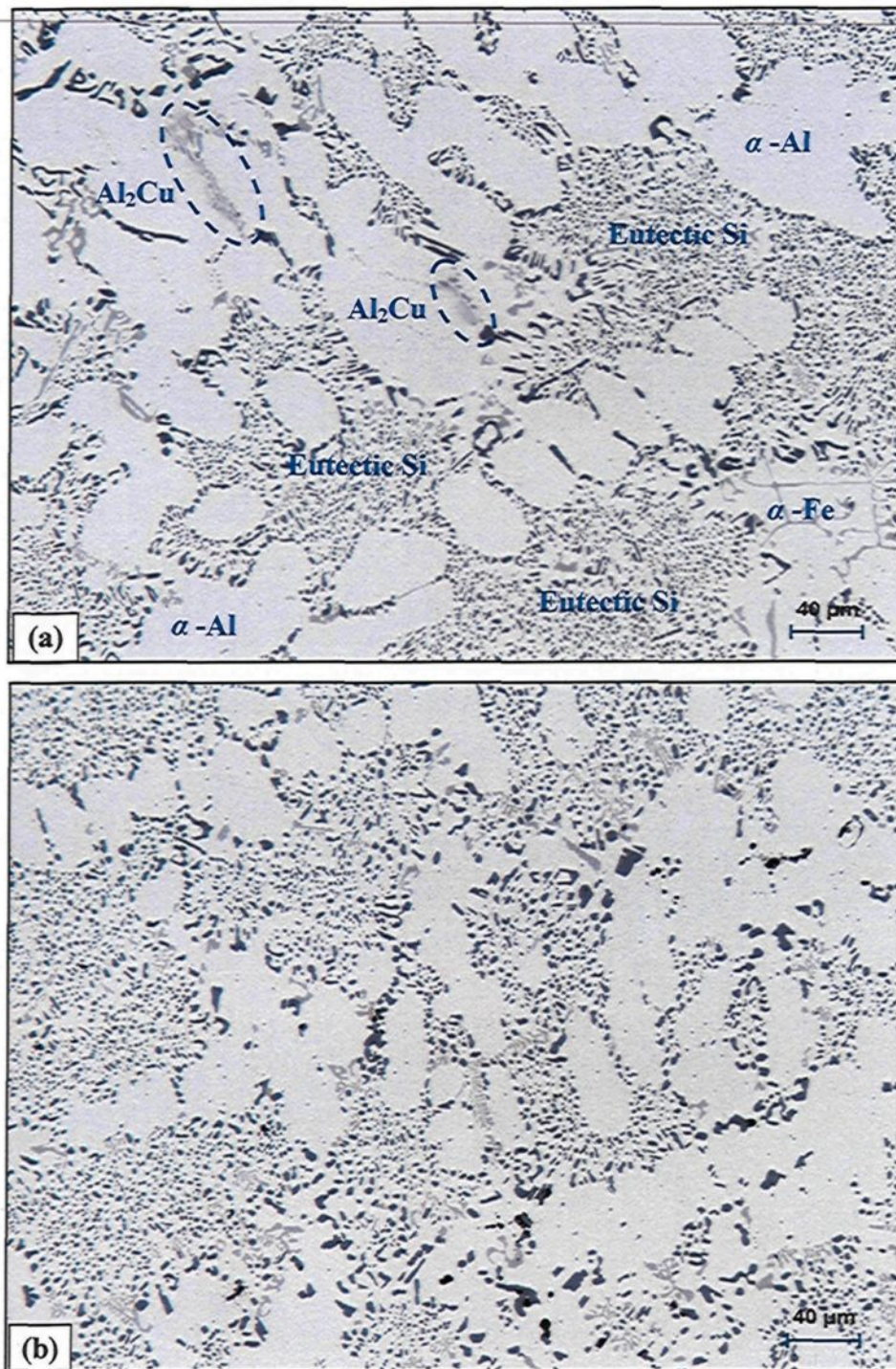


Figure 5.1 Contd.

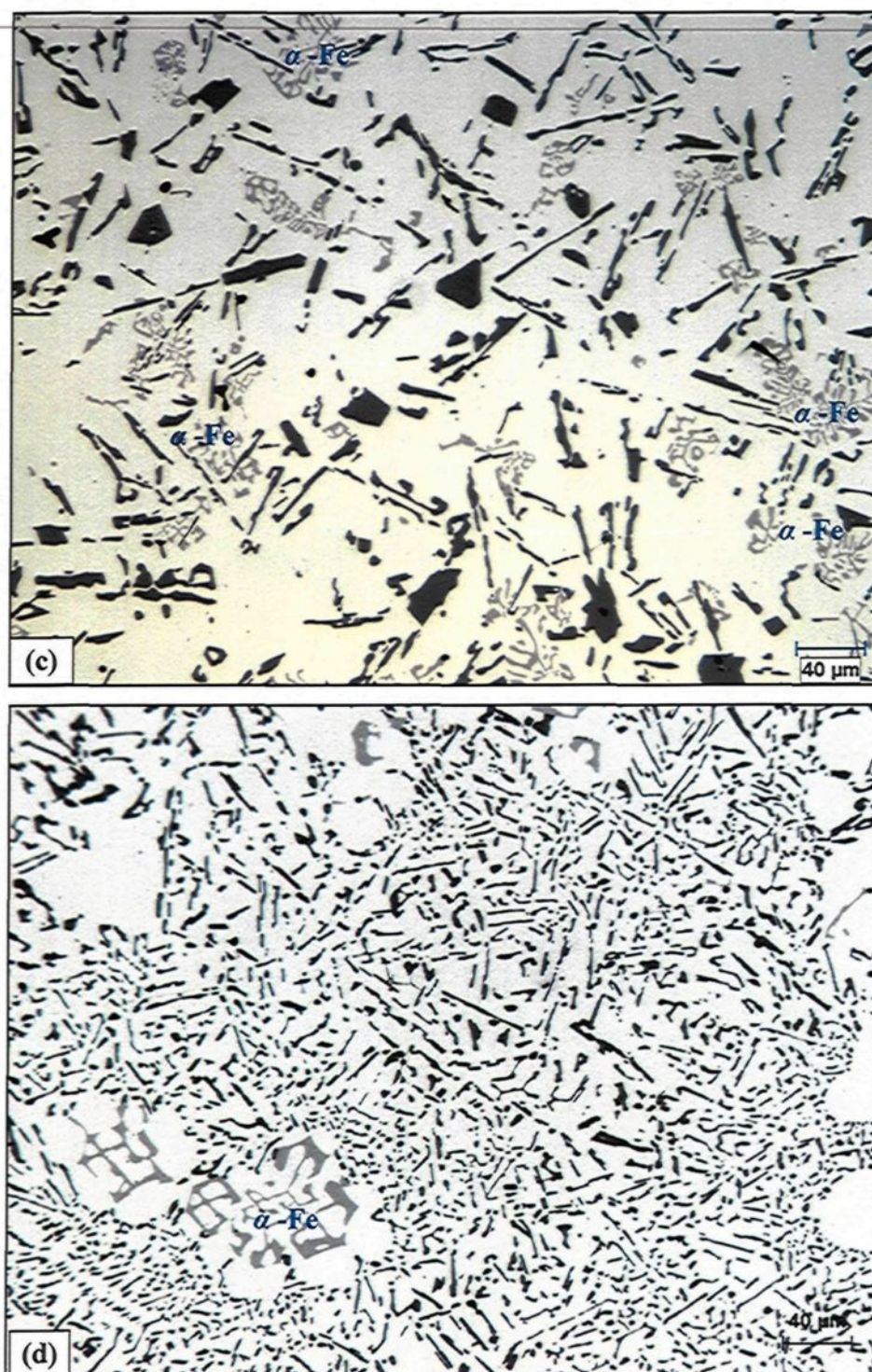


Figure 5.1 Optical micrographs showing the effects of Sn, Bi, and Pb additions on the microstructure of heat-treated 396 alloys in (a) M1 base alloy; (b) M2 (M1 + 0.15% Sn); (c) M7 (M1 + 0.5% Bi); and (d) M8 (M1 + 0.8% Pb) alloys.

5.2.2 Effects of Free-Cutting Elements on Microstructure

The microstructure of the modified, grain-refined and T6 heat-treated 396-M1 alloy, Al-11%Si, is shown in Figure 5.1(a). Eutectic silicon particles which precipitated in the form of fibrous crystals typical of a modified structure represent the main microstructural feature observed. It will also be noted that the iron precipitates in the form of the coarse α -Fe phase which is always seen to occur within α -Al dendrites, indicating that it corresponds to a predendritic reaction and thus tends to nucleate in the liquid alloy prior to solidification. The copper phase, on the other hand, may be seen mainly as small pockets of the block like Al_2Cu phase nucleating either within the aluminum matrix or at the interface of such pre-existing constituents as Si or intermetallic particles.

The size, shape, and distribution of free-machining particles are of critical importance in the machining of Al-Si casting alloys. Figure 5.2(a) shows a backscattered image, obtained at high magnification, of the heat-treated M2 alloy containing 0.15% Sn in which the precipitation of Sn in the form of β -Sn particles may be observed as the white phase. It should be noted that, according to atomic number sequence, the white phases observable in these backscattered images of the matrix are β -Sn, and that the distribution of the β -Sn particles is not uniform, rather, they appear as small clusters. This figure show also that the tin particles, or β -Sn, precipitate within the grey Al_2Cu particles and also as tiny Mg_2Sn particles on the eutectic Si particles; high Sn concentrations may be observed in Figure 5.2 (b) for the β -Sn particles shown in Figure 5.2(a). The corresponding EDX spectrum, as shown in Figure 5.3, displays strong reflections due to Sn. Both X-ray mapping and WDS analysis were also carried out to determine the distribution of Sn, Cu,

and Si within the Sn-containing particles; the application of these techniques revealed clearly that the chemical composition of this phase is β -Sn.²⁰⁹

Figures 5.4 and 5.5(a) provide low and high magnification backscattered images for the M7 alloy containing 0.5% Bi; these images show the morphology of Bi-particles precipitated in the M7 alloy, while the distribution of Bi and Mg within Bi-containing particles is shown in Figures 5.5(b) and (c), respectively. The Bi-phase is not observed as an intermetallic compound with Al, since it is independently distributed; this phase is thus not uniformly distributed in Al-Si alloy structures and has a tendency to segregate, forming a coarse phase because of the high wettability of Bi at the grain boundaries. The size of the bismuth constituents in the M7 alloy matrix varies to a certain extent, which is why a sufficiently fine distribution is preferred in this regard so that free machining would prevail throughout the workpiece. Due to the high atomic number of Bi, it may be detected easily in the form of white particles in the backscattered images.

Figure 5.6(a) shows a backscattered image of the M8 alloy containing 0.8% Pb at low magnification; in accordance with the high atomic number sequence, the white phase in the matrix is composed of Pb-particles which have precipitated within the α -Fe phase. The corresponding EDX spectrum, to be seen in Figure 5.6(b), displays a strong reflection due to the Pb-content of the Pb-containing particles.

Figure 5.7 shows the backscattered image taken from the B319.2-M14 alloy containing 0.5% Bi + 0.15% Sn showing the presence of Bi- and Sn-particles precipitated in the alloy. In the binary phase diagram for Sn-Bi, the eutectic reaction occurs at 43wt%

Sn with a melting point of 130°C; there is thus no evidence for the formation of any eutectic compound between Bi and Sn in the B319.2-M14 alloy.

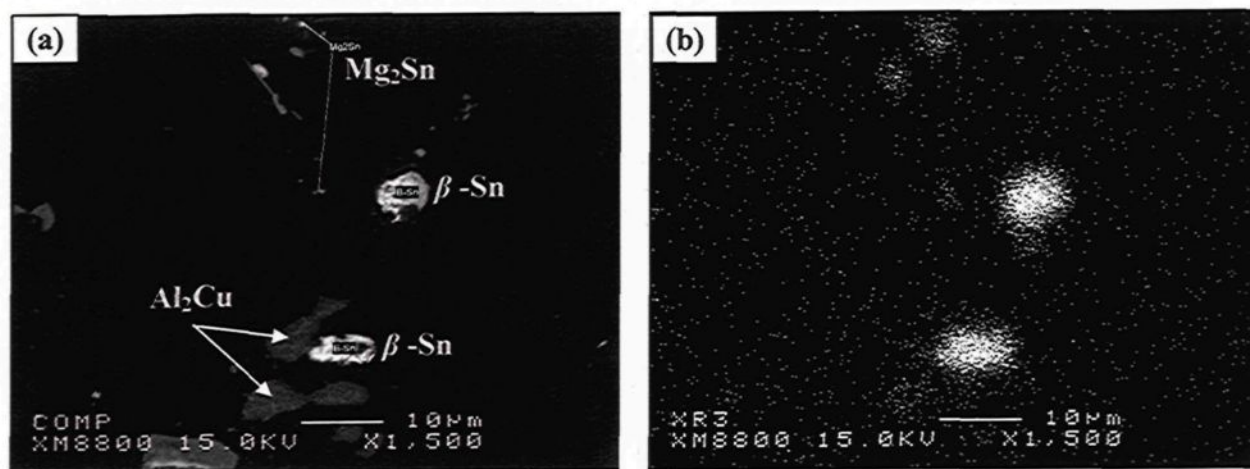


Figure 5.2 (a) High magnification backscattered image of the M2 alloy showing precipitation of β -Sn, (b) X-ray image of Sn distribution for the same particles illustrated in (a).

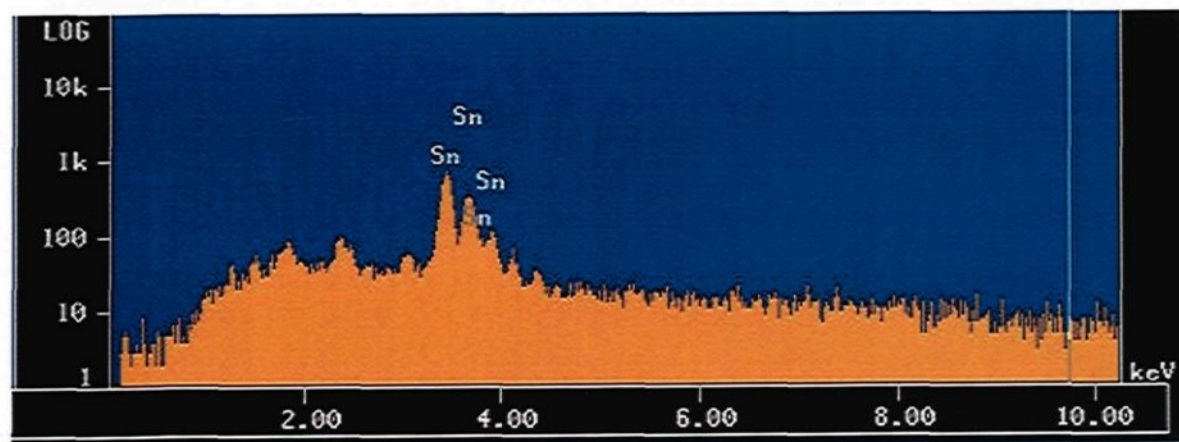


Figure 5.3 EDX spectrum corresponding to β -Sn particles observed in M2 alloy containing 0.15% Sn.

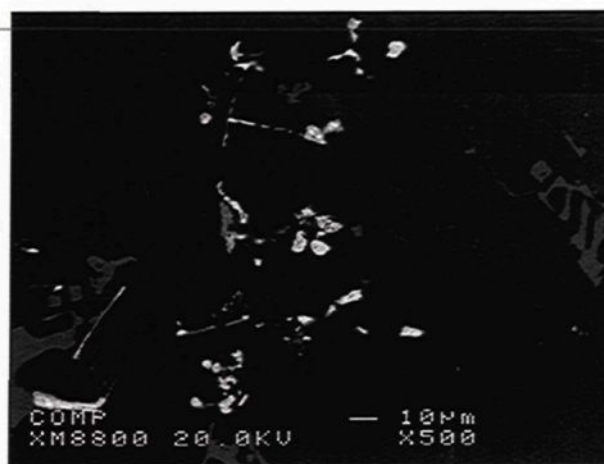


Figure 5.4 Low magnification backscattered image obtained from the M7 (M1 + 0.5% Bi) alloy showing precipitation of Bi-containing particles.

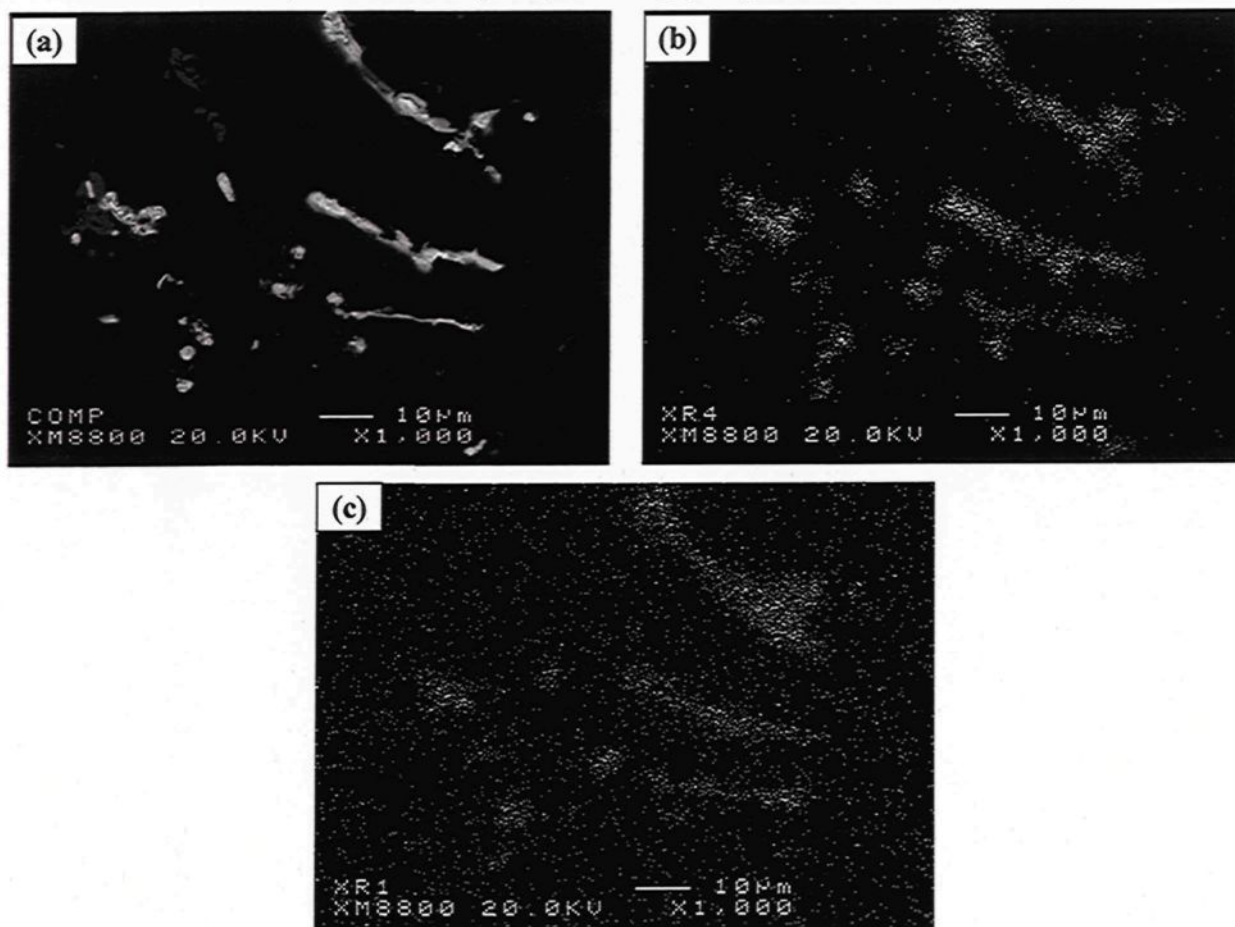
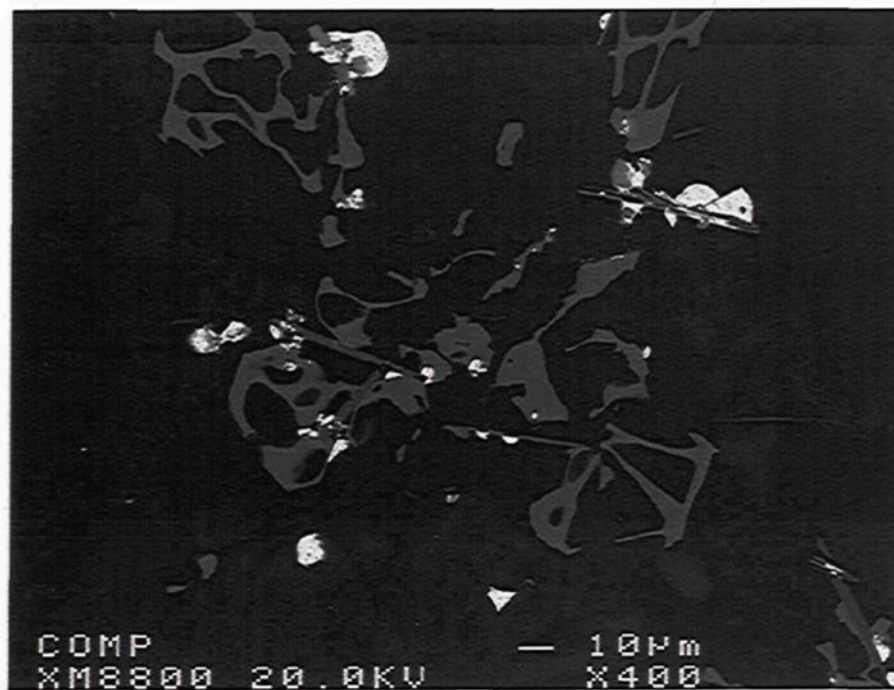
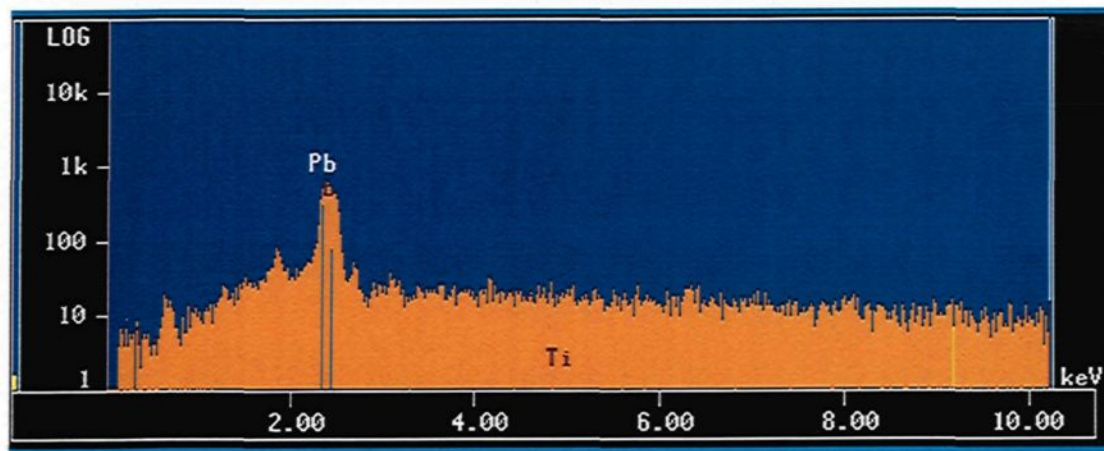


Figure 5.5 (a) Backscattered image of the M7 (M1 + 0.5% Bi) alloy showing morphology of Bi-containing particles, and X-ray images of (b) Bi and (c) Mg distribution for the same particles illustrated in (a).



(a)



(b)

Figure 5.6 (a) Backscattered image of the M8 (M1 + 0.8% Pb) alloy showing the precipitation of Pb-containing particles (white), (b) EDX spectrum corresponding to Pb-containing particles.

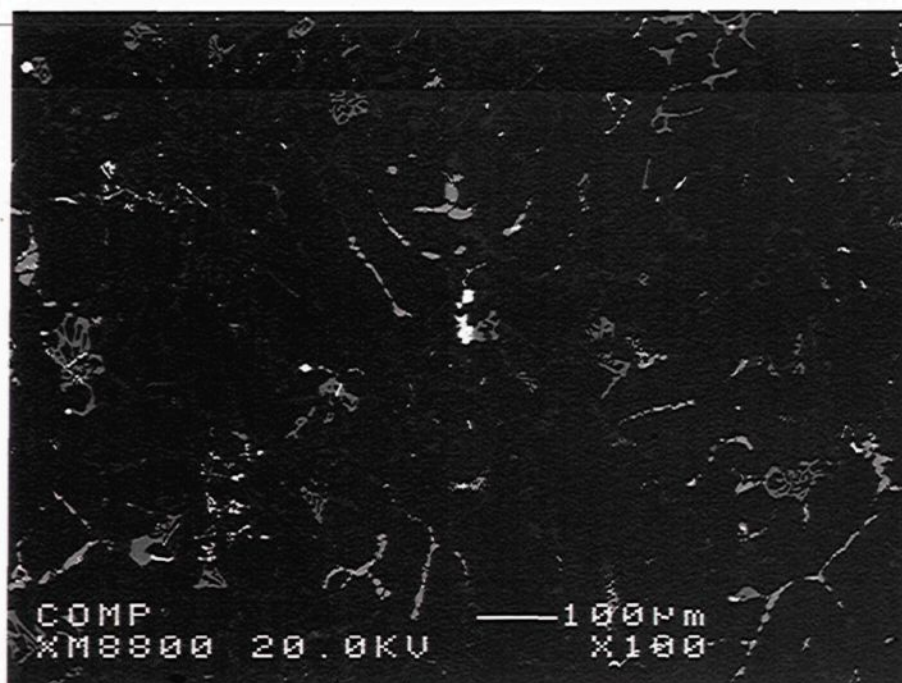


Figure 5.7 (a) Low magnification backscattered image obtained from the M12 (B319.2 + 0.15% Sn + 0.5% Bi) alloy showing the presence of Bi and Sn particles (bright white particles).

5.3 HARDNESS AND TENSILE PROPERTIES

The effects of elements having low melting-points on the mechanical properties of Al alloys have been reported in various studies. Mohamed *et al.*²¹⁰ investigated the effects of trace additions of Sn on the mechanical properties of B319.2 and A356.2 alloys; their results show that the higher ductility of Sn-containing alloys in the as-cast condition may be attributed to the stress-strain state of the matrix material associated with the fine Sn-bearing phase. In a study of the effects of Mg on the mechanical properties of secondary Al-Si-Mg alloys containing 0.1% Sn or 0.2% Pb, it was found that, with an increase of the Mg content from 0.2 to 0.5 - 0.8%, the Sn and Pb in the given concentration do not impair the mechanical properties, particularly in the heat-treated condition.²¹¹ Grebenkin *et al.*²¹²

indicated that Sn and Pb are analogs of Si in electron distribution; these elements are capable of replacing Si in compounds with Mg which prevents the formation of Mg_2Si or $Al_xMg_5Cu_4Si_4$ hardening phases in Al-Si alloys.

Table 5.2 provides the relevant data relating to T6 heat-treated mechanical properties; these include the hardness (BHN), yield strength (YS), ultimate tensile strength (UTS), and percent elongation (%El) of the Sr-modified 396 alloys after the addition of Sn, Bi, and Pb. The corresponding hardness data indicate that the M7 containing 0.5% Bi has the highest hardness values compared to the other alloys. On the other hand, the presence of 0.5% Bi in the M7 alloy results in a decrease of YS, UTS, and %El by 10%, 9%, and 34%, respectively. The significant reduction observed in the ductility value of the M7 alloy may be attributed to the effects of the addition of Bi in transforming the structure of the M1 base alloy from a well-modified to a non-modified structure, as shown earlier in the discussion on microstructure. It is important to mention here that the reduction caused in the tensile properties of the M7 alloy, compared to the M1 alloy, may be explained in terms of the Bi-Mg interaction which consumes the Mg available for the precipitation of Mg-hardening phases. It was reported that Bi is a surface active element, and its accumulation near intermetallic and Si particles may reduce the energy of the system. Most of the Bi particles were connected to intermetallic phases and Si phases, which has a deteriorating effect on the mechanical properties of the alloys.²¹³ It will be observed that the addition of 0.15% Sn causes a marginal reduction in either the hardness or the tensile properties of the 396-M1 alloy. The same results were observed in the case of the addition of 0.8% Pb. Table 5.2 also

lists the mechanical properties of the B319.2 alloys, namely M10 containing 0.15% Sn, M11 containing 0.5% Bi, and M12 containing 0.15%Sn + 0.5% Bi.

Table 5.2 Summary of mechanical properties for the alloys studied

Alloy Code	BHN (MPa)	YS (MPa)	UTS (MPa)	EI (%)
(a) 396 alloy (Al-10.8%Si)				
M1	108 ± 3.56	358.10 ± 1.55	394.04 ± 6.27	0.98 ± 0.12
M2	106 ± 3.19	351.65 ± 2.57	390.54 ± 5.73	1.02 ± 0.15
M7	115 ± 3.76	321.39 ± 3.34	360.61 ± 11	0.65 ± 0.14
M8	108 ± 1.30	335.72 ± 5.76	371.74 ± 6.52	0.93 ± 0.13
(b) B319.2 (Al-7%Si)				
M10	108 ± 3.39	392.83 ± 3.48	404.08 ± 3.75	0.77 ± 0.03
M11	111 ± 2.52	320.49 ± 7.2	380.93 ± 5.20	0.61 ± 0.03
M12	109 ± 3.68	289.00 ± 2.7	290.99 ± 11	0.626 ± 0.06

5.4 MACHINING BEHAVIOR

Free-machining elements such as Pb, Bi, In, Se, and Bi are added to aluminum alloys to cut down on chip breakage and to minimize friction, thus allowing for higher machining speeds, improved tool life, better surface finish, and greater dimensional control with a concomitant decrease in machining costs.⁸ The upcoming sections will investigate the influence of free-machining elements on the machinability of 396 and B319.2 cast alloys; it should be mentioned here that the pertinent machinability criteria relate to tool life, chip shape, and BUE evolution, together with the cutting forces and moments. A thorough understanding of the role of these elements in the alloys studied would make it possible to select suitable material and workpiece design to obtain the optimum machining combination conducive to maximum productivity.

5.4.1. Cutting Forces and Tool Life

5.4.1.1 396 Alloys (Al-11% Si)

A number of Sr-modified, grain-refined, and T6 heat-treated 396 alloys were selected in order to study the effects of the addition of free-machining elements: (i) on the mean total drilling force, (ii) on the mean total drilling moment, and (iii) on the mean drilling power, when based on the mean value of 90 holes; these free-machining elements, include Sn, Bi, and Pb. The alloys in question were individually represented by the 396 base alloy, coded M1; 396 + 0.15% Sn, coded M2; 396 + 0.5% Bi, coded M7; and 396 + 0.8% Pb, coded M8, yielding hardness values of 108, 106, 115, and 108 BHN, respectively.

The results obtained from the drilling tests reveal that the mean total drilling force, the mean total drilling moment, and the mean drilling power all increase as the number of holes drilled increases; this form of increase is clear from Figures 5.8(a), (b), and (c), respectively. It should also be noted that the greatest fluctuation values in the total drilling forces can generally be observed with a higher number of holes drilled; this analysis agrees with the mean total drilling moment and the mean drilling power of the M1 alloy. The drilling data also suggest that the effects of the addition of free-machining elements on machinability criteria is that the reduction in drilling power is more pronounced than is the reduction in total drilling forces. This observation may be explained by the fact that the drilling power responses are mostly susceptible to chip clogging in drill flutes¹¹⁷ whereas drilling force is vulnerable to changes in the geometry of the cutting edges.⁵

Figures 5.8(a), (b), and (c) show that the addition of 0.5% Bi to the M1 alloy, thereby creating M7 alloy, improves alloy machinability by lowering the mean total

drilling forces and moments, as well as the mean drilling power compared to the M1 alloy. The M7 alloy generated an average of 17% lower drilling forces ranging from 13% to 21%, and exhibited an average of 20% lower drilling moment ranging from 24% to 16%, as well as an average 28% less drilling power ranging from 30% to 25% compared to the M1 alloy over the evaluation period of 630 holes. By contrast, the presence of 0.5% Bi in the 396 alloys causes a deterioration in drill life, whereas the drill life of the M1 Bi-free alloy decreases from 2160 holes/drill to only 630 holes/drill in the Bi-containing M7 alloy, corresponding to a reduction in drill life by 71%, as shown in Figure 5.9. It may be concluded, then, that the Bi-containing M7 alloys exerts a negative influence on drill life, although its is observed to exhibit lower drilling forces, moment, and power compared to the M1 base alloy.

The addition of Sn to 396 casting alloys in small but effective amounts of ~0.15%, thereby producing the M2 alloy, significantly improves the machinability characteristics of these alloys with respect to mean drilling power; which decreases by an average 17% ranging from 20% to 13% compared to the Sn-free M1 alloy, as shown in Figure 5.8(c). On the other hand, the addition of 0.15% Sn to the M1 alloy has some slight effect in decreasing the mean total drilling force as well as the mean total drilling moment which decrease by an average 7% and 6%, respectively, over the evaluation period of 2160 holes, as shown in Figures 5.8(a) and (b). During drilling tests, it was also found that the M2 alloy containing 0.15% Sn displayed the same number of holes drilled in the M1 base alloy having 2160 holes/drill, followed by the M8 alloy containing 0.8% Pb having 1512 holes/drill, and finally the M7 alloy containing 0.5% Bi, which displayed a noticeable

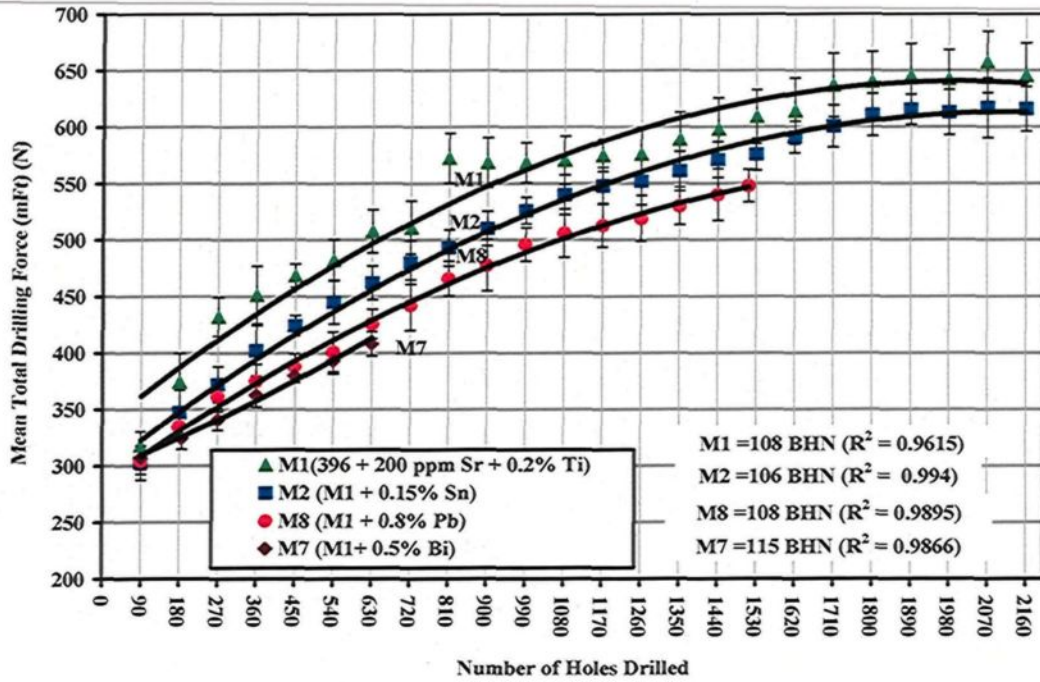
shortening of drill life having 630 holes/drill. Thus, the addition of 0.15% Sn to the 396 alloys has a positive effect on drill life since the Sn-containing alloy yields the longest drill life, *i.e.* three-and-a-half times that of the Bi-containing alloy, and one-and-a-half times that of the Pb-containing alloy. It should be mentioned here that the Sn-containing M2 alloy requires much higher values of drilling force, moment, and power than are needed by the Bi- and Pb-containing M7, and M8 alloys, respectively.

Lead (Pb) was used for the purposes of this study because it has already been recognized as a free-machining element. It is considered that the addition of Pb to aluminum alloys is the method most adequate for improving their machinability values; Pb, however, is not a suitable choice as an additive based on environmental concerns. Recent work has involved replacing Pb in free-machining wrought alloys with more environmentally friendly additives such as the elements Sn or Bi.⁵² In this study, the free-machining M8 alloy containing 0.8% Pb displays a reduction in the drilling force, the drilling moment, and in particular the drilling power which decreased by an average of 80% compared to the Pb-free M1 alloy, as shown in Figure 5.8(c).

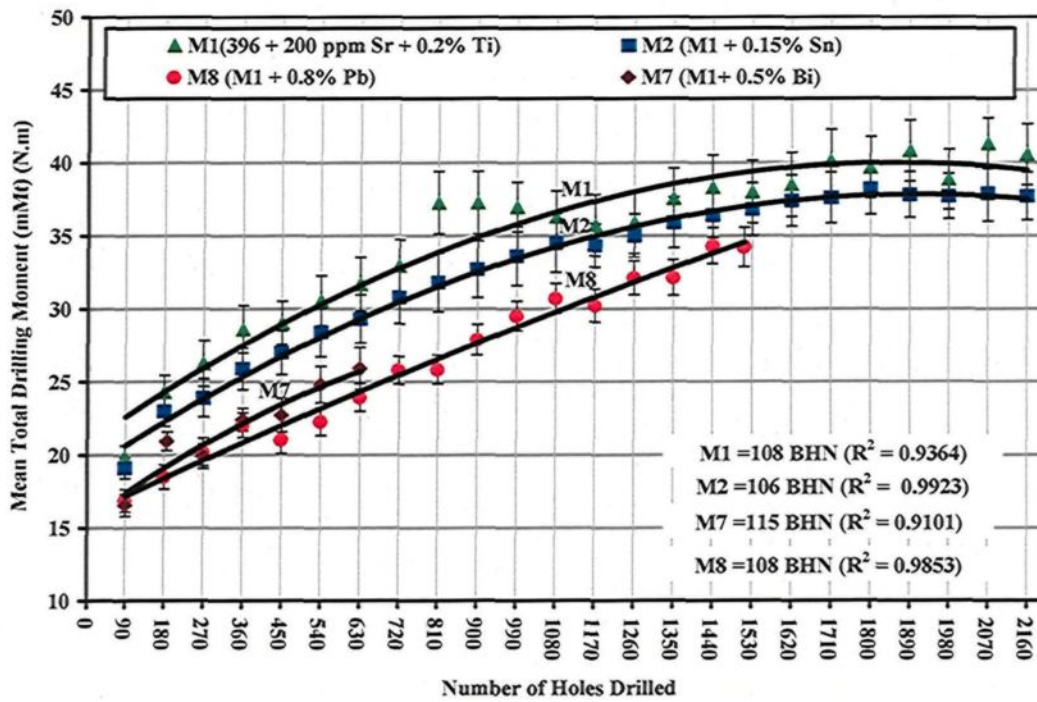
The above results show that the machinability of the alloys under investigation was significantly improved by adding small amounts of free-machining elements to the alloy. The effects of free-machining elements may be interpreted by an examination of the alloy microstructure as discussed previously in section 5.2.2 together with an analysis of the existing bibliographic data regarding the effects of these elements on the machinability of the alloys. Thus, the factors involved in reducing the drilling force and moment for the free-machining alloys may be considered in terms of the following: (i) precipitation of free-

machining elements in the form of low melting-point constituents compared to the aluminum base alloy; (ii) void formation due to the non-uniform deformation of free-machining phases and the Al matrix during the machining process; or (iii) a combination of these two events.

With regard to the Sn-containing M2 alloy, it was found that the Sn additive tends to precipitate in the elemental form at a low melting point of 232°C, being significantly lower than it is for the Al-matrix. It is presumed that Sn in its pure form will soften or melt at cutting temperatures, as shown in Figure 5.10, tending to decrease the ductility of the material in the cutting zone, thereby in turn causing a reduction in cutting forces. This observation is in satisfactory agreement with Smolej *et al.*^{52,56} who substituted Pb and Pb + Bi with Sn in the standard AA2030 and AA2011 alloys, respectively. They reported that, as a result of the extremely limited solubility of the Sn particles in the Al-matrix, these particles remain as separate entities dispersed in the matrix; during machining operations, it is believed that the temperature generated in the cutting zone is high enough to soften or even to melt these dispersed entities. Consequently, this melting gives rise to a local loss of material strength and ductility which in turn leads to the formation of broken chips. Moreover, the low-melting elements act as a lubricant during machining, thereby decreasing the friction between chip and tool edge which then results in a reduction in the cutting forces.

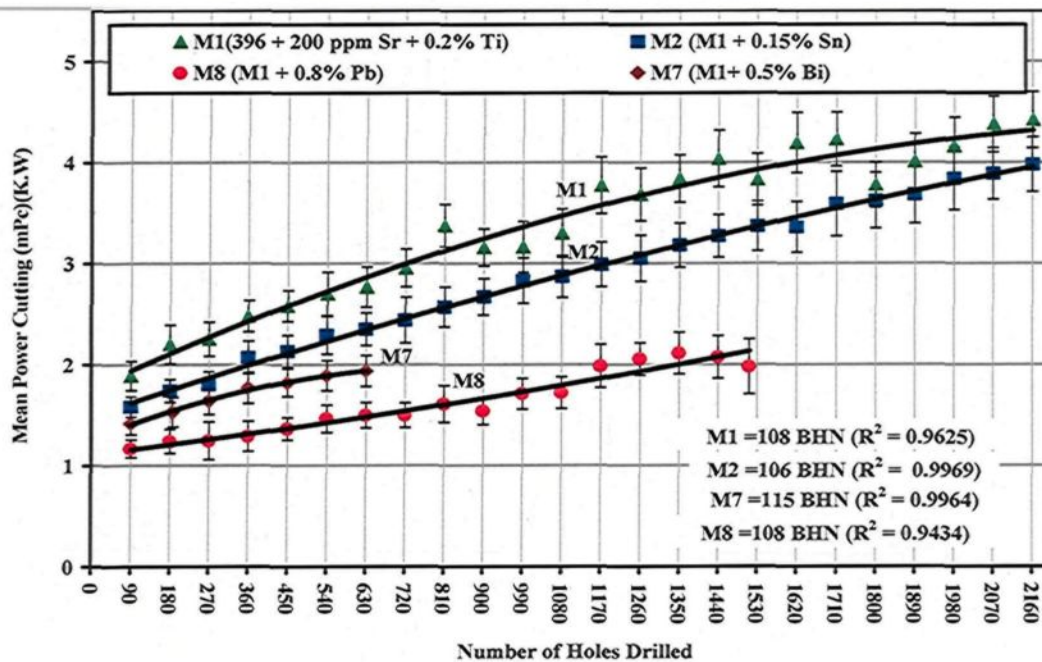


(a)



(b)

Figure 5.8 Contd.



(c)

Figure 5.8 Effects of adding Sn, Bi, and Pb on the machinability of 396 (M1, M2, M7, and M8) alloys in terms of (a) mean total drilling force; (b) mean total drilling moment; and (c) mean cutting power required for drilling 90 holes.

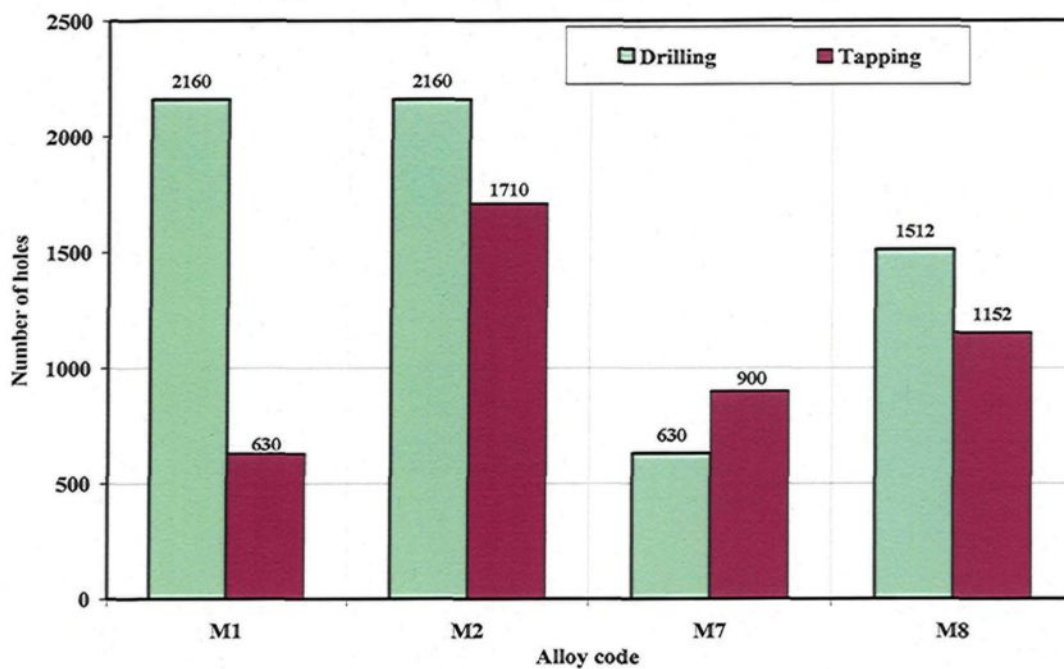


Figure 5.9 Effects of adding Sn, Bi, and Pb on the drill/tap life of the M1, M2, M7, and M8 alloys in terms of the number of holes drilled and tapped.

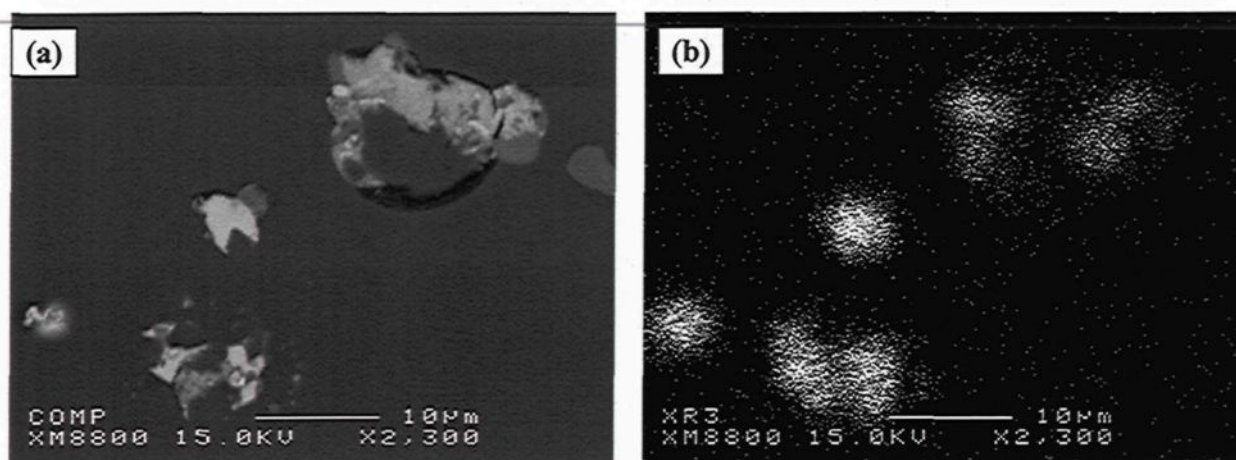


Figure 5.10 (a) High magnification backscattered image showing molten Sn particles in the M2 (M1+0.15% Sn) alloy after machining processes, (b) X-ray image of Sn distribution for the same particles illustrated in (a).

With regard to the Bi-containing M7 alloy, it should be kept in mind here that Bi, a highly reactive element, reacts not only with Sr but also with Mg to form the binary compound Bi_2Mg_3 having a very high melting point of 821°C which is considerably higher than that for 396 alloys as a whole. This type of Bi-Mg-Sr interaction was also confirmed in research carried out by Elhadad.²¹⁴ In fact, Mondolfo⁶⁶ stated that the Bi_2Mg_3 compound, once formed, is relatively hard and will attain a high melting point; from this it may be deduced that Bi additions to Al-Mg alloys do not improve the machinability values. Couper²¹⁵ also reported that the effectiveness of adding Bi in enhancing the machinability of Al-Si-Mg alloys was found to be reduced by the loss of Bi in the formation of Bi_2Mg_3 compounds. For further investigation, X-ray mapping was conducted on Bi-containing particles to determine the distribution of Bi, Mg, and Sr, as shown in Figure 5.11; in this regard, the X-ray images of Bi and Mg distribution in the Bi-containing particles were shown earlier in Figure 5.5.

The mechanism involved in decreasing the drilling force and moment for Bi-containing alloys may be explained by the fact that when the free-machining phase does not precipitate in the form of a eutectic or low melting-point compound such as the Bi phase, it may persist as a discontinuity in the aluminum alloy matrix. Consequently, when the matrix material is being subjected to drilling forces, the Bi-containing phase will tend to react to shear stress in a different manner with respect to its surrounding aluminum alloy matrix, thereby creating voids between them. The continued application of machining forces creates new voids and propagates existing ones until these voids interconnect and machining chips are formed. It may thus be concluded that the addition of Bi decreases the drilling force and moment not only through its lubricant effect when part of the Bi particles precipitate in the elemental form but also through its role in decreasing alloy ductility; the Bi-containing M7 alloy, on the other hand, causes a deterioration of the mechanical properties, particularly ductility, which decreases by 0.34% compared to the M1 alloy, as shown previously in Table 5.2.

The presence of 0.5% Bi in the 396 alloys leads to a deterioration of drill life since the drill broke down after only 630 holes although the cutting force results revealed that the Bi is more highly effective than Sn in reducing both drilling force and moment. This noticeable reduction in drill life may be explained by the fact that Bi counteracts the modification effect of Sr through Bi-Mg-Sr interactions which reduce the amount of free Sr available for Si modification; these interactions are expected to take place in the molten state prior to the precipitation of the eutectic Si. As a result, the Si appears in coarse, acicular form instead of as finely-distributed fibrous particles, as evidenced by the optical

microstructure shown in Figure 5.1(c). If the eutectic silicon structure is coarse, tool life suffers and results in an increase in the rate of drill wear. Figures 5.12(a) and (b) show the effects of the addition of Bi on the outer corner of the drill and tool edge after drilling the M7 alloy. As may be seen, wear is visible on the tool edge and at the outer cutting corner of the drill. When the corners of the drill are rounded off, the drill then sticks to the workpiece and breaks if the cutting process is not halted in time.

In the tapping test, the mean total tapping forces and moment were used as criteria for characterizing the alloys studied. The tapping results showed that the M2 alloy containing 0.15% Sn exhibited a significant reduction in the tapping force and moment; in this regard, the M2 alloy generated an average 41% lower tapping force ranging from 42% to 39%, with an average 43% lower tapping moment ranging from 44% to 41% compared to the M1 base alloy over the evaluation period of 630 holes, as shown in Figures 5.13(a) and (b). It was also found that the M2 alloy showed a higher number of holes tapped with 1710 holes/tap followed by the M8 alloy containing 0.8% Pb with 1152 holes/tap, and the M7 alloy with 0.5% Bi yielding 900 holes/tap, and finally the M1 base alloy producing 630 holes/tap, see Figure 5.9. Thus, the addition of 0.15% Sn to the 396 alloys has a beneficial effect on the tool life of both carbide drills and HSS taps. This particular effect on tool life may be explained in terms of the following facts. Firstly, eutectic silicon particles from the Sn-containing alloys tend to precipitate in uniformly distributed and fibrous crystals typical of a modified structure, as shown earlier in Figure 5.1(b). According to Miller,¹⁷ a fine, well-modified eutectic silicon structure is far less detrimental to drill life than a non-modified one. Secondly, tin particles are smaller and more uniformly distributed in

comparison with the Bi particles in the Bi-containing alloys. According to the binary phase diagram for Mg-Sn, magnesium is bonded with Sn into the intermetallic compound Mg_2Sn containing 29 wt% Sn with a melting point of 770.5°C.⁶⁶ Microstructure analysis also showed that, unlike Bi, Sn does not seem to form higher melting intermetallics with Mg in the alloy.

The addition 0.5% Bi to the 396 alloy has a noticeable effect in that it decreases the total tapping force and moment by an average of 24% and 8%, respectively, compared to the M1 base alloy. It should be mentioned here that a similar trend was also found during the tapping of the M8 alloy containing 0.8% Pb since the tapping force and moment were observed to decrease by 36% and 31%, respectively, compared to the M1 alloy, as shown in Figures 5.13(a) and (b). It is worth noting that the morphology of silicon particles affects the tapping forces and moment significantly, since HSS taps were used in the tapping tests instead of a carbide drill which was used in the drilling tests. Thus, the Bi-containing alloy exhibits higher tapping forces and moments when compared to the Sn- and Pb-containing alloys. This increase in tapping forces and moments may be explained by the presence of Bi which results in the Si particles appearing in the form of coarse, acicular plates instead of as finely-distributed fibrous particles as in the Sn-containing alloys. As was indicated previously in the discussion on microstructure, the addition of 0.5% Bi to the 396 alloy leads to a noticeable coarsening of the Si crystals since the average particle area increases from $4.30 \mu m^2$ in the Bi-free alloy to $40.6 \mu m^2$ in the Bi-containing alloy; consequently, the rate of wear on the tap increases as the silicon-particle size increases. According to Bezerra

and Coelho,¹³² HSS taps react much more sensitively to abrasive wear than do the carbide tools used for drilling.

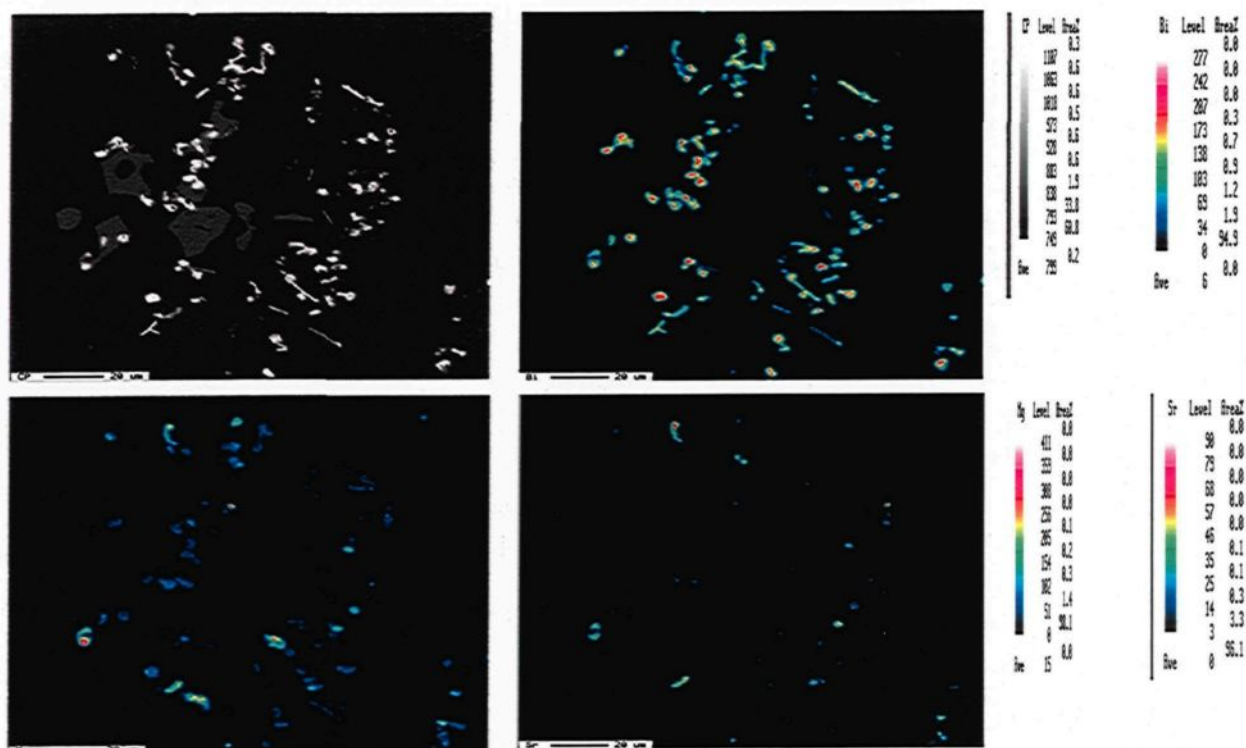
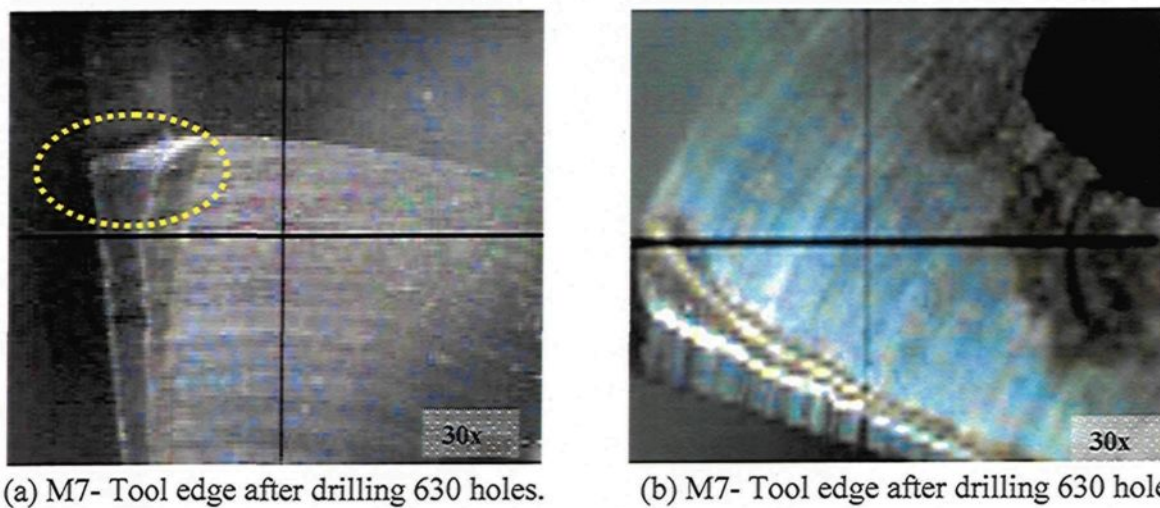


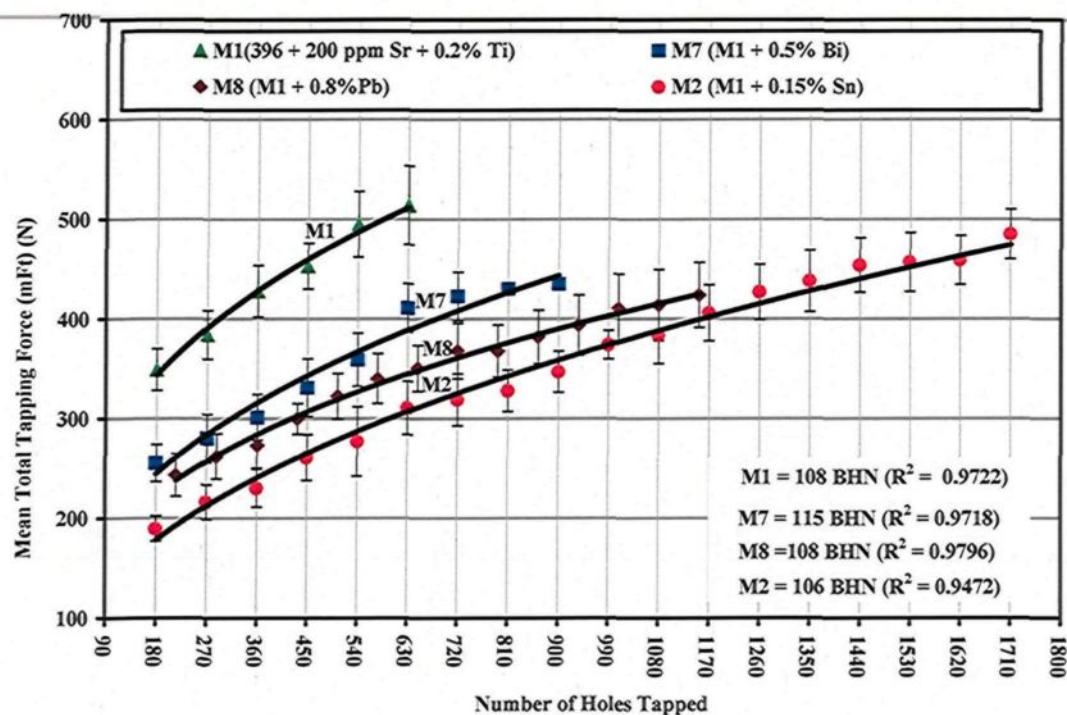
Figure 5.11 Backscattered image of the M7 alloy showing the precipitation of Bi-particles and the corresponding X-ray images of Bi, Mg, and Sr.



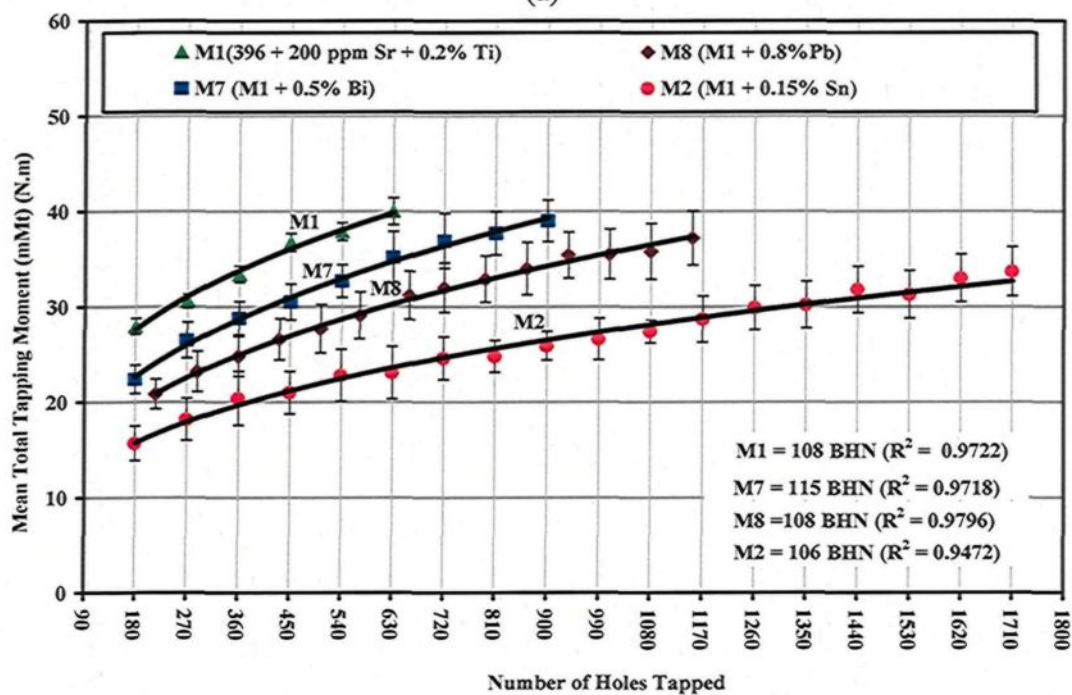
(a) M7- Tool edge after drilling 630 holes.

(b) M7- Tool edge after drilling 630 holes.

Figure 5.12 Photographs showing wear occurring on (a) outer corner and (b) cutting drill lip of the M7 alloy (containing 0.5% Bi) after stripping the BUE in a solution of NaOH.



(a)



(b)

Figure 5.13 Effects of Sn, Bi, and Pb additions on the machinability of 396 (M1, M2, M7, and M8) alloys in terms of (a) mean total tapping force; and (b) mean total tapping moment required for tapping 90 holes.

5.4.1.2 B319.2 Alloys (Al-7% Si)

The microstructure of hypoeutectic B319.2 alloys consists of the Al-based solid solution of α -Al displaying pronounced dendritic solidification and fine-grained eutectic Si particles, with the solid solution α -Al representing the soft phase of the alloy.

A number of Sr-modified, grain-refined, and T6 heat-treated B319.2 alloys containing 7% Si were selected to study the effects of individual as well as combined additions of Sn and Bi on the mean total drilling force and moment based on the mean value of 100 holes, as illustrated in Figure 5.14. The alloys in question were represented by B319.2 + 0.15% Sn, coded M10; B319.2 + 0.5% Bi, coded M11; and B319.2 + 0.15%Sn + 0.5%Bi, coded M12, yielding hardness values of 108, 111, and 108 BHN, respectively. The results revealed that the addition of 0.5%Bi to the B319.2 alloy, producing the M11 alloy, decreases the mean total drilling forces and moment compared to the M10 alloy containing 0.15% Sn. Such reductions through the addition of bismuth may be obtained either as a result of the softening of the bismuth particles from an increase in local temperature or through void formation due to a deformation mismatch between bismuth and the aluminum matrix during machining.^{71, 72}

The Bi-containing alloy, namely M11, on the other hand, has a detrimental effect on drill life, whereas the drill life of the Sn-containing M10 alloy decreases from 2100 holes/drill to only 1100 holes/drill in the M11 alloy, corresponding to a reduction of 48% in drill life. It is important to note that the detrimental effect of Bi additions on the drill life of the 396-M7 alloy is more pronounced than it is for the B319.2-M11 alloy since drill life is reduced by 71% during the machining of the 396-M7 alloy compared to 48% in the case of

the B319.2-M11 alloy which contains a similar level of Bi addition of about 0.5%. This particularity may be ascribed to the abrasiveness of the 396 alloy resulting from its higher Si content of 10.8% compared to 7% in the B319.2 alloy.

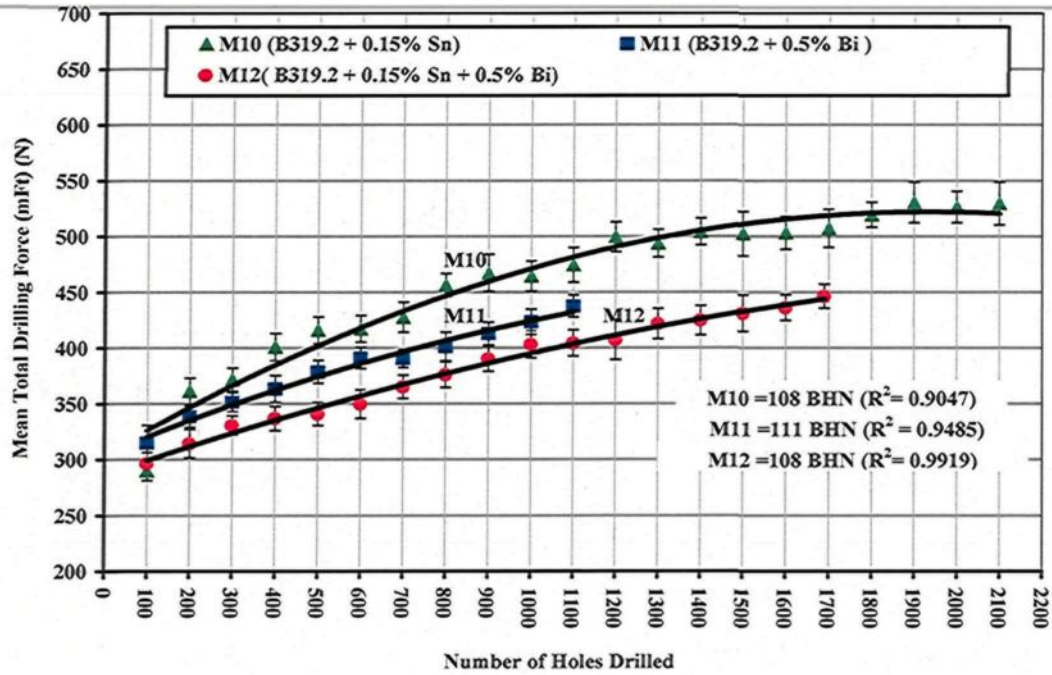
The simultaneous addition of smaller amounts of two or more elements insoluble in aluminum has a greater effect on machinability than individual additions of each element in terms of drilling force and moment. It was found that compound additions of 0.15% Sn + 0.5% Bi made to the B319.2 alloy, creating M12 alloy, lowers the drilling forces by 15% and 7% compared to the Sn-containing M10 alloy and the Bi-containing M11 alloy, respectively. It appears that the additives have the same effect on the drilling moment which was found to have decreased by 23% and 13%, respectively, as may be seen in Figures 5.14 (a) and (b). These results are consistent with work carried out by Smolej^{52,56} which confirmed that tin phases together with other phases of alloying elements and impurities reduce the cohesion of crystal grains, thereby leading either to the accelerated rupture of the material during the course of cutting or to easier breakage of chips resulting in a reduction in the cutting forces.

It was also found that the compound addition of Sn+Bi improves drill life compared to individual additions of Bi alone, whereby drill life increases from 1100 holes/drill in the M11 alloy containing 0.5% Bi to 1700 holes/drill in the M12 alloy containing 0.15% Sn + 0.5% Bi. The Sn-containing M10 alloy, however, produces the longest drill life, *i.e.* twice that of the M11 alloy and one-and-a-half times that of the M12 alloy.

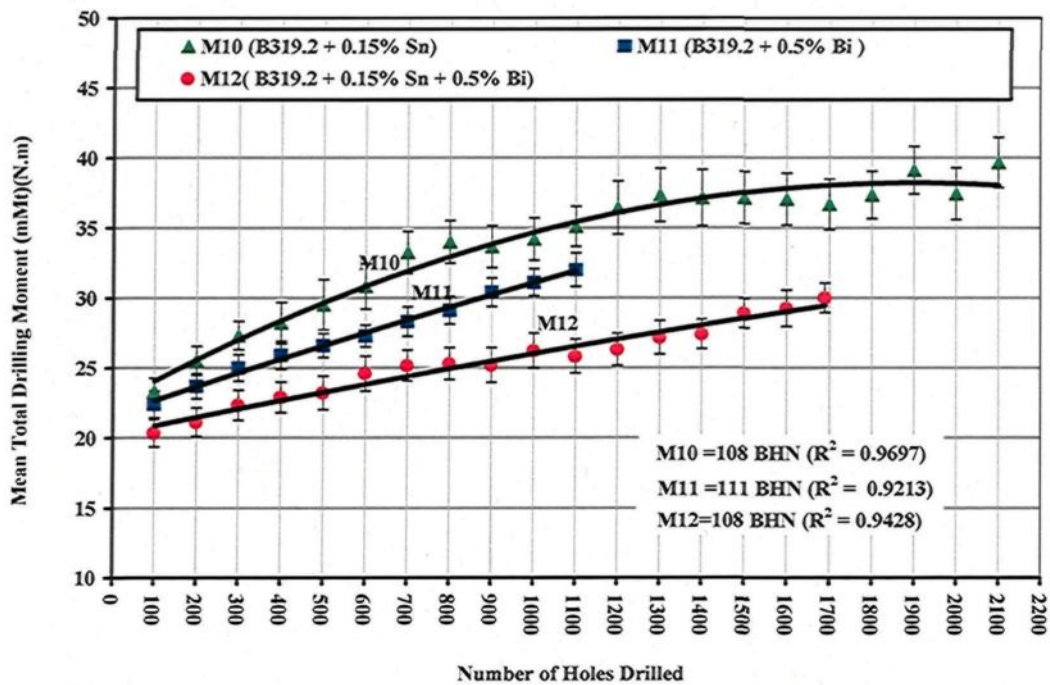
In tapping tests, it was observed that the addition of 0.5% Bi individually to the B319.2 alloy, creating the M11 alloy, or in combination with 0.15% Sn, creating the M12

alloy, produced higher mean total tapping forces and moments compared to the B319.2 alloy containing only 0.15% Sn, creating the M10 alloy, as is shown clearly in Figures 4.15 (a) and (b). It may be concluded that Bi additives have the same effects on the tapping force and moment as that observed in the drilling test. These effect, as discussed earlier, may be attributed to the presence of eutectic Si particles in the form of hard coarse, acicular plates in the Bi-containing alloys instead of fibrous particles in the Sn-containing alloy.

During the tapping of a low Si-content B319.2 alloy, it was also observed that the Sn-containing M10 alloy and Bi-containing M11 alloy present the same number of holes tapped out of the total 1500 holes, followed by the M14 alloy containing a combined addition of Sn and Bi with 1200 holes. From this finding, it may be deduced that the morphology of Si particles does not play a significant role in tap life. The difference existing in the influence of Si morphology between drill life and tap life may arise from the different cutting conditions applied in each test, since the drilling tests were carried out at high cutting speeds of around 11000 rpm with a high feed rate of about 1.17 m/min compared to the low cutting speed applied in the tapping tests of about 400 rpm with a low feed rate of about 0.56 m/min. It has been reported that the difference in Si morphology exerts only a slight influence on tool life at low cutting speeds. As the cutting speed rises, however, the effects of wear as a result of Si morphology become more pronounced.¹³

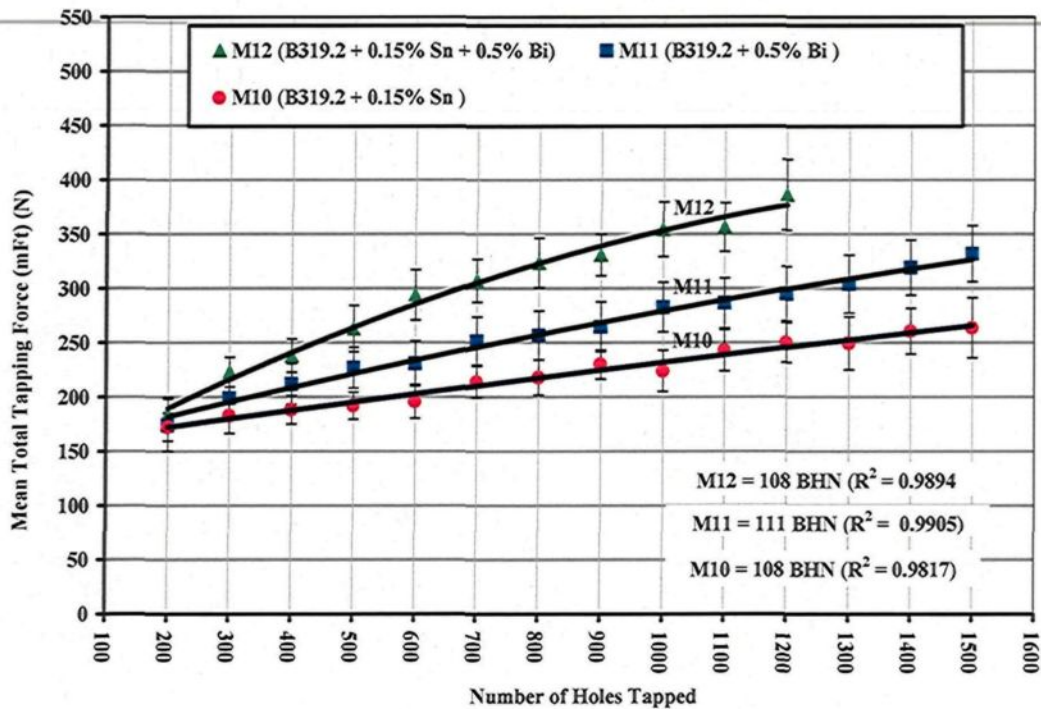


(a)

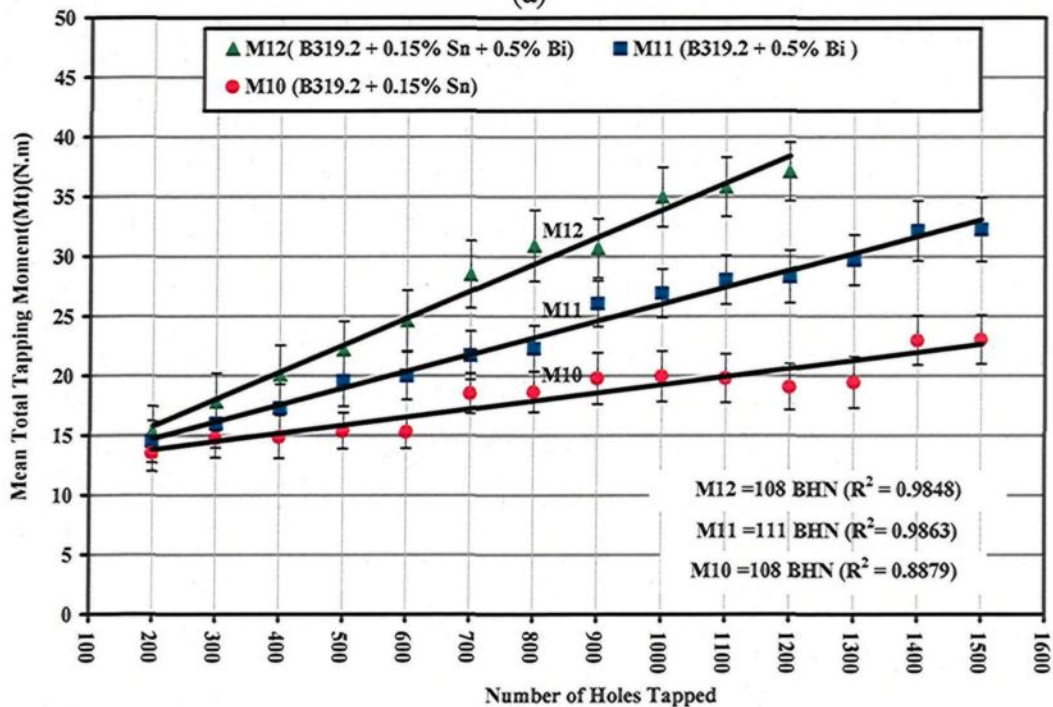


(b)

Figure 5.14 Effects of Sn and/or Bi additions on the machinability of B319.2 (M10, M11 and M12) alloys in terms of (a) mean total drilling force; and (b) mean total drilling moment required for drilling 100 holes.



(a)



(b)

Figure 5.15 Effects of Sn and/or Bi additions on the machinability of B319.2 (M10, M11 and M12) alloys in terms of (a) mean total tapping force; and (b) mean total tapping moment required for tapping 100 holes.

5.4.2 Evolution of Built-Up Edge (BUE) and Tool Wear Characteristics

Built-up edge is caused by the incidence of some strain-hardened workpiece material welding itself to the rake face and becoming a new cutting surface. In general, BUE results in the deterioration of chip size, tool life, surface finish, and part dimensional control. The evolution in the width of the BUE with the progress of the drilling process was evaluated using a toolmaker's microscope (TM-505 type) with a magnification of 30x. All of the alloys investigated left a discernible deposit, namely BUE, as drawn from the corresponding data in Table 5.3. It was found that there is no significant change to be observed in the width of the BUE with the progress of the drilling process. Figures 5.16 (b), (c), (d), and (e) illustrate the effects of Sn, Bi, and Pb additions on heat build-up formation with regard to the main cutting drill lip after drilling the 396 alloys with a different number of holes. An examination of build-up photographs indicates that the alloy containing 0.5% Bi, namely the M7 alloy, shows a slightly lower tendency to BUE formation with 0.157 mm, as may be seen in Figure 5.16 (d), compared to the M1 base alloy having a BUE width of 0.171mm. It will also be observed that the alloy containing 0.15% Sn shows a slight increase in the BUE formation of 0.192 mm compared to the base alloy and the Bi-containing alloys, as shown in Figure 15.16 (c). It is not possible to draw a firm conclusion here, however, due to the intermittent peeling off of the BUE during drilling cycles. It should also be kept in mind that the Bi-containing alloy has the greatest degree of hardness compared to the other alloys under investigation, see Table 5.2. Owing to its high hardness and low ductility values, the 396-M7 alloy shows little tendency towards built-up edge formation. These results are in satisfactory agreement with Jorstad^{14,23} who reported that

either the Sn and the Pb, or the 1% Zn, contributed slightly to the improvement in built-up height during the machining of 380 alloys.

Table 5.3 Effects of Sn, Bi, and Pb additions on the width of built-up edge (BUE)

Alloy	BUE width (mm) after drilling the specified numbers of holes								
	No. of holes drilled →	180	360	540	720	900	1080	1620	Average
396-M1(base alloy)	0.163	0.176	0.170	0.169	0.179	0.179	0.169		(0.171)
M1+ 0.15% Sn (M2)	0.193	0.186	-	0.191	-	0.195	0.196		(0.192)
M1 + 0.5%Bi(M7)	0.155	0.159	0.158	-	-	-	-		(0.157)
M1 + 0.8% Pb (M8)	0.196	0.210	0.216	0.189	0.193	0.220	-		(0.204)

As mentioned previously in Chapter 4, no systematic measurements of the flank wear on the cutting edge were considered, although it should be kept in mind that the determining factor in drill life is the quality of the hole produced when using the Go-NoGo gauge test. Drill wear differs to some extent from the wear on other cutting tools. Typically, as a result of production variations, a drill is slightly asymmetrical. Accordingly, the two corners of the drill edges wear out gradually, while maximum wear alternates from one cutting edge to the other. This alternating process continues until both lips have zero clearance at the margin. The drill then adheres to the workpiece and breaks if the cutting process is not stopped in time. The wear on the drill margins actually determines the degree of wear and is not nearly as obvious as flank wear. When the corners of the drill have become rounded off, the drill has been damaged far more than is readily apparent. Thus, for the purposes of the current study, the dominant type of wear which results in drill failure and breakage is known as outer corner wear, as shown in Figure 5.16(f) which shows the state of drill wear on the cutting drill lip after stripping the adherent workpiece material

using a solution of sodium hydroxide (NaOH). There appears to be no evidence of crater-wear at this juncture. As shown previously in Figures 5.11 (a) and (b), wear is visible on the margin point and at the outer cutting corner of the drill. Thus, aggressive wear on the carbide drill edge after drilling 630 holes during the machining of the 396-M7 alloy may be ascribed to the precipitation of coarse silicon particles in the microstructure, as noted previously in the subsection discussing microstructures.

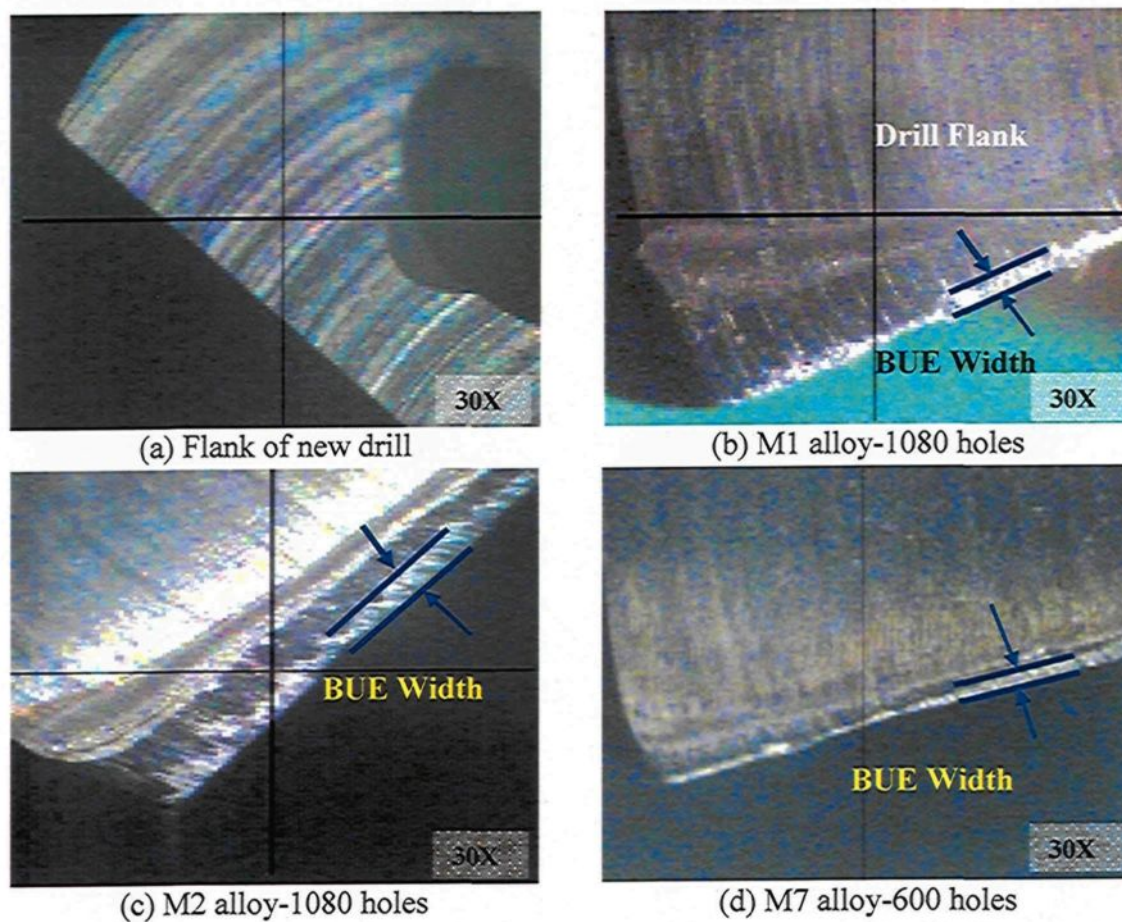


Figure 5.16 Contd.

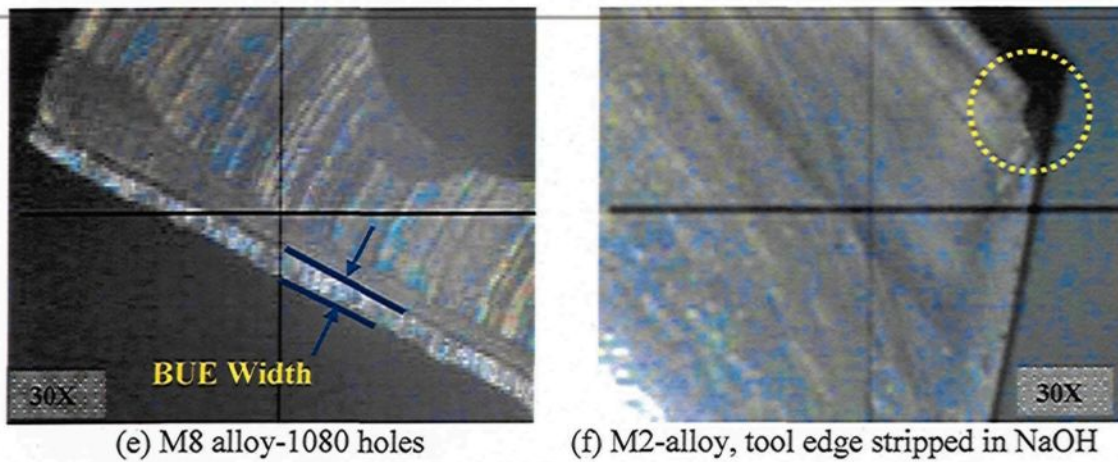


Figure 5.16 Photographs showing the effects of Sn, Bi, and Pb addition on heat build-up formation and the wear on the cutting drill lip in 396 (M1, M2, M7, M8) alloys after different stages of drilling.

5.4.3 Chip Characterization

The success of a drilling operation depends primarily on the ability to produce chips which may be readily ejected from the drilled hole. Long chips are usually not desirable because the chips, which subsequently have to be removed manually, can tangle along the drill body. Figures 5.17(b), (c), and (d) show the effects of Sn, Bi, and Pb on the typical chip formation produced during the drilling of Sr-modified, grain-refined, heat-treated 396 alloys. It was found that the fan shape was by far the predominant form, and that it is considered to be the ideal chip for the greater number of drilling applications. Most references in the literature indicate that free machinability is due to the formation of smaller chips. In the current study, chip size was not significantly different after the addition of free-machining elements. The chips were small in the absence of additives, as shown in Figure 5.17(a), and did not become obviously smaller after the inclusion of additives. The Bi-containing M7 alloy, however, produces finer chips of a fan shape than were observed in the alloys under study previously, as shown in Figure 5.17(c).

These results were supported by the data obtained after applying the chips-per-gm criterion, as provided in Figure 5.18. The corresponding data show that the chip breakability of the Bi-containing M7 alloy excelled by an increase of 35% in the number of chips per gram compared to the M1 base alloy. It should be noted that the chip breakability of each alloy is consistent with the BUE evolution for the same alloy; in this regard the Bi-containing M7 alloy, which displays a low tendency toward BUE formation, displays the best chip breakability.

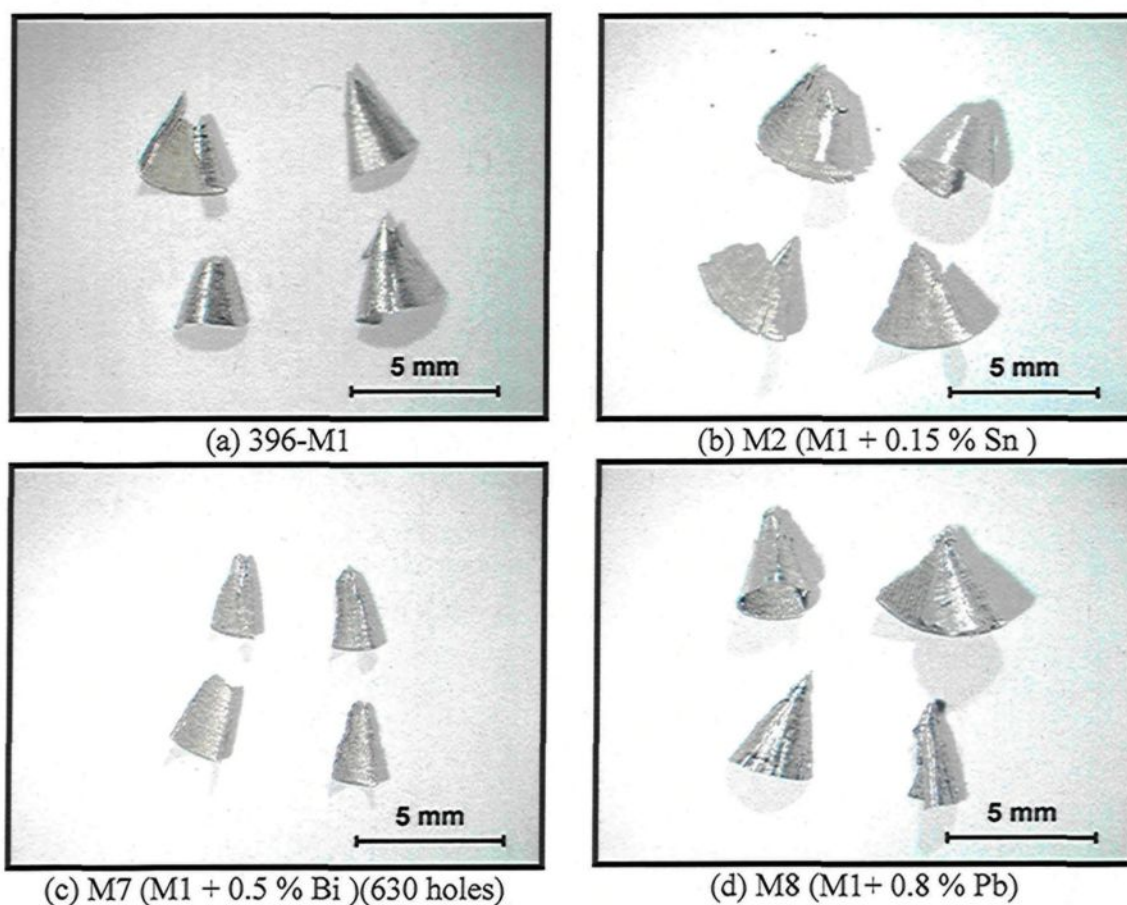


Figure 5.17 Optical micrographs showing the different types of chip obtained for M1, M2, M7, and M8 alloys after drilling the specified number of holes out of the targeted 1080 holes.

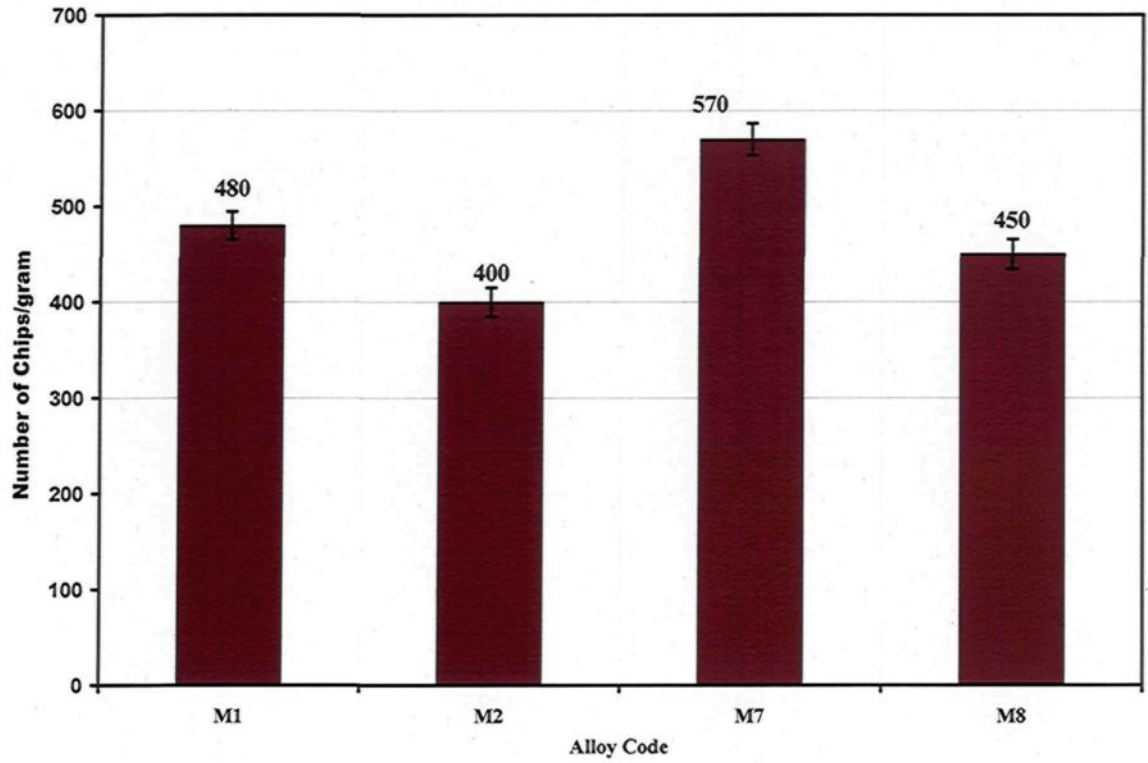


Figure 5.18 Effects of Sn, Bi, and Pb on chip breakability in terms of the chips-per-gram criterion for the alloys investigated.

CHAPTER 6
CONCLUSIONS AND RECOMMENDATIONS

CHAPTER 6

CONCLUSIONS AND RECOMMENDATIONS

The present study concentrated on a new experimental alloy belonging to the Al-Si near-eutectic cast alloy group, and containing about 10.8% Si, namely the 396 alloy. In addition, B319.2 alloys were also investigated for comparison purposes. The study was carried out with the aim of providing a better understanding of the effects that Fe-intermetallics, matrix-hardening elements, and free-machining elements would have on the machinability characteristics of this alloy. Drilling and tapping operations were carried out under fixed machining conditions as applied to the examination of the alloys under discussion. It should be mentioned here that the pertinent machinability criteria relate to forces and moments as well as to tool life, chip configuration, and built-up edge (BUE) evolution.

6.1 CONCLUSIONS

From the analysis and discussion of the results obtained, the following conclusions may be formulated:

Effects of Fe-Intermetallics

1. The results obtained from the drilling tests reveal that the 396-M1 base alloy displays a rapid increase in the mean total drilling force, moment, and power by 103%, 105%, and 134%, respectively, as the number of holes drilled increases. This particularity may be ascribed to the abrasiveness of the 396 alloy resulting from its higher Si content of 10.8%.

2. The addition of 0.25% Fe and 0.25% Mn to the M1 base alloy, producing the M3 alloy - containing sludge as a predominant phase, leads to an extremely rapid increase, of about 75%, in the total drilling force after drilling only 540 holes; similar behavior was also observed with regard to the total drilling moment and power.
3. The presence of sludge has a detrimental effect on tool life, in that it decreases drill life by about 50% compared to the M1 base alloy. It is clear that the sludge phase has a high hardness value, a high melting point, and a high specific gravity compared to the matrix, and it is consequently capable of causing significant damage to cutting tools.
4. The formation of the α -Fe phase in the M1 alloy has a beneficial effect on tool life, in that the M1 alloy produces the highest number of holes drilled compared to sludge or β -Fe containing alloys; this result may be attributed to the fact that the formation of the α -Fe intermetallic with its rounded Chinese-script morphology and its presence within the α -Al dendrites is expected to improve matrix homogeneity through the hardening of the soft α -Al dendrites.
5. Increasing the iron level from ~0.5 to 1% while maintaining the same Mn level of ~0.5% proves to be most effective in terms of cutting force and tool life in the drilling and tapping processes. The lower ductility value displayed by the β -Fe-containing alloy reduces the drill-chip friction which in turn decreases the drilling force, moment, and power.

-
6. In tapping tests, it was found that high-speed steel tools are considerably more sensitive to the Fe-intermetallic phases than the carbide tools used for drilling. The high speed steel tap (HSS-E) broke down after tapping only 630, 589, and 900 holes in the M1, M3, and M4 alloys, respectively.
 7. The addition of Fe and/or Mn to the base alloy, which would initially have been expected to reduce the edge build-up tendency through the abrasive action of hard intermetallic phases, did not measurably reduce the built-up edge width compared to the one observed for the M1 base alloy.

Effects of Cu and Mg Additions

8. The Mg-free M9 alloy displays only a slight increase in the drilling force, moment, and power with the progress of the drilling process, while in comparison, the Mg-containing M1 base alloy shows a rapid increase.
9. The M6 alloy containing high levels of Cu and Mg have a detrimental effect on drill life and cutting forces. The higher drilling force and the reduction in drill life may be attributed to the formation of large amounts of the coarse blocklike Al_2Cu phase, together with the formation of thick plates of the Al-Si-Cu-Mg phase in the alloy.
10. The Mg-free M9 alloy displays the lowest cutting force and moment in addition to producing the highest number of holes drilled/tapped compared to the Mg-containing alloys. This observation may be explained by the cooperative precipitation of the Al_2Cu , Mg_2Si , Al_2CuMg , and $\text{Al}_5\text{Si}_6\text{Cu}_2\text{Mg}_8$ hardening phases in Mg-containing alloys which confer greater strength on the alloy than would be the case with the precipitation of only the Al_2Cu phase in the Mg-free M9 alloy.

-
11. A comparison of the non-modified M0 alloy and the Sr-modified M1 alloy (containing the same level of Mg and Cu additions) in terms of the number of holes drilled, reveals that the morphology of Si particles has a noticeable effect in governing the tool life of near-eutectic Al-Si alloys.
 12. An examination of the edge build-up photographs indicates that there is little change in the width of the BUE with the progress of the drilling process. Owing to their high hardness and low ductility values, the Mg-containing alloys show an appreciably lower tendency to BUE formation compared to the Mg-free alloy.

Effects of Free-Machining Elements

13. The Bi-containing alloys have a detrimental influence on drill life, although they are observed to exhibit lower drilling forces compared to the M1 base alloys. The significant reduction in drill life may be explained by the fact that the presence of 0.5wt% Bi leads to noticeable coarsening of the Si particles. Moreover, the effectiveness of adding the low melting point Bi for the purpose of enhancing machinability is reduced by the loss of Bi in the formation of the high melting point Bi_2Mg_3 phase.
14. The addition of 0.15wt% Sn to the 396 alloy has a beneficial effect on the tool life of both carbide drills and HSS taps. Such an effect may be ascribed to the precipitation of β -Sn particles having a low melting point. In addition, these β -Sn particles are smaller and more uniformly distributed in comparison with the Bi particles in the Bi-containing alloys.

-
15. The simultaneous addition of smaller amounts of two or more elements insoluble in aluminum has a greater effect on machinability in terms of reducing the drilling force and moment than individual additions of each element.
 16. The morphology of Si particles does not play a significant role in tap life during the tapping of the B319.2 alloys. The difference existing between drill life and tap life with respect to the influence of Si morphology may arise from the different cutting conditions applied for each test.
 17. Lead is not a suitable choice as an additive because of environmental concerns. Bismuth also has several detrimental effects associated with its presence in the Al-Si alloys, including the formation of high melting point Bi_2Mg_3 phase. Bismuth also interacts with Sr which is required for Si-modification. Thus, of the free-machining elements tested, Sn is the most promising in the context of improving the alloy machinability.

Chip Characterization

18. A visual examination of the chips reveals that the fan shape is by far the predominant form during the drilling of the alloys studied, and also that it is considered to be the ideal chip for most drilling applications.
19. The chip breakability of the alloys containing Al_2Cu phase is superior to that of the alloys containing Mg_2Si . Thus combined additions of Cu and Mg are expected to further refine the size of the chips produced. Chip size is not significantly different after the addition of free-machining elements. The Bi-containing alloys, however, produce finer fan-shaped than the Bi-free 396 base alloy.

Tool Wear Characterization

20. In the drilling tests, maximum wear takes place at the outer corner edge of the drill, whereas minimum wear occurs at or near the point of the drill tip, since the maximum rotational force and the maximum drill-to-workpiece contact occur at the outer corner edge. When the corners of the drill are rounded off, the drill then sticks to the workpiece and breaks if the cutting process is not halted in time.
21. In tapping tests, the main wear mechanism observed is adhesion, although some abrasion may also occur during the tapping of the sludge-containing and Bi-containing alloys. The breakage occurs frequently at the chamfered part of the tap since it generates a major part of the resulting force, because of the larger chip cross-section related to the teeth of the chamfer.

6.2 RECOMMENDATIONS FOR FUTURE WORK

As mentioned in the objectives in Chapter 1, the main purpose of this study was the development of a new automotive alloy which would provide a performance superior to the currently used 319 and 356 Al-Si alloys. To complete the study, it is suggested that investigations be extended to cover the following aspects:

1. Investigating the high temperature performance of 396 type alloys with respect to the role of additives in preserving the mechanical properties under elevated temperature conditions.
2. Investigating the use of drill materials other than the cemented carbide tools used in the present study, from the point of view of reducing the machining costs and thereby, the overall production costs.
3. Mathematical analysis of the experimental data using factorial analysis, to provide a design for the experimental approach to such investigations, in order to reduce the time required for arriving at the optimum alloy compositions and machining conditions in the production of automotive components.
4. Investigating the addition of low melting-point elements such as tin which, with its tendency to melt during dry machining at high speeds of ~12,000 rpm, would serve as a lubricant during the machining process, thus eliminating the need for external lubricants.

REFERENCES

1. Moustafa, M.A., Samuel, F.H., Doty, H.W., "Effect of Solution Heat Treatment and Additives on the Microstructure of Al-Si (A413.1) Automotive Alloys," *Journal of Materials Science*, vol 38, pp 4507-4522 (2003).
2. Samuel, F.H., Ouellet, P., Samuel, A.M., Doty, H.W., "Effect of Mg and Sr Additions on The Formation of Intermetallics in Al-6Wt Pct Si-3.5 Wt Pct Cu-(0.45) to (0.8)Wt Pct Fe 319-Type Alloys," *Metallurgical and Materials Transactions A*, vol 29A, pp 2871-2884 (1998).
3. Grum, J., Kisin, M., "Influence of the Microstructure on Surface Integrity in Turning-Part II: The Influence of a Microstructure of the Workpiece Material on Cutting Forces," *International Journal of Machine Tools & Manufacture*, vol 43, pp 1545-1551 (2003).
4. Boothroyd, G., Knight, W.A., *Fundamentals of Machining and Machine Tools*, Third Edition, Taylor and Francis, Inc., Florida (2006).
5. Shaw, M.C., *Metal Cutting Principles*, Second Edition, Oxford University Press, New York (2005).
6. Stephenson, D.A., Agapiou, J.S., *Metal Cutting Theory and Practice*, Second Edition, Taylor and Francis, Inc., Florida (2006).
7. Kronenberg, M., *Machining Science and Application*, Elsevier Science and Technology, Pergamon, London (1966).
8. ASM Metals Handbook, vol 16, *Machining*, American Society for Metals, Materials, Park, OH, p 643 (1990).
9. KÖnig, W., Erinski, D., "Machinability of Aluminum-Silicon Pressure-Die-Cast Alloys," *Proceedings of the 20th International Machine Tool Design & Research Conference (MTDR)*, pp 337-344 (1979).
10. ASM Metals Handbook, vol 2, *Properties and Selection: Nonferrous Alloys and Special-Purpose Materials*, American Society for Metals, Materials Park, OH, (1990).
11. Trent, E.M., Wright, P.K., *Metal Cutting*, 4th Edition, Butterworth's-Heinemann, London, pp 149-166 (2000).
12. Narahari, P., Pai, B.C., Pillai, R.M., "Some Aspects of Machining Cast Al-SiCp Composites with Conventional High Speed Steel and Tungsten Carbide Tools," *Journal of Materials Engineering and Performance*, vol 8(5), pp 538-542 (1999).
13. Dwivedi, D.K., Sharma, A., Rajan, T.V., "Machining of LM13 and LM28 Cast Aluminum Alloys: Part 1," *Journal of Materials Processing Technology*, vol 196, pp 197-204 (2008).
14. Jorstad, J.L., "Influence of Aluminum Casting Alloy Metallurgical Factors on Machinability," Society of Automotive Engineers, 400 Commonwealth, PA.15096, 15 pages (1980).

15. Boileau, J.M., "The Effect of Solidification Time on the Mechanical Properties of a Cast 319 Aluminum Alloy," Ph.D. Dissertation 2000, Wayne State University, Detroit, Michigan (2000).
16. ASM Metals Handbook, vol 3, *Alloy Phase Diagrams*, American Society for Metals, Materials Park, OH, (1990).
17. Miller, J.C., "Machining High Silicon Aluminum," *Proceedings of the 11th International Die Casting Congress*, Cleveland, Ohio, pp 1-9 (1981).
18. Tash, M., Samuel, F.H., Mucciardi, F., Doty, H.W., Valtierra, S., "Effect of Metallurgical Parameters on the Machinability of Heat-Treated 356 and 319 Aluminum Alloys," *Materials Science and Engineering A*, vol 434, pp 207-217 (2006).
19. Grum, J., Kisin, M., "Influence of the Microstructure on Surface Integrity in Turning-Part I: The Influence of the Size of the Soft Phase in Microstructure on Surface-Roughness Formation," *International Journal of Machine Tools & Manufacture*, vol 43, pp 1535-1543 (2003).
20. Robert, C.L., "Metallurgical Factors Related to Machining Aluminum Castings," *SAE Transactions*, vol 76, pp 1657-1663 (1967).
21. Basavakumar, K.G., Mukunda, P.G., Chakraborty, M., "Influence of Melt Treatments and Turning Inserts on Cutting Force and Surface Integrity in Turning of Al-12Si and Al-12Si-3Cu Cast Alloys," *Surface and Coatings Technology*, vol 201, pp 4757-4766 (2007).
22. Bonsack, W., "Iron-the Problematic Factor in Quality of Aluminum Alloy Die Castings," *AFS Transactions*, vol 69, pp 712-720 (1961).
23. Jorstad, J.L., "Machinability of 380 Alloy: Effect of Minor Elements and Impurities," *Transactions of the Society of Die Casting Engineers*, Paper No.G-T79-072 (1979).
24. Lu, L., Dahle, A.K., "Iron-Rich Intermetallic Phases and Their Role in Casting Defect Formation in Hypoeutectic Al-Si Alloys," *Metallurgical and Materials Transactions, A*, vol 36A, pp 819-835 (2005).
25. Wang, L., Apelian, D., Makhlof, M.M., "Iron-Bearing Compounds in Al-Si Diecasting Alloys: Morphology and Conditions under Which They Form," *AFS Transactions*, vol 107, pp 231-238 (1999).
26. Dinnis, C.M., Taylor, J.A., Dahle, A.K., "Interactions between Iron, Manganese, and the Al-Si Eutectic in Hypoeutectic Al-Si Alloys," *Metallurgical and Materials Transactions, A*, vol 37A, pp 3283-3291 (2006).
27. Couture, A., "Iron in Aluminum Casting Alloys: A Literature Survey," *AFS International Cast Metals Journal*, pp 9-17 (1981).
28. Suárez-Peña, B., Asensio-Lozano, J., "Influence of Sr Modification and Ti Grain Refinement on the Morphology of Fe-Rich Precipitates in Eutectic Al-Si Die Cast Alloys," *Scripta Materialia*, vol 54, pp 1543-1548 (2006).
29. Gruzleski, J.E., *Microstructure Development during Metalcasting*, American Foundrymen's Society, Inc., Des Plaines, IL, p 234 (2000).

30. Moustafa, M.A., "Effect of Iron Content on the Formation of β - Al_3FeSi and Porosity in Al-Si Eutectic Alloys," *Journal of Materials Processing Technology*, vol 209, pp 605-610 (2009).
31. Pucella, G., Samuel, A.M., Samuel, F.H., Doty, H.W., Valtierra, S., "Sludge Formation in Sr-Modified Al-11.5Wt% Si Diecasting Alloys," *AFS Transactions*, vol 107, pp 117-125 (1999).
32. Shabestari, S.G., Gruzleski, J.E., "The Effect of Solidification Condition and Chemistry on The Formation and Morphology of Complex Intermetallic Compounds in Aluminum-Silicon System," *Cast Metals*, vol 6, pp 217-224 (1994).
33. Crepeau, P.N., "Effect of Iron in Al-Si Casting Alloys: A Critical Review," *AFS Transactions*, vol 103, pp 361-366 (1995).
34. Cao, X., Campbell, J., "Effect of Precipitation of Primary Intermetallic Compounds on Tensile Properties of Cast Al-11.5 Si-0.4 Mg Alloy," *AFS Transactions*, vol 108, pp 391-400 (2000).
35. Moustafa, M.A., Samuel, F.H., Doty, H.W., Valtierra, S., "Effect of Mg and Cu Additions on the Microstructural Characteristics and Tensile Properties of Sr-Modified Al-Si Eutectic Alloys," *International Journal of Cast Metals Research*, vol 14, pp 235-253 (2002).
36. Li, Z., Samuel, A.M., Samuel, F.H., Ravindran, C., Valtierra, S., "Effect of Alloying Elements on the Segregation and Dissolution of CuAl_2 Phase in Al-Si-Cu 319 Alloys," *Journal of Materials Science*, vol 38, pp 1203-1218 (2003).
37. Moustafa, M.A., Samuel, F.H., Doty, H.W., "Effect of Solution Heat Treatment and Additives on the Hardness, Tensile Properties and Fracture Behaviour of Al-Si (A413.1) Automotive Alloys," *Journal of Materials Science*, vol 38, pp 4523-4534 (2003).
38. Han, Y.M., Samuel, A.M., Samuel, F.H., Valtierra, S., Doty, H.W., "Effect of Solution Heat Treatment Type on the Dissolution of Copper Phases in Al-Si-Cu-Mg Type Alloys," *AFS Transactions*, vol 116, pp 79-90 (2008).
39. De la Sablonnière, H., Samuel, F.H., "Solution Heat Treatment of 319 Aluminum Alloy Containing~0.5wt%Mg Part 2: Microstructure and Fractography," *International Journal of Cast Metals Research*, vol 9, pp 151-225 (1996).
40. Samuel, F.H., "Incipient Melting of $\text{Al}_3\text{Mg}_8\text{Si}_6\text{Cu}_2$ and Al_2Cu Intermetallics in Unmodified and Strontium-Modified Al-Si-Cu-Mg (319) Alloys during Solution Heat Treatment," *Journal of Materials Science*, vol 33, pp 2283-2297 (1998).
41. Moustafa, M.A., Lepage, C., Samuel, F.H., Doty, H.W., "Metallographic Observations on Phase Precipitation in Strontium-Modified Al-11.7% Si Alloys: Role of Alloying Elements," *International Journal of Cast Metals Research*, vol 15, pp 609-626 (2003).
42. Ma, Z., Samuel, E., Mohamed, A.M.A., Samuel, A.M., Samuel, F.H., Doty, H.W., "Parameters Controlling the Microstructure of Al-11Si-2.5Cu-Mg Alloys," *Materials and Design*, vol 31, pp 902-912 (2009).
43. Tavitas-Medrano, F.J., Gruzleski, J.E., Samuel, F.H., Valtierra, S., Doty, H.W., "Effect of Mg and Sr-Modification on the Mechanical Properties of 319-Type

-
- Aluminum Cast Alloys Subjected to Artificial Aging,” *Materials Science and Engineering A*, vol 480, pp 356-364 (2008).
44. Ouellet, P., Samuel, F.H., “Effect of Mg on the Ageing Behaviour of Al-Si-Cu 319 Type Aluminum Casting Alloys,” *Journal of Materials Science*, vol 34, pp 4671-4697 (1999).
 45. Mohamed, A.M.A., Samuel, F.H., Samuel, A.M., Doty, H.W., “Influence of Additives on the Impact Toughness of Al-10.8%Si Near-Eutectic Cast Alloys,” *Materials and Design*, vol 30, pp 4218-4229 (2009).
 46. Tavitans-Medrano, F.J., Valtierra, S., Gruzleski, J.E., Samuel, F.H., Doty, H.W., “A TEM Study of the Aging Behaviour of 319 Type Alloys,” *AFS Transactions*, vol 116, pp 99-114 (2008).
 47. Yamada, H., Tanaka, T., “Compositional Effect of Cu and Mg on the Machinability of Casting Alloys,” *Journal of Japan Institute of Light Metals*, vol 27(11), pp 541-547 (1977).
 48. Tanaka, T., Hanasaki, S., “Effects of the Addition of Cu and Mg on the Machinability of Hypereutectic Al-Si Alloys,” *Aluminium*, vol 75, pp 590-594 (1999).
 49. Kamiya, M., Yakou, T., “Role of Second-Phase Particles in Chip Breakability in Aluminum Alloys,” *International Journal of Machine Tools and Manufacture*, vol 48, pp 688-696 (2008).
 50. Kyung-Hyun, Kim, In-Sang Chung, “Effect of Pb and Bi Element on the Cutting Characteristics in Al-Cu Alloys,” *Journal of the Korean Institute of Metals*, vol 28(3), pp 244-251(1990).
 51. Thai, L.T., “The Effects of Bismuth, Strontium and Antimony Additions on the Microstructure and Mechanical Properties of A356 Aluminum Casting Alloy,” M.Sc. Thesis, Technological University of Malaysia (2006).
 52. Smolej, A., Breskvar, B., Soković, M., Dragojević, V., Slaček, E., “Properties of Aluminum Free-Cutting Alloys with Tin, Part I,” *Aluminium*, vol 78, pp 284-288 (2002).
 53. Ang, C.C., Dasch, J.M., “Dry Machining of Aluminum Castings,” U.S. Patent, No. 0168806A1, Granted 2006.
 54. Young Sek Yang, “Free-Machinable Eutectic Al-Si Alloy,” U.S. Patent, No. 6,511,633B1, Granted 2003.
 55. Subhasish, S., “Free-Machining Aluminum Alloy and Method of Use,” U.S. Patent, No. 5,725,694, Granted 1998.
 56. Smolej, A., Breskvar, B., Soković, M., Dragojević, V., Slaček, E., “Properties of Aluminum Free-Cutting Alloys with Tin, Part II,” *Aluminium*, vol 78, pp 388-391 (2002).
 57. Zaima, S., and Takatsuji, Y., Iio, M., “Effect of Tin on the Machinability of Aluminum Silicon Alloy Castings,” *Journal of Japan Institute of Light Metals*, vol 108, pp 556-567 (1970).

58. Machovec, C.J., Byczynski, G.E., Zindel, J.W., Godlewski, L.A., "Effect of Bi-Sr Interactions on Si Morphology in a 319-Type Aluminum Alloy," *AFS Transactions*, vol 108, pp 439-444 (2000).
59. Wang, W.L., Chen, F.Y., Chen, W.H., "Effect of Process Metallurgical Factors on the Properties of 2011 Free Cutting Aluminum Alloy: on The Size and Distribution of Bi-Pb Particles," *Bulletin of Bismuth Institute*, vol 52, pp 3-7 (1987).
60. Bichsel, H., "Bismuth as an Alloying Element in Aluminum Alloys," *Bulletin of Bismuth Institute, Bulletin 19*, pp 2-3 (1978).
61. Korane, K.J., "Finding the Best Mix in Aluminum Alloys," *Machine Design*, vol 74(4), pp 94-95 (1999).
62. MacAlister, A.J., "The Al-Bi System," *Bulletin of Alloy Phase Diagrams*, vol 5(3), pp 247 (1984).
63. Sal'nikov, V.P., Zaigraikin, A.G., "Effect of Bismuth Additions on the Properties of Aluminum-Silicon Alloys," *Bulletin of Bismuth Institute, Bulletin 19*, p 2 (1978).
64. Ratke, L., Drees, S., Diefenbach, S., Prinz, B., "Microstructure Evolution in Immiscible AlSiBi Alloys under Reduced Gravity Conditions," Proceedings of the IXth European Symposium on Gravity-Dependent Phenomena in Physical Sciences Held at Berlin, Germany, vol 464, pp 154-133 (1996).
65. Tetsuya, A., and Tetsuro, A., "Morphological Influence of Bi Substituted for Pb in Free-Cutting Brass on Machinability" *Journal of the Japan Copper and Brass Research Association*, vol 40, pp 253-256 (2001).
66. Mondolfo, L.F., *Structure and Properties of Aluminium Alloys*, Butterworths, England, pp 198-230 (1979).
67. Cho, J.I., Loper, C.R., "Limitation of Bismuth Residual in A356.2 Al," *AFS Transactions*, vol 108, pp 359-367 (2000).
68. Fiorini, P., Giordano, G., "Effect of Zn and Bi Addition on Precipitation Process after Quenching and Cold Working Al-6Mg," *Metals Technology*, vol 10(2), pp 52-56 (1983).
69. Kamiya, S., "Aluminum Bearing Alloy Containing Bismuth," U.S. Patent, No. 5,286,445, Granted 1994.
70. Bhattacharya, V., Chattopadhyay, K., "Melting of Multiphase Nano-Scaled Particles Embedded in Al Matrix: Case of Pb-Sn and Bi-Sn Alloys," *Materials Science and Engineering A*, vol 449, pp 1003-1008 (2007).
71. Subhasish, S., "Free Machining Aluminum Alloy Containing Bismuth or Bismuth-Tin for Free Machining and Method of Use," U.S. Patent, No.6,409,966B1, Granted 2002.
72. Lemon, R.C., "Free Machining Aluminum Casting Alloys X310 and X335," *AFS Transactions*, vol 71, pp 315-318 (1963).
73. Dasch, J.M., Ang, C.C., Wong, C.A., Waldo, R.A., Chester, D., Cheng, Y.T., "The Effect of Free-Machining Elements on Dry Machining of B319 Aluminum Alloy," *Journal of Materials Processing Technology*, vol 209, pp 4638-4644 (2009).

74. Spillard, Colleen M., "UltrAlloy® 6020: A Lead-Free Aluminum Alloy Featuring "A" Rated Machinability," *SAE, International Congress and Exposition*, Document # 980459 (1998).
75. Wouters, O., de Hosson, J.Th.M., "Lead Induced Intergranular Fracture in Aluminum Alloy AA6262," *Materials Science and Engineering A*, vol 361, pp 331-337 (2003).
76. Pathak, J.P., Singh, V., Tiwari, S.N., "On Fracture Characteristics of Leaded Aluminium Alloys," *Journal of Materials Science Letters*, vol 11, pp 639-641 (1992).
77. Alabi, M.M., Amherst, N.Y., "Hypo-Eutectic Aluminum-Silicon Alloy Having Tin and Bismuth Additions," U.S. Patent, No 5,122,208, Granted 1992.
78. Alabi, M. M., Amherst, N.Y., "Hypo-Eutectic Aluminum-Silicon Alloy Having Bismuth Additions," U.S. Patent, No 5,122,207, Granted 1992.
79. El-Azim, A.N., Moustafa, S.F., "Machinability of Aluminum-Silicon Alloy Castings Modified With Some Additions," *International Conference on Evolution of Advanced Materials*, Milan, Italy, 1989.
80. Tash, M., "Effect of Metallurgical Parameters on the Machining Behaviour of 356 and 319 Alloys," Ph.D. Dissertation 2006, Université du Québec à Chicoutimi, Canada (2006).
81. Müller, C., Blümke, R., "Influence of Heat Treatment and Cutting Speed on Chip Segmentation of Age Hardenable Aluminium Alloy," *Materials Science and Technology*, pp 651-654 (2001).
82. Schulz, H., Abele, E., Sahm, A., "Material Aspects of Chip Formation in HSC Machining," *Annals of CIRP*, vol 50(1), pp 45-48 (2001).
83. Dwivedi, D.K. "Influence of Grain Refinement, Modification and Heat Treatment on Surface Roughness in Machining of Cast Al-Si Alloys," *Indian Foundry Journal*, vol 48 (1), pp 32-38 (2002).
84. Lim, C.S., Clegg, A.J., Loh, N.L., "The Reduction of Dendrite Arm Spacing Using a Novel Pressure Assisted Investment Casting Approach," *Journal of Materials Processing Technology*, vol 70, pp 99-102 (1997).
85. Szablewski, D., Dumitrescu, M., Elbestawi, M.A., Sokolowski, J.H., "High Speed Face milling of an Aluminum Silicon Alloy Casting," *Annals of the CIRP*, vol 53(1) pp 69-72 (2004).
86. Lorenz, G., "A Note on The Effect of Heat Treatment on The Machinability of Al-Cu Type Free-Cutting Alloy," *Annals of the CIRP*, vol 18, pp 251-256 (1970).
87. Hetke, A., and Gundlach, R.B., "Aluminum Casting Quality in Alloy 356 Engine Components," *AFS Transactions*, vol 102, pp 367-380 (1994).
88. Budinski, K.G., Budinski, M.K., *Engineering Materials: Properties and Selection*, Prentice-Hall, Englewood Cliffs, NJ (1992).
89. Burant, R.O., Skingle, T.J., "Machining the Silicon-Containing Aluminum Alloys," *SAE Technical Paper Series 800489*, pp 1-13 (1980).
90. Apelian, D., Shivkumar, S., Sigworth, G., "Fundamental Aspects of Heat Treatment of Cast Al-Si-Mg Alloys," *AFS Transactions*, vol 97, pp 367-380 (1989).

91. Shivkumar, S., Ricci, S., Steenhoff, B., Apelian, D., Sigworth, G., "An Experimental Study to Optimize the Heat Treatment of A356 Alloy," *AFS Transactions*, vol 97, pp 791-810 (1989).
92. Shivkumar, S., Keller, C., Apelian, D., "Aging Behaviour in Cast Al-Si-Mg Alloys," *AFS Transactions*, vol 98, pp 905-911 (1990).
93. Huseyin, E.M., Cuneyt, O., "Drill Wear Monitoring Using Cutting Force Signals," *Mechatronics*, vol 14, pp 533-548 (2004).
94. Rivero, A., Aramendi, G., Herranz, S., Lopez de Lacalle, L.N., "An Experimental Investigation of the Effect of Coatings and Cutting Parameters on the Dry Drilling Performance of Aluminium Alloys," *International Journal of Advanced Manufacture Technology*, vol 28, pp 1-11(2006).
95. Batzer, S.A., Haan, D.M., Rao, P.D., Olson, W.W., Sutherland, J.W., "Chip Morphology and Hole Surface Texture in the Drilling of Cast Aluminum Alloys," *Journal of Materials Processing Technology*, vol 79, pp 72-78 (1998).
96. Feng Ke, Jun Ni, Stephenson, D.A., "Continuous Chip Formation in Drilling," *International Journal of Machine Tools & Manufacture*, vol 45, pp 1652-1658 (2005).
97. Kahng, C.H., and Koegler, W.C., "A Study of Chip Breaking during Twist Drilling," *NAMRC /SME Transactions*, pp 6-11 (1977).
98. Thornley, R.H., El Wahab, A.B.I., Maiden J.D., "Some Aspects of Twist Drill Design," *International Journal of Machine Tools & Manufacture*, vol 27(3), pp 383-397 (1987).
99. Lenz, E., Mayer, J.E., "Investigation in Drilling," *Annals of the CIRP*, vol 27(1), pp 49-53 (1978).
100. Spur, G., Masuha, J.R., "Drilling with Twist Drills of Different Cross Section Profiles," *Annals of the CIRP-Manufacturing Technology*, vol 30(1), pp 31-35 (1981).
101. Morin, E., Masounave, J., Laufer, E.E., "Effect of Drill Wear on Cutting Forces in the Drilling of Metal-Matrix Composites," *Wear*, vol 184, pp 11-16 (1995).
102. Paulo Davim, J., Monteriro Baptista, A., "Relationship between Cutting Force and PCD Cutting Tool Wear in Machining Silicon Carbide Reinforced Aluminium," *Journal of Materials Processing Technology*, vol 103, pp 417-423 (2000).
103. Hamade, R.F., Ismail, F., "A Case for Aggressive Drilling of Aluminum," *Journal of Materials Processing Technology*, vol 166, pp 86-97 (2005).
104. Vernaza-Peña, K.M, Mason, J.J., Li, M., "Experimental Study of the Temperature Field Generated during Orthogonal Machining of an Aluminum Alloy," *Experimental Mechanics*, vol 42, pp 221-229(2002).
105. Jawahir, I.S., van Luttervelt, C.A, "Recent Developments in Chip Control Research and Applications," *Annals of the CIRP*, vol 42(2), pp 695-693 (1993).
106. Sakurai, K., Adachi, K., Kawai, G., Sawai, T., Ogawa, K., "High Feed Rate Drilling of Aluminum Alloy," *Materials Science Forum*, vols 331-337, pp 625-630 (2000).
107. Kishawy, H.A., Dumitrescu, M., Elbestawi, M.A., "Effect of Coolant Strategy on Tool Performance, Chip Morphology and Surface Quality during High-Speed

- Machining of A356 Aluminum Alloy,” *International Journal of Machine Tools & Manufacture*, vol 45, pp 219-227 (2005).
108. Haan, D.M., Batzer, S.A., Olson, J.W., Sutherland, J.W., “An Experimental Study of Cutting Fluid Effects in Drilling,” *Journal of Materials Processing Technology*, vol 71, pp 305-313 (1997).
 109. Bhowmick, S., Alpas, A.T., “Minimum Quantity Lubrication Drilling of Aluminium-Silicon Alloys in Water Using Diamond-Like Carbon Coated Drills,” *International Journal of Machine Tools & Manufacture*, vol 48, pp 429-1443 (2008).
 110. Schneider, G., *Cutting Tool Applications*, 2002,
http://www.manufacturingcenter.com/online_book/chap_8.pdf, G. Schneider,
 111. Walker, John R., *Machining Fundamentals: From Basic to Advanced Techniques*, 6th Edition, Goodheart-Wilcox Company, Inc. Tinley Park, Illinois (2004).
 112. Edmund Isakov, *Engineering Formulas for Metal Cutting*, Industrial Press, Inc. New York (2004).
 113. <http://www.me.metu.edu.tr/me535/Lecture%20Notes/Chapter%204/index.html>, Department of Mechanical Engineering, Metal Cutting, Machinability, 2005.
 114. Nouari, M., List, G., Girot, F., Coupard, D., “Experimental Analysis and Optimisation of Tool Wear in Dry Machining of Aluminum Alloys,” *Wear*, Vol. 225, pp 1359-1368 (2003).
 115. Wain, N., Thomas, N.R., Hickman, S., Wallbank, J., Teer, D.G., “Performance of Low-Friction Coatings in the Dry Drilling of Automotive Al-Si Alloys,” *Surface & Coatings Technology*, vol 200, pp 1885-1892 (2005).
 116. List, G., Nouari, M., Gehin, D., Gomez, S., Manaud, J.P., Le Petitcorps, Y., Girot, F., “Wear Behaviour of Cemented Carbide Tools in Dry Machining of Aluminium Alloy,” *Wear*, vol 259, 1177-1189 (259).
 117. Dasch, J.M., Ang, C.C., Wong, C.A., Cheng, Y.T., Weiner, A.M., Lev, L.C., Konca, E., “A Comparison of Five Categories of Carbon-Based Tool Coatings for Dry Drilling of Aluminum,” *Surface & Coatings Technology*, vol 200, pp 2970-2977 (2006).
 118. Kalidas, S., DeVor, R.E., Kapoor, S.G., “Experimental Investigation of the Effect of Drill Coatings on Hole Quality Under Dry and Wet Drilling Conditions,” *Surface & Coatings Technology*, vol 148, pp117-128 (2001).
 119. Bhowmick, S., Alpas, A.T., “The Performance of Hydrogenated and Non-Hydrogenated Diamond-Like Carbon Tool Coatings during the Dry Drilling of 319 Al,” *International Journal of Machine Tools & Manufacture*, vol 48, pp 802-814 (2010).
 120. Sreejith, P.S., Ngoi, B.K.A., “Dry Machining: Machining of the Future,” *Journal of Materials Processing Technology*, vol 101, pp 287-291 (2000).
 121. Arumugam, P.U., Malshe, A.P., Batzer, S.A., “Dry Machining of Aluminum-Silicon Alloy Using Polished CVD Diamond-Coated Cutting Tools Inserts,” *Surface & Coatings Technology*, vol 200, pp 3399-3403 (2006).

122. Nouari M., List, G., Girot, F., Géhin, D., "Effect of Machining Parameters and Coating on Wear Mechanisms in Dry Drilling of Aluminium Alloys," *International Journal of Machine Tool & Manufacture*, vol 45, pp 1436-1442 (2005).
123. Cselle, T., "New Directions in Drilling," *Manufacturing Engineering*, vol 115(2), pp 77-80 (1995).
124. Aronson, R.B., "Why Dry Machining," *Manufacturing Engineering*, vol 114(1) pp 33-37 (1995).
125. Klocke, F., Eisenblätter, G., "Dry Cutting," *Annals of the CIRP*, vol 46 (2), pp 519-526 (1997).
126. Braga, D.U., Diniz, A.E., Miranda, G.W.A., Coppini, N.L., "Using a Minimum Quantity of Lubricant (MQL) and a Diamond Coated Tool in the Drilling of Aluminum-Silicon Alloys," *Journal of Materials Processing Technology*, vol 122, pp 127-138 (2002).
127. Heine, H.J., "Dry Machining: A Promising Option," *Foundry Management & Technology*, vol 126(8), pp 44-49 (1998).
128. Liu, M., Takagi, J., Yanagida, K., "A Study of the Chip Formation and Chip Removal in Dry Drilling of Aluminum Cast Alloy," *Key Engineering Materials*, vols 257-258, pp 575-580 (2004).
129. Johnson, M., "Tapping," *Machining in Metals Handbook Series*, Edition 9, vol 16, 1989, pp 255-267, American Society for Metals, Metals Park, OH.
130. Henderer, W.E., "On the Mechanics of Tapping by Cutting," *Transactions of the ASME-Journal of Engineering for Industry*, pp 257-262 (1977).
131. Dogra, Ajit Pal S., Kapoor, S. G., DeVor, R.E., "Mechanistic Model for Tapping Process with Emphasis on Process Faults and Hole Geometry," *Transactions of the ASME-Journal of Manufacturing Science and Engineering*, vol 124, pp 18-25 (2002).
132. Bezerra, A.A., Coelho, R.T., "Tool Wear Aspects when Applying High-Speed Tapping on Grey Cast Iron," *Proceedings of the Institution of Mechanical Engineers, Part B: Journal of Engineering Manufacture*, vol 222(2), pp 129-136 (2008).
133. Agapiou, J.S., "Evaluation of the Effect of High Speed Machining on Tapping," *Transactions of the ASME-Journal of Engineering for Industry*, vol 116, pp 457-462 (1994).
134. Schneider, G., *Cutting Tool Applications*, 2002, http://www.manufacturingcenter.com/online_book/chap_11.pdf, G.Schneider.
135. Cao, T., Sutherland, J.W., "Investigation of Thread Tapping Load Characteristics through Mechanistic Modeling and Experimentation," *International Journal of Machine Tool & Manufacture*, vol 42, pp 1527-1538 (2002).
136. Puzovic, R., Kokotovic, B., "Prediction of Thrust Force and Torque in Tapping Operations Using Computer Simulation," *FME Transactions*, vol 34(1), pp 1-5 (2006).
137. Kelly, J.F., Cotterell, M.G., "Minimal Lubrication Machining of Aluminium Alloys," *Journal of Materials Processing Technology*, vol 120, pp 327-334 (2002).

138. Jantunen, E., "A Summary of Methods Applied to Tool Condition Monitoring in Drilling," *International Journal of Machine Tool & Manufacture*, vol 42, pp 997-1010 (2002).
139. Lin, S.C., Ting, C.J., "Tool Wear Monitoring in Drilling Using Force Signals," *Wear*, vol 180, pp 53-60 (1995).
140. Liu, T.I., Anantharaman, K.S., "Intelligent Classification and Measurement of Drill Wear," *ASME Transactions-Journal of Engineering for Industry*, vol 116, pp 392-397 (1994).
141. Bakkal, M., Shih, A.J., McSpadden, S.B., Scattergood, R.O., "Thrust Force, Torque, and Tool Wear in Drilling the Bulk Metallic Glass," *International Journal of Machine Tools & Manufacture*, vol 45, pp 863-872 (2005).
142. Axinte, D.A., Belluco, W., De Chiffre, L., "Evaluation of Cutting Force Uncertainty Components in Turning," *International Journal of Machine Tool & Manufacture*, vol 41, pp 719-730 (2001).
143. Thangaraj, A., Wright, P.K., "Drill Wear Sensing and Failure Prediction for Untended Machining," *Robotic and Computer-Integrated Manufacturing*, vol 4, p 429 (1998).
144. Brinksmeier, E., "Prediction of Tool Fracture in Drilling," *Annals of the CIRP-Manufacturing Technology*, vol 39 (1), pp 97-100 (1990).
145. Subramanian, K., Cook, N.H., "Sensing of Drill Wear and Prediction of Drill Life," *Transactions of the ASME-Journal of Engineering for Industry*, vol 99, pp 295-301 (1977).
146. Bandyopahyay, P., Gonzalez, E.M., Huang, R., Wu, S.M., "A Feasibility Study of on-Line Drill Wear Monitoring by DDS Methodology," *International Journal of Machine Tool Design and Research*, vol 26(3), pp 245-257 (1986).
147. Jalali, S.A., Kolarik, W.J., "Tool Life and Machinability Models for Drilling Steels," *International Journal of Machine Tools & Manufacture*, vol 31 (3), pp 273-282 (1991).
148. Zhang, M.Z., Liu, Y.B., Zhou, H., "Wear Mechanism Maps of Uncoated HSS Tools Drilling Die-Cast Aluminum Alloy," *Tribology International*, vol 34, pp 727-731 (2001).
149. Mubarakhi, B., Bandyopadhyay, S., Fowle, R., Mathew, P., "Drilling Studies of an Al₂O₃-Al Metal Matrix Composite: Part 1-Drill Wear Characteristics," *Journal of Materials Science*, vol 30, pp 6273-6280 (1995).
150. Kannatey-Asibu, E., "A Transport Diffusion Equation in Metal Cutting and its Application to Analysis of the Rate of Flank Wear," *Journal of Engineering for Industry*, vol 107(1), pp 81-89 (1985).
151. Moufki, A., Molinari, A., Dudzinski, D., "Modelling of Orthogonal Cutting with a Temperature Dependent Friction Law," *Journal of the Mechanics and Physics of Solids*, vol 46, pp 2103-2138 (1998).
152. Carrilero, M.S., Bienvenido, R., Sanchez, J.M., Alvarez, M., Gonzalez, A., Marcos, M., "A SEM and EDS Insight into the BUL and BUE Differences in the Turning

- Processes of AA2024 Al-Cu Alloy,” *International Journal of Machine Tools & Manufacture*, vol 42, pp 215-220 (2002).
153. Tanaka, T., Akasawa, T., “Machinability of Hypereutectic Silicon-Aluminum Alloys,” *ASM International-Journal of Materials Engineering and Performance*, vol 8(4), pp 463 (1999).
 154. Liu, H.S., Lee, B.Y., Tarng, Y.S., “In-Process Prediction of Corner Wear in Drilling Operations,” *Journal of Materials Processing Technology*, vol 101, pp 152-158 (2000).
 155. Choi, Y.J., Park, M.S., Chu, C.N., “Prediction of Drill Failure Using Features Extraction in Time and Frequency Domains of Feed Motor Current,” *International Journal of Machine Tools & Manufacture*, vol 48, pp 29-39 (2008).
 156. El-Wardany, T.I., Gao, D., Elbestawi, M.A., “Tool Condition Monitoring in Drilling Using Vibration Signature Analysis,” *International Journal of Machine Tools & Manufacture*, vol 36, pp 678-711 (1996).
 157. Kanai, M., Kanda, Y., “Statistical Characteristics of Drill Wear and Drill Life for the Standardized Performance Tests,” *Annals of the CIRP*, vol 27, pp 61-66 (1978).
 158. Worthington, B., Rahman, M.H., “Predicting Breaking with Grooved Type Breakers,” *International Journal of Machine Tool Design and Research*, vol 19, pp 121-132 (1979).
 159. Colding, B.N., “Machinability Determinations Based on Chip Deformation and Friction,” *International Journal of Machine Tool Design and Research*, vol 2, pp 297-316 (1962).
 160. Van Luttervelt, C.A., Pekelharing, A.J., “Chip Formation in Machining Operation at Small Diameter,” *Annals of the CIRP-Manufacturing Technology*, vol 25(1), pp 71-76 (1976).
 161. Davies, D.W., “Machinability and Microstructure of Some Common Non-Ferrous Metals and Alloys,” *Metals Technology*, vol 3(5/6), pp 272-284 (1976).
 162. Nakayama, K., and Ogawa, M., “Basic Rules on the Form of the Chip in Metal Cutting,” *Annals of the CIRP*, vol 27(1), pp 17-21 (1978).
 163. www.Kistler.com, Kistler, 2005.
 164. Joenoes, A.T., Gruzleski, J.E., “Mg Effects on the Microstructure of Unmodified and Modified Al-Si Alloys,” *International Journal of Cast Metals Research*, vol 4(2), pp 62-71 (1991).
 165. Liu, L., Mohamed, A.M.A., Samuel, A.M., Samuel, F.H., Doty, H.W., “Precipitation of β -Al₅FeSi Phase Platelets in Al-Si Based Casting Alloys,” *Metallurgical and Materials Transactions A*, vol 40A, pp 2457-2469 (2009).
 166. Mohamed, A.M.A., Samuel, A.M., Samuel, F.H., Doty, H.W., “Influence of Additives on the Microstructure and Tensile Properties of Near-Eutectic Al-10.8%Si Cast Alloy,” *Materials and Design*, vol 30, pp 3943-3957 (2009).
 167. Shabestari, S.G., “The Effect of Iron and Manganese on the Formation of Intermetallic Compounds in Aluminum-Silicon Alloys,” *Materials Science and Engineering A*, vol 383, pp 289-298 (2004).
 168. Jorstad, J.L., “Understanding Sludge,” *Die Casting Engineer*, pp 30 (1986).

169. Samuel, A.M., Samuel, F.H., Doty, H.W., "Observation on the Formation of β -AlFeSi Phase in 319 Type Al-Si Alloys," *Journal of Materials Science*, vol 31, pp 5529-5539 (1996).
170. Villeneuve, C., Samuel, F.H., "Fragmentation and Dissolution of β -Al₅FeSi Phase during Solution Heat-Treatment of Al-13% Si-Fe Alloys," *International Journal of Cast Metals Research*, vol 12(3), pp 145-160 (1999).
171. Lasa, L., Rodriguez-Ibabe, J.M., "Evolution of the Main Intermetallic Phases in Al-Si-Cu-Mg Casting Alloys during Solution Treatment," *Journal of Materials Science*, vol 39, pp 1343-1355 (2004).
172. Hatch, J.E., *Aluminum Properties and Physical Metallurgy*, 1st Edition, American Society for Metals, Metals Park, Ohio (1988).
173. Alfonso, I., Maldonado, C., Gonzales, G., Bedolla, A., "Effect of Mg Content and Solution Treatment on the Microstructure of Al-Si-Cu-Mg Alloys," *Journal of Materials Science*, vol 41, pp 1945-1952 (2006).
174. Tavitas-Medrano, F.J., Mohamed, A.M.A., Gruzleski, J.E., Samuel, F.H., Doty, H.W., "Precipitation-Hardening in Cast Al-Si-Cu-Mg Alloys," *Journal of Materials Science*, vol 45, pp 641-651 (2010).
175. Ma, Z., Samuel, A.M., Samuel, F.H., Doty, H.W., Valtierra, S., "A Study of Tensile Properties in Al-Si-Cu and Al-Si-Mg Alloys: Effects of β -Iron Intermetallics and Porosity," *Materials Science and Engineering A*, vol 490, pp 36-51 (2008).
176. Xiufang, B., Guohua, C., Jiayi, M., "The Spheroidisation of Needle-Form Iron Compound in an Al-Si Alloy," *Cast Metals*, vol 5(1), pp 39-42 (1992).
177. Grum, J., Kisin, M., "The Influence of the Microstructure of Three Al-Si Alloys on the Cutting-Force Amplitude during Fine Turning," *International Journal of Machine Tools & Manufacture*, vol 46, pp 769-781 (2006).
178. Demir, H., Gunduz, S., "The Effects of Aging on Machinability of 6061 Aluminum Alloy," *Materials and Design*, vol 30, pp 1480-1483 (2009).
179. Colwell, D.L., Tichy, O., "Machinability of Aluminum Die Castings," *AFS Transactions*, vol 64, pp 236-241 (1956).
180. Komiyama, Y., Uchida, K., Gunshi, M., "Effect of Fe, Mn, Zn, and Ti on Mechanical Properties and Microstructure of Al-Si-Cu-Mg Casting Alloy," *Journal of Japan Institute of Light Metals*, vol 26(7), pp 311-319 (1976).
181. Cáceres, C.H., Svensson, I.L., Taylor, J.A., "Strength-Ductility Behaviour of Al-Si-Cu-Mg Casting Alloys in T6 Temper," *International Journal of Cast Metals Research*, vol 15, pp 531-543 (2003).
182. Tavitas-Medrano, F.J., Samuel, F.H., Valtierra, S., Doty, H.W., "Artificial Aging Behavior of 319-Type Cast Aluminum Alloys with Mg and Sr Additions," *AFS Transactions*, vol 115, pp 135-150 (2007).
183. Tash, M., Samuel, F.H., Mucciardi, F., Doty, H.W., "Effect of Metallurgical Parameters on the Hardness and Microstructural Characterization of As-Cast and Heat-Treated 356 and 319 Aluminum Alloys," *Materials Science and Engineering A*, vol 443, pp 185-201 (2007).

184. Froehlich, A.R., Jacques, R.C., Strohaecker, T.R., Mombro, R., "The Correlation of Machinability and Microstructural Characteristics of Different Extruded Aluminum Alloys," *Journal of Materials Engineering and Performance*, vol 16(6), pp 784-791 (2007).
185. Yamada, H., Tanaka, T., "Machinability of Al-Si Casting Alloys on Super-High Speed Machining," *Journal of Japan Foundry Engineering Society*, vol 47(5), pp 332-337 (1975).
186. Zaima, S., Inabe, M., Hirono, M., "Contribution to Wear in Turning of Hypereutectic Al-Si Alloys," *Journal of Japan Institute of Light Metals*, vol 22(4), pp 275-280 (1972).
187. Zaima, S., Suzuki, M., Yamada, S., "Turning of Hypereutectic Al-Si Alloys by Use of CBN Tools," *Journal of Japan Institute of Light Metals*, vol 131(12), pp 780-786 (1981).
188. Tsunoda, K., M., Hirono, M., "Tool Deposits and Their Influences on Tool Wear in Turning of Hypereutectic Al-Si Alloy," *Journal of Japan Institute of Light Metals*, vol 30(4), pp 190-195 (1980).
189. Muromachi, S., Takatsuji, Y., Tada, S., "Effects of Additional Elements on Machinability of Hypereutectic Al-Si Alloy," *Journal of Japan Institute of Light Metals*, vol 19(12), pp 543-549 (1969).
190. Edward, J.D., Frary, F.C., Jeffries, Z., "The Aluminum Industry-Aluminum Products and Their Fabrication," *Chapter IV-Properties of Aluminum Alloys*, pp 176.
191. Yakou, T., Yoshida, S., Matsuoka, H., Hasegawa, T., "Machinability of Age-Hardened Al-Cu, Al-Cu-Pb, Bi and Al-Cu-Si Alloys From a View Point of Chip Breaking," *Transactions of Japan Society of Mechanical Engineers, Series C* 66, pp 3772-3777 (2000).
192. Konig, W., Erinski, D., "Machining and Machinability of Aluminum Cast Alloys," *Annals of the CIRP*, vol 32(2), pp 535-540 (1983).
193. Vermolen, F., Vuik, K., van der Zwaag, S., "A Mathematical Model for the Dissolution Kinetics of Mg₂Si-phases in Al-Mg-Si Alloys During Homogenisation Under Industrial Conditions," *Materials Science and Engineering A*, vol 254, pp. 13-32 (1998).
194. Lasa, L., Ibabe, J., "Characterization of the Dissolution of Al₂Cu Phase in Two Al-Si-Cu-Mg Casting Alloys Using Calorimetry," *Materials Characterization*, vol 48, pp 371-378 (2002).
195. Kang, H.G., Kida, M., Miyahara, H., Ogi, K., "Age-Hardening Characteristics of Al-Si-Cu-Base Cast Alloys," *AFS Transactions*, vol 107, pp 507-515 (1999).
196. Wang, G., Sun, Q., Feng, L., Hui, L., Jing, C., "Influence of Cu Content on Ageing Behavior of AlSiMgCu Cast Alloys," *Materials and Design*, vol 28, pp1001-1005 (2007).
197. Mocellin, R., Fougeres, P., Gobin, F., "A Study of Damage Under Tensile Loading in a New Al-Si-Fe Alloy Processed by the Osprey Route," *Journal of Materials Science*, vol 28, pp. 4855-4861(1993).

198. Nishido, S., Kaneso, M., Kobayashi, T., Toda, H., "Role of Si Particle Damage on Fatigue Characteristics of Cast Al-Si Alloys," *International Journal of Cast Metals Research*, vol 17(6), pp 345-350 (2004).
199. Trent, E.M. "Metal Cutting and the Tribology of Seizure: I Seizure in Metal Cutting," *Wear*, vol.128, pp 29-45 (1988).
200. Bao, H., Stevenson, M.G., "An Investigation of Built-Up Edge Formation in the Machining of Aluminum," *International Journal of Machine Tool Design and Research*, vol 16, pp 165-178 (1976).
201. Trent, E.M. "Metal Cutting and the Tribology of Seizure: II Movement of Work Material over the Tool in Metal Cutting," *Wear*, vol 128, pp 47-64 (1988).
202. Williams J.E., Rollason E.C., "Metallurgical and Practical Machining Parameters Affecting Built-up Edge Formation in Metal Cutting," *Journal of Japan Institute of Light Metals*, vol 98, pp144-153 (1970).
203. Kei-Lin Kuo, "Experimental Investigation of Ultrasonic Vibration-Assisted Tapping," *Journal of Materials Processing Technology*, vol 192-193, pp 306-311 (2007).
204. Sha, J., "Monitoring, Diagnosis, and Control of Tapping Process," Ph.D. Dissertation, The University of Wisconsin, Madison (1989).
205. Hardy, H.K., "The Effect of Small Quantities of Cd, In, Sn, Sb, Ti, Pb, or Bi on the Aging Characteristics of Cast and Heat-Treated Al-4%Cu-0.15%Ti Alloy," *Journal of the Institute of Metals*, vol 78, pp 169-194 (1950).
206. Goswami, R., Chattopadhyay, K., "The Solidification Behavior of Bi particles Embedded in an Al Matrix," *Acta Materialia*, vol 44 (6), pp 2421-2429 (1996).
207. Campbell, J., *Castings*, pp 221, Butterworth-Heinemann, Reed Educational and Professional Publishing Ltd, (1991).
208. Emadi, D., Whiting, L.V., Gertsman, V.Y., Sahoo, M., "Effect of Tin on the Mechanical Properties of Aluminum 319 Alloy," *AFS Transactions*, vol 114 (2006).
209. Mohamed, A.M.A., Samuel, F.H., Samuel, A.M., Doty, H.W., Valtierra, S., "Influence of Tin Addition on The Microstructure and Mechanical Properties of Al-Si-Cu-Mg and Al-Si-Mg Casting Alloys," *Metallurgical and Materials Transactions A*, vol 39A, pp 490-501 (2008).
210. Mohamed, A.M.A., Samuel, F.H., Samuel, A.M., Doty, H.W., Valtierra, S., "Precipitation of Tin in Cast 319 and 356 Aluminum Alloys," *AFS Transactions*, vol 115, (2007).
211. Kliauga, A.M., Vieira, E.A., Ferrante, M., "The Influence of Impurity Level and Tin Addition on the Aging Heat Treatment of the 356 Class Alloy," *Materials Science and Engineering A*, vol 480, pp 5-16 (2008).
212. Grebenkin, V.S., Sil'chenko, T.V., Gorshkov, A.A., Dzykovich, I.Y., "Effect of Magnesium on the Distribution of Tin and Lead in Al-Si Alloys," *Metals Science & Heat Treatment*, vol 3, pp 50-54 (1972).
213. Chen, P., Alpas, A.T., "Mechanical Properties and Machinability of an Aluminum-16 wt.% Silicon Alloy Modified by 0.5 and 1.0 wt.% Bismuth," *AFS Transactions*, vol 118 (2010).

-
214. Elhadad, S., "Effect of Trace Elements on the Microstructure and Porosity Formation in 319 Type Al-Si-Cu Alloys," M.Sc. Dissertation 2003, Université du Québec à Chicoutimi, Canada.
 215. Couper, M.J., "6XXX Series Aluminum Alloys," U.S. Patent, No. 6,364,969B1, Granted 2002.

